

**AN EVALUATION OF DEEP EUTECTIC SOLVENTS  
FOR CHARGE/DISCHARGE TESTS USING ALL-  
VANADIUM REDOX COUPLES FOR FLOW BATTERIES**

**LALEH BAHADORI**

**THESIS SUBMITTED IN FULFILMENT OF THE  
REQUIREMENTS FOR THE DEGREE OF DOCTOR OF  
PHILOSOPHY**

**FACULTY OF ENGINEERING  
UNIVERSITY OF MALAYA  
KUALA LUMPUR**

**2015**

**UNIVERSITI MALAYA**

**ORIGINAL LITERARY WORK DECLARATION**

**Name of Candidate: Laleh Bahadori (Passport No: H95658880)**

**Registration/Matric No.: KHA100019**

**Name of Degree: Doctor of Philosophy (Ph.D.)**

**Title of Project Paper/Research Report/Dissertation/Thesis (“this Wrok”):**

**AN EVALUATION OF DEEP EUTECTIC SOLVENTS FOR  
CHARGE/DISCHARGE TESTS USING ALL-VANADIUM REDOX COUPLES  
FOR FLOW BATTERIES**

**Field of Study: Chemical Engineering**

**I do solemnly and sincerely declare that:**

- (1) I am the sole author/writer of this Work;
- (2) This Work is original;
- (3) Any use of any work in which copyright exists was done by way of fair dealing and for permitted purposes and any excerpt or extract from, or reference to or reproduction of any copyright work has been disclosed expressly and sufficiently and the title of the work and its authorship have been acknowledged in this Work;
- (4) I do not have any actual knowledge or ought I reasonably to know that the making of this Work constitutes an infringement of any copyright work;
- (5) I hereby assign all and every rights in the copyright to this Work to the University of Malaya (“UM”), who henceforth shall be owner of the copyright in this Work and that any reproduction or use in any form or by any means whatsoever is prohibited without the written consent of UM having been the first had and obtained;
- (6) I am fully aware that if in the course of making this Work I have infringed any copyright whether intentionally or otherwise, I may be subject to legal action or any other action as may be determined by UM.

**Candidate’s Signature**

**Date:**

**Subscribed and solemnly declared before,**

**Supervisors’s signature**

**Date:**

**Name:**

**Designation:** Department of Chemical Engineering,  
Faculty of Engineering, University of Malaya, Kuala Lumpur, 50603, Malaysia  
Tel./Fax: +60 379675294/ +60 379675319



## ABSTRACT

One of the key constraints limiting the widespread commercialization of redox flow batteries (RFBs) appears to be their low energy density. A mean of overcoming this drawback has been the employment of non-aqueous electrolyte solvents that can offer a wide potential window of operation and increase the energy capacity of the system. In the present study, low cost ionic liquids analogues, namely deep eutectic solvents (DESs), have been proposed as non-aqueous electrolytes for potential application in the RFB. The proposal is based upon diffusion coefficient and electrode rate kinetics data. Different DESs, based on ammonium and phosphonium salts with various hydrogen bond donors (HBDs) including acids, alcohols and amid have been prepared. The evaluation of DESs as new electrolytes demands a perception of their main physicochemical and electrochemical properties. For this purpose, selected properties of the prepared DESs were measured and documented. The DESs were employed as electrolytes to determine the effects of electrode type and solvent on the electrochemical system studied. Two organometallic redox couples, ferrocene/ferrocenium ( $\text{Fc}/\text{Fc}^+$ ) and cobaltocenium/cobaltocene ( $\text{Cc}^+/\text{Cc}$ ) were utilized as internal reference redox systems to provide a known and stable reference point in different DESs. Diffusion coefficient ( $D$ ) of  $\text{Fc}/\text{Fc}^+$  and  $\text{Cc}/\text{Cc}^+$  was found to be of the order of  $10^{-10}$  to  $10^{-8}$   $\text{cm}^2 \text{ s}^{-1}$  in all studied DESs, and these values do not change significantly with concentration. The kinetics of the  $\text{Fc}/\text{Fc}^+$  and  $\text{Cc}^+/\text{Cc}$  electrochemical systems have been investigated over a temperature range from 298 to 338 K. The standard heterogeneous electron transfer rate constant ( $k^0$ ) was calculated at different temperatures by means of a logarithmic analysis. From the comparison of results, it can be inferred that the  $D$  and  $k^0$  for ammonium based DES prepared from ethylene glycol HBD was greater than those for other DESs.

In spite of the importance of DESs and their interesting advantages, their applications in redox flow battery are scarce. The present work is an attempt to describe a single-element non-aqueous redox system based on vanadium (III) acetylacetonate ( $V(acac)_3$ ) in DES, in order to overcome the key technological barriers of developing vanadium redox battery, such as the stability of electrolyte. The solubility of  $V(acac)_3$  was determined in selected DESs and the maximum solubility was approximately 0.1 M in the ammonium salt:ethylene glycol DES. Subsequently, the potential application and kinetic behavior of the selected DES were evaluated using cyclic voltammetry. The cyclic voltammetry show that the DES was stable in a functional potential range (-2.12–1.22 V). The  $D$  of  $V(acac)_3$  in the DESs electrolytes were estimated to be in the range of  $0.02\text{--}0.69\times 10^{-6} \text{ cm}^2 \text{ s}^{-1}$  at room temperature. Charge–discharge performance was determined using a static H-type electrochemical cell and coulombic efficiencies near 50% at 50 % state of charge (SOC) were achieved. The charge/discharge results were very similar to the use of acetonitrile as a solvent. This research will open up new opportunities for evaluating different types of DESs for enhancing the performance of all-vanadium RFB.

PENILAIAN PELARUT EUTEKTIK DALAM UNTUK UJIAN CAJ / DISCAS  
MENGUNAKAN KESEMUA PASANGAN REDOKS VANADIUM

**ABSTRAK**

Salah satu faktor utama yang menghadkan pengkomesialan meluas bateri aliran redoks (RFBs) adalah kerana mempunyai ketumpatan tenaga yang rendah. Bagi mengatasi kelemahan ini, penggunaan pelarut elektrolit bukan akues boleh memberikan operasi tingkap keupayaan yang luas dan dapat meningkatkan kapasiti tenaga bagi sistem. Dalam kajian ini, analog cacair ionik yang berkost rendah, yang dinamakan pelarut eutektik dalam (DESs) telah dicadangkan sebagai elektrolit bukan akues yang berpotensi untuk aplikasi dalam RFBs. Cadangan ini adalah berdasarkan kepada pekali resapan dan data kadar kinetik elektrod. Pelbagai DESs yang berasaskan garam amonium dan fosforus dengan penderma ikatan hidrogen (HBD) menggunakan asid, alkohol dan amid telah disediakan. Penilaian DESs sebagai elektrolit baru memerlukan persepsi terhadap ciri-ciri fizikokimia utama dan elektrokimia. Untuk tujuan ini, beberapa ciri-ciri tertentu bagi DESs yang telah disediakan, diukur dan didokumenkan. DESs ini digunakan sebagai elektrolit untuk menentukan kesan jenis elektrod dan pelarut terhadap sistem elektrokimia yang dikaji. Dua pasangan redok organologam, ferosena/ferosenium ( $\text{Fc}/\text{Fc}^+$ ) dan cobaltocenium / cobaltocene ( $\text{Cc}^+/\text{Cc}$ ) telah digunakan sebagai rujukan dalaman sistem redok supaya memberikan titik rujukan yang stabil dan diketahui dalam DESs yang berbeza. Pekali resapan ( $D$ )  $\text{Fc}/\text{Fc}^+$  dan  $\text{Cc}/\text{Cc}^+$  didapati dalam turutan  $10^{-10}$ - $10^{-8}$   $\text{cm}^2\text{s}^{-1}$  dalam kesemua DESs yang dikaji, dan tiada perubahan ketara terhadap nilai ini dengan perubahan kepekatan. Kinetik sistem elektrokimia bagi  $\text{Fc}/\text{Fc}^+$  dan  $\text{Cc}/\text{Cc}^+$  telah dikaji dalam julat suhu 298-338 K. Kadar malar pemindahan elektron heterogen asas ( $k^0$ ) telah dihitung pada suhu yang berbeza menggunakan analisis logaritma. Daripada perbandingan keputusan, ianya boleh

disimpulkan bahawa  $D$  dan  $k^{\circ}$  untuk DES berasaskan ammonium yang disediakan daripada etilena glikol sebagai HBD adalah lebih besar daripada DESs yang lain.

Walaupun DESs berkepentingan dan mempunyai kelebihan yang menarik, aplikasi pelarut ini dalam bateri aliran redok masih terhad. Kajian ini adalah percubaan untuk menerangkan sistem redok bukan akues satu elemen berasaskan vanadium (III) acetylacetonate ( $V(acac)_3$ ) dalam DES, dalam usaha untuk menghadapi kekangan utama teknologi pembangunan bateri redok vanadium, seperti kestabilan pelarut. Kebolehlarutan  $V(acac)_3$  telah dilakukan dalam DESs terpilih dan keterlarutan maksimum adalah sebanyak 0.1 M dalam eutektik garam ammonium : etilena glikol. Seterusnya, aplikasi keupayaan dan ciri kinetik DES terpilih telah dinilai dengan menggunakan kaedah siklik voltametri. Siklik voltametrik ini menunjukkan DES beroperasi dengan stabil pada keupayaan (-2.12–1.22 V). Pekali resapan bagi  $V(acac)_3$  dalam DES elektolit ini adalah dalam julat  $0.02\text{--}0.69 \times 10^{-6} \text{ cm}^2 \text{ s}^{-1}$  pada suhu bilik. Prestasi caj-discaj telah ditentukan menggunakan sel elektrokimia jenis H statik dan pencapaian kecekapan coulumbic menghampiri 50%. Keputusan caj/discaj adalah hampir sama apabila acetonitril digunakan sebagai pelarut. Kajian ini akan membuka peluang yang baru untuk menilai jenis DESs yang berbeza bagitujuan peningkatan prestasi kesemua RFB vanadium.

## ACKNOWLEDGMENTS

I extend my immense gratitude to my supervisors; Prof. Dr. Mohd Ali Hashim, Dr Mohammed Harun Chakrabarti, Assoc. Prof. Dr. Inas Muen AlNashef, Assoc. Prof. Dr. Farouq Sabri Mjalli and Dr Ninie Suhana Abdul Manan for their incessant support, guidance, constructive comments and encouragement.

A special thanks to all my friends and lab mates in the University of Malaya for their helpfulness and friendship throughout.

Last but definitely not least, my deepest and most heart-felt gratitude to my beloved mum, dad and brother for their endless love and supports.



## TABLE OF CONTENTS

TITLE PAGE.....	i
ORIGINAL LITERARY WORK DECLARATION FORM.....	ii
ABSTRACT.....	iii
ABSTRAK.....	v
ACKNOWLEDGMENT.....	vii
TABLE OF CONTENTS.....	viii
LIST OF FIGURES.....	xiii
LIST OF TABLES.....	xv
LIST OF SYMBOLS AND ABBREVIATIONS.....	xvi
NOMENCLATURE.....	xvii
<b>CHAPTER 1: INTRODUCTION.....</b>	<b>1</b>
1.1 Overview.....	1
1.2 Research Objectives.....	5
1.3 Research Methodology.....	5
1.4 Thesis Outline.....	6
<b>CHAPTER 2: LITERATURE REVIEW.....</b>	<b>8</b>
2.1 Renewable Energy.....	8
2.2 Introduction to Redox Flow Batteries.....	9
2.3 Vanadium System Overview.....	13
2.3.1 The Principle of VRBs.....	14
2.3.2 Why vanadium?.....	16
2.4 Conventional Electrolytes Used in Redox Flow Batteries and Their Drawbacks.....	17
2.4.1 Aqueous Electrolytes.....	17
2.4.2 Non-aqueous Systems.....	22

2.5	Introduction to ILs.....	25
2.5.1	Physical Properties of ILs.....	29
2.5.2	Applications of ILs in Electrochemical Engineering Based Processes.....	33
2.5.2.1	Electrochemical applications of ILs in metal processing.....	34
2.5.2.2	Destruction of halogenated hydrocarbons.....	35
2.5.2.3	Electrochemical energy storage application.....	36
2.5.2.4	Dye sensitized solar cells (DSSCs) for renewable energy storage.....	39
2.5.2.5	Applications of ionic liquids in redox flow batteries.....	39
2.6	Definition of DESs.....	42
2.6.1	Physical Properties of DESs.....	47
2.6.1.1	Melting Point (Freezing Point).....	47
2.6.1.2	Density.....	48
2.6.1.3	Viscosity.....	49
2.6.1.4	Ionic conductivity.....	50
2.6.2	Feasibility of Using DES for RFB Applications.....	51
2.7	Electrochemistry.....	53
2.7.1	Internal reference redox system.....	53
2.7.2	Reference electrodes.....	54
	<b>CHAPTER 3: RESEARCH METHODOLOGY.....</b>	<b>56</b>
3.1	Synthesis of DESs.....	56
3.1.1	Materials.....	56
3.1.2	Synthetic Procedure.....	57
3.2	DESs Characterization.....	58
3.2.1	Viscosity.....	59
3.2.2	Electrical Conductivity.....	59

3.2.3	Melting temperature.....	59
3.2.4	Density.....	60
3.2.5	pH.....	61
3.3	Electrochemical Experiments.....	61
3.3.1	Electrochemical Cell.....	61
3.3.2	Cyclic Voltammetry.....	61
3.3.3	Chronoamperometric Experiments.....	62
3.4	Measuring the solubility of Vanadium Acetylacetonate Compound in DESs.....	62
3.5	Charge/discharge Experiment.....	64
3.5.1	Instrumentation.....	64
3.5.2	H-type cell.....	64
<b>CHAPTER 4: RESULTS AND DISCUSSIONS.....</b>		<b>67</b>
4.1	Synthesis and Characterization of Different DESs.....	67
4.1.1	Density.....	68
4.1.2	Viscosity.....	71
4.1.3	Ionic and Molar Conductivity.....	75
4.1.4	pH.....	82
4.2	Electrochemical Behaviour of Fc and Cc <sup>+</sup> in DESs.....	84
4.2.1	Electrochemical Potential Window.....	85
4.2.2	Cyclic Voltammetry for Oxidation of Fc and Reduction of Cc <sup>+</sup> in Various DESs.....	91
4.2.3	Chronoamperometric Transients of Fc and Cc <sup>+</sup> in DESs.....	96
4.2.4	The Heterogeneous Electron-transfer Rates for the Fc and Cc <sup>+</sup> in DESs....	97
4.2.5	Temperature Dependence of the Voltammetric Data, <i>D</i> and <i>k</i> <sup>0</sup> for Fc/Fc <sup>+</sup> and Cc <sup>+</sup> /Cc in DESs.....	99
4.2.6	Concentration Dependence of <i>D</i> of Fc/Fc <sup>+</sup> .....	107

4.2.7	Stokes–Einstein Behaviour of Metallocene Derivatives.....	109
4.3	Electrochemical Behaviour of V(acac) <sub>3</sub> in DESs.....	111
4.3.1	Voltammetry of Vanadium Electrolytes in DESs.....	111
4.3.2	Kinetics of Electrode Reactions.....	116
4.4	Charge/discharge Performance.....	123
 <b>CHAPTER 5: CONCLUSIONS</b>		
5.1	Summary and Conclusions.....	127
5.2	Recommendations for Future Work.....	131
	REFERENCES.....	132
	LIST OF PUBLICATIONS AND PAPERS PRESENTED.....	155

## LIST OF FIGURES

Figure 2.1	General schematic of a redox flow battery.	11
Figure 2.2	The principle of VRB.	15
Figure 2.3	The main components of the VRB stacks.	16
Figure 2.4	Charging profile for 0.1 M ruthenium acetylacetonate and 1 M TEABF <sub>4</sub> in CH <sub>3</sub> CN at a current of 1 mA.	24
Figure 2.5	Phase diagram for urea-choline chloride (ChCl/U) system.	45
Figure 2.6	DES includes bulky cations and smaller anions attached to HBD.	46
Figure 3.1	Structures of the salts and hydrogen bond donors applied in this study.	58
Figure 3.2	(a) The scheme of H-type glass cell battery; (b) Photograph of an H-type charge/discharge cell.	65
Figure 4.1	Dependence of densities ( $\rho$ ) on temperature for; (a) DESs based on ammonium salts and polyol HBDs; (b) ammonium based salts and acids, amine, amide, zinc nitrate HBDs; (c) phosphonium based salts and polyol HBDs.	70
Figure 4.2	Dependence of viscosity ( $\eta$ ) on temperature for; (a) DESs based on ammonium salts and polyol HBDs; (b) ammonium based salts and acids, amine, amide, zinc nitrate HBDs; (c) phosphonium based salts and polyol HBDs.	72
Figure 4.3	Arrhenius plot of viscosity ( $\eta$ ) for; (a) DESs based on ammonium salts and polyol HBDs; (b) ammonium based salts and acids, amine, amide, zinc nitrate HBDs; (c) phosphonium based salts and polyol HBDs.	74
Figure 4.4	Dependence of ionic conductivity ( $\sigma$ ) on temperature for; (a) DESs based on ammonium salts and polyol HBDs; (b) ammonium based salts and acids, amine, amide, zinc nitrate HBDs; (c) phosphonium based salts and polyol HBDs.	77
Figure 4.5	Arrhenius plot of viscosity ( $\eta$ ) for; (a) DESs based on ammonium salts and polyol HBDs; (b) ammonium based salts and acids, amine, amide, zinc nitrate HBDs; (c) phosphonium based salts and polyol HBDs.	79
Figure 4.6	Walden plot for for; (a) DESs based on ammonium salts and polyol HBDs; (b) ammonium based salts and acids, amine, amide, zinc nitrate HBDs; (c) phosphonium based salts and polyol HBDs.	82
Figure 4.7	Temperature-dependency of pH for; (a) DESs based on ammonium salts and polyol HBDs; (b) ammonium based salts and acids, amine, amide, zinc nitrate HBDs; (c) phosphonium based salts and polyol HBDs.	84
Figure 4.8	PWs of DESs based on ammonium salts and polyol HBDs using (a) GC working electrode; (b) Pt. microelectrode.	87
Figure 4.9	PWs of DESs based on ammonium salts and acids, amine, amide, zinc nitrate HBDs (a) GC working electrode; (b) Pt. microelectrode.	88
Figure 4.10	PWs of DESs based on phosphonium based salts and polyol HBDs. (a) GC working electrode; (b) Pt. microelectrode.	90
Figure 4.11	Cyclic voltammetry for the; (a) oxidation of 5.21 mM Fc; (b) reduction of Cc <sup>+</sup> in DES11 on a Pt electrode (diameter 20 $\mu$ m) at varying scan rates of 10, 30, 50, 70 and 100mV s <sup>-1</sup> .	92

Figure 4.12	Linear dependence of peak current vs. square root of scan rates (SR) for; (a) Fc and; (b) Cc <sup>+</sup> using a Pt electrode in DES11.	95
Figure 4.13	Cottrell plot for the oxidation of Fc in DES3.	96
Figure 4.14	Cyclic voltammetry for; (a) oxidation of Fc and; (b) reduction of Cc <sup>+</sup> in the DES1 at varying temperatures of (i) 298 K, (ii) 308 K, (iii) 318 K, (iv) 328 K, (v) 338 K and (vi) 348 K, at 100 mV s <sup>-1</sup> .	100
Figure 4.15	Double potential step chronoamperometry measured; (a) on the DES1 across the Fc/Fc <sup>+</sup> ; (b) on the DES11 across the Cc <sup>+</sup> /Cc at temperatures of 298, 308, 318 and 338 K.	104
Figure 4.16	Dependence of diffusion and rate constant on temperature using Arrhenius rule for; (a) Fc/Fc <sup>+</sup> in DES1 and; (b) Cc <sup>+</sup> /Cc in DES11	107
Figure 4.17	Experimental (–) and fitted theoretical (o) chronoamperometric transients for the oxidation of 1.08, 5.21, 10.13, 20.18 and 30.06 mM Fc in DES11 at a 20 μm Pt microelectrode.	109
Figure 4.18	Plot of <i>D</i> against the inverse of viscosity ( $\eta^{-1}$ ) for the DESs based on glycerol and ethylene glycol HBDs	110
Figure 4.19	Cyclic voltammograms recorded at a glassy carbon electrode in 0.5 M TEABF <sub>4</sub> in CH <sub>3</sub> CN (---) and 0.01 M V(acac) <sub>3</sub> and 0.5 M TEABF <sub>4</sub> in CH <sub>3</sub> CN (—) at 0.1 V s <sup>-1</sup> .	112
Figure 4.20	Cyclic voltammograms recorded at 0.1 V s <sup>-1</sup> at a glassy carbon electrode in 0.01 M V(acac) <sub>3</sub> and 0.5 M TEABF <sub>4</sub> in different DESs.	116
Figure 4.21	Cyclic voltammetry recorded at a glassy carbon electrode in 0.01 M V(acac) <sub>3</sub> and 0.5 M TEABF <sub>4</sub> in CH <sub>3</sub> CN at different scan rate.	117
Figure 4.22	Cyclic voltammograms for (a) V(acac) <sub>3</sub> , (b) the V(II)/V(III) redox couple and (c) the V(III)/V(IV) redox couple at a glassy carbon electrode in 0.01 M V(acac) <sub>3</sub> /0.5 M TEABF <sub>4</sub> in DES3.	118
Figure 4.23	Cyclic voltammograms at a glassy carbon electrode in 0.01 M V(acac) <sub>3</sub> /0.5 M TEABF <sub>4</sub> in DES11 at different scan rate.	120
Figure 4.24	Cyclic voltammograms at a glassy carbon electrode in 0.01 M V(acac) <sub>3</sub> /0.5 M TEABF <sub>4</sub> in DES9 at different scan rate.	120
Figure 4.25	Plot of the Nernst equation for a single-electron disproportionation reaction with a 2.01 V cell potential (DES3).	122
Figure 4.26	Charge/discharge curves for 0.01 M V(acac) <sub>3</sub> /0.5 M TEABF <sub>4</sub> in CH <sub>3</sub> CN. The charge current was 1 mA and the discharge current was 0.1 mA.	123
Figure 4.27	Charge/discharge curves for 0.01 M V(acac) <sub>3</sub> /0.5 M TEABF <sub>4</sub> in DES3. The charge current was 0.1 mA and the discharge current was 0.01 mA.	124
Figure 4.28	Charge/discharge curves during the 3th and 12th cycles for 0.01 M V(acac) <sub>3</sub> /0.5 M TEABF <sub>4</sub> in DES3. The charge current was 0.1 mA and the discharge current was 0.01 mA.	125

## LIST OF TABLES

Table 2.1	Reduction potentials of vanadium redox couples	17
Table 2.2	Prices of some commercially available ILs prepared at the Queen's University Belfast and sold by Acros Organics	43
Table 2.3	Commercial prices of DESs manufactured in Leicester and sold throughout the UK	44
Table 3.1	List of DESs obtained by complexation between hydrogen acceptor and hydrogen-bond donor molecules	57
Table 3.2	Equipments utilized for characterization of DESs with their uncertainties.	58
Table 3.3	Properties of AMI-7001S anion exchange membrane.	66
Table 4.1	Physical properties of the different DESs synthesized in this study.	68
Table 4.2	The adjustable parameters for density of all studied DESs.	70
Table 4.3	Regression parameters for viscosity of studied DESs.	75
Table 4.4	Regression parameters for ionic conductivity of studied DESs.	79
Table 4.5	The adjustable parameters for pH of all studied DESs.	84
Table 4.6	Electrochemical potential windows for the DESs based on ammonium salts and polyol HBDs obtained by means of GC and Pt. electrodes.	89
Table 4.7	Cyclic voltammetric data for oxidation of FC in DESs.	93
Table 4.8	Kinetic parameters and $D$ for $\text{Fc}/\text{Fc}^+$ and $\text{Cc}^+/\text{Cc}$ in DESs.	98
Table 4.9	The experimental voltammetric data for $\text{Fc}/\text{Fc}^+$ and $\text{Cc}^+/\text{Cc}$ in DESs with different operating temperatures.	101
Table 4.10	Temperature dependence of Kinetic parameters and diffusion coefficients for $\text{Fc}/\text{Fc}^+$ and $\text{Cc}^+/\text{Cc}$ in DESs.	105
Table 4.11	Activation energies of the diffusion coefficients and rate constants for $\text{Fc}/\text{Fc}^+$ and $\text{Cc}^+/\text{Cc}$ in studied DESs.	106
Table 4.12	Concentration dependent of the diffusion coefficients of Fc in DESs solution.	108
Table 4.13	The Stokes–Einstein products of Fc and $\text{Cc}^+$ in some DESs.	111
Table 4.14	Summary of $\text{V}(\text{acac})_3$ performance characteristics in selected DESs.	121

## LIST OF ABBREVIATIONS

[MOPMPip <sup>+</sup> ][TFSI <sup>-</sup> ]	1-(3-methoxypropyl)-1-methylpiperidinium bis(trifluoromethylsulfonyl) imide
[BMIM]Cl	1-butyl-3- methylimidazolium chloride
EMI-FSI	1-ethyl-3-methyl imidazolium bis(fluorosulfonyl)imide
[C <sub>2</sub> mim]I	1-ethyl-3-methylimidazolium iodide
[C <sub>2</sub> mim][BF <sub>4</sub> ]	1-ethyl-3-methylimidazolium tetrafluoroborate
[HMPyrr <sup>+</sup> ][TFSI <sup>-</sup> ]	1-hexyl-1-methyl-pyrrolidinium bis (trifluoromethylsulfonyl) imide
[bmim][PF <sub>6</sub> ]	1-n-butyl-3-methylimidazolium hexafluorophosphate
[bmim][BF <sub>4</sub> ]	1-n-butyl-3-methylimidazolium tetrafluoroborate
CH <sub>3</sub> CN	Acetonitrile
VRB	All-vanadium Redox Flow Battery
[N(CF-SO <sub>2</sub> ) <sub>2</sub> ]	Bis(trifluoromethyl)sulfonylamide
ChCl	Choline Chloride
CA	Chronoamperometry
Cc <sup>+</sup> /Cc	Cobaltocenium/Cobaltocene
CE	Coulombic Efficiency
CV	Cyclic Voltammetry
DES	Deep Eutectic Solvent
DCA	Dicyanamide
DSC	Differential Scanning Calorimetry
DSSCs	Dye Sensitized Solar Cells
EDLC	Electric Double layer Capacitor
EE	Energy Efficiency
EG	Ethylene Glycol
Fc/Fc <sup>+</sup>	Ferrocene/Ferrocenium
GC	Glassy Carbon
AuNPs	Gold Nanoparticles
HBD	Hydrogen Bond Donor
ICP-AES	Inductively Coupled Plasma-Atomic Emission Spectrometer
IEM	Ion Exchange Membrane
IL	Ionic Liquid
TEA-BF <sub>4</sub>	<i>N,N,N,N</i> -tetraethylammonium-tetrafluoroborate
PYR <sub>14</sub> TFSI	<i>N</i> -butyl- <i>N</i> -methylpyrrolidinium bis (trifluoromethanesulfonyl) imide
OCP	Open-Circuit Potential
Pt	Platinum Electrode
PEMFC	Polymer Electrolyte Membrane Fuel Cell
PW	Potential Window
PC	Propylene Carbonate
QRE	Quasi-Reference Electrodes
RFB	Redox Flow Battery
G2	Second Generation
AgBF <sub>4</sub>	silver tetrafluoroborate
SEI	Solid Electrolyte Interface
SOC	State Of Charge
B(CN) <sub>4</sub>	Tetracyanoborate
TEABF <sub>4</sub>	tetraethylammonium tetrafluoroborate
SCN	Thiocyanate
TCM	Tricyanomethanide
V(acac) <sub>3</sub>	Vanadium (III) acetylacetonate
VE	Voltage Efficiency



## NOMENCLATURE

$E_{\eta}$	Activation Energy Of Viscosity ( kJ mol <sup>-1</sup> )
$E_{pa}$	Anodic Peak Potential
$k_B$	Boltzmann Constant(m <sup>2</sup> kg s <sup>-2</sup> K <sup>-1</sup> )
$E_{pc}$	Cathodic Peak Potential
$C_o$	Concentration Of The Electroactive Species (mol cm <sup>-3</sup> )
$\sigma$	Conductivity (mS cm <sup>-1</sup> )
$\rho$	Density (g cm <sup>-3</sup> )
$D$	Diffusion Coefficient(cm <sup>2</sup> s <sup>-1</sup> )
$A$	Electrode Area (cm <sup>2</sup> )
$V_e$	Equivalent Weight (gm)
$F$	Faraday's Constant( C mol <sup>-1</sup> )
$T_f$	Freezing Point(K)
$E_{1/2}$	Half Wave Potential (V)
$k^0$	Heterogeneous Rate Constant (cm s <sup>-1</sup> )
$R$	Ideal Gas Constant ( kPa.L.mol <sup>-1</sup> .K <sup>-1</sup> )
$M_w$	Molecular Weight (g mol <sup>-1</sup> )
$i_p$	Peak Current (A)
$\Delta E_p$	Peak-to- Peak Potential Separation(V)
$v$	Scan Rate (mV s <sup>-1</sup> )
$s$	Solubility(M)
$\eta D T^{-1}$	Stokes–Einstein Product( g cm s <sup>-2</sup> K <sup>-1</sup> )
$T$	Temperature(K)
$t$	Time (s)
$\eta$	Viscosity (mPa s)

# CHAPTER 1: INTRODUCTION

## 1.1 Overview

Exploration and development of renewable energies from sources like solar, wind and wave are amongst a few of the central topics of our time (Skyllas-Kazacos et al., 2009, Skyllas-Kazacos et al., 2011). However, the variable and intermittent nature of renewable energy is the most critical issue affecting the final quality of power output, so there is often the problem of matching the supply to meet the demand (Hart et al., 2012). Large scale energy storage systems, is the key technology to solve this problem. Energy storage can increase the stability of energy that can be derived from wind or other forms of renewable energy. For instance, electricity supply from photovoltaic cells that convert solar energy can be stabilized significantly if coupled to an efficient energy storage system (Li et al., 2011). Of all the new energy storage technologies the all-vanadium redox flow battery (VRB) possesses features such as flexible design, long life, low pollution emission, high storage capacity and quick response (Kear et al., 2009; Huang et al., 2008, Rahman and Skyllas-Kazacos, 2004, Fabjan et al., 2001).

The VRB, proposed by Maria Skyllas-Kazacos in 1985, operates on the principle of two electrolyte tanks containing active soluble species of vanadium in different valence states (in the positive tank: the V(IV)/V(V) redox couple; in the negative tank: the V(II)/(III) redox couple) in sulfuric acid solution, two pumps, and a battery stack section where the redox electrode reaction takes place (Li et al., 2011; Zhao et al., 2006). The electrolytes are pumped into the stack separated by an ion exchange membrane. Electrical balance is achieved by the migration of hydrogen ions across the membrane separating the electrolytes (Rychcik and Skyllas-Kazacos, 1988). All of the reactants and products of the electrode reactions remain dissolved in one or other of the two electrolytes and, if solution crossover happened, the vanadium half-cell electrolytes

can be mixed again and the system make return to its original state, although with a loss of energy efficiency. No significant phase change reactions or electro-recrystallization processes occur in the VRB system (Ponce de Leon et al., 2006). Furthermore, the difficulty of electrolytes cross contamination through the battery separator was overcome, because of using only vanadium species in both halves of the cell (Skylas-Kazacos et al., 1991, Vafiadis et al., 2006). Based on these attractive features, more and more attention has been paid to the VRB recently (Herr et al., 2014, Wandschneider et al., 2014; Wu et al., 2014, Burt et al., 2014).

Low energy density seems to be a major barrier toward commercialization of redox flow batteries (Chakrabarti et al., 2014). In order to overcome this significant difficulty, non-aqueous electrolyte solvents offering a wide potential window of operation and increase the energy capacity of the system (Chakrabarti et al., 2007, Chakrabarti et al., 2011). In contrast of organic systems which are environmentally unfriendly, ILs have recently emerged as a new class of non-aqueous electrolytes with energy storage applications (Skylas-Kazacos et al., 2011; Soloveichik et al., 2011, Katayama et al., 2002; Hirao et al., 2000). ILs have their own limitations due to its high cost and its electrochemistry can be severely affected in the presence of water (Nkuku and Lesuer, 2007). This problem can be eliminated by replacement of DES with ILs (Chakrabarti et al., 2013).

ILs are defined generally as salts composed of discrete cations and anions that melt at or below 100°C (Earle and Seddon, 2000). Since the last decade, due to some fascinating properties of ILs, they have attracted more attention and became interesting for various applications. ILs have been described as designer solvents (Zhao and Baker, 2012), and this means that their properties can be tuned to suit the requirements of a particular process. Their advantageous properties include negligible vapour pressure,

good thermal and chemical stability, high polarity and non-flammability (AlNashef et al., 2001, Endres and Zein El Abedin, 2006, MacFarlane et al., 2006). Some ILs also show no miscibility with water, allowing the development of novel separation processes (Appetecchi et al., 2006). ILs have been intensively studied as electrolytes due to their attractive characteristics such as broad potential windows, intrinsic conductivities and high thermal stabilities (zhao et al., 2008, Galinski et al., 2006) in comparison to common organic solvents like acetonitrile (Chakrabarti et al., 2007). In addition, some ILs are so stable with respect to electrochemical decomposition, that reactive metals, such as sodium and lithium can be deposited from them (Fuller et al., 1997).

ILs have great potential for use as “green” solvents for industrial processes (AlNashef et al., 2002; Plechkova et al., 2008). However, their large scale applications in industry have remained a challenge, due to issues associated with high cost, purity and toxicity (Hou et al., 2008, Abbott et al., 2003). Thus deep eutectic solvents (DESs) have been identified as alternatives for ILs (Abbott et al., 2009, Abbott et al., 2004). A DES is a eutectic mixture of an organic salt (ammonium or phosphonium) and a hydrogen bond donor (HBD), that is, made up of different components such as amides, metal salts, alcohols, carboxylic acids and amines that may be used as complexing agents (typically a H-bond donor) (Boisset et al., 2013, Rub and Konig, 2012 ). DESs have a melting point that is far below that of either individual constituent. The mechanism is that the complexing agent interacts with the anion and increases its effective size. This, in turn, decreases the anion interaction with the cation thereby reducing the melting point of the mixture (Abbott et al., 2003). These liquids are easy to prepare in a pure state, they are non-reactive with water and most importantly they are biodegradable due to which, the toxicological properties of the components are well characterized (Abbott et al., 2007). These compounds share many characteristics of conventional ILs (e.g. they have intrinsic electrical conductivity, low-volatility,

biodegradability, high thermal and chemical stability, good electrochemical stability, non-flammability) and they are simple to synthesize on a large scale (Leron and Li et al., 2012, Zhang et al., 2012, Carriazo et al., 2012). These properties have been explored for promising applications such as solvents for electrodeposition and electropolishing (Steichen et al., 2011, Abbott et al., 2009), electrochemistry (Nkuku and LeSuer, 2007), separation processes (Pang et al., 2012), chemical and enzyme reactions (Lindberg et al., 2010), biochemistry (Dai et al., 2013) as well as organic and inorganic synthesis (Abbott et al., 2006, Abbott et al., 2005).

Despite the significance of DESs and their remarkable advantages, their applications in a redox flow battery (RFB) are either negligible or even absent. In this work, we prepared several DESs based on quaternary ammonium and phosphonium salts and different hydrogen bond donors (HBD) for potential use as solvents and electrolytes in RFB. Furthermore, their physicochemical and electrochemical properties (viscosity, conductivity, electrochemical stability, diffusion coefficient, etc.) in a similar manner to that for ILs have been evaluated. The synthesized DESs are applied as electrolyte to determine the effects of the electrode and solvent on the electrochemical system. Ferrocene/ferrocenium ( $\text{Fc}/\text{Fc}^+$ ) or cobaltocenium/cobaltocene ( $\text{Cc}^+/\text{Cc}$ ) redox couples have been investigated as candidates of internal references to provide a known and stable reference point in various DESs.

In addition, a single-element non-aqueous redox system based on vanadium (III) acetylacetonate ( $\text{V}(\text{acac})_3$ ) in selected DES is described. The potential application of DESs in non-aqueous RFBs was evaluated using cyclic voltammograms and charge-discharge characteristics of the system were estimated using a static H-type electrochemical cell with an anion-exchange membrane separator.

## 1.2 Research objectives

This project is an attempt to adapt work from the development of a novel redox flow battery and uses the H-type electrochemical cell employing DES and a range of active electrolytes for efficient charge/discharge purposes. In the proposed research, DESs will be synthesized from different available chemical sources. Then, these DESs will be utilized as electrolytes for vanadium redox flow battery applications. Thus, in summary, the objectives of this study are as follows:

1. Synthesis of different DESs in the laboratory.
2. Measure the physical properties of DESs relevant to battery applications.
3. Test the electrochemical behaviours of DES using cyclic voltammetry and chronoamperometry using reversible redox couple as an internal potential standard.
4. Study the solubility of  $V(acac)_3$  in selected DESs.
5. Study the detailed electrochemical kinetics for the  $V(II)/V(III)$  and  $V(IV)/V(V)$  couples.
6. Conduct charge/discharge experiments with the DES that shows best performance obtained from preliminary electrochemical screening tests.

## 1.3 Research methodology

The methodology that will be followed to obtain the objectives will be considered comprehensively in chapter three. A summary of the methodology is listed below:

1. Synthesis of DESs.
2. Characterization of physical properties of these electrolytes using several equipments.
3. Testing Cyclic voltammetry experiments on  $V(acac)_3$  in acetonitrile.

4. Preparation of solubility experiments of  $V(acac)_3$  in DESs.
5. Analysis of the samples using Induced Coupled Plasma (ICP) analysis.
6. Testing electrochemical properties of reversible vanadium species in DESs using cyclic voltammetry.
7. Fabrication of an H-type electrochemical cell.
8. Performing charge/discharge experiments with electrochemically reversible DES using the glass cell reactor.

#### **1.4 Thesis outline**

This report contains five chapters dealing with different aspects relevant to the topic of the study as follows:

1. Chapter One - INTRODUCTION: This chapter includes a brief introduction to the research and objectives of the study.
2. Chapter Two - LITERATURE REVIEW: This chapter presents the literature survey concerning the renewable energies, vanadium redox flow battery, ionic liquids, deep eutectic solvents and their application.
3. Chapter Three - METHODOLOGY: this chapter includes chemical and material used in this work, the synthesis of deep eutectic solvents and measuring their physical properties, solubility experiment, cyclic voltammetry and chronoamperometry and Charge/discharge experiments.
4. Chapter Four - RESULTS AND DISCUSSIONS: experimental results are discussed thoroughly.

5. Chapter Five - CONCLUSIONS: conclusions are drawn over the results obtained and their analysis.



## CHAPTER 2: LITERATURE REVIEW

### 2.1 Renewable energy

Renewable energy has been growing in demand throughout the world due to environmental issues such as global warming or acid rain. These problems have resulted due to an excessive use of fossil fuels as a consequence of unprecedented growth in agricultural, domestic and industrial activities especially in emergent countries (Banos et al., 2011, Liming et al., 2009). In response, there are strong possibilities of replacing fossil fuels with renewable sources of energy in the future due to their significantly lesser impact upon the environment (Panwar et al., 2011). Renewable energy also presents important drawbacks, such as the discontinuity of generation, as most resources depend on climatic conditions (Marques et al., 2011, Negro et al., 2012). Despite that, combining these renewable energy sources with back-up units to form a hybrid system can provide a more economic, environment friendly and reliable supply of electricity in comparison to the single-usage of such systems (Erdinc and Uzunoglu, 2012). Another alternative means of improving the sustained supply of the renewable and yet intermittent energy involves the design and deployment of efficient energy storage technologies (Lund and Mathiesen, 2009, Hajimolana et al., 2011). Each technology has some inherent disadvantages that make it practical or economical for only a limited range of applications (Evans et al., 2012). When combining operation requirements with cost, electrochemical systems are seen to be superior to the other forms of energy storage which are mainly mechanical in nature and therefore have relatively longer response times (Skylas-Kazacos et al., 2011, Leung et al., 2012).

Efficient renewable energy storage needs to accumulate energy during times when demand is low (peak shaving) and to supply it when demand is high in order to ensure efficient energy handling (load leveling) (Skylas-Kazacos et al., 2011). A number of

technologies based on electrical, chemical, electrochemical and mechanical processes have been proposed to address the energy storage needs of electrical grids (Soloveichik, 2011, Sheikh, 2010, Sahir and Qureshi, 2008). Electrochemical storage systems are found to be robust due to their relative ease of siting as well as fast response times. Electrochemical energy storage systems provide direct conversion between chemical and electrical energy and are therefore particularly suited to the storage of the latter (Skylas-Kazacos et al., 2011). Electrochemical storage technologies also offer additional advantages compared with other types of energy storage systems, including (Leung et al., 2012):

- Modularity whereby they can be used in applications ranging from a few kWh to several MWh.
- Simultaneous application for both power quality and energy management.
- Low environmental impact, which means they can be sited near residential areas.

## **2.2 Introduction to redox flow batteries**

Redox flow batteries (RFBs) are rechargeable electrochemical systems that rely on the redox states of various soluble species for the purposes of storing and releasing energy via highly efficient charge/discharge processes (Weber et al., 2011, Bartolozzi, 1989). The use of the redox flow cell can be traced back to the zinc/chlorine system that was developed in 1884 by Charles Renard and Arthur Krebs to power their army airship “La France” (Yang et al., 2011, Posner, 1955). Later, this concept was re-visited by Posner in the mid-1950s (Posner, 1955), and an independent investigation was conducted in Japan around 1968 (Soloveichik, 2011, Bae et al., 2011). The modern iron/chromium RFB was invented by Lawrence Thaller at the National Aeronautics and

Space Administration (NASA) in the USA (Thaller, 1974, Bae et al., 2011). In the last two decades following the invention of this technology, it was developed and used in small to medium-scale field tests (Diaz-Gonzalez et al., 2012). Because fully soluble redox couples and inert electrodes are used (Skyllas-Kazacos et al., 2011, Leung et al., 2012, Chakrabarti et al., 2007), undesirable electrode processes are eliminated (especially structural changes of the electrode), in contrast with secondary battery systems (Palacin et al., 2009). The energy storage capacity of the system is determined by the concentrations of the reactants and the size of the storage tanks, and the system power is determined by the number of individual cells in the battery stack and their electrode area (Rychcik and Skyllas-Kazacos, 1988). Consequently, it is possible to independently optimise the flow cell's storage capacity and power output. This feature makes RFBs unique in their ability to provide specific power and energy requirements for each application. The storage capacity can be increased to reduce the incremental costs of each additional energy storage capacity unit relative to other batteries by adding additional electrolytes. Thus, the cost per kWh of the system substantially decreased as the storage capacity increased, making the RFB particularly attractive for applications requiring storage times in excess of 4–6 h (Skyllas-Kazacos et al., 2011).

Furthermore, RFBs are different from other types of rechargeable batteries because liquid electrolytes supply their energy rather than solid electrodes. For example, in a lithium-ion cell, lithium ions from the liquid electrolyte are inserted into the electrodes. The capacity of the lithium-ion battery is controlled by the size of the lithium component in the electrode and the electrolyte. The power of lithium-ion batteries is enhanced by increasing the electrode size, which couples the power and energy (Sato et al., 2004, Garcia et al., 2004, Hayashi et al., 2005).

In comparison, the RFB prospect separates the power capacity from the energy capacity. The electrodes in the reactors supply sources or sinks for electrons and are theoretically inert. In addition, the number of cell reactors piled together and the sizes of the electrodes in each cell specify the overall power. The total mass of the electrolytic solution flowing through the reactor stack specifies the energy-storage capacity (Ponce de Leon et al., 2006, Li et al., 2011). This separation of energy and power uses flexible and scalable RFBs to meet client requirements. Due to the relatively low energy densities of liquid electrolytes, RFBs are mainly employed for stationary applications, specifically, large power plants. One additional benefit of RFBs is that the electrochemical reactions at the liquid/solid interface are fast (Ponce de Leon et al., 2006, Li et al., 2011). Because the electrodes of Li-ion batteries exhibit mechanical exhaustion with time due to insertion reactions, the electrodes in the RFB should not. Consequently, the RFB lifetimes are much longer than those in other battery systems (Ponce de Leon et al., 2006, Li et al., 2011).

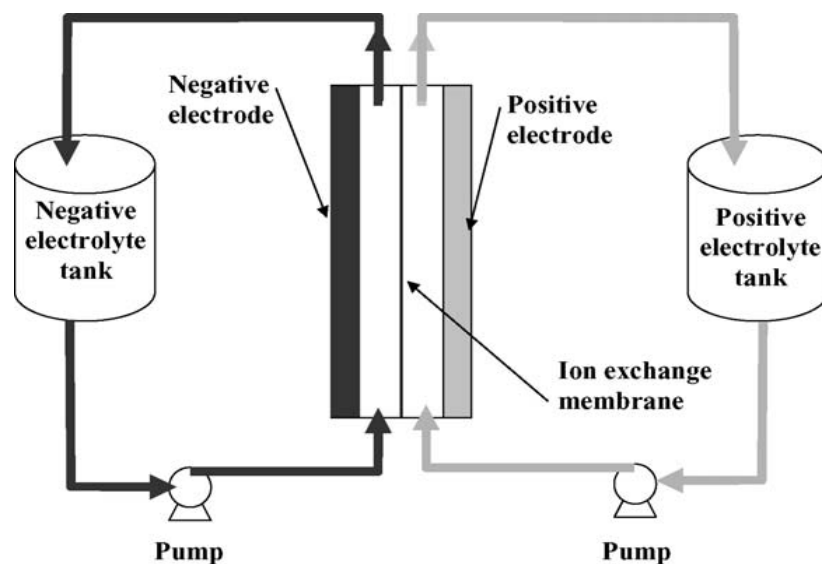


**Figure 2.1:** General schematic of a redox flow battery (Ponce de Leon et al., 2006)

Generally, an RFB contains a main cell, electrolyte tanks, and a flow system, displayed schematically in Figure 2.1. An electrical power source, such as a solar cell, is used to charge the RFB. The electrolyte is pumped from the storage tanks through two

separate compartments in the main cell while the battery is performing. The electrolyte storage tanks are generally greater than the main reactor in which redox reactions occur. The cell includes two current collectors, an anode, a cathode, and an ion-exchange membrane that separates the anode compartment from the cathode compartment. Electrons flow through the electrode/solution interfaces and drive redox reactions that include the active materials dissolved in the liquids if a voltage difference exists between the electrodes. To increase their area, the electrodes are composed of high surface area porous materials, such as carbon (Ponce de Leon et al., 2006, Li et al., 2011). The membrane that separates the negative and positive electrolytes is used to keep the solutions electronically isolated while allowing ion exchange between the compartments. Ion-selective membranes were used to minimise the self-discharge reactions in the cell interior (Skylas-Kazacos et al., 2011). Because electrons flow through the electrodes and charge is passed across the electrode/liquid interfaces, ions are transferred through the membrane to sustain overall charge neutrality. The separator is a principle cause of transport restrictions in an RFB and can considerably influence the power and energy efficiency of the battery (Arora and Zhang et al., 2004).

The liquid electrolytes in a RFB have three main components, redox active species, the supporting electrolyte, and the solvent. The active species are oxidised or reduced to transform the electricity into chemical energy. The composition and structure of the active species control the features of the battery, including the reversibility, kinetics, and cell potential (Shinkle et al., 2014, Leung et al., 2012). The supporting electrolyte is an observer in the reaction and only supplies conductivity to the solution (Shinkle et al., 2014, Leung et al., 2012). The solvent controls the solubility of the active species and supports the electrolytes, which influence the energy and power density. In addition, the solvent affects most of the physical properties of the solution (Shinkle et al., 2014, Leung et al., 2012). In the mixture, the solvent and supporting electrolyte generally

define the stability window of the solution, which can restrict the possible active-species reactions that can be used to store energy (Shinkle et al., 2014, Leung et al., 2012).

### **2.3 Vanadium system overview**

The vanadium redox flow battery (VRB), which was originally proposed by Skyllas-Kazacos and co-workers, has recently received considerable attention due to its technical benefits (Sum and Skyllas-Kazacos, 1985, Skyllas-Kazacos et al., 1986). Since then, research regarding this technology has continued (Kear et al., 2012, Joerissen et al., 2004, Zhang et al., 2012, Huang et al., 2008). These benefits include the flexibility in design, the facility to regenerate the electrolyte solution and the reliability of large-scale energy storage, among others (Mai et al., 2011). In iron/chromium and bromine/polysulphide systems, a chief concern and liability is the incompatibility between and the sensitivity of the two electrolyte streams regarding their contamination of each other. If a species crosses over and reacts irreversibly with the elements in the opposite stream; it includes an efficiency loss from that special charge/discharge cycle and a capacity loss and degradation in the overall operation of the system, which may result in costly electrolyte separation and reactant recovery (Weber et al., 2011). Thus, it is helpful to develop a system with more than two oxidation states of the same element, where crossover only represents an efficiency loss because no species are irreversibly consumed or removed from their reactive electrolytic solutions (Li et al., 2011, Oriji et al., 2004, Weber et al., 2011). As a promising technology for storing intermittent renewable energy, VRB systems have potentially received the most attention among RFBs recently (Watt-Smith et al., 2013, Zhang et al., 2012, Kear et al., 2012). While energy density is not necessarily an initial effect for stationary, grid applications, the VRB energy density is limited by the solubility of vanadium in the electrolyte stream

and precipitation can occur. In addition, the solubility limits depend on the temperature and acid concentration (Skyllas-Kazacos et al., 1996).

### **2.3.1 The principle of VRBs**

The VRB is an electrochemical system that can comprehend alterations between chemical energy and electrical energy (Chakrabarti et al., 2014, Zhao et al., 2006). As shown in Figure 2.2, VRBs have two electrolyte tanks, including active vanadium species in different valence states. The V(II)/V(III) redox couple is used at the negative electrode, while the V(IV)/V(V) redox couple is used at the positive electrode (Sum and Skyllas-Kazacos, 1985, Zhang et al., 2011). All active species are dissolved in a sulphuric acid medium. The vanadium ion and sulphuric acid concentrations were 1–3 M and 1–2 M, respectively (Li et al., 2011). During the charge/discharge procedures, the active species are oxidised or reduced to convert between chemical energy and electrical energy (Ponce de Leon et al., 2016). The electrical balance was obtained by transporting the protons or sulphate ions for the anion exchange membrane in the electrolytes across the membrane during the performance of the cell. Characterised by the dissolved redox species in the re-circulated solution, the flow battery differs from the other batteries storing the energy in electrode structures, such as lithium-ion batteries and lead-acid batteries. The characteristic structure of the VRB allows for the independent design of the power rating and storage capacity (Huang et al., 2008, Weber et al., 2011, Li et al., 2011). In addition, VRBs have a unique advantage over other flow batteries because their positive and negative electrolytes are identical in their discharged states (Vafiadis and Skyllas-Kazacos, 2006, Oriji et al., 2004, Li et al., 2011).

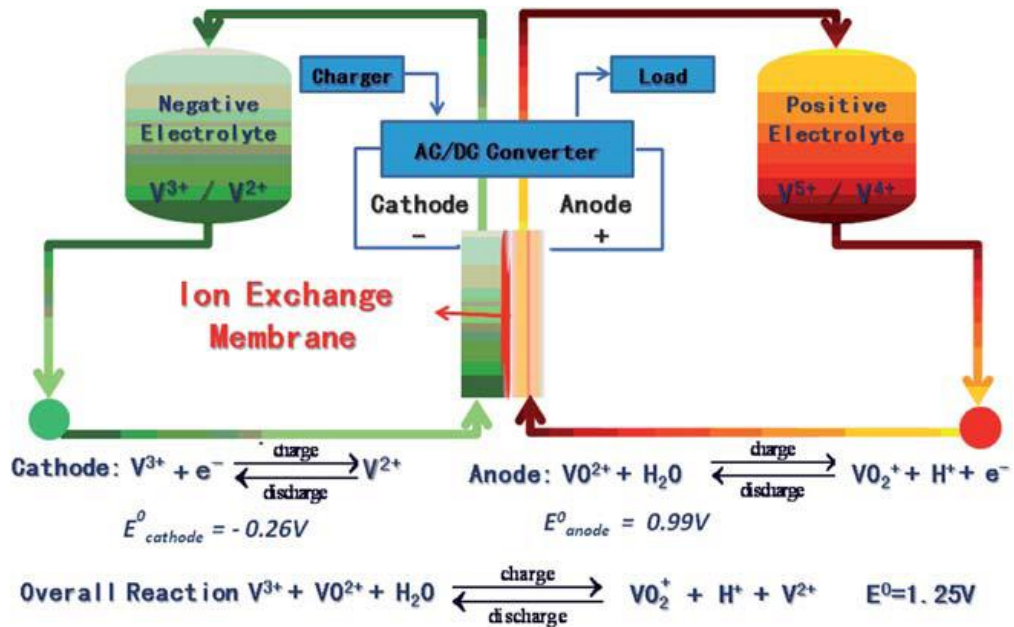


**Figure 2.2:** The principle of VRB (Li et al., 2011).

This arrangement makes shipping and storing the electrolyte easier and more economical, further simplifying their management during use. Moreover, there the ions from one electrolyte do not contaminate the other electrolyte in their discharge state because the active species in both electrolytes are the same (Li et al., 2011).

An individual VRB cell is mainly composed of two half cells, two solid electrodes and one ion exchange membrane (IEM) (Zhao et al., 2006). The reactions occur on the surface of the solid electrodes during charge and discharge. High surface area carbon materials are commonly used as electrodes in VRB. These materials perform over a certain range of voltage potentials with minimal hydrogen and oxygen gas progression (Li et al., 2011). The IEMs between these materials isolate both electrolytes but allow proton transport (Zhang et al., 2011). In addition, VRBs are constructed by assembling various cells in series to form a VRB stack in applicable applications, as shown in Figure 2.3. The number of cells assembled is determined from the desired output voltage level of the battery (Li et al., 2011).



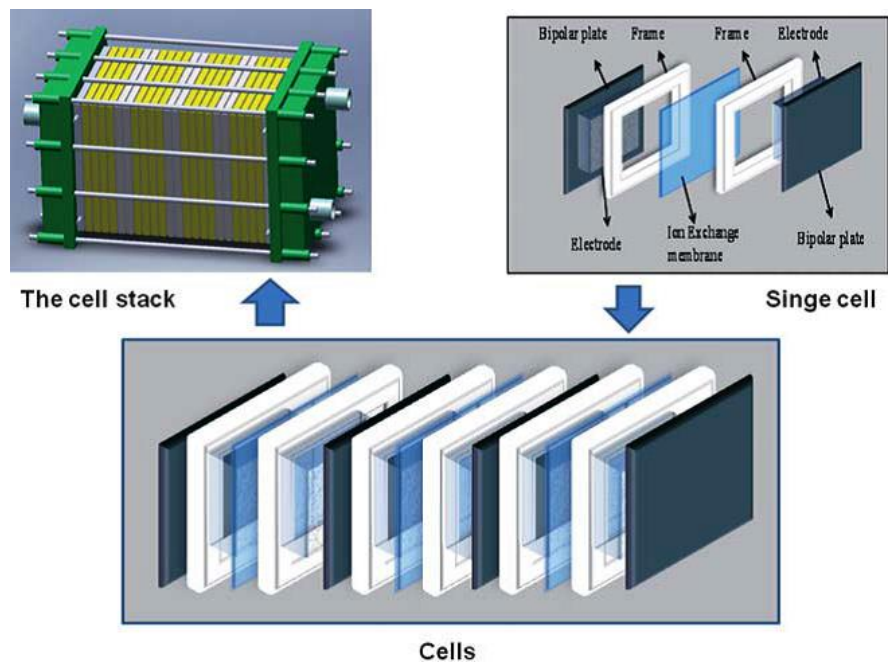


**Figure 2.3:** The main components of the VRB stacks (Li et al., 2011).

### 2.3.2 Why vanadium?

The cross contamination of electrolytes with different elements, which increases the cost of electrolyte regeneration, is one of the challenges of using RFBs. Thus, the same elements are used as redox couples for negative and positive electrodes (Kear et al., 2012, Ponce de Leon et al., 2006). The vanadic, vanadyl, vanadous and hypovanadous ions can be recognised during cell performance by their coloration, with light yellow, blue, green and violet corresponding with soluble vanadium species in the (II), (III), (IV) and (V) oxidation states, respectively (Kear et al., 2012). Table 2.1 lists the broad span between the standard reduction potentials of V(III)/V(II) and V(V)/V(IV). The solubility of VRB in acidic aqueous solutions satisfies the requirements of a flow battery (Gattrell et al., 2004, Sun and Skyllas-Kazacos, 1991). Using vanadium solutions in both half-cells in batteries is beneficial for the following reasons: (a) the electrolyte can be easily regenerated after contamination; (b) the electrochemical reversibility of the vanadium redox couple makes high-energy efficiency accessible; and (c) vanadium occurs naturally in approximately sixty five various minerals and in fossil fuel deposits, making its commercial use possible (Li et al., 2011).

**Table 2.1:** Reduction potentials of vanadium redox couples (Joerissen al., 2004, Li et al., 2011).

Redox couple	Reduction potential (V)
$V^{3+}/V^{2+}$	-0.255
$VO_2^+/VO^{2+}$	0.999
$VO^{2+}/V^{3+}$	0.337

## 2.4 Conventional electrolytes used in redox flow batteries and their drawbacks

Generally, most of the RFBs reported in the literature employ aqueous electrolytes. Therefore, their operating potential is constrained by the electrochemical stability window of water (depending on pH, generally lower than 2.0 V) (Chakrabarti et al., 2007). Organic solvents offer a much higher potential window, e.g. 5 V for acetonitrile ( $CH_3CN$ ), with which, much higher power and energy output can be obtained (Liming et al., 2009, Low et al., 2013). However, organic solvents tend to be detrimental to the environment due to high vapor pressures, toxicity and flammability.

### 2.4.1 Aqueous electrolytes

The most notable aqueous-based systems were the iron/chromium, all-vanadium and bromide/polysulfide technologies. The all-vanadium system achieved commercial fruition, while the other two systems faced limitations when scaling up (Yufit et al., 2013). Despite commercial success, the all-vanadium systems suffer from several drawbacks, including high costs due to the IEM, a low open-circuit potential (OCP) (which results in less power output), and a lower energy density (ca. 25 Wh  $kg^{-1}$ ) (Skylas-Kazacos et al., 2011, Leung et al., 2012). The low energy density problem was solved by inventing a vanadium/bromine redox system (Skylas-Kazacos, 2003). Preliminary studies have been conducted using a 3–4 M vanadium–bromide solution in the negative half-cell and an 8–10 M HBr solution in the positive half-cell (Skylas-Kazacos, 2003) and different membrane materials (Skylas-Kazacos et al., 2011, Vafiadis and Skylas-Kazacos, 2006). For this concentration of active ions, it was

possible to reach energy densities of up to  $50 \text{ Wh kg}^{-1}$  (Vafiadis and Skyllas-Kazacos, 2006). This cell showed a rapid loss of capacity due to the transfer of vanadium ions across the membrane to the positive half-cell solution (Skyllas-Kazacos et al., 2011). To overcome this problem, vanadium–bromide was added to both half-cells, resulting in the G2 (second generation) V–Br cell technology that employs the same electrolytes in both half-cells. Similar to the all-vanadium battery, the G2 V–Br overcame this cross contamination problem. However, the higher solubility of vanadium halides compared with vanadium sulphate salts resulted in much higher energy densities (Skyllas-Kazacos et al., 2011). This technology was patented in 2008 (Skyllas-Kazacos, 2008, Skyllas-Kazacos et al., 2011). Nonetheless, one potential concern of V–Br redox systems is the release of toxic bromine-vapour during operation. Consequently, Skyllas-Kazacos (Skyllas-Kazacos et al., 2010) used bromine complexing agents, such as tetrabutylammonium bromide, polyethylene glycol, N-methyl-N-ethyl morpholinium bromide, and N-methyl-N-ethylpyrrolidinium bromide, to decrease the hazards associated with this process (Yufit et al., 2013). A similar problem related to the toxic discharge of hydrogen sulphide gas was reported for the bromide/polysulfide system (Lessner et al., 1992). Despite achieving higher energy densities with the V–Br system, the electrochemical decomposition of water limited its potential power output.

All of the early RFBs used multiple redox-active species in the liquid electrolytes, a formation known as a “dual-active-species”. Samples of dual-active-species RFBs include RFBs containing iron/titanium (Savinell et al., 1979) and iron/chromium (O'Donnell et al., 1976), as well as commercial zinc/bromine (Lim et al., 1977, Besenhard et al., 1977) hybrids and sodium-polysulfide/bromine (Ge et al., 2004, Price et al., 1999, Zhao et al., 2005) systems. The attendance of distinct active species is important because the crossover of active species affects all RFBs. Dual-active-species

RFBs frequently demand periodical electrolyte reactivation after long-term performance (Arora, P. and Z. Zhang, 2004, Assink, 198

4, Wiedemann et al., 2005) because they can be irreversibly degraded when constituents of the catholyte and anolyte merge or reach the electrode surfaces.

The first single-active-species RFB, which was based on vanadium, was first used by Skyllas-Kazacos and co-workers (Skyllas-Kazacos et al., 1986). The aqueous all-vanadium chemistry, which was patented in 1986, was recently the most studied RFB system (Skyllas-Kazacos et al., 1986). In sulphuric acid at a pH of nearly zero, the following VRB half-reactions occurred (Sum et al., 1985, Sum and Skyllas-Kazacos, 1985, Oriji et al., 2005, Li et al., 2011)



Therefore, the overall cell reaction is



In addition, it is important to observe that the support acid in an all-vanadium RFB supplies protons for the overall cell reaction, which makes the equilibrium cell potential pH dependent. At the negative electrode, V(II) oxidises on the electrode surface as V(III) and frees an electron during its release (Li et al., 2011). The electron crosses the external circuit to the cathode and hydrogen ions pass through the membrane from the anode compartment to the cathode compartment to sustain charge neutrality. At the positive electrode, V(V) is reduced to V(IV), consuming two hydrogen ions and an electron while producing water. During charging, energetic electrons are provided by an external source, and the reactions at the positive and negative electrodes are reversed (Watt-Smith et al., 2013).

The aqueous VRB can obtain coulombic efficiencies of 95 %. Thus, the majority of the current input to the battery can be removed (Skyllas-Kazacos et al., 1986). Skyllas-Kazacos et al. proposed that the coulombic efficiency was less than 100 %, mainly due to crossover through the membrane. However, a second reason for reduced efficiency could be water electrolysis, which occurs near the potential of the V(II)/V(III) redox couple. Overall, energy efficiencies of 80-85 % were obtained, which were estimated from the ratio of energy input to energy output (Kazacos and Skyllas-kazacos, 1989).

Many researchers have concentrated on adjusting the original VRB (Watt-Smith et al., 2013, Huang et al., 2008, Zhao et al., 2006). Recent cell chemistry modifications replace the V(IV)/V(V) couple because it is not steady in many popular membranes (Shinkle et al., 2014, Zhang et al., 2012). The use of vanadium/bromide was examined by Skyllas-Kazacos et al. (Skyllas-Kazacos et al., 2010) but resulted in a lower cell potential, efficiency, and current density than the all-vanadium chemistry. Xue et al. (2008) demonstrated that a vanadium/manganese system using manganese on the positive electrode had an efficiency of 63 %, likely due to crossover through the membrane. Several researchers reported using a vanadium/cerium (Paulenova et al., 2002, Fang et al., 2002, Xia et al., 2002) flow cell with a cylindrical geometry. This system was capable of reaching a coulombic efficiency of 90 % when applying a porous Vycor frit in place of a costly proton exchange membrane. State-of-the-art RFB systems use active-species concentrations of up to 3 M (Rahman and Skyllas-Kazacos et al., 1998). These RFB systems achieved 60-70 % energy efficiencies, 75-85 % coulombic efficiencies, and discharge potentials of nearly 1.5 V in an H-cell configuration (Hall et al., 2008, Tsuda et al., 1997). Complex reactor designs have been successfully used to increase the coulombic efficiencies to up to 97 % and the energy efficiencies to up to 86 % (Kazacos and Skyllas-kazacos, 1997) using IEM (Sukkar and Skyllas-Kazacos, 2003) or microporous separators (Arora and Zhang, 2004).

Aqueous RFB systems are associated with several limitations, such as membrane cost/stability, membrane crossover, water electrolysis, and low energy densities. Membranes with small pore sizes and/or functionalization for enhancing ion selectivity are used to mitigate crossover (Skylas-Kazacos et al., 2011). The resistance of the membranes increases as the pore size decreases, which results in an energy loss within the battery system. Therefore, the chosen membrane must balance the resistance of the membrane with crossover and the balance depends on the electrolytes used. For example, the zinc/bromine system demands the use of a flocculent to stop crossover (Lim et al., 1977, Barnartt and Forejt et al., 1964) or a constant separation process. The all-vanadium system begins with similar complexes in both electrolytes and is crossover resistant.

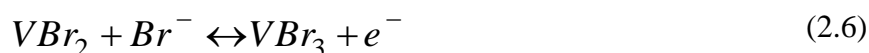
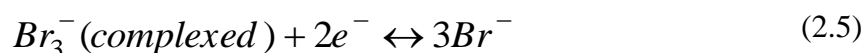
Many recent studies have focused on membrane stability due to the V(V) oxide species in commercial membranes (Skylas-Kazacos et al., 2011). Most early research of VRBs included Nafion membranes (sulfonic-acid ionomer membranes with perfluorinated backbones), which have low ionic resistances and outstanding selectivity. However, due to cost cuts, a host of commercially available membranes were examined. The Nafion and “New Selemion anion exchange membrane” are known to supply sufficient stability. Both membranes have similar costs (Skylas-Kazacos et al., 2011). In addition, membranes based on cross-linked, sulfonated polyethylene (called “Daramic”) separator materials have been manufactured (Mohammadi and Skylas-Kazacos, 1995).

One fundamental issue with aqueous RFBs is their relatively narrow stability window (1.23 V, not accounting for the over potential associated with water-splitting), which is limited by water electrolysis (Sum et al., 1985). Thus, it is difficult to achieve long term cycling of aqueous VRB without losing some water to the formation of hydrogen (Sum and Skylas-Kazacos, 1985).

Another limitation of aqueous RFBs is their energy density. The energy density of RFBs generally scales with the potential window (VCell), solution concentration (c<sub>active</sub>), and the number of electrons transferred (n) as follows:

$$E \propto \frac{1}{2} n F V_{Cell} c_{active} \quad (2.4)$$

The recent progresses of Skyllas-Kazacos et al. (2010) have pushed aqueous RFB systems to their performance thermodynamically possible limits in the presence of water. Their latest battery chemistry uses active vanadium bromide species to reach a two-electron transfer reaction in one electrolyte based on the following reaction scheme:



This system was cycled with 3-4 M vanadium bromide and 8-10 M hydrogen bromide (Skyllas-Kazacos, 2003). Because this system already uses multiple electrons at high concentrations, increasing the cell potential is the last possible strategy that can be used to increase the energy density. Thus, the presence of water creates a hard ceiling on the maximum energy density that is possible in existing RFB systems. Due to these issues, researchers have considered the application of non-aqueous solvents as potential electrolytes in RFBs around the world (Low et al., 2013).

#### 2.4.2 Non-aqueous systems

Non-aqueous systems can sustain cell reactions with potentials up to 5 V, depending on the solvent used (Bard and Faulkner, 2000). Replacing the solvent could enable the use of RFBs in extreme climates where they currently are not viable. For instance, acetonitrile (CH<sub>3</sub>CN, also abbreviated as ACN), an attractive non-aqueous solvent, is a liquid at temperatures between -45 and 82 °C and is suitable for colder

climates, while dimethylformamide is a liquid between  $-61$  and  $153$  °C. OCP potential as high as  $2.6$  V were reported using acetonitrile, but overall energy efficiency was limited to 40% (Matsuda et al., 1988). Non-aqueous solvents permit the use of many high-energy RFB reactions and will thus be the focus of this dissertation. There are several reports of non-aqueous RFBs using chemistries based on uranium, ruthenium, manganese, chromium, and vanadium (Chakrabarti et al., 2007, Yamamura et al., 2002, Liu et al., 2009, Sleightholme et al., 2011, Liu et al., 2010).

Matsuda et al. (1988) studied ruthenium complexes (ruthenium acetylacetonate and tris(2,2'-bipyridine) ruthenium (II) tetrafluoroborate) in non-aqueous electrolytes for RFB applications. They employed tetraethylammonium tetrafluoroborate (TEABF<sub>4</sub>) as the supporting electrolyte and CH<sub>3</sub>CN as the solvent. Cyclic voltammetry experiments showed a cell voltage of  $2.6$  V for the system. The conductivity was optimised, and charge/discharge experiments were performed to determine the efficiency. The optimum efficiency as a function of active-species concentration occurred in the range of  $0.02$ - $0.05$  M, while very low efficiencies were observed for concentrations greater than  $0.1$  M or less than  $0.01$  M. Crossover of active species is expected to be the cause of the low efficiencies at high concentrations due to the increased diffusion driving force (Matsuda et al., 1988).

A paper published in 2007 by Chakrabarti and co-workers reported charge/discharge curves from an investigation of the feasibility for RFBs of ruthenium and iron complexes (ruthenium acetylacetonate, tris(2,2'-bipyridine)ruthenium (II) tetrafluoroborate, tris(2,2'-bipyridine)iron (II) perchlorate, and rubrene) in CH<sub>3</sub>CN with TEABF<sub>4</sub> as a supporting electrolyte (Chakrabarti et al., 2007). The results from these non-aqueous systems were compared with those for aqueous VRB. OCPs of  $1.77$  V and  $2.41$  V were measured for the ruthenium and iron complexes, respectively. Charge/discharge experiments on the ruthenium system revealed the behaviour shown



in Figure 2.4. Chakrabarti et al. (2007) attributed the unexpected increase in potential at 1000 minutes to a side reaction and stopped charging at 12% of the theoretical capacity. The discharge voltage corresponding to this charge cycle was also low (1.3 V).

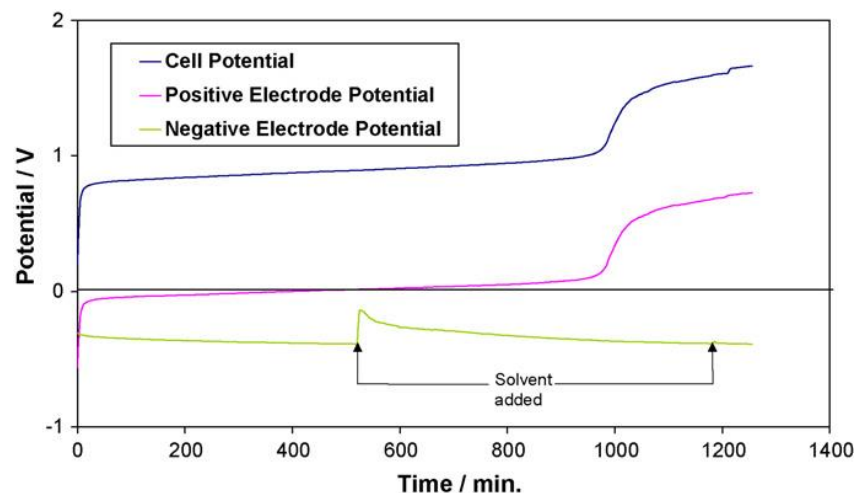


**Figure 2.4:** Charging profile for 0.1 M ruthenium acetylacetonate and 1 M TEABF<sub>4</sub> in CH<sub>3</sub>CN at a current of 1 mA (Chakrabarti et al., 2007).

Chakrabarti et al. (2011) also recently reported the use of a ruthenium active species (ruthenium acetylacetonate) within a novel cell design. These experiments were performed using a membrane-less flow cell based on two counter current laminar flow streams, with the same electrolyte on each side of the battery. To keep the flow laminar, very low flow rates were employed to reduce the propensity for crossover; in spite of the control of the flow, the voltage efficiency was 55%. To test the feasibility of the flow-cell design, Chakrabarti et al. (2013) also studied the operation of several other RFB chemistries in the laminar flow-cell configuration. The aqueous all-vanadium system had the highest energy efficiency, at 13.4%, using a 0.02 M vanadium solution.

Yamamura et al. (2002) worked on uranium RFB in 2002 as a creative way to apply depleted uranium. They succeeded in changing the solubility by three orders of magnitude by changing the structure of the ligand in the metal complex. Unfortunately, the electrochemistry resulted in cell potentials of only 1.0 to 1.2 V, and significant

amounts of ligand shedding (with corresponding irreversible loss of active material) occurred with cycling. The reactions were stated to be:



Different limitations are associated with non-aqueous RFB technologies. RFBs have been recognised to have low solubility limits of active species and supporting electrolytes, resulting in low energy densities. They also have low internal conductivity, resulting in high overpotentials, and additional safety concerns related to aqueous systems (Weber et al., 2011, Li et al., 2009, Soloveichik et al., 2011). The high cost of organic solvents and their high vapour pressures introduce severe restrictions to the system (Low et al., 2013). For these reasons, as well as concerns regarding the safe handling of organic and flammable solvents, alternative non-aqueous solvents are required that could provide a high potential window of operation without having the inherent disadvantages of their organic counterparts. Ionic liquids and deep eutectic solvents appear to have some answers to overcome these issues (Chakrabarti et al., 2014).

## 2.5 Introduction to ILs

ILs, also called molten salts, are defined as liquid mixtures of cations and anions that melt below 100 °C and are stable up to 300°C (Galinski et al., 2006, Zhao et al., 2012). Structurally, they contain cations, which are usually organic compounds, and anions of inorganic or organic components. The ions in ILs are large and bulky, with the cationic component inclined to have a very low degree of symmetry (Zhang et al., 2006). Due to the poor packing associated with the asymmetric nature of ILs, crystal forming is restrained and ILs remain liquids over a wide range of temperatures. By

careful selection of these components, it is possible to prepare ILs that are liquids around and below room temperature, which has initiated great interest in them (Plechko et al., 2008). The first IL formed, [EtNH<sub>3</sub>][NO<sub>3</sub>], which has a freezing point of 12 °C, was introduced in 1914 by Paul Walden. However, interest in them remained at a low level until the detection of binary ionic liquids prepared from mixtures of N-alkylpyridinium and aluminium(III) chloride (Chum, 1975) or 1,3-dialkylimidazolium chloride (Wilkes, 1982). The key problem of chloroaluminate-based ILs was their instability in the presence of water and air. In addition, they are reactive towards various organic compounds, which restricted their application. In 1970, a work was presented for developing ILs as electrolytes for batteries and space probes (Chen, 2001, Keskin et al., 2007) that required molten salts to operate. These molten salts were hot enough to damage nearby materials, so researchers sought salts that remained liquid at lower temperatures. They ultimately recognised pyridinium and alkyl-substituted imidazolium cations with tetrahalogenoaluminate or halide anions as suitable for this purpose. Wilkes and co-workers (1982) upgraded particular ILs for use as battery electrolytes. In the 1980s, imidazolium-based cations were found to have better properties, such as air/moisture stability and more potential for variation (Kölle and Dronskowski, 2004, Sheldon et al., 2002, Carmichael and Seddon, 2000, Aki et al., 2001). In the 1990s, applications of air-stable ILs such as 1-n-butyl-3-methylimidazolium hexafluorophosphate ([bmim][PF<sub>6</sub>]) and 1-n-butyl-3-methylimidazolium tetrafluoroborate ([bmim][BF<sub>4</sub>]) as well as water-stable ILs were enhanced quickly to the extent that ILs became among the most promising solvents in chemical processes (Wasserscheid et al., 2002, Aki et al., 2001).

Common ionic liquids consist of ammonium, phosphonium, sulfonium, imidazolium, lithium, pyridinium, thiazolium, oxazolium, picolinium, triazolium or pyrrolidinium as the cationic component and bromide, chloride, nitrate, aluminium

chloride, iodide, benzoate, and acetate as the anionic component. ILs are referred to as designer solvents due to the wide range of possible cation and anion combinations that enables the tuning of properties such as melting point, viscosity, density, polarity, refractive index and hydrophobicity to satisfy the requirements of a particular process (Kirchner et al., 2010, Zhang et al., 2006).

ILs can be sorted into two principal classes: (1) simple salts (single anion and cation) and (2) binary ILs (salts where equilibrium is included). For example, [EtNH<sub>3</sub>][NO<sub>3</sub>] is a simple salt, while the mixture of 1,3-dialkylimidazolium chloride and aluminium(III) chloride (a binary IL system) consists of several different ionic species, and its melting point and properties depend upon the mole fractions of the two components (Earle and Seddon, 2000).

Due to severe regulations imposed on industry, the application of common organic solvents such as diethyl ether, toluene or methanol is limited. In contrast, ILs are green solvents that are not subject to these restrictions (Keskin et al., 2007).

The synthesis of ILs usually includes two phases: the formation of the desired cation followed by anion exchange to give the desired product. The cation should be unsymmetrical and have a poorly localised positive charge, stopping the formation of a regular lattice and thereby decreasing the melting point of the resulting salt (Rauter et al., 2010).

The synthesis of ILs generally starts with the quaternisation of an amine, an imidazole or phosphine to produce the cationic component (Wilkes et al., 1982, and Wasserscheid and Keim, 2000). Examples of ILs that can be formed by direct quaternisation are [EMIM]CF<sub>3</sub>SO<sub>3</sub> and [BMIM]Cl (Wasserscheid and Keim, 2000). An anion exchange reaction is another method for synthesising ILs. It is achieved by using one of three methods:

i) Metathesis of a halide salt with a salt of the desired anion:

Generally, imidazolium and pyridinium halides can be acquired using this method.

These types of reactions are divided into two classes depending on the water solubility of the object IL. One is metathesis by free acids or ammonium salts of alkali metals, and another one is metathesis by silver salt. The production of water-miscible ILs is difficult because it demands separation of the by-products from the desired IL. For instance, 1-ethyl-3-methylimidazolium tetrafluoroborate  $[\text{C}_2\text{mim}][\text{BF}_4]$  was produced in 1992 by the metathesis reaction of 1-ethyl-3-methylimidazolium iodide  $[\text{C}_2\text{mim}]\text{I}$  and silver tetrafluoroborate ( $\text{AgBF}_4$ ) in methanol. The metathesis reaction is able to synthesise novel ILs, but they are contaminated with a small quantity of halide ions that may react with the solute materials (Wilkes and Zaworotko, 1992, Bao et al., 2003).

ii) Acid-base neutralisation:

Monoalkylammonium nitrates are produced by the neutralisation of aqueous solutions of a base with nitric acid. The ILs are separated by removing extra water under vacuum. In a similar reaction, tetraalkylammonium sulfonates are synthesised mixing sulfonic acid and tetraalkylammonium hydroxide. To ensure the purity of the ILs, they were dissolved in either tetrahydrofuran or acetonitrile and treated with activated charcoal for at least 24 h, and the organic solvent was ultimately removed under vacuum (Wasserscheid and Keim, 2000).

iii) Direct combination of a halide salt with a metal halide:

Halogenaluminate(III)- and chlorocuprate(I)-based ILs are prepared by this method. However, chlorocuprate(I) ILs are sensitive to oxygen and have not established widespread usage in synthesis (Wasserscheid and Keim, 2000).

### 2.5.1 Physical properties of ILs

Recently, much interest has been generated in ILs for their potential use as solvent media due to their unique combination of properties. As it is possible to change the structure of ILs, it is also possible to tune their physical properties as needed (Zhao and Baker, 2013, Menne et al., 2013, Shiddiky and Torriero et al., 2011). They are good solvents for a wide variety of inorganic and organic components. Therefore, it is possible to bring unusual combinations of reagents into a single phase. ILs have the potential to be highly polar yet non-coordinating solvents, as they are composed principally of poorly coordinating ions. ILs are also immiscible with a large number of organic solvents and therefore supply a non-aqueous, polar alternative for two-phase systems. They are ordinarily non-volatile (Bhatt et al., 2007, Bhatt et al., 2008, Earle et al., 2006, Wasserscheid and Keim, 2000).

ILs have lower melting or freezing points than do traditional inorganic salts. Alkali metal chlorides such as KCl and NaCl have high melting points of 772 °C and 801 °C, respectively. When the cation is replaced with a suitable organic cation such as [BMIM]<sup>+</sup> or [EMIM]<sup>+</sup>, the melting points drastically decrease to 65 °C and 87 °C, respectively (Wilkes et al., 1982). Cations with low symmetry and poor intermolecular bonding are responsible for the lowering of the melting point of ILs. The melting point can be further reduced by increasing the anion size, such as by replacing the chloride ions with [BF<sub>4</sub>], [PF<sub>6</sub>] or [CF<sub>3</sub>CO<sub>2</sub>]. For instance, 1-butyl-3-methylimidazolium chloride [BMIM]Cl has a melting point of 65 °C, whereas [bmim] [PF<sub>6</sub>] has a melting point of 6.5 °C (Wilkes et al., 1982).

The fact that ILs have no measurable vapour pressure is one of their defining characteristics (Earle et al., 2006, Wasserscheid and Keim, 2000). For instance, [bmim] [PF<sub>6</sub>] has an extremely low vapour pressure of 100 Pa at 298 K compared to 3 kPa at

298 K for water. However, Earle and co-workers have shown that a number of imidazolium- and pyridinium-based ILs can be distilled under vacuum at 200-300 °C and then re-condensed at lower temperatures, for example, the distillation of [hmim][NTf<sub>2</sub>] at a pressure of 0.07 mbar and a temperature of 200 °C (Earle et al., 2006).

The density of ILs is generally on the order of 1 to 1.6 g cm<sup>-3</sup>. These values are typically higher than those of water and organic solvents (Jacquemin et al., 2006, Jacquemin et al., 2008). The density increases with the decreasing length of the alkyl chain present in the imidazolium cation (Wilkes, 2004) and with an increase in the molecular mass of the anion in the approximate order [FAP] > [NTf<sub>2</sub>] > [PF<sub>6</sub>] > [OTf] > [BF<sub>4</sub>] (Barrosse-Antle et al., 2010). Various groups have reported an approximately linear decrease of density with temperature. The density is significant in establishing the kinematic viscosity, which plays an important role in rotating disk and other hydrodynamic forms of voltammetry experiments (Dzyuba and Bartsch, 2002, Gu and Brennecke, 2002, Fredlake et al., 2004).

The viscosity of ILs is a significant consideration in electrochemical studies due to its strong effect on the rate of mass transport within a solution (Wu et al., 2011). ILs tend to be more viscous than conventional organic solvents. The strength of their van der Waals interactions and their tendency to form hydrogen bonds are the main factors that contribute to the viscosity of ILs (Bonhote et al., 1996). The impact of van der Waals forces on viscosity is apparent in some hydrophobic ILs that include fluorinated anions, such as [BMIM][CF<sub>3</sub>SO<sub>3</sub>], which has a viscosity of 90 cP at 20 °C (Bonhote et al., 1996). The structure of the cation also affects the viscosity of ILs. Larger or fluorinated alkyl side chains have stronger van der Waals forces and thus show a higher viscosity. Lower viscosities are inclined to be the result of low molar mass side chains that have high mobility. Abbott has proposed an explanation for this using a hole theory

that supposes the generation of empty spaces when an ionic component melts due to thermally generated fluctuations in the local density (Abbott, 2004).

As with any solvent used in an electrochemical process, the conductivity of an IL is of critical importance (Buzzeo et al., 2004). ILs have conductivities equivalent to organic solvents with supplemented inorganic electrolytes but not significantly larger (Endres and Zein El Abedin, 2006). While their absolute conductivity is a small improvement over conventional non-aqueous solvents, ILs propose the advantage that this property is inherent to the pure liquid and does not demand the addition of a separate salt (O'Mahony et al., 2008). This could be advantageous in the investigation of reactions in which a supporting electrolyte may interfere or can simplify the removal and purification of the product from an electrosynthetic process. Among several IL structures, conductivity appears to be most strongly linked to viscosity, most likely because of the correlation between viscosity and ion mobility (Buzzeo et al., 2004). For a single anion with a range of cations, conductivity usually increases in the order tetraalkylammonium > N,N-dialkylpyrrolidinium > 1-alkyl-3-methylimidazolium, and this has been related to an increase in the planarity of the cationic core; the flatness of the imidazolium ring appears to give a higher conductivity than the tetrahedral arrangement of alkyl groups in the ammonium salts, with the pyrrolidinium-based ILs adopting an intermediate geometry and conductivity (MacFarlane et al., 1999). Hagiwara and co-workers reported the synthesis of an IL that is significantly more conductive than all of those considered above (Hagiwara et al., 2002). This salt was produced by the reaction of 1-ethyl-3-methylimidazolium (EMIM) chloride with anhydrous hydrogen fluoride. A conductivity of  $100 \text{ m}\Omega^{-1}\text{cm}^{-1}$  at 298 K was reported, along with a very low viscosity of 4.85 mPa (Hagiwara et al., 2002, Buzzeo et al., 2004).



A solvent is only appropriate for managing a range of electrochemical processes on species dissolved within it if these species are more simply reduced or oxidised than the solvent itself. In ILs, it is usually discovered that the component anions are oxidised at adequately wide potentials and that at sufficiently low ones, the organic cations endure reduction (Hultgren et al., 2002). An itemised comparison of several potential windows (PWs) studied in the literature is not feasible for a number of reasons:

- i) The presence of electroactive impurities can limit the true PW where the purity of an IL is uncertain.
- ii) The potential for solvent breakdown may differ slightly on different electrode surfaces.
- iii) The data are studied relative to different reference and quasi-reference systems that cannot be easily interconverted (Hultgren et al., 2002, Evans et al., 2003, Buzzeo et al., 2004).

Many voltammetric examinations performed in IL solvents have used quasi-reference electrodes, often silver or platinum wires (Boxall et al., 2002, Quinn et al., 2002, Bahadori et al., 2013, Zhang et al., 2003). The PWs in an aprotic organic solvent containing supporting electrolytes can be much wider, for instance, 3.5 V for dichloromethane, 4.4 V for dimethylsulfoxide and 5.0 V for acetonitrile (Bard and Faulkner, 2001) Some aprotic ILs also contain wide PWs in the range of 4.0 to 6.0 V (Buzzeo et al., 2004) due to the strengths of the cations and anions in their structure. The PWs discovered in protic ILs have been discussed in detail and are usually smaller than those studied in aprotic ones due to the ease of the reduction of the proton (Zhao et al., 2008). The size of the window is dependent on the electrode potential and voltammetric data, as well as the particular cation and anion admixture employed and the electrode material. Moreover, the PW is calculated in a pure solvent and may differ from those established in the presence of solutes. For instance, imidazolium salts may

be restricted in the negative potential area, as the reduction of this IL cation is catalysed by radical anions present at negative potentials. Large PWs in ILs have been used in electrodeposition investigations in which definite metals and semi-conductors have been deposited at potentials that are out of the range of conventional solvents (Endres and Zein El Abedin, 2006). Hultgren and co-workers have reported the use of the organometallic reference redox as a voltammetric reference standard for ILs (Hultgren et al., 2002). When examined in [BMIM][PF<sub>6</sub>], a reversible, one-electron reduction process was achieved for Cc<sup>+</sup> with a potential independent of electrode material, scan rate and concentration. Fc was discovered to be poorly soluble in this metallocene, but it may function as a less costly alternative to other ILs.

All the discussion above is general and based on the most commonly employed ILs. Nonetheless, it should be observed that there are many ILs that include different anions and cations, and their properties cover a large range. Hence, the above statements should not be applied in a general manner to all synthesised ILs and to those designed in the future (Keskin et al., 2007).

### **2.5.2 Applications of ILs in electrochemical engineering based processes**

These compounds are liquid over a wide range of temperatures (down to -81 °C), possess high thermal and chemical stability as well as high density and electrical conductivity in comparison to other solvents (Suarez et al., 1998, Dullius et al., 1998). Due to such advantages, ILs have enjoyed plenty of applications as electrolytes in sensors (Wei and Ivaska, 2008), electrochemical capacitors (Lu et al., 2009), lithium ion batteries (Galinski et al., 2006), lead acid batteries (Rezaei et al., 2006), dye-sensitized solar cells (Jhong et al., 2009) and fuel cells (De Souza et al., 2003) amongst many others (Lloyd et al., 2011, Armand et al., 2009). Several reviews are dedicated to the electrochemistry of ILs (Armand et al., 2009, Endres, 2004, Buzzeo et al., 2004, Abbott

et al., 2007). While ILs have many inherent advantages, issues such as complex synthetic steps (Shahbaz et al., 2011), cost, lack of toxicity data and availability limit their practical use for large scale applications (Abbott et al., 2007).

### **2.5.2.1 Electrochemical applications of ILs in metal processing**

Ambient temperature ILs have been applied for the extraction of gold and silver from a mineral matrix (Whitehead et al., 2004). Some work has also been carried out on the electrowinning of aluminum from ILs (McCluskey et al., 2002). In the application of ILs and DESs to metal processing the major advantage is a significant reduction in the volume of aqueous streams required (Abbott et al., 2011).

Some ILs have been designed to contain ions which are known to have lower toxicity than normal and these include functionalized imidazoles (Gathergood et al., 2006), lactams (Du et al., 2005), amino acids (Fukumoto et al., 2005) and choline (Abbott et al., 2003). It is only the last of these that have been extensively applied to metal processing (Abbott et al., 2011). Electrodeposition of metals from ILs became an area of periodic research from the 1930s onwards (Audrieth et al., 1936). The first major breakthrough was the development of protic haloaluminate eutectics in the 1950s by Hurley and Wier (1951). A further improvement was the development of the aluminum chloride and 1-methyl-3-ethylimidazolium chloride ( $\text{AlCl}_3$  and EMIM-Cl) system in the 1980s (Lloyd et al., 2011). The biggest drawback of chloroaluminate systems was their reactivity with water, which drastically limited their applications. Since the early 1990s attention was shifted to the use of other anions, for instance bis(trifluoromethyl)sulfonylamide [ $\text{N}(\text{CF}_3\text{SO}_2)_2^-$ ], which resulted in liquids that were stable in the presence of air and water. Recently, metal nanoparticles stabilized by ILs have been synthesized with some unique properties (Shan et al., 2008). Dupont and co-workers reported that iridium nanoparticles stabilized by the imidazolium IL showed a

large increase in activity for the biphasic hydrogenation of various olefins and arenes under mild reaction conditions (Fonseca et al., 2003, Dupont et al., 2002). Itoh and co-researchers (2004) synthesized AuNPs (gold nanoparticles) modified by an imidazolium cationic based IL. The IL-modified AuNPs could change color in aqueous solutions via anion exchange of the IL moiety (Shan et al., 2008). Tatumi and Fujihara (2005) reported that gold nanoparticles stabilized by a zwitterionic imidazolium sulfonate-terminated thiol exhibited a remarkably high stability in aqueous solutions with high concentrations of electrolytes, ILs, and proteins. Metal nanoparticles, as discussed above, were all stabilized by small IL derivatives. Other workers synthesized a gold-nanoparticle-containing an IL derived polymer by conducting the UV irradiation of 1-decyl-3-vinylimidazolium chloride in the presence of an aqueous solution of  $\text{HAuCl}_4$  (chloroauric acid) (Shan et al., 2008, Batra et al., 2007).

### **2.5.2.2 Destruction of halogenated hydrocarbons**

Recently, the superoxide ion was intensively investigated by researchers using numerous solvents (Hayyan et al., 2012). For ILs, generation of the superoxide ion by electro-reduction of  $\text{O}_2$  in imidazolium chloride–aluminum chloride molten salt was reported by Carter and co-workers. These researchers found that the generated superoxide ion was unstable and could not be utilized in reactions (Carter et al., 1991). In spite of this, AlNashef and co-researchers managed to stabilize the generated superoxide within the imidazolium based ILs in separate investigations (AlNashef et al., 2001, AlNashef et al., 2002). This work was further extended to report the successful destruction of chlorobenzenes in ILs such as  $[\text{MOPMPip}^+][\text{TFSI}^-]$  {1-(3-methoxypropyl)-1-methylpiperidinium bis (trifluoromethylsulfonyl) imide} and  $[\text{HMPyrr}^+][\text{TFSI}^-]$  {1-hexyl-1-methyl-pyrrolidinium bis (trifluoromethylsulfonyl) imide} under ambient conditions (Hayyan et al., 2012).

### 2.5.2.3 Electrochemical energy storage applications

During the last few years there has been increasing interest in ILs as electrolytes for lithium or lithium-ion batteries (Armand et al., 2009, Lewandowski and Swiderska-Mocek et al., 2009). The formation of the solid electrolyte interface (SEI) on the anode surface is critical to the correct operation of the system. ILs used as electrolyte components in Li-ion batteries are quaternary ammonium salts, such as those based on the tetraalkylammonium  $[R_4N^+]$  ion or cyclic amines that may be both aromatic (pyridinium, imidazolium) and saturated (piperidinium or pyrrolidinium) in nature. A good example of some typical ILs applied for Li-ion batteries is the N-butyl-N-methylpyrrolidinium bis (trifluoromethanesulfonyl) imide (PYR<sub>14</sub>TFSI) (Appetecchi et al., 2009, Kuhnel et al., 2011). PYR<sub>14</sub>TFSI is an air-stable, hydrophobic IL with very good thermal stability (up to 300 °C) as well as promising conductivity and viscosity at 20 °C (1.85 mS cm<sup>-1</sup> and 95 mPa s, respectively) (Liang et al., 2001). In addition, liquid imidazolium salts show stability of ca. 4 V, while piperidinium and pyrrolidinium or tetraalkylammonium salts, especially based on the imide anion, show stability at the level of ca. 6 V. Such stability is sufficient towards the use of ILs as electrolytes in Li-ion batteries (Lewandowski and Swiderska-Mocek, 2009). There are no systematic studies on transport numbers of Li<sup>+</sup> containing ILs. This is a significant missing link in the literature as low values of lithium transportation numbers may lead to a concentration polarization of the battery (Chakrabarti et al., 2014).

The electric double layer capacitor (EDLC) is an energy storage device based on the operating principle of the electric double layer that is formed at the interface between an activated carbon material and an electrolyte (McEwen et al., 1997, Yuyama et al., 2006, Sato et al., 2004). This device stores electricity physically and lacks the chemical reactions found in rechargeable batteries during charging and

discharging (Yuyama et al., 2006). Various solvents and salts (solutes in other word) are available, offering specific advantages such as high capacitance and low temperature performances (Sato et al., 2004). Generally, an organic electrolyte that is a solid quaternary ammonium salt, such as N,N,N,N-tetraethylammonium-tetrafluoroborate (TEA-BF<sub>4</sub>), dissolved in propylene carbonate (PC, which has a high dielectric constant), has been used for high voltage EDLCs of 2 V or more. When compared to rechargeable batteries, the EDLC has a remarkably long cycle life and high power density (Sato et al., 2004, Largeot et al., 2011).

ILs generally have high viscosity so that their ionic conductivity is lower than that of common organic electrolytes. This may cause a deterioration of power density in EDLCs (Handa et al., 2008). The decrease in viscosity of ILs is, therefore, essential for improving the EDLC's performance. In the recent past, ILs based on imidazolium salts have been widely investigated because they have relatively low viscosity and high ionic conductivity (Yuyama et al., 2006, Zhou et al., 2004, Ue et al., 2003, Yoshida et al., 2007, Lockett et al., 2008). For example EDLCs prepared with EMI-FSI [1-ethyl-3-methyl imidazolium bis(fluorosulfonyl)imide] show good performance despite the presence of a binder in an activated carbon-based electrode (Handa et al., 2008). The self-discharge is suppressed by using the IL. A cycling durability test show that the cell with EMI-FSI keeps over 90% of the initial capacitance even after 10,000 cycles.

As low-volatility conductive media with good thermal stability, ILs are finding applications as fuel cell electrolytes and as proton conductors in proton exchange membranes, often in combination with polymer gels (Galinski et al., 2006, MacFarlane et al., 2007, Devanathan, 2008). Typically, "protic" ILs, formed through the reaction of a strong acid with a base, is used as proton conductors.

Several systematic studies on the use of ILs in fuel cells have been reported and promising results were obtained (Nakamoto and Watanabe, 2007, Fericola et al., 2008, Sekhon et al., 2006). An efficiency of 67% was achieved using ILs such as 1-butyl-3-methylimidazolium tetrafluoroborate [BMI][BF<sub>4</sub>] as electrolytes in an alkaline fuel cell (De Souza et al., 2003) for instance. Watanabe and co-workers show that some ILs are electro-active for H<sub>2</sub> oxidation and O<sub>2</sub> reduction under non-humidifying conditions (Susan et al., 2003). In addition, some reports on utilizing ILs to substitute water in Nafion™ or directly as a liquid electrolyte for laboratory fuel cells are also available in literature (De Souza et al., 2003, Doyle et al., 2000). The use of IL aqueous solutions for wetting the membrane electrode assembly (MEA) used in fuel cells yield an impressive performance enhancement (Padilha et al., 2010). Compared with the classic polymer electrolyte membrane fuel cell (PEMFC), which uses only water on the polymeric membrane, the IL-PEMFC, using [BMI][BF<sub>4</sub>] IL aqueous solutions, enhances the current density 50-fold, the power density 73-fold and increases the overall efficiency by 21% (De Souza et al., 2003, Padilha et al., 2010).

The application of ILs as membranes in fuel cells have also been reported (Ye et al., 2008). For example polybenzimidazole membranes nano impregnated with phosphoric acid have been studied as electrolytes in PEMFCs for more than a decade (Asensio et al., 2010). Novel membranes consisting of an anhydrous proton solvent H<sub>3</sub>PO<sub>4</sub>, the protic IL propyl-3-methylimidazolium di-hydrogen phosphate and polybenzimidazole (PBI) as a matrix have also been prepared and characterized for PEMFCs intended for operation at elevated temperatures (120–150 °C) (Ye et al., 2008). More recently, several copolymers and related derivatives have attracted many researchers' attention, adding variety to the field (Asensio et al., 2010). Besides phosphoric acid, many other strong inorganic acids, as well as alkaline electrolytes have been used to impregnate benzimidazole membranes. However, phosphoric acid-doped PBI membrane-based fuel

cells are not good for a pure hydrogen feed, and they provide inferior performance to that of Nafion-based fuel cells. Therefore they do not show much promise in comparison to perfluorosulfonic acid ionomer membranes, especially at temperatures less than 80 °C (Zhang and Shen, 2012).

#### **2.5.2.4 Dye sensitized solar cells (DSSCs) for renewable energy storage**

Till now, ILs based on imidazolium salts have been widely used as solvents for DSSCs (Jhong et al., 2009). Unfortunately, pure imidazolium iodide/triiodide ILs are too viscous and obstruct the diffusion of the redox couple ( $I^-/I_3^-$ ) in the electrolyte, thereby hampering device performance. The use of some binary IL electrolytes allows the reduction of electrolyte viscosity. It has been reported that ethylmethylimidazolium-based ILs with anions including tetracyanoborate ( $B(CN)_4^-$ ), tricyanomethanide (TCM), dicyanamide (DCA) and thiocyanate (SCN) appear to be promising for high performance DSSCs incorporating pure imidazolium iodide (Kuang et al., 2006, Gratzel, 2001, Wang et al., 2005, Wang et al., 2003, Wang et al., 2004). Then again, their applications as electrolytes in DSSCs are limited by their high costs and toxicological issues (Jhong et al., 2009, Gratzel, 200). The same is true for ether-functionalized imidazolium iodides due to their high viscosities and low conductivities (Tang et al., 2012). Therefore, better alternatives are considered necessary for practical applications.

#### **2.5.2.5 Applications of ionic liquids in redox flow batteries**

A room temperature molten salt consisting of 1-ethyl-3-methylimidazolium chloride (EMICl) and aluminum trichloride ( $AlCl_3$ ) was found to have low melting point and a wide electrochemical potential window for applications in RFBs (Katayama et al., 2002). A number of metal chlorides were found to dissolve in EMICl– $AlCl_3$  molten salt



due to its adjustable Lewis acid–base property. Most of the soluble redox couples have been reported and studied under basic conditions (Gau and Sun, 1996, Anderson et al., 1991, Sun and Hussey, 1989, Strubinger et al., 1990, Lipsztajn and Osteryoung, 1985) probably because the metal species of several high oxidation states were stabilized after forming chloro-complexes (Katayama et al., 2002). This fact was confirmed in a separate study whereby the Fe(III)/Fe(II) electron transfer process was irreversible in acidic ionic liquids, while this redox reaction became reversible in basic ionic liquids probably due to complex formation (Yamagata et al., 2007).

The standard formal potentials of the redox couples of various metal chloro-complexes were found to be distributed widely within the electrochemical potential window of a basic EMICl–AlCl<sub>3</sub> molten salt (Katayama et al., 2002). As a consequence, rechargeable RFBs having high cell voltages were envisaged by combining these redox couples in a basic EMICl–AlCl<sub>3</sub> molten salt. The redox reactions of some transition metals, such as iron, samarium, europium and ytterbium in BMPTFSI [BMP<sup>+</sup>, 1-n-butyl-1-methylpyrrolidinium; TFSI<sup>-</sup>, bis(trifluoromethylsulfonyl)imide] ionic liquid were investigated as the negative and positive electrode reactions of the RFB (Yamagata et al., 2006). Among these studies, it was found that the redox reactions of M(III)/M(II) (M=Fe, Sm, Eu and Yb) were quasi-reversible or irreversible when M(III) or M(II) was introduced into BMPTFSI by dissolving M(TFSI)<sub>n</sub> (n=2 or 3) and that the diffusion coefficients of M(III) or M(II) were less than  $\sim 10^{-7}$  cm<sup>2</sup> s<sup>-1</sup> (Yamagata et al., 2007). These results suggested that the interaction between these metallic species and TFSI<sup>-</sup> anions led to the formation of complexes such as M<sub>x</sub>(TFSI)<sub>y</sub><sup>-</sup>, which caused slow electrode kinetics and low diffusivity. This complex formation was important for understanding the redox reactions of metallic species in BMPTFSI. With regard to bromo- and chloro-aluminate ionic liquids, it was reported that the electrochemical

behavior of iron species was affected by the Lewis acidity of the ionic liquids (Laher and Hussey, 1982, Nanjundiah et al., 1982).

In another study, the redox reactions of some lanthanides were examined as the candidates for the half cell reactions of the RFB using 1-ethyl-3-methylimidazolium and 1-n-butyl-1-methylpyrrolidinium bis(trifluoromethanesulfone) imide (EMITFSI and BMPTFSI) molten salt systems. Unfortunately, cyclic voltammetry indicated that the redox reaction of the Eu(III)/Eu(II) couple was irreversible electrochemically. The slow electrode kinetics may have been due to the formation of some complexes of Eu(III) probably with TFSI<sup>-</sup>, which was suggested by UV-vis spectroscopy (Skyllas-Kazacos et al., 2011).

Very recently, Sandia National Laboratories have developed new types of metallic based ionic liquids for applications in RFBs (Pratt et al., 2013). The compounds consist of manganese, iron, cobalt, nickel, copper, zinc, or cerium coordination cations and weakly coordinating anions such as 2-ethylhexanoate, triflate, triflimide, or tetrafluoroborate that may simultaneously act as a solvent and electrolyte (Anderson et al., 2010, Pratt et al., 2011, Hoogerstraete et al., 2012). Most compounds are quite inexpensive to produce and some show promising viscosity, conductivity or electrochemical reversibility (Pratt et al., 2013). Theoretical calculations show that metal ion concentrations up to 6.5 M are possible in the ILs thereby opening up windows for future high energy density RFBs. From preliminary investigations that considered the application of methylimidazolium iron chloride molten salt system in RFB applications (Katayama et al., 2002), it was predicted that if a sodium chloride-sodium electrode was combined with this EMICI-FeCl<sub>2</sub>-FeCl<sub>3</sub> molten salt, a high energy density per unit volume may be expected (Skyllas-Kazacos et al., 2011). Since Na(I)/Na couple in EMICI-AlCl<sub>3</sub> system had the formal potential of -2.15 V at room temperature (Scordilis-Kelley et al., 1992), the electromotive force of approximately 2 V

was expected for the Na/EMICl–FeCl<sub>2</sub>–FeCl<sub>3</sub> battery. Even though this battery appeared to have the advantage of a low operating temperature and a long cycle life compared with Na–S and Zebra cells (Wen et al., 2006), further work with this system appeared to be lacking in the literature. Instead recent work reported upon the application of 1-ethyl-3-methyl imidazolium hexafluorophosphate ILs as supporting electrolytes for organic RFBs (Zhang et al., 2012). The efficiencies obtained were not as good as those reported using standard supporting electrolytes such as tetrabutylammonium hexafluorophosphate. Further work on this topic has not been reported to date. One reason for the lack of activity in the area of ionic liquids for RFBs is the fact that these materials are known to be sensitive to air and moisture, which makes their handling difficult in large-scale commercial applications (Skylas-Kazacos et al., 2011, Leung et al., 2012). These materials also tend to be quite expensive and are unlikely to be economically viable for RFB applications compared to the lower cost aqueous-based systems. In contrast, given the large electrochemical window of many ionic liquids, the possibility of using redox couples that fall outside the decomposition potential of water may open the way to the development of high voltage flow cells that offer much higher power and energy densities than current aqueous-based systems (Skylas-Kazacos et al., 2011, Leung et al., 2012). Further investigation of such couples could therefore prove fruitful as long as practical systems can be shown to offer better performance, cell voltage and cycle life than the all-vanadium RFB to offset the high costs of these electrolytes (Chakrabarti et al., 2014).

## **2.6 Definition of DESs**

While ILs have many inherent advantages, issues such as complex synthetic steps (Shahbaz et al., 2011), cost, lack of toxicity data and availability limit their practical use for large scale applications (Abbott et al., 2007). An alternative approach

to simplifying the synthesis of ILs is to start with a straightforward quaternary ammonium halide and decrease the freezing point by complexing the anion to effectively delocalize the charge (Abbott et al., 2006). These mixtures form eutectics where the depression of freezing point can occur up to 200 °C. The use of simple amides, acids and alcohols as complexing agents makes the liquids very versatile and to distinguish them from other ILs the term deep eutectic solvents (DESs) is used (Abbott et al., 2006 Abbott et al., 2007). These liquids have high conductivities, viscosities, and surface tensions. The fact that some of the hydrogen bond donors are commonly available as bulk commodity chemicals such as urea and oxalic acid gives them the potential for large-scale applications (Abbott et al., 2006).

**Table 2.2:** Prices of some commercially available ILs prepared at the Queen's University Belfast and sold by Acros Organics (Chakrabarti et al., 2014).

No.	Name of ionic liquid	Pack size (g)	Price (US\$)
1	1-Butyl-2,3-dimethylimidazolium tetrafluoroborate	5	177.50
2	1-Butyl-2,3-dimethylimidazolium trifluoromethansulfonate	10	157.63
3	1-Butyl-3-methylimidazolium (L)-lactate	5	155.15
4	1-Butyl-3-methylimidazolium tetrafluoroborate	5	155.15
5	1-Butyl-3-methylimidazolium trifluoromethansulfonate	10	151.42
6	1-Butylpyridinium tetrafluoroborate	5	155.15
7	1-Butylpyridinium trifluoromethansulfonate	10	147.71
8	1-Decyl-3-methylimidazolium chloride	10	121.40
9	1-Dodecyl-3-methylimidazolium chloride	10	113.57
10	1-Ethyl-3-methylimidazolium (L)-lactate	5	145.22
11	1-Hexadecyl-3-methylimidazolium chloride	10	127.84
12	1-Hexyl-2,3-dimethylimidazolium tetrafluoroborate	5	182.46
13	1-Hexyl-2,3-dimethylimidazolium trifluoromethansulfonate	10	157.63
14	1-Hexyl-3-methylimidazolium hexafluorophosphate	25	118.84
15	1-Hexyl-3-methylimidazolium tetrafluoroborate	5	187.11
16	1-Hexyl-3-methylimidazolium trifluoromethansulfonate	10	141.50

In addition, the primary advantages of DESs are the extremely low cost of the precursors and their general biodegradability (Lloyd et al., 2011). Table 2.2 shows the commercial price of ILs synthesized at Queen's University Belfast while Table 2.3 gives commercial rates for DESs prepared in the University of

Leicester (Chakrabarti et al., 2014). Clearly DESs can be manufactured at much lower costs than ILs.

**Table 2.3:** Commercial prices of DESs manufactured in Leicester and sold throughout the UK (Chakrabarti et al., 2014).

Product description	Price (US\$/kg)
Glyceline	313.29
Ethaline	313.29
Maline	391.61
Oxaline	313.29
Reline	313.29

DESs are eutectic-based IL and include bulky cations and smaller anions that are bound to a hydrogen bond donor (HBD) or a metal halide (Zhang et al., 2012). Abbott and co-workers introduced DESs using quaternary ammonium salts  $R_1R_2R_3R_4N^+X^-$  complexed with metal halide (type 1), hydrated metal halide (type 2) or HBD such as acids, amides and alcohols (type 3). The same group also explained a fourth type of DES which is of metal chlorides (e.g.  $ZnCl_2$ ) complexed with several HBDs such as ethylene glycol, urea, acetamide or hexanediol (type 4) (Abbott et al., 2004, Abbott et al., 2007, Abbott et al., 2008) The phase diagram of the two component system containing choline chloride (ChCl) and urea (U) system is shown in Figure 2.5. The melting point of choline chloride is 302 °C and urea is 133 °C. But when they are mixed together in a 2:1 molar ratio (urea: choline chloride), they form an eutectic mixture at 12 °C (Morrison et al., 2009, Abbott et al., 2003).

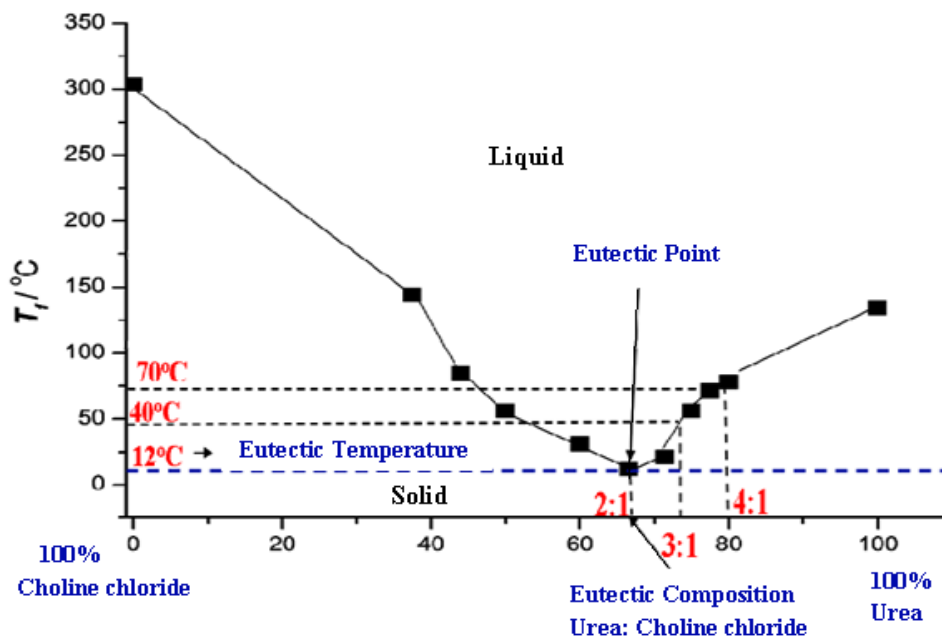


**Figure 2.5:** Phase diagram for urea-choline chloride (ChCl/U) system (Morrison et al., 2009).

The charge delocalization happening through hydrogen bonding between the halide anion and the hydrogendonor moiety is responsible for the decrease in the freezing point of the mixture concerning the melting points of the individual components as shown in Figure 2.6 (Morrison et al., 2009, Abbott et al., 2003). The melting point of a mixture of chemical compounds depends on degrees of interaction between the components. When the interaction between components is weak, the melting point of the mixture including the components steadily increases or decreases based on the composition (Abbott et al., 2004, Zhang et al., 2012). Although, when a mixture contains highly interactive components, the melting point of it presents a large decrement at a specific composition which is known as the eutectic point, and herein the word eutectic was originated from the Greek term for ‘easily melted’ (Endres et al., 2008). Due to ChCl low cost, biodegradability and low toxicity, ChCl most of the research laboratories around the world used as an organic salt to produce eutectic mixtures ordinarily with cheap and safe HBDs such as glycerol, urea, carbohydrate-derived polyols or renewably sourced carboxylic acids (Zhang et al., 2012, Zhao et al., 2011).

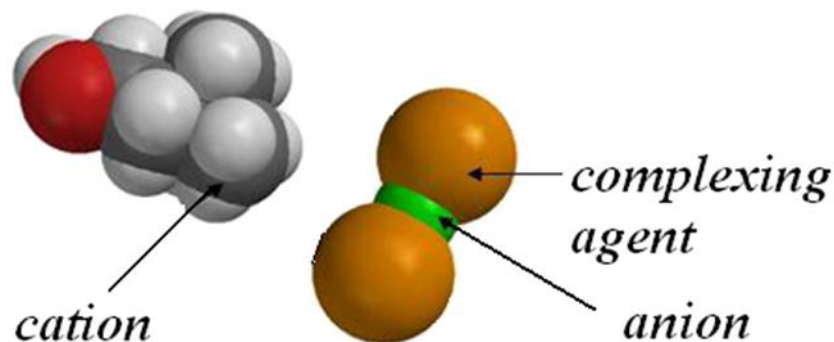


**Figure 2.6:** DES includes bulky cations and smaller anions attached to HBD (Abbott et al., 2004)

Moreover, the other research group (Chakrabarti et al., 2013, Kareem et al., 2010, Bahadori et al., 2013a, Bahadori et al., 2013b, Hayyan et al., 2012, Shahbaz et al., 2011) has employed quaternary phosphonium salts-based DESs. The salts under examination are methyltriphenylphosphonium bromide, benzyltriphenylphosphonium chloride, tetrabutylphosphonium bromide and ethyltriphenylphosphonium iodide. The phosphonium salts for apply in DESs' preparation have their own pros. Fraser and McFarlane (2009) reported that phosphonium salts are promising due to the numerous reasons. They are readily available and usually less costly than ammonium salts (Bradaric et al., 2003). The global production of these salts is in millions of tons. They are thermally more stable than ammonium salts that they can be applied in applications at the temperature above 100 °C (Tsunashima and Sugiya, 2007). Finally, densities of alkylphosphonium salts are less than water (Adamova et al., 2012).

DESs are fascinating since they present similar physicochemical properties to conventional imidazolium-based ILs and therefore can beneficially substitute them in different applications. DESs are not observed as volatile organic solvents and not flammable as compared to conventional organic solvents which making their storage easy. From the approach point of green chemistry, DESs are even more charming since some of them have been examined to be biodegradable and compatible with enzymes

further increasing their interest. Moreover, preparation of DESs is 100% economical, simple to handle and no extra purification is demanded, therefore making their large-scale use achievable (Zhang et al., 2012, Carriazo et al., 2012, Zhao and Baker, 2013, Tang and Row, 2013).

### **2.6.1 Physical properties of DESs**

DESs are chemically designable solvents since they can be formed by combining different quaternary ammonium and phosphonium salts with HBD in various molar ratios to tune their physicochemical properties. It was examined that the change in one of these components or the molar ratios with which the DES is synthesized leads to an alteration in the physical properties of the resulting DES (Bahadori et al., 2013, Kareem et al., 2010). Therefore, different DESs with various physicochemical properties, such as freezing point, viscosity, conductivity and pH can be obtained. Numerous efforts have been dedicated to the physicochemical characterization of DESs due to their favorable applications.

#### **2.6.1.1 Melting Point (Freezing Point)**

The difference of the lattice energies of the salt and the HBD rely on the anion-HBD interaction and the entropy changes emerge from the formation of the solvent. Factors that contribute to the reduction of the melting point are cation with small size and low symmetry. The anions with high hydrogen bond strength and small size have also impact the melting point and produce higher freezing temperature depression (Zhang et al., 2012). For example, in combination with urea, the melting point of a choline salt derived DES increase in the order  $\text{BF}_4^- < \text{Cl}^- < \text{NO}_3^- < \text{F}^-$ , recommending a correlation with the hydrogen bond strength (Zhang et al., 2012). Abbott and co-workers displayed that DESs of ChCl:U had some unique solvent's properties. It was revealed that the self-association occurring between the salt and the HBD depends on



the employed components, and moreover their molar ratios impact in controlling the melting point of the DES (Abbott et al., 2003). Shahbaz and co-workers (2010) reported that for DESs prepared from  $\text{ChCl}$  with either 2,2,2 trifluoroacetamide or ethylene glycol, the difference of the salt:HBD molar ratio has the same impact on the melting point of the DESs.

Kareem et al. (2010) presented same results for phosphonium-based DESs as well as Hayyan et al. (2013) validated the controlling role of salt:HBD molar ratio in glucose based DESs.

### **2.6.1.2 Density**

Densities of DESs are generally investigated by means of a specific gravity meter. The majority of DESs show higher densities than water (Kareem et al., 2010, Shabaz et al., 2012a). For example,  $\text{ZnCl}_2$ -HBD eutectic mixtures have densities higher than  $1.3 \text{ g cm}^{-3}$ . Density of  $\text{ZnCl}_2$ -urea (1:3.5) and  $\text{ZnCl}_2$ -acetamide (1:4) are different ( $1.63$  and  $1.36 \text{ g cm}^{-3}$ , respectively) (Zhang et al., 2012). This remarkable variation of density might be ascribed to a different molecular arrangement or packing of the DESs. Both of DESs have higher density than those of neat HDBs. This fact could be demonstrated by the hole theory. DESs are comprised of holes or empty vacancies same as imidazolium based ILs. For example, the average hole radius was decreased when  $\text{ZnCl}_2$  was combined with urea, therefore density of the DES increased as compared to that of pure urea (Abbott et al., 2007b). The variation in organic salt/HBD molar ratio also has an apparent impact on the densities of DES. This phenomenon was demonstrated by the work of Shahbaz et al. (2011c). Recently, researchers (Bahadori et al., 2013, Kareem et al., 2010, Abbott et al., 2011, Shahbaz et al., 2011c, Hayyan et al., 2013) have reported the investigation of densities of DESs over different range of temperatures.

### 2.6.1.3 Viscosity

Viscosity is a significant issue that needs to be addressed, particularly when fluids and liquids specifically are used as lubricants. It is defined as the resistivity of a fluid to flow in streams.

Most DESs systems have relatively high viscosities at ambient temperature, except for ChCl-ethylene glycol (EG) eutectic mixture (Zhang et al., 2012). The high viscosity of DESs is ascribed to the attendance of a comprehensive hydrogen bond network between each component, which causes a lower mobility of free species within the DES. Van der Waals interactions or electrostatic forces and also the big ion size and tiny void volume of DESs may contribute to the high viscosity of DES (Ghatee et al., 2010, Sanchez et al., 2009).

In general, viscosities of eutectic mixtures are strongly influenced by the atomic structure of its components, organic salt/HBD molar ratio, the water content, and the operating temperature (Zhang et al., 2012). Hole theory has been applied to account for viscosity in DES (Abbott et al., 2007c). This theory presumes that DES contains unoccupied space that is created from thermal fluctuations in local density. The holes are of random size and location, and in constant flux. As the viscosity is related to the free volume in the fluid and the probability to find holes of appropriate dimensions for the ions to move into, it is possible to decrease the viscosity by increasing the free volume of the solvent (Abbott et al., 2007c).

Viscosities of most DESs alter remarkably as a function of the temperature. The profiles of viscosity versus temperature also follow an Arrhenius-like behaviour. As the temperature enhances, the viscosity reduces (Zhang et al., 2012, Bahadori et al., 2013).

#### 2.6.1.4 Ionic conductivity

Ionic conductivity is one of the most important physical properties which represent how well a material can conduct electrical current. It is a functional measurement, as in the case of applying liquids as electrolytes in electrochemical processes, such as in batteries or in electroplating process (Galinski et al., 2006, Ju et al., 2012, Ishikawa et al., 2006). In engineering applications, it is critical to estimate the ionic conductivity of an electrolyte in order to design, control and optimize the electrolytic processes and the manufacture of electrochemical power sources (Galinski et al., 2006). For corrosion protection, ionic conductivity supplies applicable data for estimation the corrosivity of aqueous media and for cathodic protection system (Holbery et al., 2003).

In DES, the ionic conductivity is controlled by the mobility of the charge carriers rather than by their number. The mobility is restricted by the accessibility of holes of appropriate measures for the charge transport. Since the fraction of suitable sized holes at ambient temperature (21° C) is very low, the holes can be presumed to be at infinite dilution (Abbott et al., 2004).

Most of DESs present poor ionic conductivity due to their relatively high viscosity around or lower than 2 mS cm<sup>-1</sup> at ambient temperature (Zhang et al., 2012). Like viscosity, molecular structure and changes of the organic salt/HBD molar ratio dramatically impacts the ionic conductivity of DESs. Abbott and co-workers (2007c) reported the conductivity of DES increases with increasing the ChCl content.

Ionic conductivity and its behavior as a function of temperature for different ammonium and phosphonium based DES is demonstrated in Chapter 4 of this thesis. Conductivity of DESs generally increases significantly as the temperature increases due to a decline in the viscosity.

Therefore, Arrhenius-like equation can also be accustomed to predict the conductivity behavior of a DES.

### **2.6.2 Feasibility of using DES for RFB applications**

The feasibility of applying DESs in RFBs can be ascertained from both economic and environmental impact analyses. It is obviously sensible to estimate the performance of recently reported DESs in RFBs (Lloyd et al., 2013a, Lloyd et al., 2013b) with that of the commercially developed VRB (Watt-Smith et al., 2013). Assuming a typical 2 kW/30 kWh VRB installation reported by Walsh and co-workers (Kear et al., 2012), an economic analysis reveals an amortized capital cost of \$850 and a cost of stored electricity of  $\$0.10 \text{ kW}^{-1} \text{ h}^{-1}$ . When the cost of electricity from wind power is added to the energy storage cost a total combined generation/storage cost of  $\$0.15\text{--}0.18 \text{ kW}^{-1} \text{ h}^{-1}$  is obtained. From Table 2.3, it is clear that the commercial cost of the most commonly investigated DES, i.e. ethaline is about an order of magnitude higher than that of the commonly available VRB electrolyte. However the future of VRBs may not be very bright considering the high extraction costs of vanadium (Wadia et al., 2011). For this reason, it is logical to develop simple, cost effective systems using materials exhibiting fewer supply constraint such as DESs (Lloyd et al., 2013a). In addition, a recent report has revealed that DESs are environmentally benign as they are produced naturally by plants and used for their metabolism processes (Choi et al., 2011). Compare this with the environmental impacts of acidic based electrolytes that are normally applied in VRBs. Therefore DESs show strong potential as future electrolytes for RFB applications (Chakrabarti et al., 2014).

So far, there have been two direct reports related to the study of redox species in DESs for applications in RFBs (Lloyd et al., 2013a, Lloyd et al., 2013b). In addition, several DESs have been electrochemically characterized using redox couples such as

ferrocene/ferrocenium (Nkuku and Lesuer, 2007, Bahadori et al., 2013), copper (II)/copper (I) (Lloyd et al., 2011) and other metallic ions in ethaline (Abbott et al., 2011b). The rate kinetics of the copper (II)/(I) redox couple was shown to be appreciably higher in ethaline (Lloyd et al., 2011b) in comparison to ILs reported in the literature (Abbott et al., 2009, Nanjundiah and Osteryoung, 1983). Similarly, the heterogeneous rate constant of ferrocene in DES (Nkuku and Lesuer, 2007) was of the same order of magnitude as that in ionic liquids (Chakrabarti et al., 2013, Bahadori et al., 2013, Lewandowski et al., 2013, Fontaine et al., 2009).

The electrochemistry of DES is not severely affected if experiments are conducted in the open atmosphere (Nkuku and Lesuer, 2007). This gives it an edge over acetonitrile or ionic liquids as solvents, because in most cases, non-aqueous electrolytes have been reported to undergo experiments under inert atmospheres (i.e., either purging the solutions with nitrogen or argon to remove dissolved oxygen and moisture or else experiments remain confined within expensive glove boxes) (Sleightholme et al., 2011, Nanjundiah and Osteryoung, 1983). In addition, solubility of metal oxides based on vanadium, chromium, iron and zinc are reasonably high in DESs based upon urea or malonic acid, which shows some promise towards applications in RFBs (Abbott et al., 2011a). Abbott and co-workers also reported that the solubility of such metallic species can be improved in the presence of iodine as an electrocatalyst (Abbott et al., 2011b). This would be extremely beneficial in improving the energy densities of RFBs running on DES-based electrolytes, thereby encouraging their implementation in future electric vehicles.

In a nutshell, application of DES appears quite promising for RFBs due to the possibility of manufacturing the materials in bulk at reasonably low costs as well as due to the high heterogeneous rate constants of several metallic species in such

solvents (Bahadori et al., 2013). DESs can also be produced from different salts and hydrogen bond donors thereby adding versatility to the process.

## 2.7 Electrochemistry

### 2.7.1 Internal reference redox system

Establishing solvent independent reference electrodes for the comparison of redox potentials in aqueous and non-aqueous systems has a long history (Gagne et al., 1980). In 1947, Pleskov introduced the concept of  $\text{Rb}|\text{Rb}^+$  or  $\text{Rb}(\text{Hg})|\text{Rb}^+$  as a pilot ion, followed by the proposal to use organometallic redox couples (Inzelt et al., 2013). In order to limit the number of possible reference redox systems based on organometallic redox couples IUPAC recommended that the systems ferrocene/ferrocenium ion ( $\text{Fc}/\text{Fc}^+$ ) and bis(biphenyl)chromium<sup>(0)/(I)</sup> ( $\text{BCr}/\text{BCr}^+$ ) should be used as reference redox systems in non-aqueous media (Gritzner and Kuta, 1984).

During the last decade a considerable number of papers dealing with ILs were published, including their possible application as solvent-free electrolytes (Brooks and Doherty, 2004, Galinski et al., 2006, Fernicola et al., 2006, Waligora et al., 2009, Wu et al., 2011).

Organometallic redox couples, where both the oxidized and the reduced form are soluble, have been proposed in non-aqueous solvents and solvent mixtures (Waligora et al., 2009, Wu et al., 2011). So far, the electrochemical behavior of the redox couples  $\text{Cc}/\text{Cc}^+$  and ethylferrocene/ethylferrocenium ion on gold, glassy carbon and platinum disc electrodes in 1-*n*-butyl-3-methylimidazolium hexafluorophosphate and the electrochemical behavior of several substituted ferrocenes, which adhered to the working electrode surface, have been studied (Rogers et al., 2008, Hultgren et al., 2002). The cobaltocene/cobaltocenium couple was studied and suggested as possible reference redox couples in 1-*n*-butyl-3-methylimidazolium hexafluorophosphate in 1-

ethyl-3-methylimidazolium bis(trifluoromethanesulphonyl)imide as well as in 1-butyl-1-methylpyrrolidinium bis(trifluoromethanesulphonyl) imide (Lewandowski et al., 2013). Current literature indicates that the Fc/Fc<sup>+</sup> ion redox couple as possible reference system for ILs suffers from poor solubility in several ILs (Buzzeo et al., 2004), prompting the research group to emphasize Cc<sup>+</sup>/Cc ion as a possible internal potential standard for electrode potential measurements in ILs (Lewandowski et al., 2013). It must be kept in mind that a redox couple must fulfill the requirements of a Fc redox system in many ILs before it may be accepted as a reference redox system. Hopefully, a redox couple, which has been proposed as reference redox system in organic solvents could also be employed in ILs (Nagy et al., 2006, Fu et al., 2011, Eisele et al., 2006, Tsierkezos, 2007).

Additional research is thus needed including organometallic redox couples, for which data in non-aqueous solvents and solvent mixtures are available. In this work we sought to investigate the electrochemistry of Nernstian redox couples, Fc and Cc<sup>+</sup> in different DESs to set a benchmark for typical electrochemical behavior in these solvents.

### **2.7.2 Reference electrodes**

The employment of quasi-reference electrodes, QRE, is a frequent practice in electrochemical probe in non-aqueous solvents. The case with IL examinations, well-defined reference electrodes are difficult to supply and stabilize (Torriero et al., 2012). In most ILs volatility is not an issue contrasted to the condition prevailing in some organic solvents in which evaporation can alter the composition of the reference electrode half-cell (Fu et al., 2011, Torriero et al., 2012). However, the small volume of IL usually used, in general several hundred of microliters, in order to perform simple and cost-efficient research, justifies the use of this kind of reference system (McHale et

al., 2008). Most of studies that use QRE in ILs are established upon platinum (Suarez et al., 1997, Caban et al., 2004), silver (AlNashef et al., 2002, Chakrabarti et al., 2013, Bahadori et al., 2013), or lithium metal (Lewandowski and Swiderska-Mocek, 2010) immersed directly into the IL system. Magnesium is less usually employed (Nuli et al., 2005). The role of platinum or silver wire as a QRE is established upon the presence of several compounds on the metal surface, where the precise identity of the redox couples are not known with any certainty (Snook et al., 2006). Moreover, the quantity of the oxidized component, which is quite little when contrasted to commercial aqueous reference electrodes, is also mysterious (Snook et al., 2006). Hence, the potential of the QRE is probably to alter extremely in the event of:

- (a) Reaction with the IL components or impurities present in the media;
- (b) Dissolution of the oxidized compounds in the IL;
- (C) Polarization, because of shortage of potentiostatic control (Torriero et al., 2012).

These changes can take place dynamically throughout the time period when the wire is immersed in the IL as a result of the electrochemical experiment. Therefore, the presumption that the potential of the electrochemical processes of interest inscribed versus a QRE can be adjusted, at some stage, versus a appropriate reference electrode or a standard redox compound, cannot always be relied upon to supply an exact potential value over the whole range of potentials measured (Torriero et al., 2012).



## CHAPTER 3: RESEARCH METHODOLOGY

In this Chapter, the procedures used to achieve the objectives of this work are reported. Five main sections will be presented in this chapter. Section 3.1 describes the syntheses of studied DESs; section 3.2 describes the characterization procedure of the physical properties of some of the synthesized DESs; Section 3.3 explains electrochemical experiments; Section 3.4 presents the experimental procedure for measuring the stability of vanadium acetylacetonate in some of the DESs. Finally, section 3.5 describes charge/discharge experiments.

### 3.1 Synthesis of DESs

#### 3.1.1 Materials

Choline chloride (ChCl) ( $C_5H_{14}ClNO$ ), methyltriphenylphosphonium bromide ( $C_{19}H_{18}PBr$ ), N,N-diethylenethanol ammonium chloride ( $C_6H_{16}ClNO$ ), glycerin ( $C_3H_8O_3$ ), ethylene glycol ( $C_2H_6O_2$ ), triethylene glycol ( $C_6H_{14}O_4$ ), malonic acid ( $CH_2(COOH)_2$ ), oxalic acid ( $HOOC-COOH$ ), triethanolamine ( $N(CH_2CH_2OH)_3$ ), zinc nitrate hexahydrate ( $Zn(NO_3)_2 \cdot 6H_2O$ ) and 2,2,2-trifluoroacetamide ( $F_3C-CO-NH_2$ ), were purchased from Merck Chemicals (Germany) with high purity ( $\geq 98\%$ ). All chemicals were used as supplied by the manufacturer and utilized for the synthesis of DESs without further purification and were stored in an inert glove box purged with argon. The synthesized DESs were stored in tight-capped bottles to prevent them from being affected by atmospheric humidity. Moreover, the water mass fraction in these chemicals, as per the manufacturer's guide, was  $< 10^{-4}\%$ .

#### 3.1.2 Synthesis procedure

The original procedure of synthesizing DESs as reported by Abbott et al. (2004) was used in this work. A jacketed cup with magnetic stirrer was used to mix both the

salt and HBD at 383.15 K (as a maximum) and atmospheric pressure for a minimum period of 3 hours until a homogenous liquid was formed. The synthesis experiments were conducted in a glove box with firm humidity control of less than 4 ppm water. Figure 3.1 shows the chemical structures of the salts and hydrogen bond donors that make up the DESs chosen for this study and Table 3.1 presents the compositions and abbreviation of the different DESs synthesized in this study.

**Table 3.1:** List of DESs obtained by complexation between hydrogen acceptor and hydrogen-bond donor molecules

Hydrogen acceptor(Salts)	Hydrogen-bond donor	Molar ratio (salt:HBD)	Abbreviation
Choline chloride	Triethylene glycol	1:3	DES1
Choline chloride	Glycerol	1:2	DES2
Choline chloride	Ethylene glycol	1:2	DES3
Choline chloride	Malonic acid	1:1	DES4
Choline chloride	Oxalic acid	1:1	DES5
Choline chloride	Triethanolamine	1:2	DES6
Choline chloride	Zinc nitrate hexahydrate	1:1	DES7
Choline chloride	2,2,2-Trifluoroacetamide	1:2	DES8
N,N-Dimethylmethyleiminium chloride	Triethylene glycol	1:3	DES9
N,N-Dimethylmethyleiminium chloride	Glycerol	1:2	DES10
N,N-Dimethylmethyleiminium chloride	Ethylene glycol	1:2	DES11
N,N-Dimethylmethyleiminium chloride	Malonic acid	1:1	DES12
N,N-Dimethylmethyleiminium chloride	Zinc nitrate hexahydrate	1:1	DES13
Methyltriphenylphosphonium bromide	Triethylene glycol	1:4	DES14
Methyltriphenylphosphonium bromide	Glycerol	1:3	DES15
Methyltriphenylphosphonium bromide	Ethylene glycol	1:2	DES16

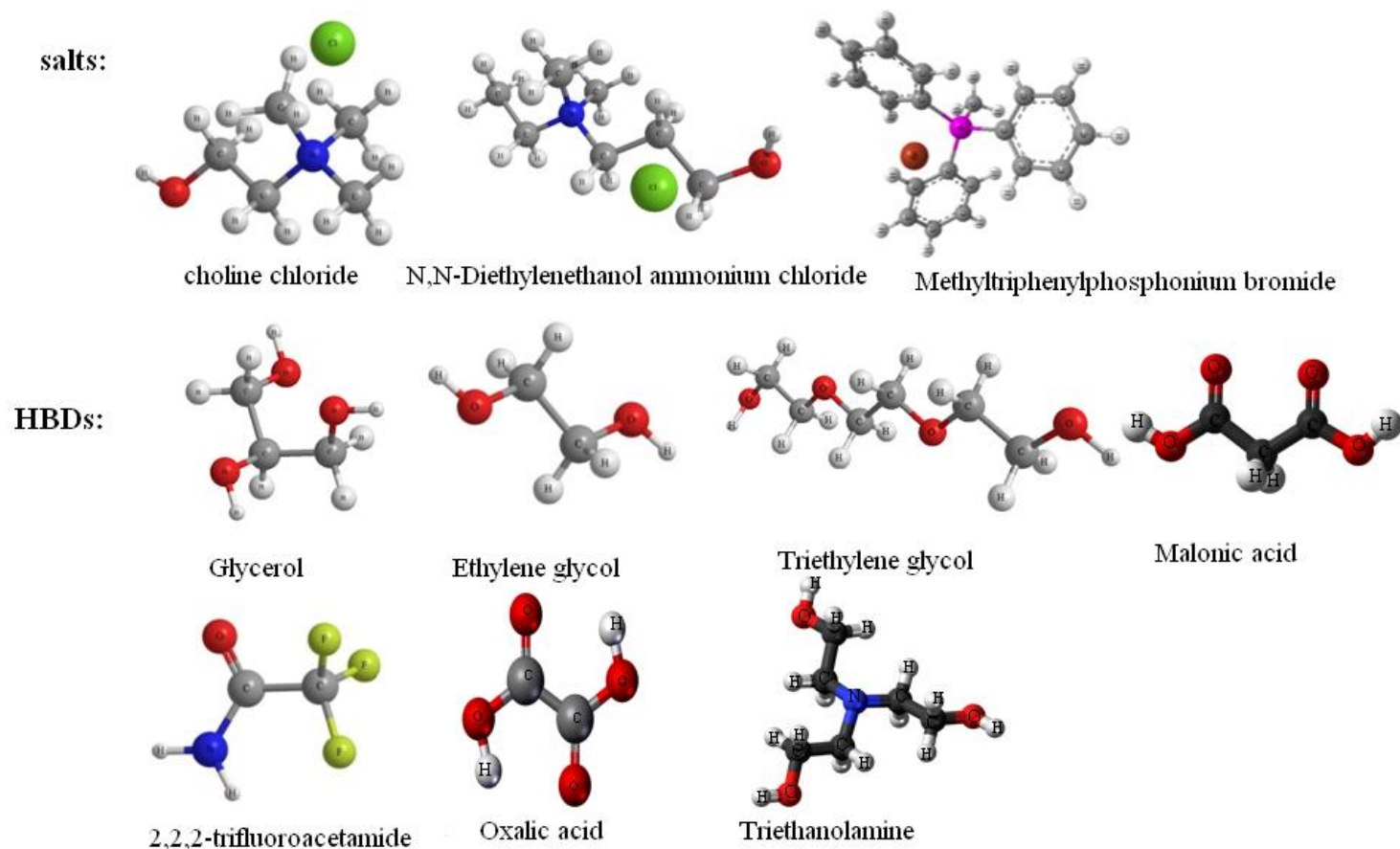


**Figure 3.1:** Chemical structures of the salts and hydrogen bond donors applied in this study.

### 3.2 DESs characterization

DESs can be considered as tailor-made solvents since they can be formed by correctly mixing different quaternary ammonium or phosphonium salts with different hydrogen bond donors. Therefore, task-specific DESs with various physicochemical properties such as viscosity, conductivity, melting temperature, density, and pH can be prepared. To characterize a DES intends to comprehend its physical behaviour as a function of temperature. A list for the characterization equipment and the measurements obtained along with the uncertainties in measurement are presented in Table 3.2.

**Table 3.2:** Equipment used in this work for characterization of DESs with uncertainties in measurements.

Property	Equipment	Estimated Uncertainty
Viscosity	Brookfield DV-II + Pro EXTRA instrument	(1 to 3) % of measured value
Freezing temperature	Mettler Toledo Differential Scanning Calorimetry (DSC)	$\pm 0.22$ °C
Conductivity	Cheetah DZS-708 Multi-parameter analyzer	$\pm 5$ $\mu\text{S}\cdot\text{cm}^{-1}$
pH	Metrohm pH meter	$\pm 0.05$
Density	Anton Paar DMA 4100 Density Meter (U-Tube)	$\pm 0.00008$ $\text{g}\cdot\text{cm}^{-3}$

In the following sub-sections, the detailed procedures for measuring each physical property are described.

### **3.2.1 Viscosity**

The viscosities of the DESs were obtained by averaging each measurement at least three to five times, using a Brookfield DV-II +Pro EXTRA instrument. The temperature control was achieved by using an external water bath that was connected to the instrument. Viscometer is supplied with a set of 4 spindles and a narrow guard leg. The equipment was calibrated with standard values of pure water and glycerol.

### **3.2.2 Electrical conductivity**

The measurement of the electrical conductivity of DESs is performed using Cheetah multi parameters meter model DZS - 780. This device has a wide temperature range for measurements, i.e. from -5 °C up to 135 °C. The meter was calibrated by standard buffer solutions provided by the manufacturer. The measurements of the electrical conductivities at different temperatures were carried out by placing the DES on a hot plate, equipped with a temperature controller. To ascertain that the temperature displayed by the hot plate was accurate, external thermometers were used to measure the temperature inside the DES.

### **3.2.3 Melting temperature**

The Differential Scanning Calorimetry (DSC) is a device that measures the heat flow emitted from a sample upon heating over a range of temperatures. The basis of this method is that when a sample passes through its melting temperature upon heating, it emits a certain amount of heat which is detectable by micro-scale sensors. A sample of less than 10 mg is placed inside a particular pan made principally from aluminium and a hole is made in the cover of that pan. The temperature of the sample is gently increased.

The hole permits the heat emitted to transfer outside the pan whereby specific sensors will estimate this heat and record it. If the sample is liquid at room temperature, then it must be cooled down till it freezes. The measurement starts from a point at which the sample is in the solid state. If the sample is solid at room temperature, then the heating program may start from the ambient temperature to a temperature at which the sample is in the liquid state. The heating of the sample from below its melting temperature to above this temperature is carried out through a computerized program. On the initiation of the program the sample starts to emit a certain amount of heat till it reaches the glass transition point whereby only a few molecules of the sample change from the solid state to liquid state. At the glass transition point, the amount of heat emitted will be reduced sharply to assist in converting the state of the sample. The specialized sensors detect this sudden depression and it is drawn as a drop in the curve of the heat flow. When the entire sample has melted down, the heat emission will be uniform again. This sudden drop in the heat flow curve will be identified on the x-axis which represents the temperature, and this temperature will be the melting temperature of the sample. In this work, a Mettler Toledo Differential Scanning Calorimetry (DSC) was used. The DSC was calibrated versus known standards (water and 2-propanol) to ensure the measurement's accuracy.

#### **3.2.4 Density**

Densities of the synthesized DESs in this work were measured using a DMA 4500 vibrating tube density/specific gravity meter (Anton Paar, Austria). Anton Paar U-tube density meter is an apparatus using sophisticated systems to weigh the mass of the injected liquid sample in the U-tube. The apparatus can only be utilized for samples which are liquid at room temperature as the procedure includes injection of the sample in the apparatus utilizing a syringe until the U-tube is full of the sample. Then a

temperature at or above the room temperature can be set using a pre-programmed method and the measurement of the density at that temperature is given by the apparatus. The values of the density and the specific gravity at that special temperature are then exhibited on the screen of the apparatus. Density measurements were carried out at temperatures from 298 to 363K at 5 K intervals with three replicates for each reading.

### **3.2.5 pH**

The pH was determined by means of a Metrohm pH meter, which was calibrated using standard pH buffer solutions. The temperature control of all properties, from 298 to 368 K, was ensured by a Wisecircu thermostatic water bath.

## **3.3 Electrochemical experiments**

### **3.3.1 Electrochemical cell**

The electrochemical cell consisted of a typical three-electrode set-up. The counter electrode was a Pt wire, and an Ag wire (immersed in 65% HNO<sub>3</sub> prior to experiments, then rinsed thoroughly with water and ethanol) was used as a quasi reference electrode (QRE). A platinum microelectrode (20 μm diameter) and Glassy Carbon (GC, 3 mm diameter) were used as working electrodes. The working electrodes were carefully polished before each voltammetry experiment with 0.3 μm alumina paste (Wirth Buehler) and ultrasonically rinsed in acetone. The electrochemical cell was assembled within a Faraday cage, which in turn was situated inside the dry argon-filled glove box.

### **3.3.2 Cyclic voltammetry**

All electrochemical experiments were performed using a computer-controlled Autolab PGSTAT302N Potentiostat/Galvanostat (Ecochemie, Netherlands) with Nova software.

Basic electrochemical behaviour of a system was obtained by performing a series of different potential steps and recording the current-time response curves. The potential was usually varied linearly with time at scan rates ( $\nu$ ) ranging from 10  $\text{mVs}^{-1}$  to 1000  $\text{mVs}^{-1}$  with conventional electrodes. The technique allows both oxidation and reduction processes to be measured for the system because the polarization of the electrode is reversed on the reverse scan.

### 3.3.3 Chronoamperometric Experiments

Potential step chronoamperometric transients were achieved using a sample time of 0.01 s. The pre-treatment step comprised of holding the potential at a point of zero current (with 20 s pre equilibration time), after which the potential was stepped from a position of zero current to a chosen potential after the oxidative peak and the current was measured for 10 s. The nonlinear curve fitting function in the software package Origin 6.0 (Microcal Software Inc.), following the Shoup and Szabo approximation (Eq. 3.1-3.3) was used to fit the experimental data (Shoup and Szabo, 1982, Roger et al., 2008).

$$I = -4nFDcr_d f(\tau) \quad (3.1)$$

$$f(\tau) = 0.7854 + 0.8863\tau^{-1/2} + 0.2146\exp(-0.7823\tau^{-1/2}) \quad (3.2)$$

$$\tau = \frac{4Dt}{r_d^2} \quad (3.3)$$

### 3.4 Measuring the solubility of vanadium acetylacetonate compound in DESs

The solute is added to the solvent and the mixture is stirred for 24 hours or longer in the shaker. Uninterrupted observation is demanded to estimate if the solute has totally dissolved or not. If it is totally dissolved, addition of more solute is demanded and the

observation is done again. By observing the presence of undissolved solute in the solvent after several additions of the solute saturation is obtained and confirmed.

Samples from the solution are then taken from the upper part that does not hold suspended undissolved compound. The sample may require filtering if suspended compound is suspected to be present. After filtration, samples are taken for chemical analysis. To prevent crystallization, dilution may be necessary in certain cases of sample preparation. If necessary, the samples are diluted with de-ionized water. Finally, samples are analyzed using Perkin-Elmer Optima 5300DV inductively coupled plasma-atomic 69 emission spectrometer (ICP-AES). For reasons of accuracy, each analysis was repeated three times and the average of the three analyses was determined. Shake flask method was used in this work as it is the most accurate method to determine solubility.

In the present work, the solubility of vanadium acetylacetonate ( $V(acac)_3$ ) was measured in various DESs. This was carried out by adding about 0.01 g of compound to 10 g of DES and stirred for 24 – 48 hours at constant temperature. If the solvent was able to dissolve all the 0.01 g of compound, more salt was added and observation was focused to ensure that a saturated solution was achieved. During these measurements, two important factors were taken into consideration. Firstly, the solvent and compound must be of high purity. This is because any amount of impurities, no matter how small, will affect the measured solubility. For this reason, all the chemicals used in the present work were of synthesis grade. Secondly, the samples withdrawn from the saturated solutions did not contain any undissolved salt.



## **3.5 Charge/discharge experiment**

### **3.5.1 Instrumentation**

Charge–discharge testing is another experimental technique utilized in this work. These tests will be used to demonstrate how active species perform in an applied RFB cell over time. Charge/discharge tests are designed to imitate the conditions a battery would experience under long-term performance. The ‘charge’ step includes the addition of energy to the system, while the ‘discharge’ step includes energy extraction. The charge/discharge steps can be performed at constant applied potential, current, or resistive load – or a sequence of any or all of these conditions. In this work, experiments were accomplished under the frequently utilized constant current condition (potential response was measured) because the resulting data were more readily analyzed. Galvanostatic method was performed for charge/discharge tests using an H-type glass cell. In this work, the galvanostat used was an Autolab PGSTAT302N Potentiostat/Galvanostat (Ecochemie, Netherlands).

### **3.5.2 H-type cell**

An H-type glass cell was designed and fabricated for the constant current charge and discharge tests of a small redox battery with vanadium redox couples. This H-type glass cell consists of principal three parts, the anodic and cathodic compartments and the membrane placed between the two compartments. The H-type cell is commonly utilized to screen electrolytes (Skylas-Kazacos et al., 1986, Shinkle et al., 2012, Zhang et al., 2012). It is used because it is very easy to set up and versatile (electrodes, membranes, and liquids are easily changed). The scheme and photograph of H-type glass cell battery is shown in Figure 3.2.

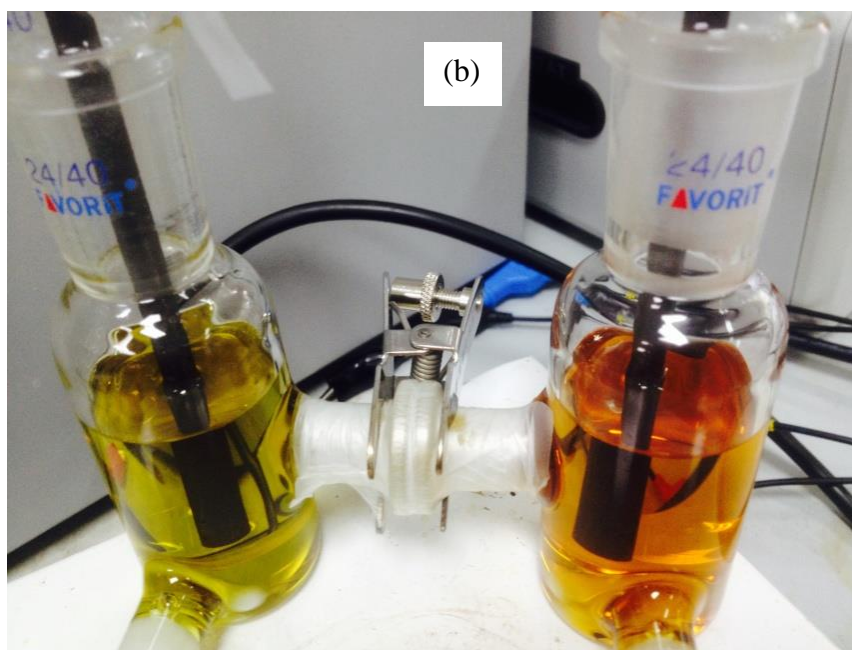
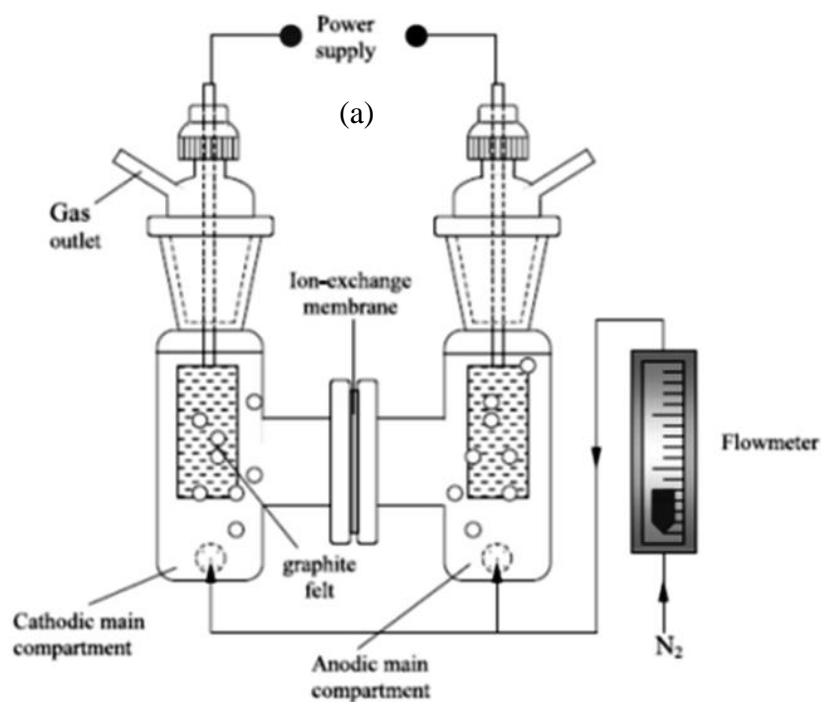


**Figure 3.2:** (a) The scheme of H-type glass cell battery; (b) Photograph of an H-type charge/discharge cell.

6 mm graphite felt electrode was utilized as both anode and cathode for the charge–discharge of the H-type cell, which were polished with 15  $\mu\text{m}$  silicon carbide paper, sonicated for 15 min, and dried for 8 h prior to the experiment. Acetonitrile (anhydrous

grade) was used as a means for comparing the performance of the  $V(\text{acac})_3$  system with that of different DESs. Tetraethylammoniumtetrafluoroborate ( $\text{TEABF}_4$ ) was used as the supporting electrolyte to improve conductivity of the solvents. Each compartment comprised 15 ml electrolyte with a magnetic stirring.

An AMI-7001S anion exchange membrane from American Membranes International Inc was utilized in the H-type cell. The membrane was situated between two O-shaped silicon rubber gaskets and sealed to each gasket with silicon sealant in order to prevent any leakage. Expansion of AMI-7001S membrane from dry (as-shipped) to wet conditions is small; therefore its size does not alter importantly during the experiments. The characteristics of this membrane are shown in Table 3.3.

**Table 3.3:** Properties of AMI-7001S anion exchange membrane.

Technical Specification	AMI-7001S
Polymer structure	Gel polystyrene cross linked with divinylbenzene
Functional group	Quaternary ammonium
Ionic formed as shipped	chloride
color	Light yellow
Electrical resistance ( $\text{ohm.cm}^2$ )	<40
0.5 mol/L NaCl	
Permselectivity (%)	91
0.1 mol KCl/Kg / 0.5 mol KCl/Kg	
Total exchange capacity (meq/g)	1.3±0.1
Thermal stability ( $^{\circ}\text{C}$ )	90
Chemical stability range (pH)	1-10

## CHAPTER 4: RESULTS AND DISCUSSIONS

Different types of DESs were synthesized and utilized in different parts of this research. Of the studied DESs, DES7 and DES13 are novel and have not been reported before. To simplify the text, each DES was given an abbreviation. These DESs are summarized in Table 3.1. The results of this study are arranged into four main sections. Section 4.1 includes the results of the synthesis and characterization of the DESs. Section 4.2 presents the results of applying DESs as electrolyte for electrochemical behaviour of Fc and  $Cc^+$ . Section 4.3 comprises voltammetric behavior of  $V(acac)_3$  and kinetics of electrode reactions in DESs. Section 4.4 deals with the results of charge/discharge experiments.

### 4.1 Synthesis and characterization of different DESs

The structures of the DESs prepared in this work and their abbreviations are shown in Table 3.1. In order to get a better understanding of the interactions in these DESs and investigate their potential applications in industry, selected important physical properties of these DESs were measured. The measured properties include: electrical conductivity ( $\sigma$ ), viscosity ( $\eta$ ), density ( $\rho$ ), freezing point ( $T_f$ ) and pH. The results are summarized in Table 4.1.

**Table 4.1:** Physical properties of the different DESs synthesized in this study

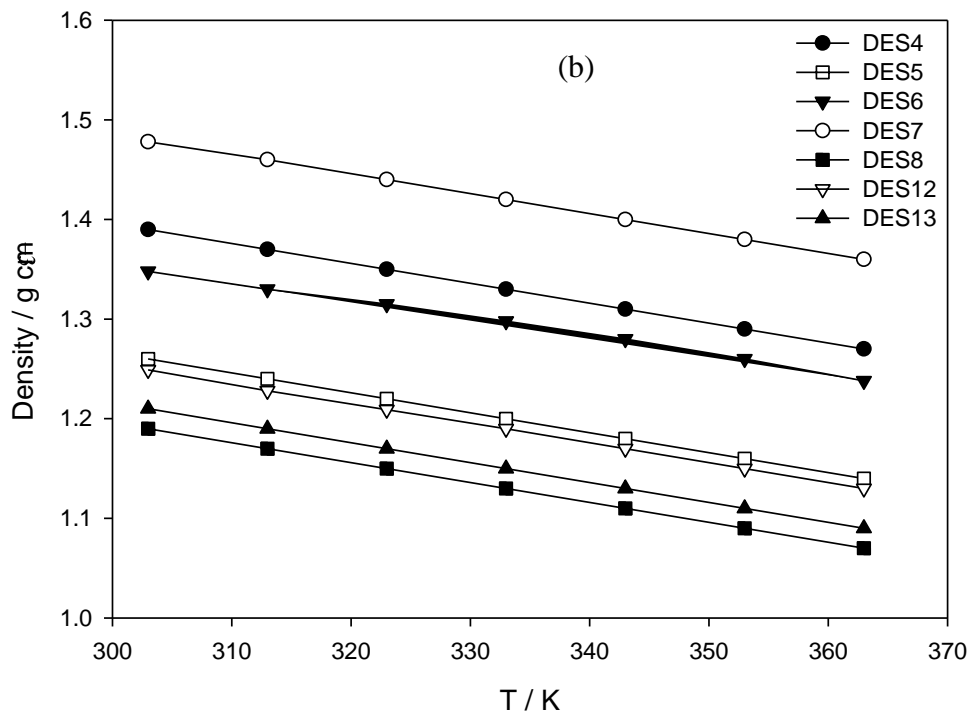
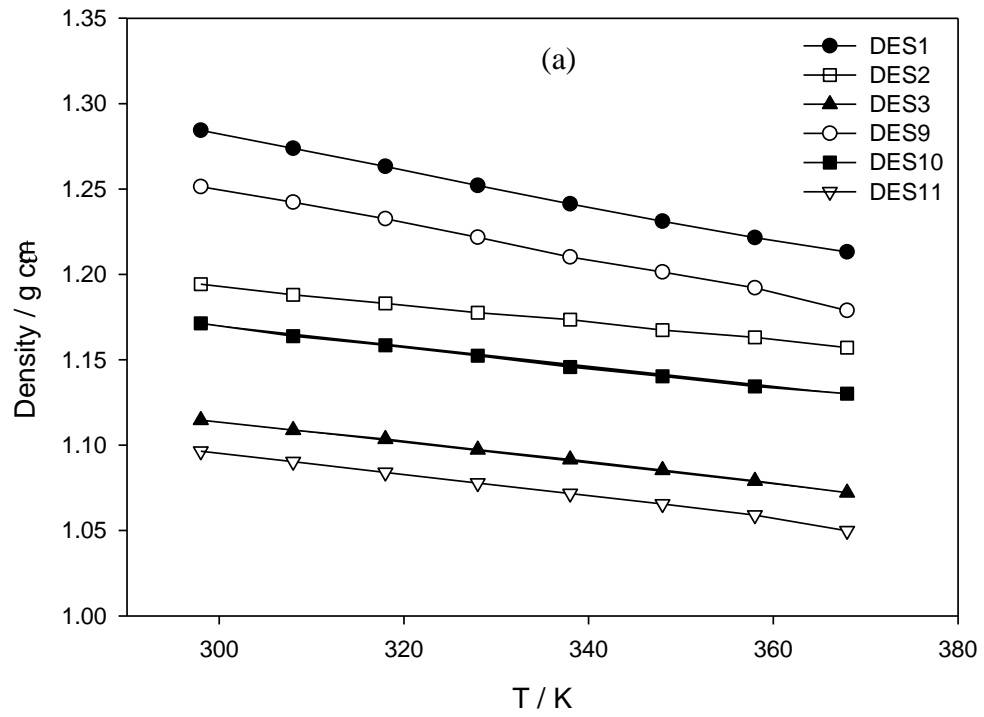
DESs	$M_w$ (g mol <sup>-1</sup> )	$\rho$ (g cm <sup>-3</sup> )	$\eta$ (mPa s)	$\sigma$ (mS cm <sup>-1</sup> )	pH	$T_f$ (K)
DES1	147.52	1.28	164	1.78	5.70	-
DES2	107.93	1.19	322	0.65	2.22	237
DES3	87.92	1.11	66	5.26	4.01	207
DES4	121.84	1.37	828	0.91	1.67	283
DES5	114.82	1.24	458	1.88	-	307
DES6	146.00	1.33	838	0.65	10.66	-
DES7	218.55	1.46	106	9.28	1.00	-
DES8	121.90	1.17	77	2.48	2.36	226
DES9	151.03	1.25	229	1.24	5.12	-
DES10	112.60	1.17	577	0.25	2.04	267
DES11	92.59	1.10	58	5.72	3.89	242
DES12	128.85	1.23	541	1.13	0.98	-
DES13	225.57	1.20	163	7.05	0.52	-
DES14	191.58	1.20	270	0.62	5.53	254
DES15	158.38	1.29	3040	0.08	5.60	267
DES16	160.46	1.25	213	1.43	6.12	230

#### 4.1.1 Density

The densities of the DESs were determined in the temperature range of 298-368 K at atmospheric pressure. As expected, it was observed (Figure 4.1) that the densities of the DESs decreased linearly with increasing temperature because of thermal expansion. The difference in the values of density for the studied DESs could be ascribed to a different molecular association or packing of the DES and the difference in the density of the HBDs. In general, there was a good agreement between the values obtained in this work and those reported in the literature (Shahbaz et al., 2012). The following equation fits the experimental data for the densities ( $\rho$ ) of the DESs very well over the entire temperature range:

$$\rho = AT + B \quad (4.1)$$

Where  $T$  is the absolute temperature (K) while  $A$  and  $B$  are empirical constants that depend on the type of DES.



‘Figure 4.1, continued’

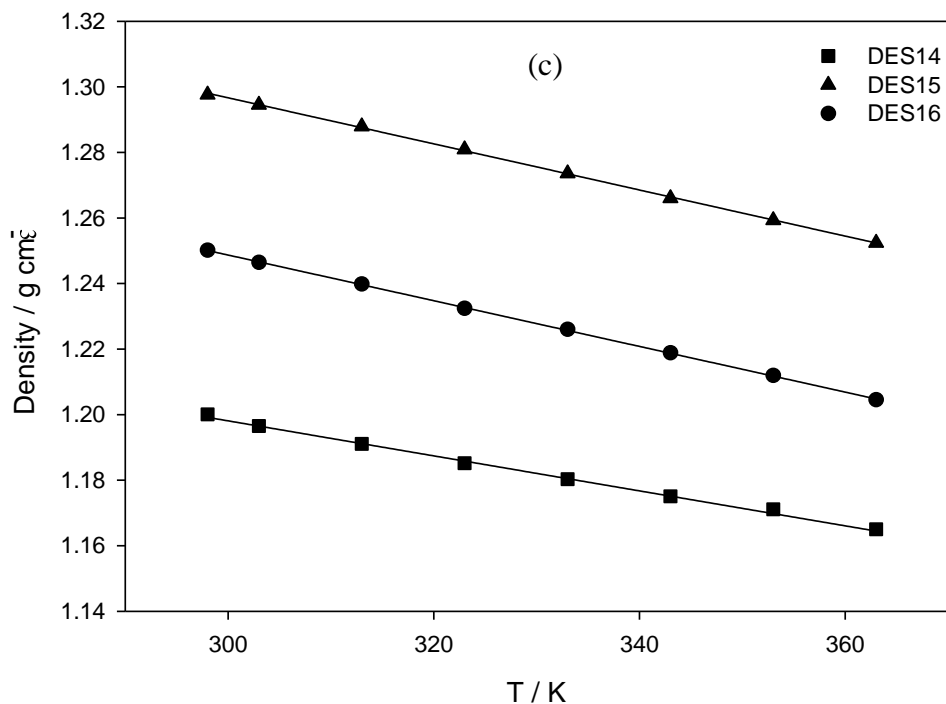


**Figure 4.1:** Dependence of densities ( $\rho$ ) on temperature for; (a) DESs based on ammonium salts and polyol HBDs; (b) ammonium based salts and acids, amine, amide, zinc nitrate HBDs; (c) phosphonium based salts and polyol HBDs.

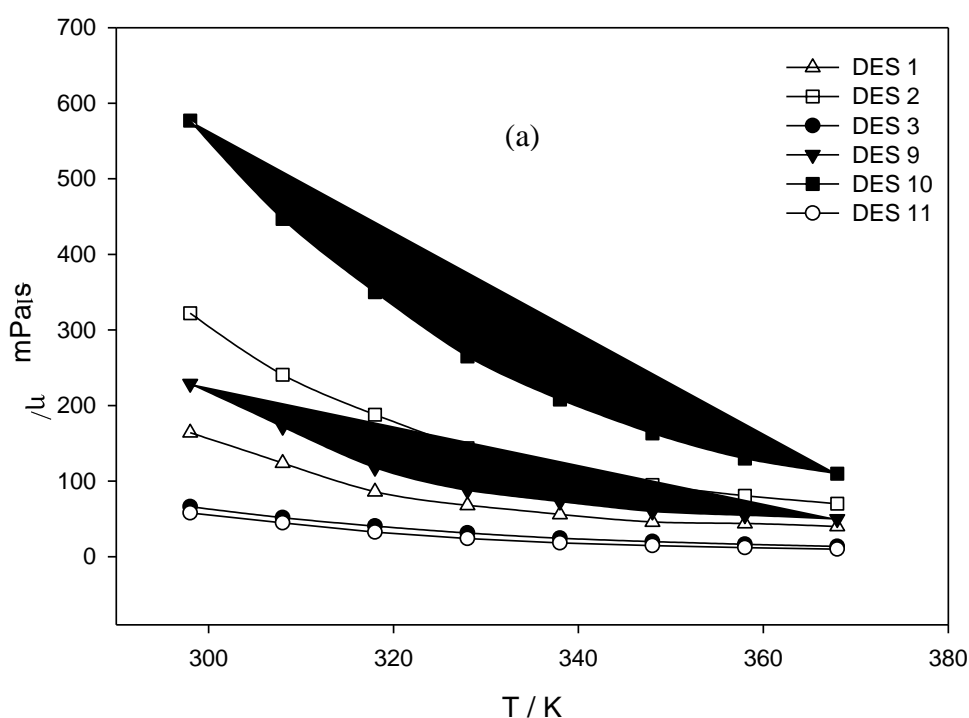
As shown in Table 4.1, DES7 has a higher density due to a higher intermolecular packing of the compound's denser structure. The density of ethylene glycol based DESs were found to be slightly less than those of other polyol-based counterparts. The adjustable parameters of equation (3.1) for the density of all studied DESs are displayed in Table 4.2.

**Table 4.2:** The adjustable parameters for density of some studied DESs.

DES	Density		DES	Density	
	A	B		A	B
DES1	-0.0010	1.5740	DES9	-0.0010	1.5530
DES2	-0.0005	1.3417	DES10	-0.0006	1.3503
DES3	-0.0006	1.2938	DES11	-0.0006	1.2852
DES4	-0.0020	1.9960	DES12	-0.0021	1.8459
DES5	-0.0019	1.8660	DES13	-0.0020	1.8160
DES6	-0.0018	1.8962	DES14	-0.0005	1.3582
DES7	-0.0020	2.0786	DES15	-0.0007	1.5077
DES8	-0.0019	1.7960	DES16	-0.0007	1.4578

### 4.1.2 Viscosity

The viscosity is a very important parameter in electrochemical studies due to its strong effect on the rate of mass transport within the solution. It significantly influences the diffusion coefficient of species which are dissolved or dispersed in a media such as an IL (Wu et al., 2011). The viscosity can be influenced by various parameters such as the relative capacity to form hydrogen bonds, anionic species, size, higher alkalinity, van der Waals forces and the size of the cation (Bandres et al., 2011). The viscosity is generally affected by the interaction of the salt with the HBD and their ability to coordinate. Figure 4.2 indicates that as the temperature increases from 298 to 368 K, the viscosity of the DESs decreases due to the higher mobility of ions. DESs with the glycerol HBD exhibits higher viscosities than other polyol based DESs, thus resulting in lower conductivities (Figure 4.2(a)). Moreover, choline chloride based DESs show lower viscosities in comparison to diethylenethanol ammonium chloride based DESs. The value of viscosity at 298 K follows the order **DES15 > DES6 > DES4 > DES10 > DES12 > DES5 > DES2 > DES14 > DES9 > DES16 > DES1 > DES13 > DES7 > DES8 > DES3 > DES11.**





'Figure 4.2, continued'

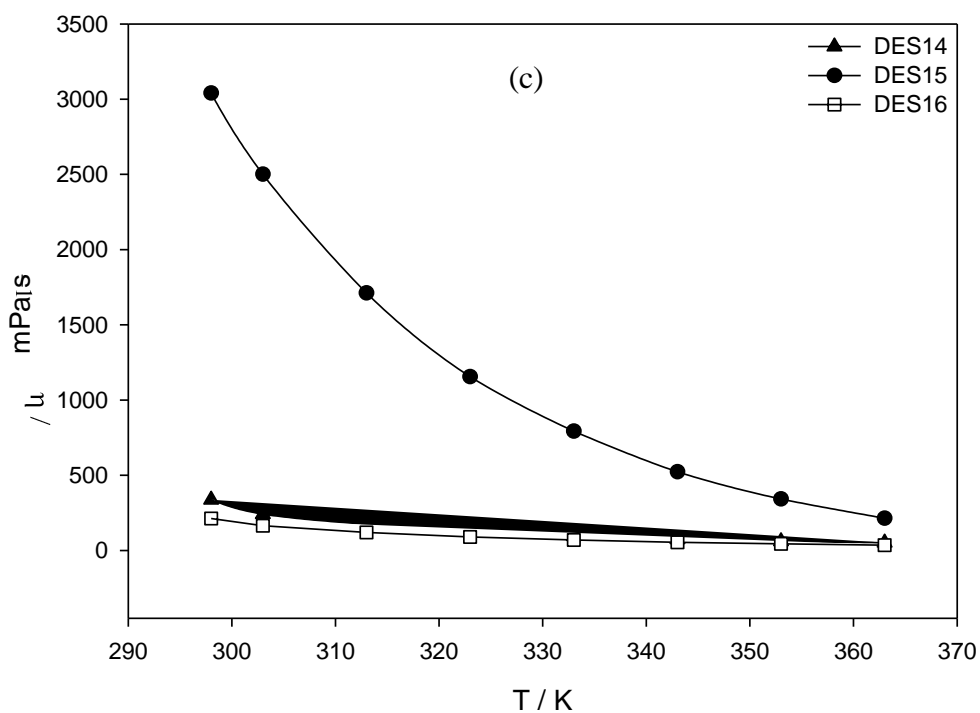
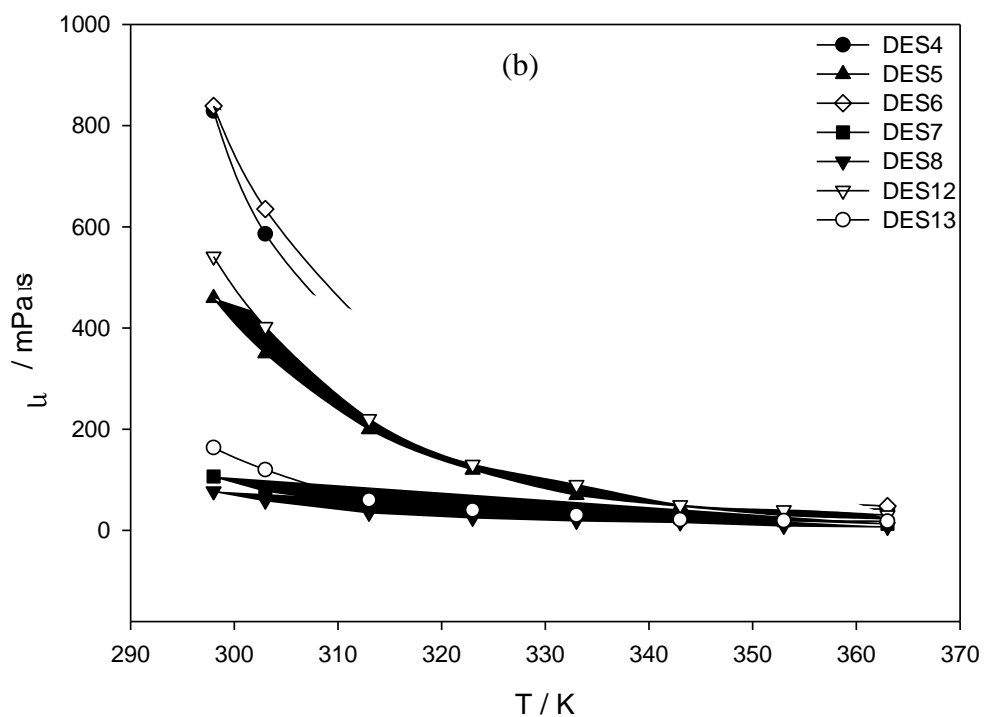
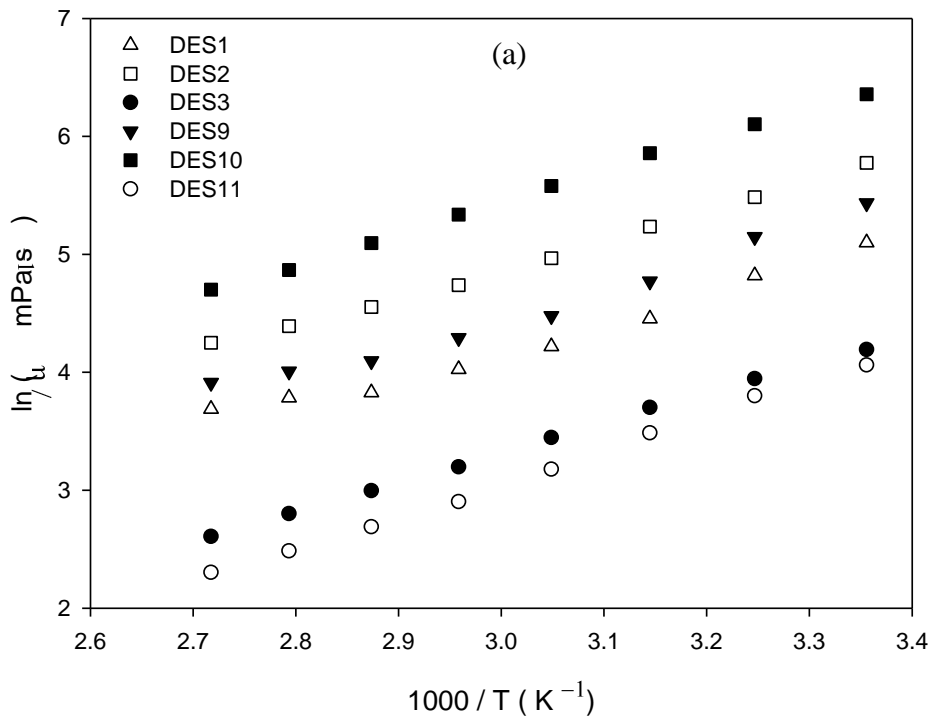


**Figure 4.2:** Dependence of viscosity ( $\eta$ ) on temperature with shear rate between  $0.01$ - $100 \text{ s}^{-1}$  for; (a) DESs based on ammonium salts and polyol HBDs; (b) ammonium based salts and acids, amine, amide, zinc nitrate HBDs; (c) phosphonium based salts and polyol HBDs .

As can be seen in Figure 4.2(c), the viscosity of DES15 has a large value at low temperatures in comparison to DES14 and DES16. However, it decreases sharply with increasing temperature and reaches a value of around 2.14 Pa.s at 363K.

The temperature dependency of the viscosity ( $\eta$ ) for the DESs and the profiles are fitted to the Arrhenius equation (Eq. 4.2), which describes the temperature dependence for non-associating electrolytes (Bonhote et al., 1996), as depicted in Figure 4.3. Where  $T$  is the temperature in Kelvin,  $\eta$  is the viscosity in mPa.s,  $E_\eta$  is the activation energy,  $\eta_0$  is a constant and  $R$  is the universal gas constant in  $\text{kPa.L.mol}^{-1}.\text{K}^{-1}$ .

$$\ln \eta = \ln \eta_0 + \frac{E_\eta}{RT} \quad (4.2)$$



The experimental method used to measure the viscosity could have an effect on the obtained viscosity data, and within this effect it should be remarked that some DESs are non-Newtonian fluids, which should be considered when analyzing their rheological properties.

'Figure 4.3, continued'

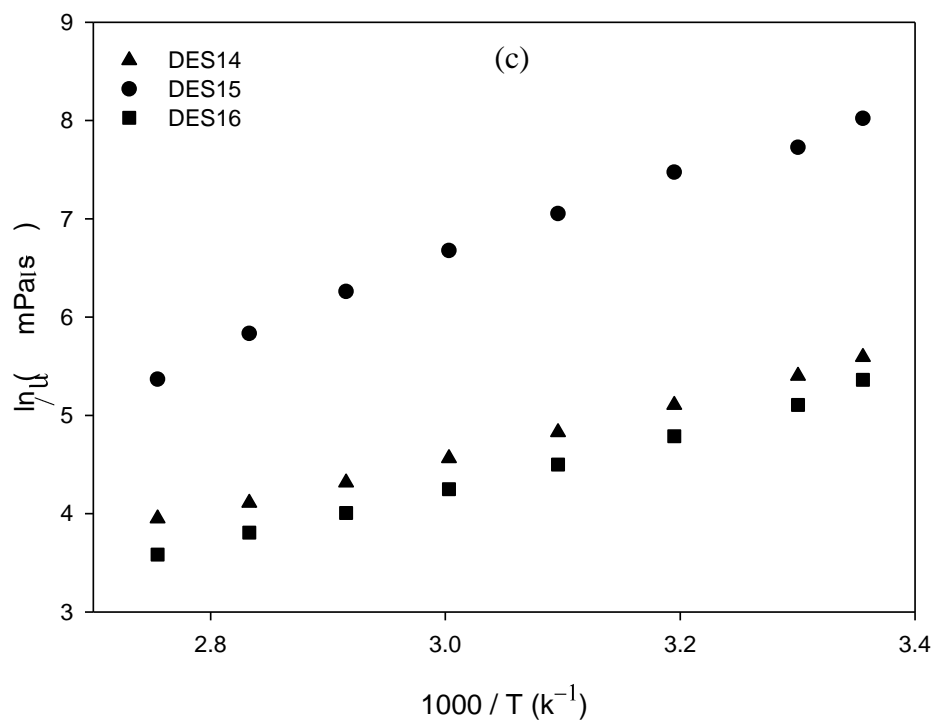
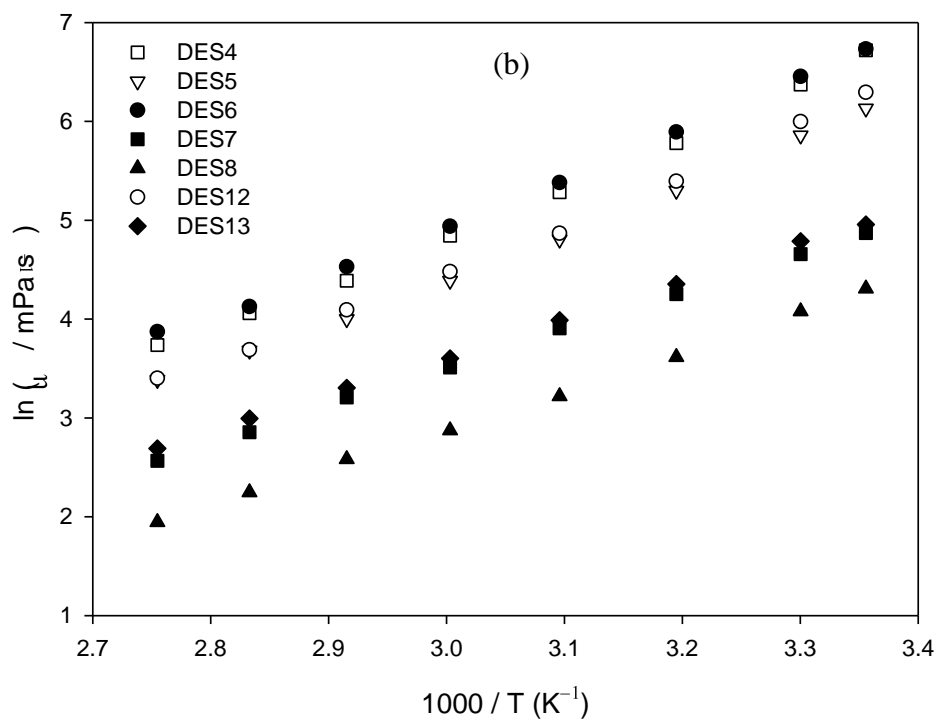


**Figure 4.3:** Arrhenius plot of viscosity ( $\eta$ ) for; (a) DESs based on ammonium salts and polyol HBDs; (b) ammonium based salts and acids, amine, amide, zinc nitrate HBDs; (c) phosphonium based salts and polyol HBDs.

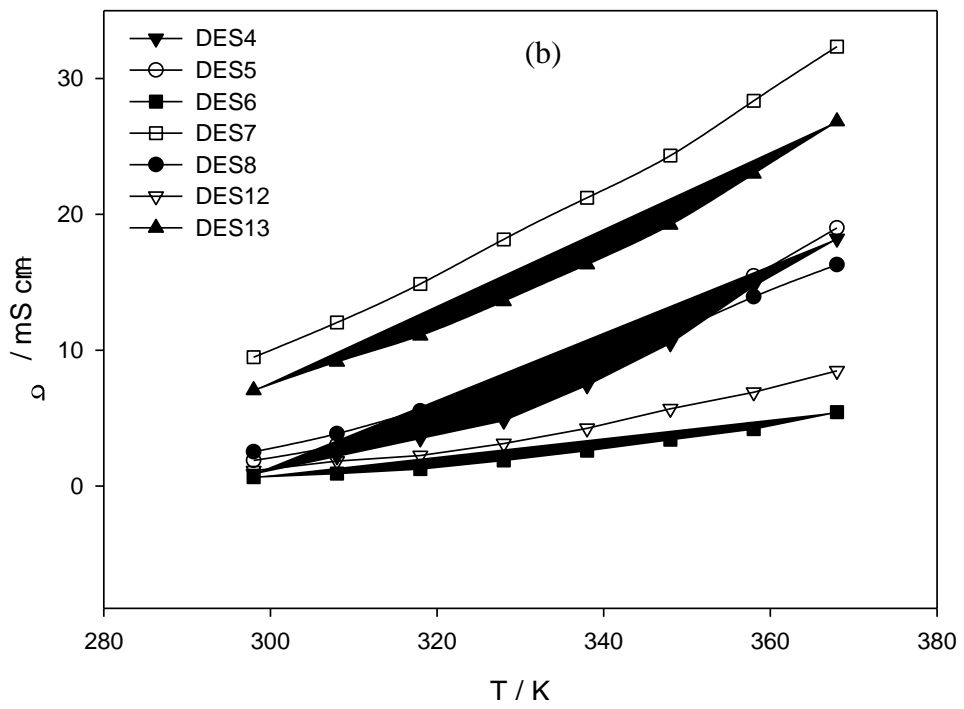
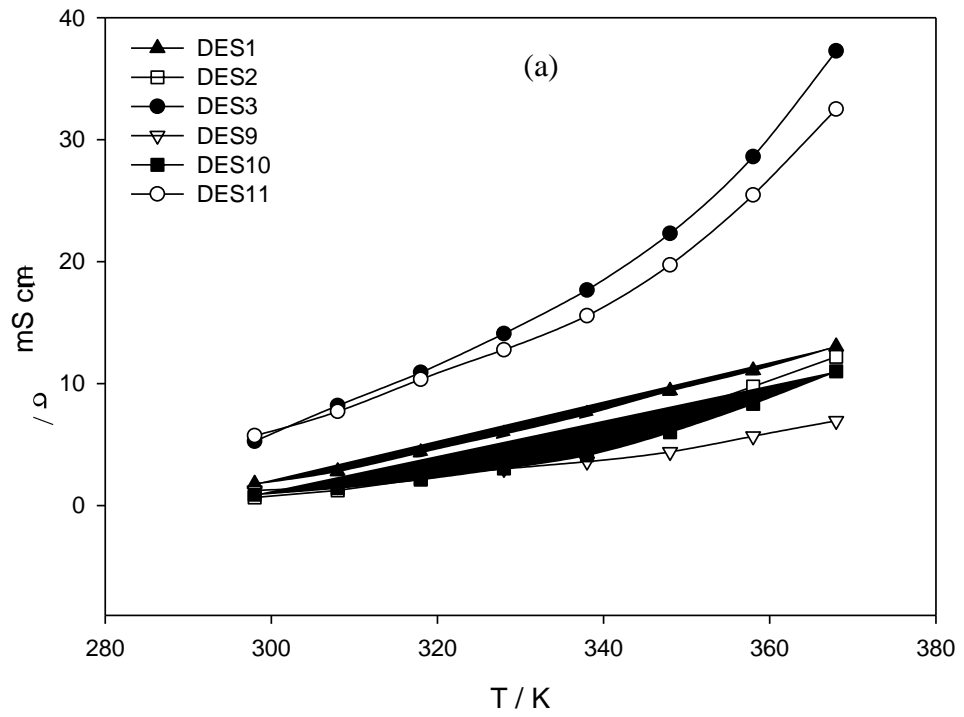
The value of  $E_\eta$ ,  $\eta_0$  and sums of square errors are listed in Table 4.3. The regression correlation coefficients have values higher than 0.97 showing a reasonably good fit.

**Table 4.3:** Regression parameters for viscosity of studied DESs.

DES	$\eta_0/ \text{mPa s}$	$E_\eta/ \text{kJ mol}^{-1}$	$SSE_\eta$	DES	$\eta_0/ \text{mPa s}$	$E_\eta/ \text{kJ mol}^{-1}$	$SSE_\eta$
DES1	1.85	20.68	0.036	DES9	1.08	21.30	0.028
DES2	2.59	22.55	0.066	DES10	2.80	23.96	0.034
DES3	4.47	20.46	0.035	DES11	5.69	19.00	0.054
DES4	10.01	41.25	0.067	DES12	9.99	40.17	0.068
DES5	9.39	38.32	0.062	DES13	7.77	31.57	0.018
DES6	9.57	40.31	0.054	DES14	3.70	22.97	0.031
DES7	7.99	31.88	0.016	DES15	6.55	36.36	0.089
DES8	8.80	32.40	0.031	DES16	4.37	23.93	0.042

### 4.1.3 Ionic and molar conductivity

Ionic conductivity is a function of both the mobility and number of carrier ions. Conductivity evolution can be attributed to various factors, such as the geometrical and electronic structure of the salts and hydrogen bond donors, the diffusion coefficient of protons and hydrogen-bond interactions. As the temperature rises, conductivity of DESs generally increases significantly as a consequence of faster movement of ions at higher temperatures as well a slower viscosity of the neat DES. The temperature dependence of conductivity for the DESs is depicted in Figure 4.4. It can be observed from Figure 4.4 that the ionic conductivity for most ammonium based DESs is higher than that for the corresponding phosphonium based DESs. The maximum conductivity achieved in this research was for DES3 at 368K which is  $37.26 \text{ mS cm}^{-1}$ . Together with the finding that ammonium-based DESs possessed lower melting temperatures and lower viscosities than the phosphonium-based DESs, it is more evident now that the electrochemistry of DESs at moderate temperatures has more potential to be carried out in ammonium based DESs.



‘Figure 4.4, continued’

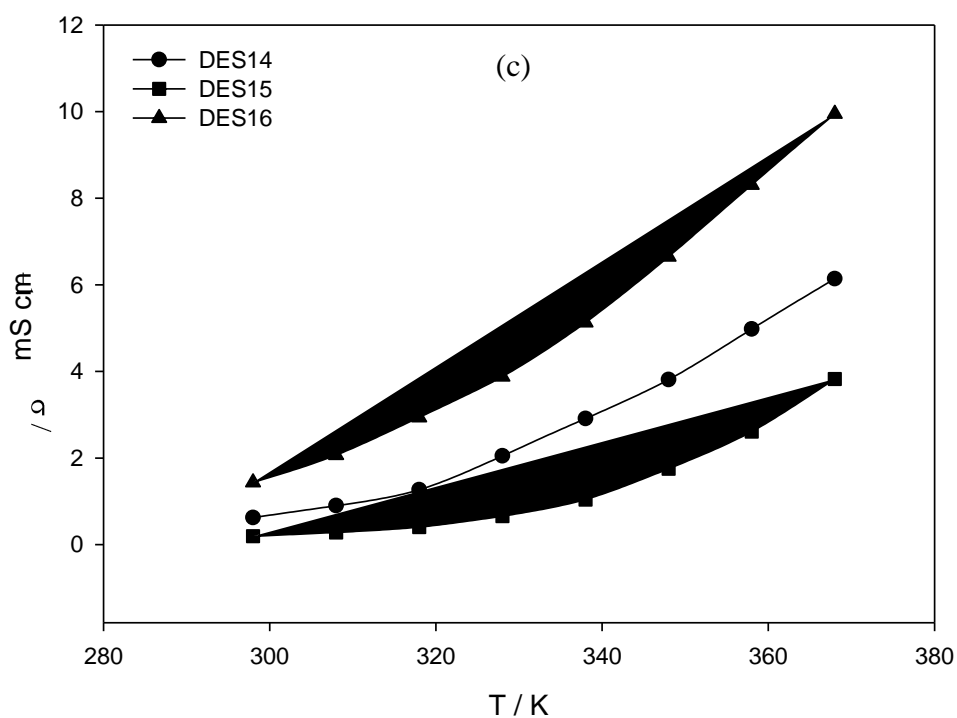


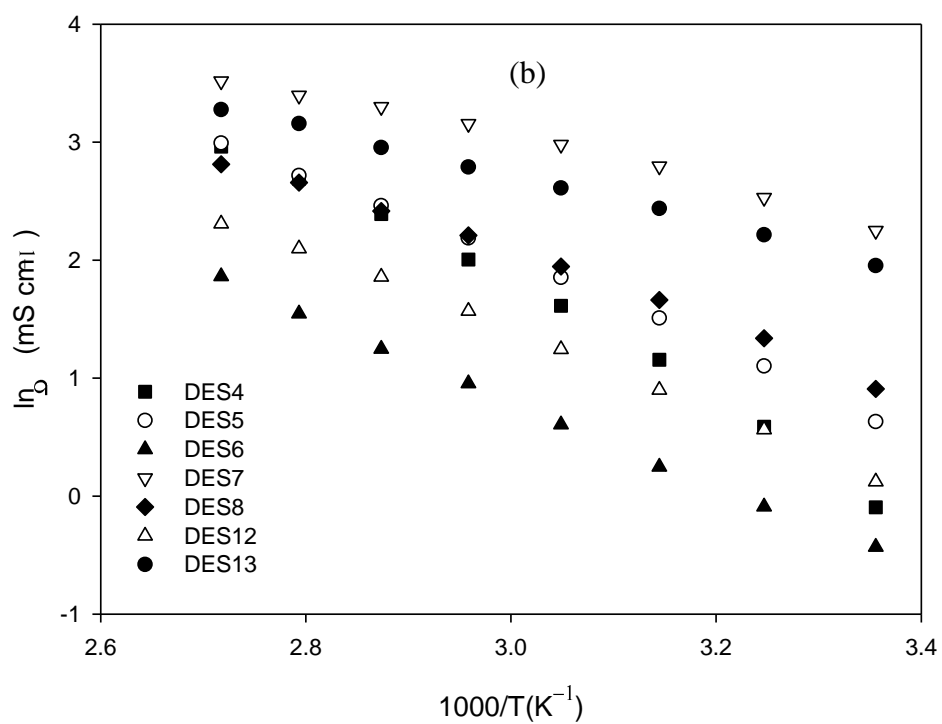
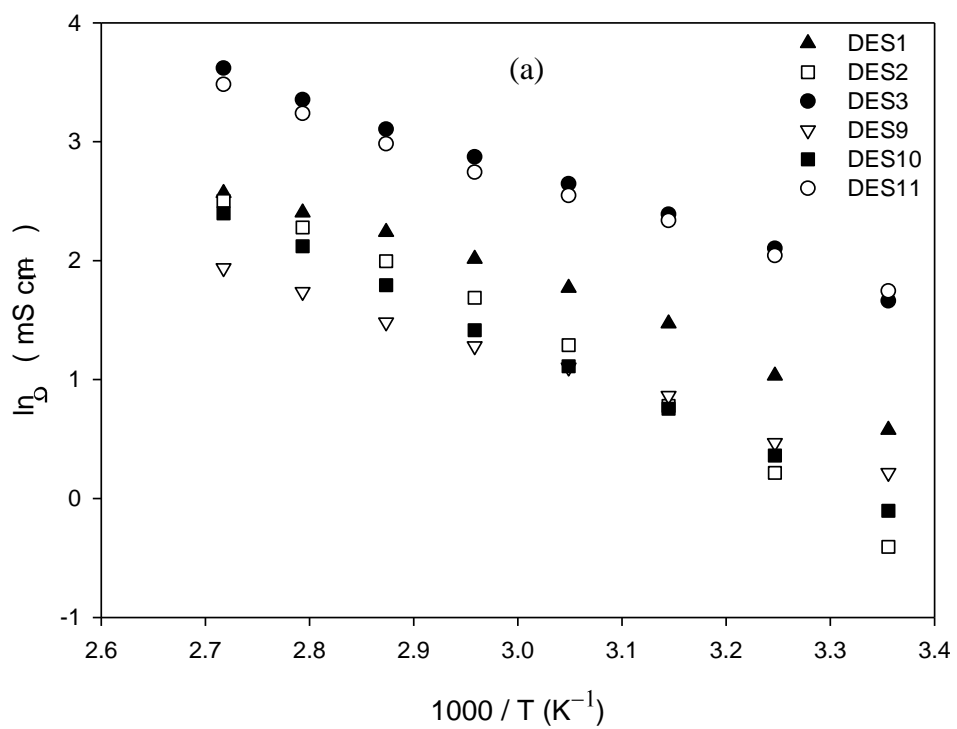
**Figure 4.4:** Dependence of ionic conductivity ( $\sigma$ ) on temperature for; (a) DESs based on ammonium salts and polyol HBDs; (b) ammonium based salts and acids, amine, amide, zinc nitrate HBDs; (c) phosphonium based salts and polyol HBDs.

The conductivity of DESs ( $\sigma$ ) varies over the entire temperature range according to

Equation 4.3:

$$\ln\sigma = \ln\sigma_o + \frac{E_\sigma}{RT} \quad (4.3)$$

Where  $T$  is the temperature,  $\sigma_o$  is a constant and  $E_\sigma$  is the activation energy for conduction. Consequently, from Equation 4.3  $E_\sigma$ ,  $\sigma_o$  and sums of square errors are shown in Table 4.4. The regression correlation coefficients are of values higher than 0.96.



‘Figure 4.5, continued’

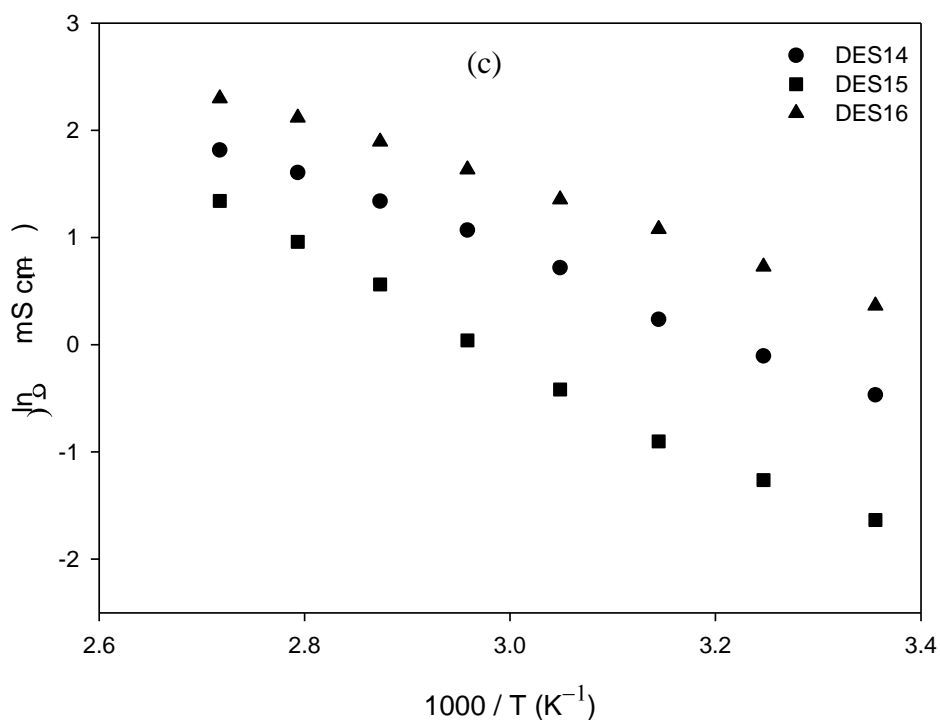


**Figure 4.5:** Arrhenius plot of viscosity ( $\eta$ ) for; (a) DESs based on ammonium salts and polyol HBDs; (b) ammonium based salts and acids, amine, amide, zinc nitrate HBDs; (c) phosphonium based salts and polyol HBDs.

**Table 4.4:** Regression parameters for ionic conductivity of studied DESs.

DES	$\sigma_o/\text{mS cm}^{-1}$	$E_\sigma/\text{kJ mol}^{-1}$	$SSE_\sigma$	DES	$\sigma_o/\text{mS cm}^{-1}$	$E_\sigma/\text{kJ mol}^{-1}$	$SSE_\sigma$
DES1	10.02	23.97	0.068	DES9	11.13	25.70	0.102
DES2	15.44	38.48	0.197	DES10	16.03	40.72	0.160
DES3	10.56	21.61	0.097	DES11	8.88	17.52	0.046
DES4	16.35	39.9551	0.178	DES12	12.01	29.05	0.090
DES5	13.26	30.8320	0.102	DES13	9.07	17.40	0.051
DES6	11.99	30.6116	0.042	DES14	12.30	25.32	0.032
DES7	9.06	16.5350	0.087	DES15	14.30	39.85	0.103
DES8	11.14	24.9039	0.103	DES16	11.93	30.74	0.058

Molar conductivity  $\Lambda$  ( $\text{m}^2\text{Smol}^{-1}$ ) of the DESs as electrolytes was calculated using the expression  $\Lambda = V_e \sigma$ . The equivalent weight ( $V_e$ ) of the DESs is measured from the experimental density using the equation  $V_e = M/\rho$ , where  $\rho$  is the density and  $M$  is the molar mass.



In order to discuss the ionic behavior, the plot of the equivalent conductivity against the inverse of viscosity (Walden plot) for all the studied DESs over a temperature range of 298–368K is shown in Figure 4.6. When the conductivity is strongly correlated with the viscosity, the Walden rule can be written as follows:

$$\Lambda\eta^\alpha = C \quad (4.4)$$

Where  $\alpha$  is the slope of the line in the Walden plot, which reflects the decoupling of the ions and  $C$  (Walden product) is a temperature-dependent constant. This scheme provides a useful basis for classifying and arranging the ILs (Wu et al., 2011, Angell et al., 2007, MacFarlane et al., 2009) due to the practical measure for examining the ion pairing problem in electrolytes. It also helps in understanding the relationship between conductivity and low vapor pressure that is, otherwise, not so apparent. The mobility of ions in ILs is significantly different from that in non-aqueous solvents and there have been very few assays to model the conductivity of ILs. Deviations from the Walden rule seen in proton transfer ILs have previously been used to illustrate ionic association (Martino et al., 2006, Wu et al., 2003). This rule is not fully feasible to ILs as it is only applicable for ions at infinite dilution where ion-ion interactions can be disregarded, which is obviously not the case in ILs. While there is clearly no validity behind the application of the Walden rule to ILs it is interesting to perform this analysis for DESs to observe how they compare with ILs with discrete anions.

The dotted ideal line in Figure 4.6 represents the data for aqueous KCl solutions at high dilution, which corresponds to a system composed of equally mobile and fully dissociated ions. In comparison to the ideal line it can be seen that most of DESs lie below the ideal Walden line. DESs with zinc nitrate hexahydrate HBD examined from Walden plots lie above the ideal line. DES2, DES4 and DES10 examined from Walden plot lie closely to the ideal line which indicates that they are good ILs. The deviations of

the Walden plot of these DESs from the ideal line show an increased electrostatic interaction between the salts and the HBDs.

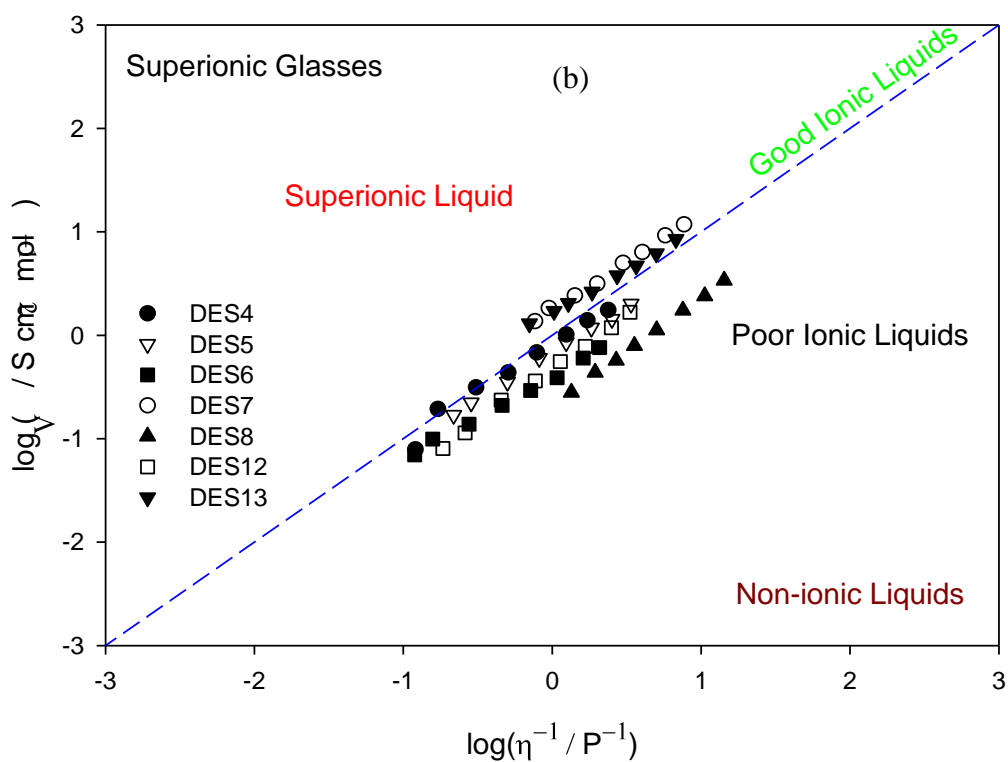
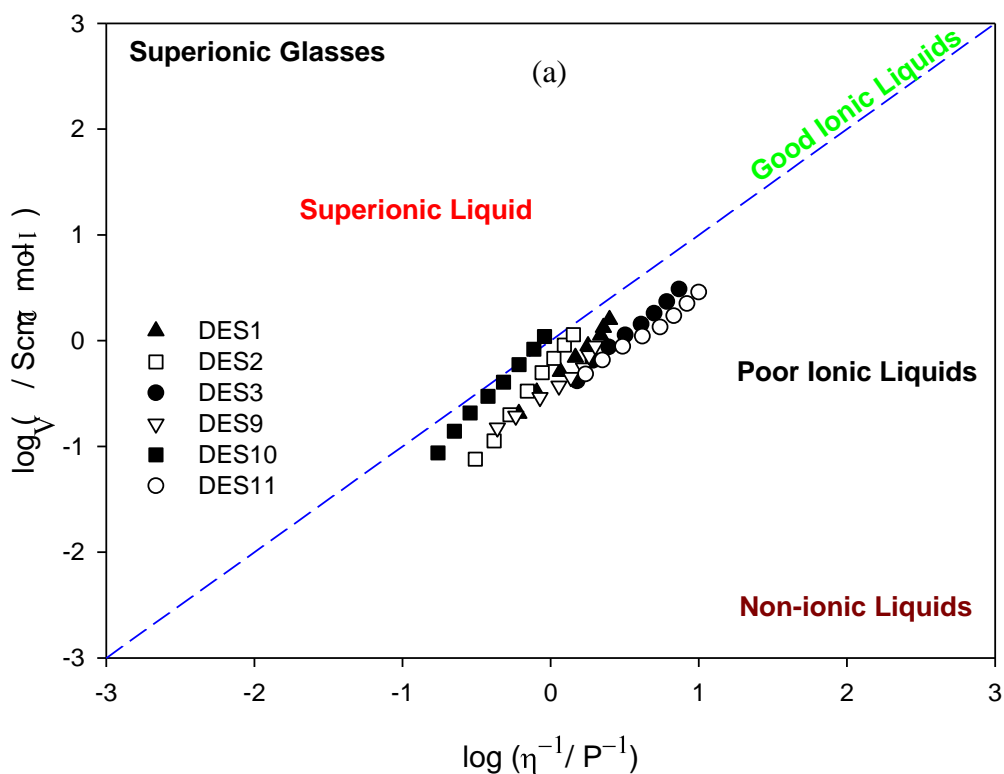
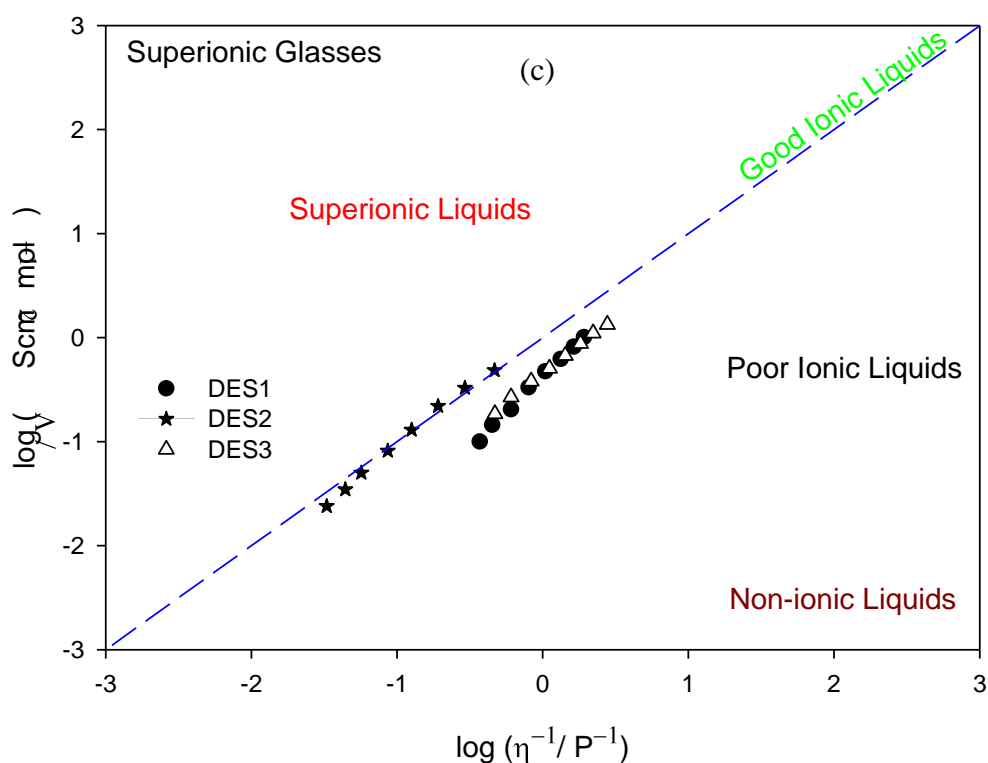


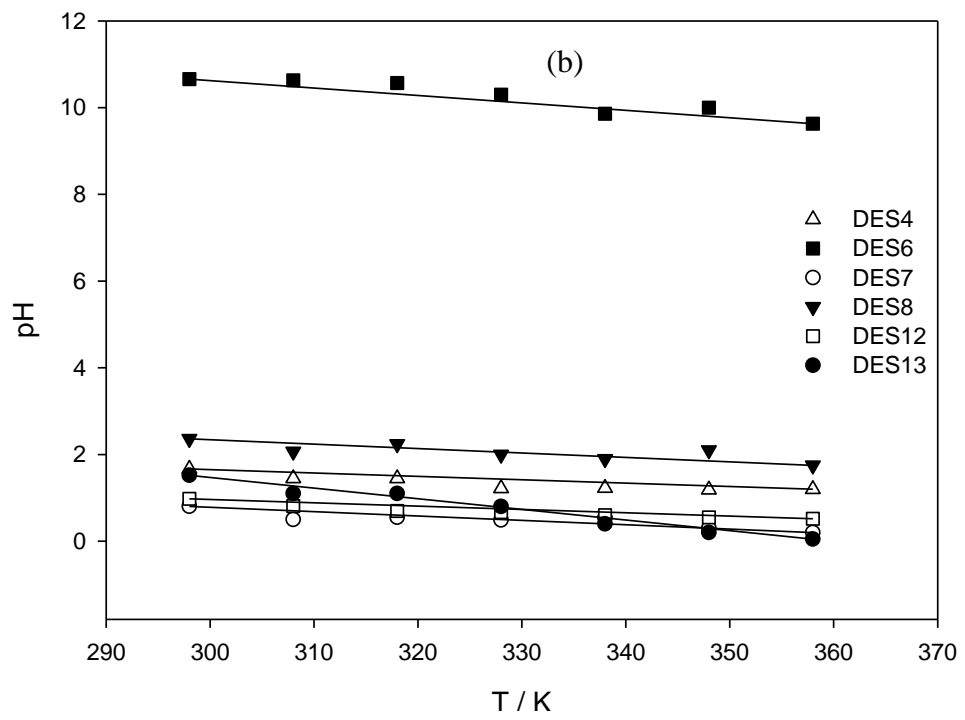
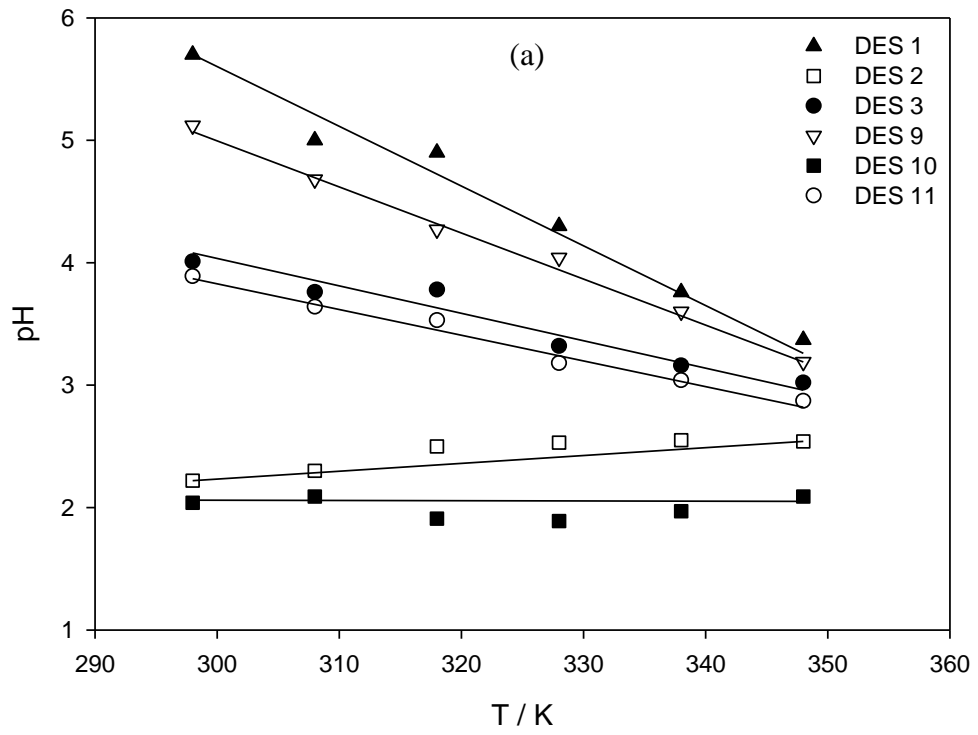
Figure 4.6, continued



**Figure 4.6:** Walden plot for for; (a) DESs based on ammonium salts and polyol HBDs; (b) ammonium based salts and acids, amine, amide, zinc nitrate HBDs; (c) phosphonium based salts and polyol HBDs.

#### 4.1.4 pH

In this study, we also measured the pH of the synthesized DESs as a function of temperature as indicated in Figure 4.7. The temperature dependence of pH was fitted linearly and the parameters for fitting are depicted in Table 4.5. It seems that the type of the HBD has a strong effect on determining the acidity and alkalinity of the DESs as compare to the salts. The temperature dependence of pH has been fitted linearly and the parameters needed for fitting are shown in Table 4.5. These results indicate that the pH increases with rising temperature for DES2 and DES14. On the other hand, the pH of DES1, DES3, DES6, DES9, DES11, DES13, DES15 and DES16 tends to decrease with temperature. The pH of DES4, DES7, DES8, DES10 and DES12 do not change much with temperature.



‘Figure 4.7, continued’

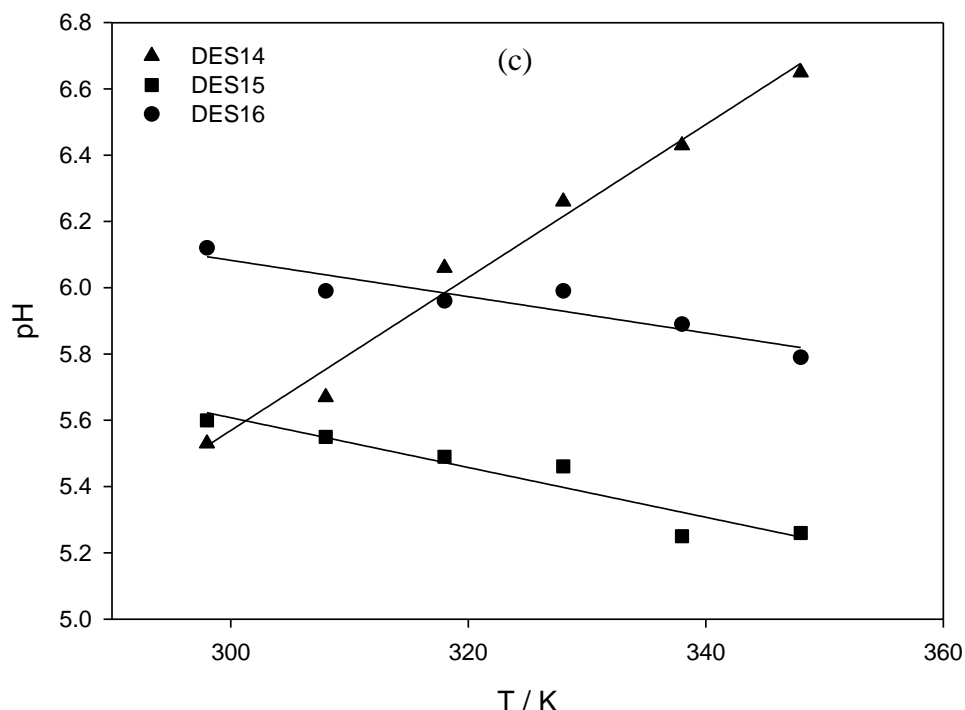


**Figure 4.7:** Temperature-dependency of pH for; (a) DESs based on ammonium salts and polyol HBDs; (b) ammonium based salts and acids, amine, amide, zinc nitrate HBDs; (c) phosphonium based salts and polyol HBDs.

**Table 4.5:** The adjustable parameters for pH of all studied DESs.

DES	pH		DES	pH	
	A	B		A	B
DES1	-0.0456	19.2430	DES9	-0.0375	16.2579
DES2	0.0068	0.2436	DES10	0.0004	2.1183
DES3	-0.0206	10.1621	DES11	-0.0207	10.0490
DES4	-0.0077	3.8629	DES12	-0.0071	3.0329
DES5	-	-	DES13	-0.0247	8.8331
DES6	-0.0181	16.1631	DES14	0.0231	-1.3567
DES7	-0.0079	3.0900	DES15	-0.0075	7.8614
DES8	-0.0075	4.5317	DES16	-0.0055	7.7286

## 4.2 Electrochemical behaviour of Fc and Cc<sup>+</sup> in DESs

It is essential to employ either a reference electrode of a familiar potential against a standard hydrogen electrode or refer all data to a procedure whose reversible potential is to be independent of the DESs, in order to compare voltammetric data from different eutectic solvents. The Ferrocene/ferrocenium (Fc/Fc<sup>+</sup>) or cobaltocenium/cobaltocene (Cc<sup>+</sup>/Cc) redox couples is most prevalently used as an internal potential scale standard

in voltammetry in conventional organic solvent media (Gritzner and Kuta, 1984, Bond et al., 2000). This process is also used in IL electrochemistry (Zhang and Bond, 2005, Rogers et al., 2008). This work may be one of the few reports that provide a detailed account on the determination of electrochemical potential windows, internal potential references (based on the reduction of  $Cc^+$  and oxidation of Fc), diffusion and rate coefficients of Fc and  $Cc^+$  as well as the Stokes–Einstein products of Fc and  $Cc^+$  in such DESs (Bahadori et al., 2013a).

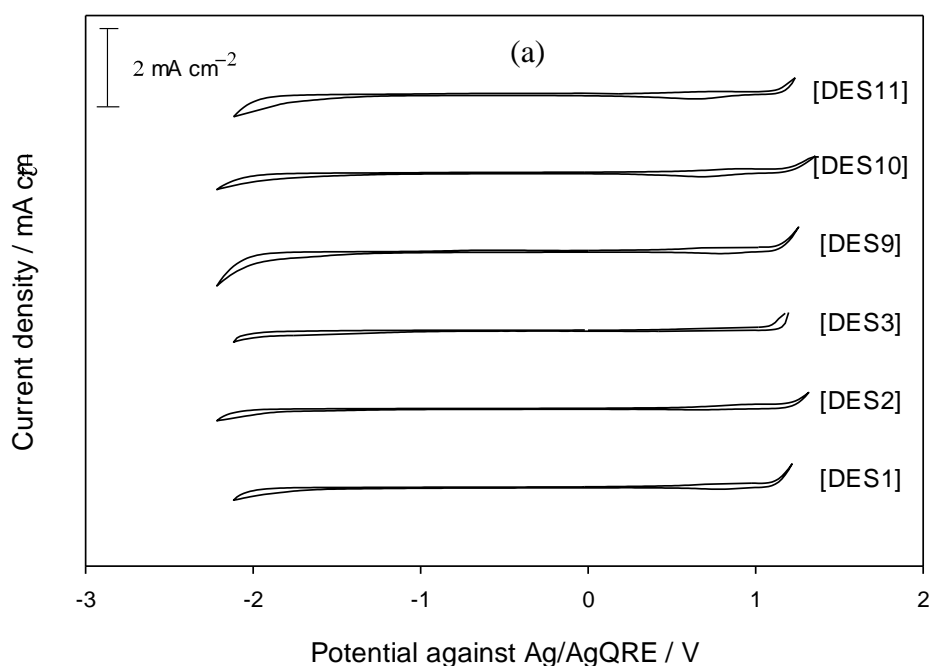
In addition, no fundamental study on the effect of temperature range variations for the Fc/Fc<sup>+</sup> oxidation and Cc<sup>+</sup>/Cc reduction processes in DESs is available. DESs perform the dual function of electrolyte and solvent and in this perception depict a different kind of medium for electrochemical applications, so care in extrapolation of concepts to the DES case is required. In the present work the electrochemical data and kinetics of the Fc/Fc<sup>+</sup> and Cc<sup>+</sup>/Cc redox couples obtained with cyclic voltammetry and chronoamperometry methods in different DESs based on a quaternary phosphonium and ammonium salts are reported over a range of temperatures (Bahadori et al., 2013b).

#### **4.2.1 Electrochemical potential window**

The electrochemical potential window (PW) is one of the most important characteristics to be identified for electrolytes and solvents used in electrochemical applications. PW is dependent on the type of electrodes, the measurement situation, and the references employed. The arbitrary current cut-off used to define the onset of redox processes (typically between 0.1 and 1.0 mA cm<sup>-2</sup>) may not be strictly electrochemically determined. This difficulty is further combined in the case of ILs due to their sensitivity to air, water, and other impurities (Ong et al., 2011). The PW is a significant indicator of electrochemical stability, when DESs are used as electrolytic media for electrochemical devices. This is because the redox couple of an analyte must

fall within the PW of the DESs. The cathodic stability of DESs is mainly determined by the potential at which the reduction of the cations (salts) takes place, while the anodic stability is measured where oxidation of the anions (HBDs) is expected to occur. For particular applications (e.g., supercapacitors), it is the overall potential window that matters, while in other applications, the actual anodic and cathodic limits associated to some reference is the restricting factor.

The limiting reduction and oxidation potentials of the DESs are analyzed by performing cyclic voltammetry using a GC working electrode and a Pt microelectrode at ambient temperature and scan rate of  $0.1 \text{ V s}^{-1}$  as shown in Figures 4.8, 4.9 and 4.10 where the limiting current density reached  $0.2 \text{ mA cm}^{-2}$ . It is discovered that some tested DESs have similar potential ranges as compared to typical ILs (Lu et al., 2012). However, some ILs have wider electrochemical windows (Wu et al., 2011, Suarez et al., 1997). The screened PW may assist in selection of proper DESs as electrolytes and solvents in various spectroscopic and electrochemical applications.



'Figure 4.8, continued'

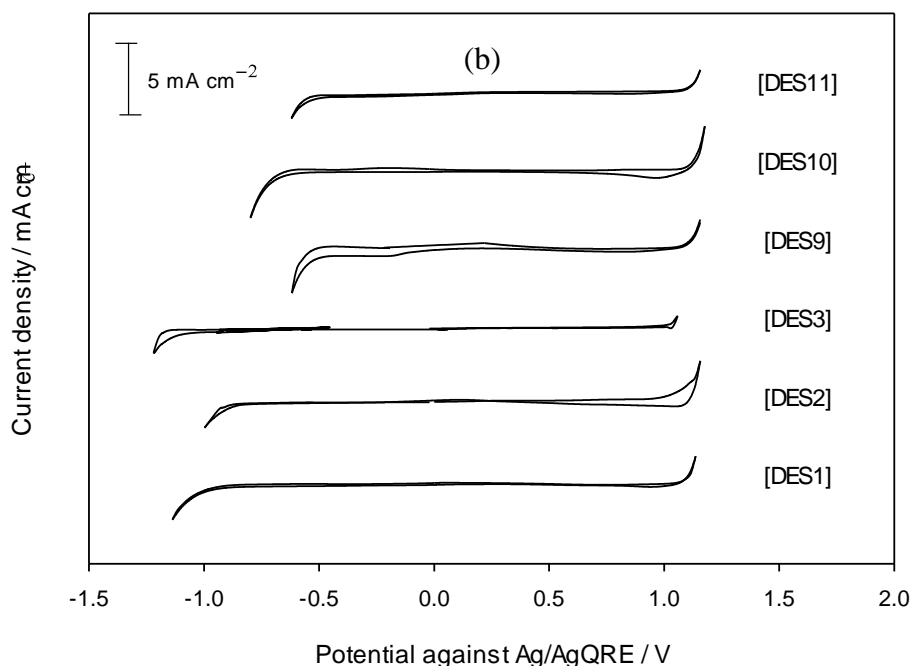


**Figure 4.8:** Electrochemical windows of DESs based on ammonium salts and polyol HBDs using (a) GC working electrode; (b) Pt. microelectrode.

The limiting anodic and cathodic potentials of the DESs are listed in Table 4.6. The potential window lies approximately between 2.02 and 6.65 V vs. Ag/AgQRE for the GC electrode and between approximately 1.43 and 2.48V vs. Ag/AgQRE for the Pt. microelectrode. The largest potential window is obtained using the GC working electrode. The cathodic limit for the Pt. working electrode is smaller than that of its GC counterpart. The anodic limit obtained at a Pt. microelectrode is smaller to those obtained by means of the GC electrode except DES1, DES5, DES6 and DES7. The cathodic and anodic potential limits are indicative of the PW of the DESs. However, establishing a sequence of PW is difficult for all salts and HBDs combinations because a suitable potential reference scale is not always available. However, when this is not a problem, the cathodic and anodic limiting potentials are found to vary even when the salts or HBDs present are common. For example, the oxidation potential limit occurs at 1.22 V (vs Ag/Ag<sup>+</sup>) in [choline chloride][ethylene glycol], 1.26 V (vs Ag/Ag<sup>+</sup>) in [N,N-Dimethylmethyleiminium chloride][ethylene glycol], and 0.69 V (vs Ag/Ag<sup>+</sup>) in



[methyltriphenylphosphonium bromide][ ethylene glycol] at a GC electrode, and the reduction potential limit for the [methyltriphenylphosphonium bromide] series is -0.89 and -0.96 V (vs Ag/Ag<sup>+</sup>) in [glycerol] and [ethylene glycol], respectively, but this limit is more negative in [Methyltriphenylphosphonium bromide][ Triethylene glycol] (-1.25 V vs Ag/Ag<sup>+</sup>) at a GC electrode. The variation of these potentials implies that association of salts or HBDs plays an important role in their PW.

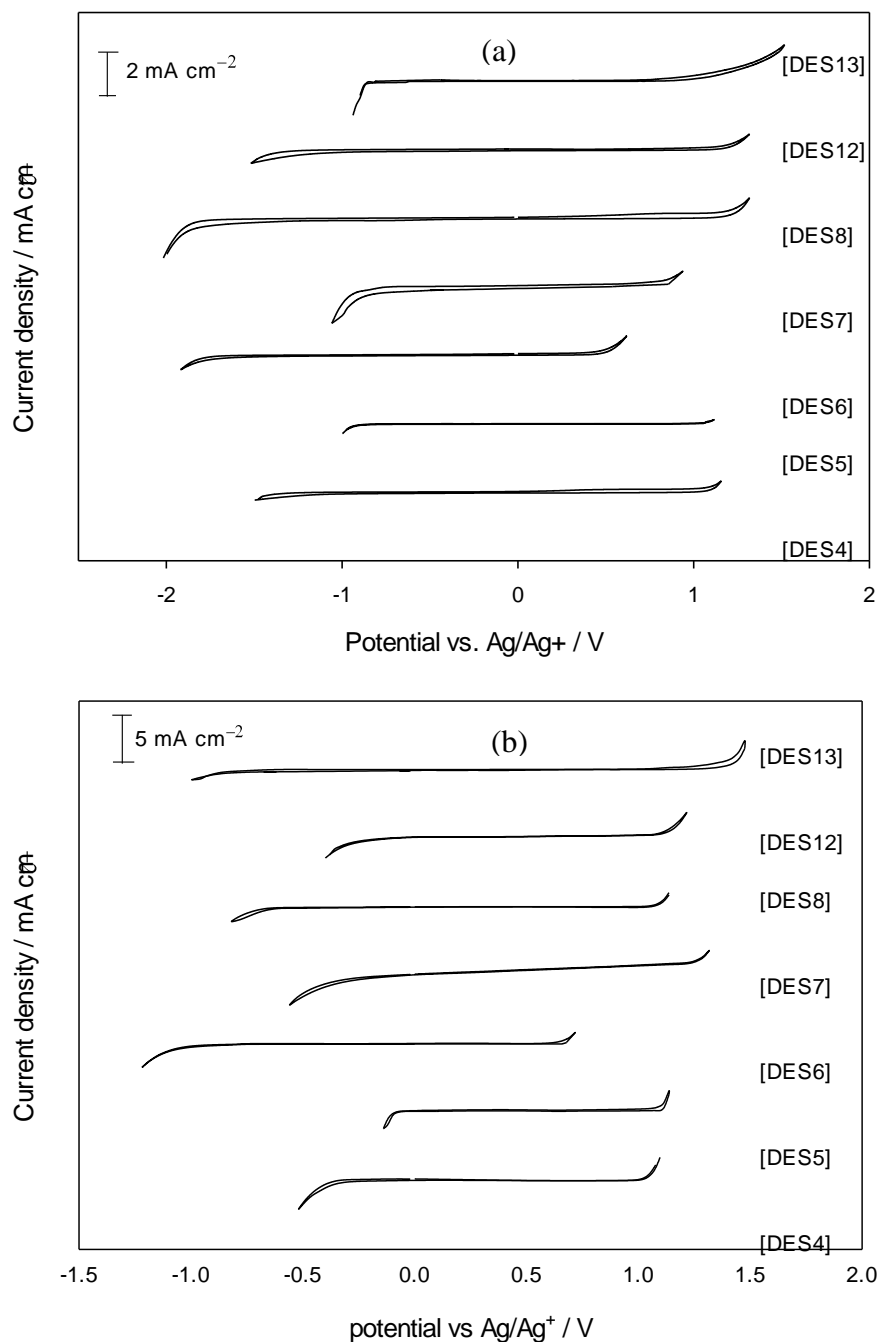


**Figure 4.9:** Electrochemical windows of DESs based on ammonium salts and acids, amine, amide, zinc nitrate HBDs (a) GC working electrode; (b) Pt. microelectrode.

**Table 4.6:** Electrochemical potential windows for the DESs based on ammonium salts and polyol HBDs obtained by means of GC and Pt. electrodes.

DESs	Electrode Material	Anodic limit/ V	Cathodic limit / V	Potential windows
DES1	GC	1.23	-2.13	3.36
	Pt	1.27	-1.21	2.48
DES2	GC	1.31	-2.19	3.50
	Pt	1.28	-1.08	2.36
DES3	GC	1.22	-2.12	3.34
	Pt	1.11	-1.22	2.33
DES4	GC	1.15	-1.49	2.64
	Pt	1.11	-0.51	1.62
DES5	GC	1.11	-0.99	2.10
	Pt	1.14	-0.29	1.43
DES6	GC	0.61	-1.91	2.52
	Pt	0.65	-1.11	1.76
DES7	GC	0.93	-1.09	2.02
	Pt	1.31	-0.55	1.86
DES8	GC	1.31	-2.01	3.32
	Pt	1.13	-0.81	1.94
DES9	GC	1.30	-2.18	3.48
	Pt	1.18	-0.72	1.90
DES10	GC	1.35	-2.17	3.52
	Pt	1.21	-0.90	2.11
DES11	GC	1.26	-2.13	3.39
	Pt	1.19	-0.75	1.94
DES12	GC	1.31	-1.51	2.82
	Pt	1.21	-0.39	1.60
DES13	GC	1.51	-0.91	2.42
	Pt	1.47	-0.97	2.44
DES14	GC	2.67	-3.89	6.65
	Pt	0.79	-1.25	2.04
DES15	GC	1.21	-1.84	3.05
	Pt	0.75	-0.89	1.64
DES16	GC	1.03	-1.63	2.66
	Pt	0.69	-0.96	1.65

Figure 4.8 shows the cathodic potential on the Pt. electrode decreased for the DESs in the order DES1 >DES2 >DES3 when using the choline chloride salt. However, for DESs made with the diethylenethanol ammonium chloride salt the cathodic potential values are similar. Such variations are not seen for the anodic potential.

It needs to be noted that some tested DESs, e.g., DES2, DES9, DES14 have a relatively high reduction limit. This allows the use of these DESs in many important electrochemical processes like the generation of a stable superoxide ion (Hayyan et al., 2012).

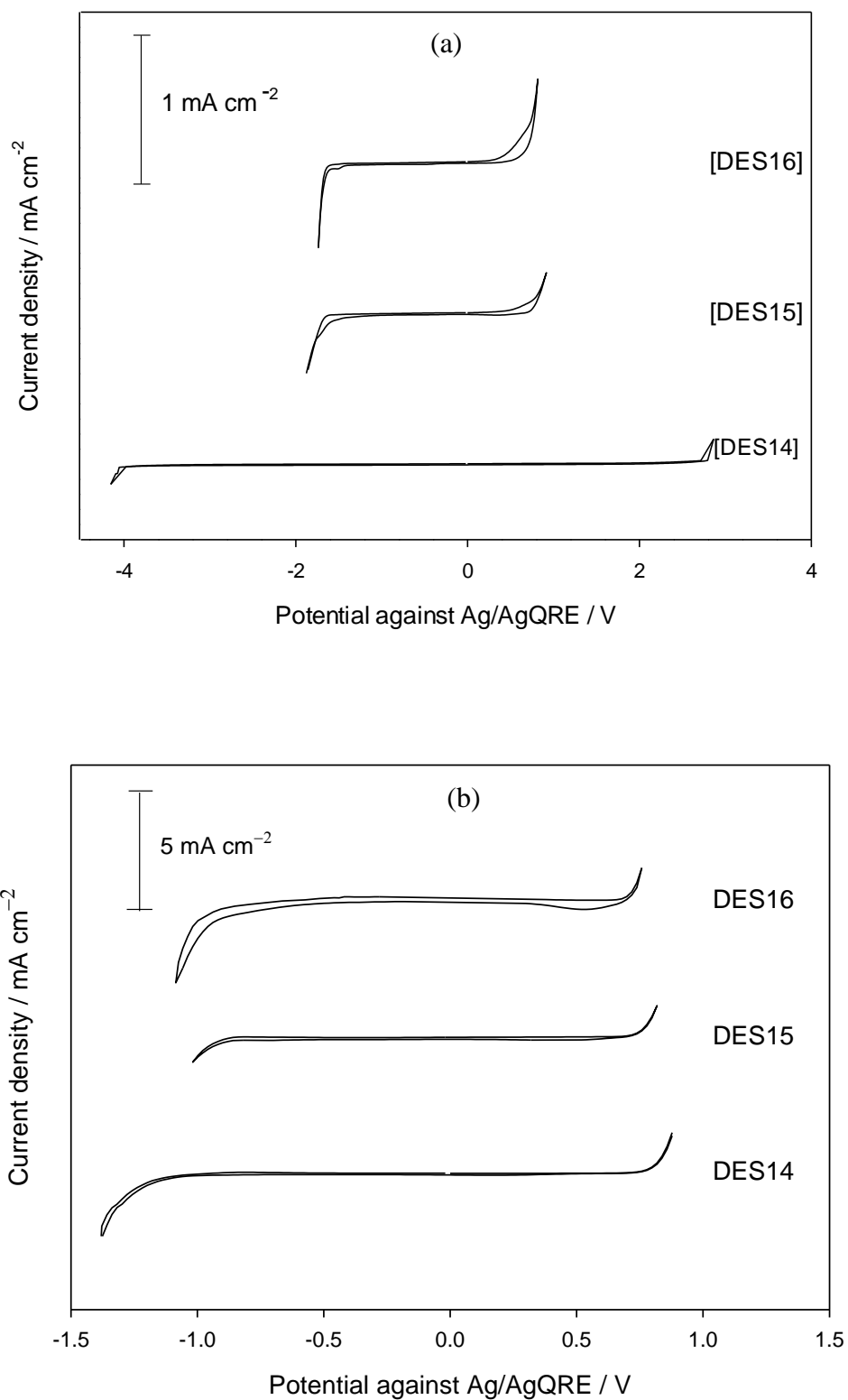
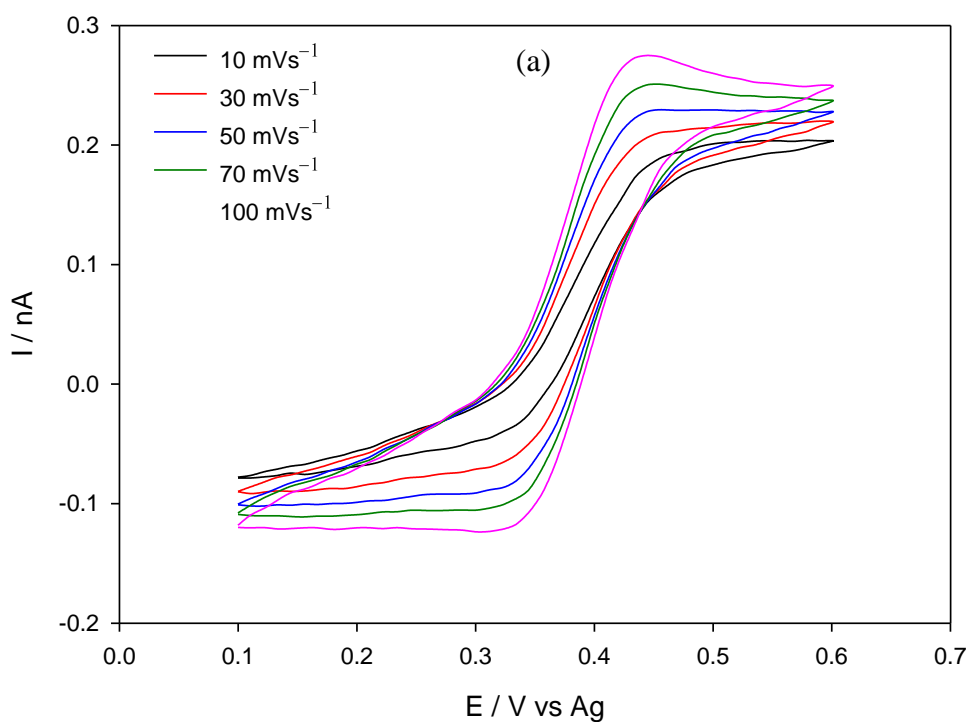
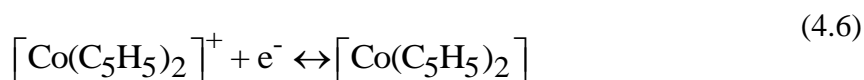
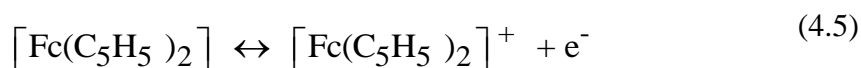


**Figure 4.10:** Electrochemical windows of DESs based on phosphonium based salts and polyol HBDs. (a) GC working electrode; (b) Pt. microelectrode.

## 4.2.2 Cyclic voltammetry for oxidation of Fc and reduction of $Cc^+$ in various DESs

Figure 4.11 shows typical cyclic voltammograms for the oxidation of 5.21 mM solution of Fc and  $Cc^+$  in DES11 on a platinum microelectrode (20  $\mu\text{m}$  diameter) at scan rates ranging from 10 to 100  $\text{mV s}^{-1}$ . The voltammetry is reported against a silver wire quasi-reference electrode and Pt counter electrode. The scan rate dependence indicates that the oxidation of Fc to  $Fc^+$  in DESs follows Equations 4.5 and 4.6.



‘Figure 4.11, continued’

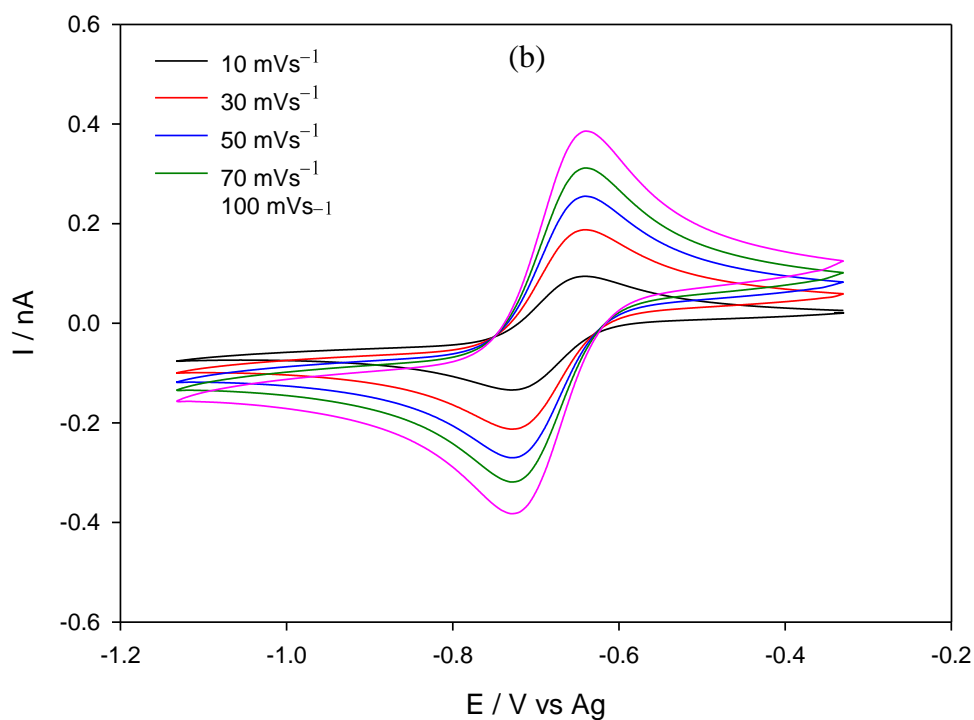


**Figure 4.11:** Cyclic voltammetry for the; (a) oxidation of 5.21 mM Fc; (b) reduction of  $Cc^+$  in DES11 on a Pt electrode (diameter 20  $\mu m$ ) at varying scan rates of 10, 30, 50, 70 and 100  $mV s^{-1}$ .

The quantitative relationship of data in conventional voltammetric experiments of DESs such as values of the reversible half wave potential ( $E_{1/2}$ ) calculated as the average of anodic and cathodic peak potentials ( $(E_{pa} + E_{pc})/2$ ), the peak-to-peak potential separation ( $\Delta E_p = E_{pa} - E_{pc}$ ), the ratio of the peak current for oxidation and reduction components ( $i_{pa}/i_{pc}$ ) and the peak width at half-height ( $W_{1/2}$ ) for both oxidation and reduction processes of Fc in some DESs, are shown in Table 4.7.

**Table 4.7:** Cyclic voltammetric data for oxidation of FC in DESs

DESs	$\nu / (\text{V}\cdot\text{s}^{-1})$	$i_{\text{pa}}/i_{\text{pc}}$	$\Delta E_p / (\text{mV})$	$E_{1/2} / (\text{mV})$	$W_{1/2}(\text{mV})$	
					Oxidized species	Reduced species
DES2	0.01	1.22	80	352	138	145
	0.05	1.05	80	353	148	122
	0.07	1	80	352	155	153
	0.1	1.02	85	352	152	161
	0.5	1.02	95	356	158	177
	1	1.2	96	353	155	149
DES3	0.01	1.06	100	372	138	127
	0.05	1	101	375	159	159
	0.07	1.15	101	376	149	173
	0.1	1.02	103	373	156	158
	0.5	1.2	106	372	155	177
	1	1.24	110	372	163	172
DES10	0.01	1	78	372	140	152
	0.05	1.06	79	377	141	150
	0.07	0.98	81	375	140	149
	0.1	0.96	88	372	143	151
	0.5	1	92	376	139	148
	1	0.98	98	377	140	152
DES11	0.01	0.99	89	389	142	168
	0.05	1.05	89	388	140	148
	0.07	1	89	389	141	155
	0.1	0.98	89	387	139	143
	0.5	1.05	92	394	141	138
	1	0.97	100	398	142	151
DES15	0.01	0.98	70	381	136	117
	0.05	1.02	71	379	139	140
	0.07	1	73	379	144	155
	0.1	0.96	73	383	145	139
	0.5	0.98	80	381	145	158
	1	1.08	80	380	149	148
DES16	0.01	1.12	91	386	147	171
	0.05	1.08	91	388	142	178
	0.07	1.02	91	388	150	176
	0.1	0.98	91	386	153	171
	0.5	0.99	91	386	149	169
	1	0.97	93	386	150	170

In investigated DESs, the cathodic and anodic peak currents increased with increasing scan rate and the peak current ratio of the reverse and the forward scans was close to unity ( $i_{\text{pa}}/i_{\text{pc}}=1.0$ ) and was independent of the scan rate. The peak-to-peak potential separation ( $\Delta E_p$ ) of Fc and  $\text{Cc}^+$  in the cyclic voltammograms, at different scan rates was estimated in the range of 0.06 – 0.1 V. A fast, reversible, one-electron transfer would ideally have a  $\Delta E_p = 0.059$  V at 298 K. The discrepancy from this ideal value at

higher concentrations and scan rates in DESs was attributed to the effect of either slow heterogeneous electron transfer kinetics or the enhanced impact of Ohmic drop as was previously described by other researchers (Zhao et al., 2008, Sukardi et al., 2008, Zhang and Bond, 2003). Also it was observed that for different scan rates the  $E_{1/2}$  and  $W_{1/2}$  remained constant. The redox potential for a couple was better approximated by the half-wave potential ( $E_{1/2}$ ) rather than by the cathodic peak ( $E_{pc}$ ) or anodic peak ( $E_{pa}$ ) potentials, because both  $E_{pa}$  and  $E_{pc}$  change with the scan rates while  $E_{1/2}$  was independent of the scan rate; as was expected for a reversible system.

In consideration of the above, we assumed that the electrochemical reaction of  $Fc/Fc^+$  and  $Cc^+/Cc$  was reversible at the respective scan rates in order to calculate the diffusion coefficients of  $Fc$  and  $Cc^+$ . The peak current was linearly varying with the square root of the scan rate on platinum microelectrode as exhibited in Figure 4.12. This confirms that the process is mainly regulated by the diffusion of  $Fc/Fc^+$  and  $Cc^+/Cc$  in the DESs.

The diffusion coefficients ( $D$ ) have been calculated using the Randles-Sevcik equation (Eq. 4.7) (Randles, 1948), which presumes that mass transport occurs only by a diffusion process and they are shown in Table 4.8. According to the Randles-Sevcik equation,  $i_{pa}$  and  $i_{pc}$  are proportional to  $v^{1/2}$  and hence a plot of  $i_{pa}$  or  $i_{pc}$  versus  $v^{1/2}$  gives a straight line; the slope of which can be used to determine the  $D$ .

$$i_p = 0.4463(nF)^{3/2}(RT)^{-1/2}AD^{1/2}C_0v^{1/2} \quad (4.7)$$

where  $i_p$  is the peak current (A),  $n$  is the number of electron equivalent exchanged during the redox process (electron stoichiometry),  $A$  is the electrode area ( $cm^2$ ),  $D$  is the diffusion coefficient of the electroactive species ( $cm^2 s^{-1}$ ),  $v$  is the voltage scan rate ( $V s^{-1}$ ),  $C_0$  is the bulk concentration of the electroactive species ( $mol cm^{-3}$ ),  $R$  is the universal gas constant,  $T$  is the absolute temperature (K) and  $F$  is Faraday's constant.

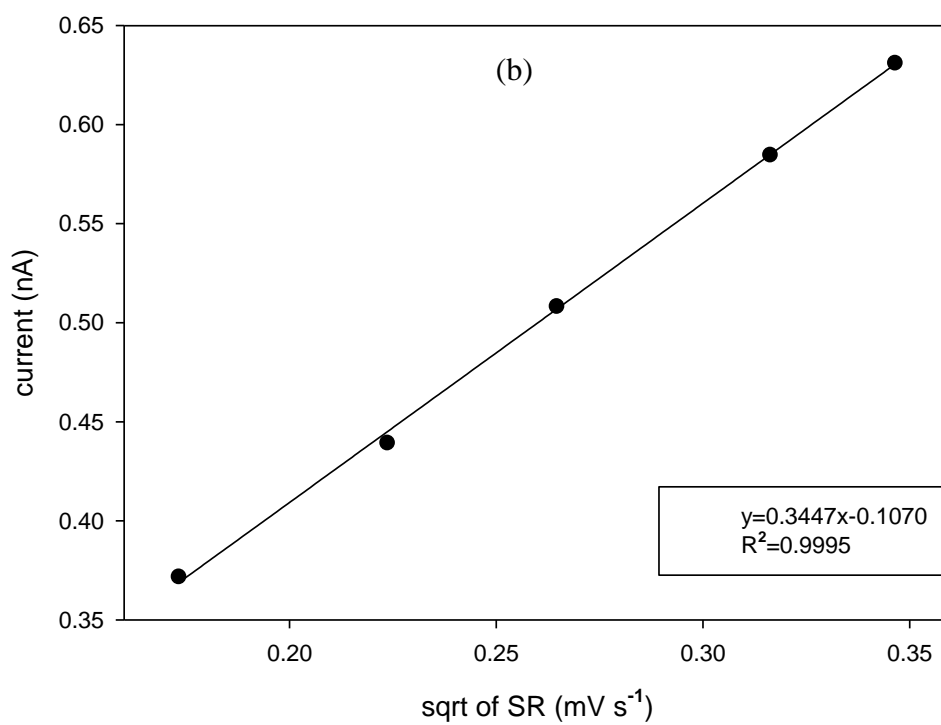
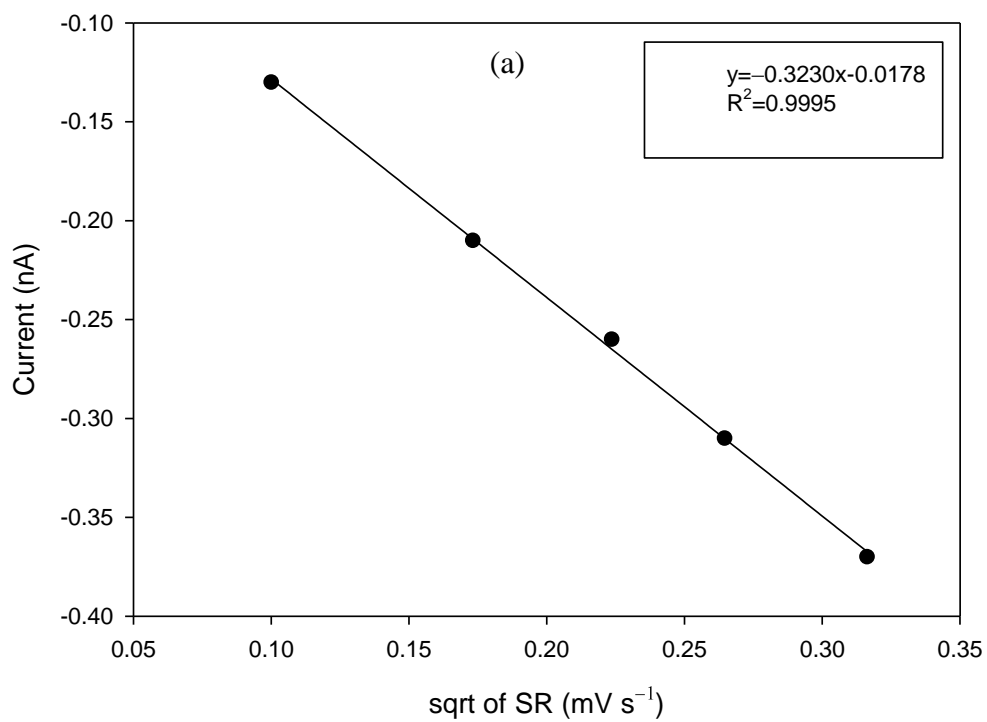


**Figure 4.12:** Linear dependence of peak current vs. square root of scan rates (SR) for; (a) Fc and; (b)  $\text{Cc}^+$  using a Pt electrode in DES11.



### 4.2.3 Chronoamperometric transients of Fc and Cc<sup>+</sup> in DESs

Potential step simulations were first applied to the aqueous one-electron oxidation of Fc to Fc<sup>+</sup> since the  $D$  of both species are well established in the literature (Adams, 1969). Potential step chronoamperometry was conducted using a platinum microelectrode immersed in solutions of Fc and Cc<sup>+</sup> in DESs at various concentrations in order to calculate diffusion coefficients of Fc and Cc<sup>+</sup>. The potential was stepped from 0 to +0.60 V (oxidation of Fc to Fc<sup>+</sup>) and -0.40 to -1 V (reduction of Cc<sup>+</sup> to Cc), and the current was calculated for 5 s. The potential was then stepped back to 0 V (reduction of Fc<sup>+</sup> to Fc) and -0.40 V (oxidation of Cc to Cc<sup>+</sup>), and the current response calculated for a further 5 s. The transient procured is exhibited in Figures 4.15 and 4.17. The  $D$  of both Fc and Cc<sup>+</sup> have been determined using the Cottrell equation (Eq. 4.8). The experimental plots of  $i$  versus  $t^{-1/2}$  with the best fits in order to determine the  $D$  for Fc and Cc<sup>+</sup> were employed (Figure 4.13).

$$i_p = nFACD^{1/2}\pi^{-1/2}t^{-1/2} \quad (4.8)$$

In this equation,  $n$  is the number of electrons,  $A$  is the electrode area (cm<sup>2</sup>),  $F$  is Faraday's constant,  $t$  is time (s) and  $C$  is the bulk concentration (mol cm<sup>-3</sup>).

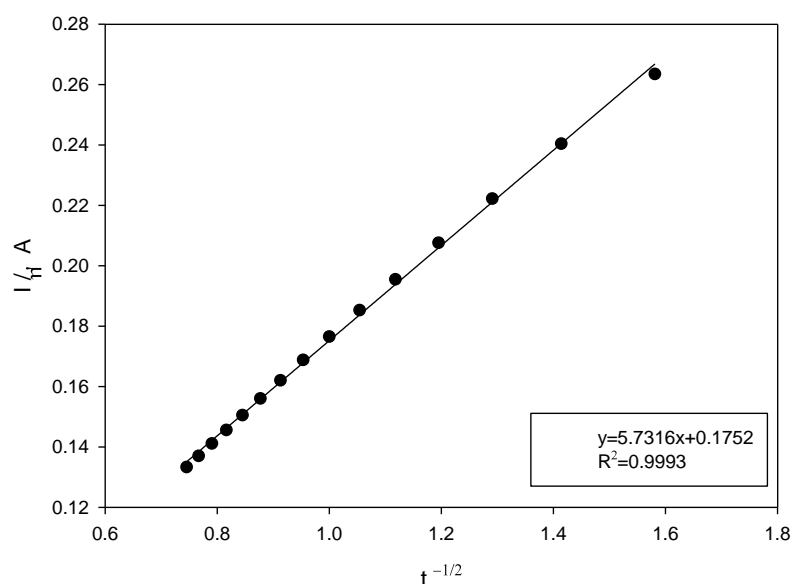


**Figure 4.13:** Cottrell plot for the oxidation of Fc in DES3.

To further support this conclusion and analyse these transients, the data from the first potential step were initially fitted to the analytical Shoup and Szabo expression (Shoup and Szabo, 1982) in order to determine  $D$  for Fc and  $Cc^+$  after inputting values for the concentration and electrode radius. A close fit between the experimental and simulated transients of Fc/Fc<sup>+</sup> and Cc<sup>+</sup>/Cc was achieved, as shown for a typical experimental transient in Figure 4.15. The values for  $D_{Fc}$  and  $D_{Cc}$  using chronoamperometry technique are displayed in Table 4.8. Herein,  $D$  was found to be lower than those determined in organic solvents due to higher viscosities of DESs (Tsierkezos, 2007). However, the  $D$  of Fc reported here are of the same order of magnitude with those of ILs (Zhao et al., 2008, Rogers et al., 2008) and  $D$  of Cc<sup>+</sup> was found to be 10 times lower than those reported by Lewandowski et al. (2013).

#### 4.2.4 The heterogeneous electron-transfer rates for the Fc and Cc<sup>+</sup> in DESs

Nicholson's method (Nicholson, 1965) was the first approach used to evaluate the heterogeneous rate constant ( $k^0$ ). Anodic and cathodic peak separations from a background were subtracted from a voltammogram for a simple one electron transfer reaction and further used to determine  $\psi$  from which ( $k^0$ ) was achieved using Eq. 4.9:

$$\psi = \frac{k^0}{(\pi a D_0)^{1/2}} \quad (4.9)$$

Where  $a = nF\nu/R$ ,  $D_0$  is the diffusion coefficient,  $\nu$  is the scan rate,  $\psi$  is a kinetic parameter and all other symbols have their usual meaning. For this experiment the data has been acquired at 298 K,  $C = 5.21$  mM,  $\nu = 0.1$  V s<sup>-1</sup> and thus linear diffusion was expected to dominate. If  $D$  has been determined, either from cyclic voltammetry for a reversible system or using a suitable chronoamperometric technique,  $k^0$  can be estimated by measuring cyclic voltammograms at various scan rates and fitting the observed variation in peak separation to tabulated values.  $k^0$  of Fc and Cc<sup>+</sup> in DESs were

summarized in Table 4.8. The  $k^0$  calculated for Fc was between  $5.87 \times 10^{-5}$  and  $5.36 \times 10^{-4}$   $\text{cm s}^{-1}$ . Other reports in the literature (Kim et al., 2013, Pan et al., 2012, Matsumiya et al., 2006) showed that  $k^0$  for Fc/Fc<sup>+</sup> was lower in DESs as compared to those in ILs and common organic electrolyte solutions (Matsumiya et al., 2006). It was reported that the  $k^0$  could be correlated to the solution's viscosity. The  $k^0$  calculated for Cc<sup>+</sup> was between  $1.91 \times 10^{-5}$  and  $4.35 \times 10^{-4}$   $\text{cm s}^{-1}$ . As noted by Tsierkezos et al. (2008), studies of the  $k^0$  for the Cc/Cc<sup>+</sup> reaction in organic solvents produced values about 100× higher than those determined in DESs.

**Table 4.8:** Kinetic parameters and  $D$  for Fc/Fc<sup>+</sup> and Cc<sup>+</sup>/Cc in DESs.

Redox species	DES	$D / \text{cm}^2 \text{s}^{-1}$		$k^0 / \text{cm s}^{-1}$
		CV	CA	
Fc/Fc <sup>+</sup>	DES1	$1.68 \times 10^{-8} (\pm 0.03)$	$1.71 \times 10^{-8} (\pm 0.06)$	
	DES2	$4.07 \times 10^{-9} (\pm 0.08)$	$3.96 \times 10^{-9} (\pm 0.09)$	$2.18 \times 10^{-4}$
	DES3	$3.08 \times 10^{-8} (\pm 0.09)$	$3.12 \times 10^{-8} (\pm 0.04)$	$3.08 \times 10^{-4}$
	DES4	$1.23 \times 10^{-9} (\pm 0.03)$	$1.36 \times 10^{-9} (\pm 0.04)$	$9.19 \times 10^{-5}$
	DES5	$3.70 \times 10^{-9} (\pm 0.10)$	$4.05 \times 10^{-9} (\pm 0.08)$	$4.25 \times 10^{-4}$
	DES6	$1.13 \times 10^{-9} (\pm 0.08)$	$1.16 \times 10^{-9} (\pm 0.02)$	$5.87 \times 10^{-5}$
	DES7	$8.54 \times 10^{-9} (\pm 0.04)$	$8.63 \times 10^{-9} (\pm 0.05)$	$3.23 \times 10^{-4}$
	DES8	$3.11 \times 10^{-8} (\pm 0.10)$	$3.32 \times 10^{-8} (\pm 0.05)$	$5.36 \times 10^{-4}$
	DES9	$4.01 \times 10^{-9} (\pm 0.08)$	$4.41 \times 10^{-9} (\pm 0.04)$	$2.31 \times 10^{-4}$
	DES10	$3.25 \times 10^{-9} (\pm 0.03)$	$3.40 \times 10^{-9} (\pm 0.04)$	$1.68 \times 10^{-4}$
	DES11	$3.22 \times 10^{-8} (\pm 0.10)$	$3.95 \times 10^{-8} (\pm 0.02)$	$5.44 \times 10^{-4}$
	DES12	$3.21 \times 10^{-9} (\pm 0.06)$	$3.39 \times 10^{-9} (\pm 0.08)$	$1.72 \times 10^{-4}$
	DES13	$6.24 \times 10^{-9} (\pm 0.02)$	$6.67 \times 10^{-9} (\pm 0.05)$	$2.15 \times 10^{-4}$
	DES14	$3.26 \times 10^{-9} (\pm 0.05)$	$3.76 \times 10^{-9} (\pm 0.07)$	$1.38 \times 10^{-4}$
	DES15	$9.12 \times 10^{-10} (\pm 0.06)$	$8.88 \times 10^{-10} (\pm 0.05)$	$2.09 \times 10^{-4}$
	DES16	$4.56 \times 10^{-9} (\pm 0.06)$	$3.86 \times 10^{-9} (\pm 0.08)$	$1.72 \times 10^{-4}$
Cc <sup>+</sup> /Cc	DES1	$0.60 \times 10^{-8} (\pm 0.09)$	$0.65 \times 10^{-8} (\pm 0.08)$	$1.96 \times 10^{-4}$
	DES2	$3.21 \times 10^{-9} (\pm 0.07)$	$3.26 \times 10^{-9} (\pm 0.04)$	$1.92 \times 10^{-4}$
	DES3	$2.13 \times 10^{-8} (\pm 0.07)$	$2.22 \times 10^{-8} (\pm 0.05)$	$2.68 \times 10^{-4}$
	DES4	$1.03 \times 10^{-9} (\pm 0.03)$	$1.18 \times 10^{-9} (\pm 0.04)$	$7.95 \times 10^{-5}$
	DES5	$2.21 \times 10^{-9} (\pm 0.10)$	$2.66 \times 10^{-9} (\pm 0.08)$	$2.77 \times 10^{-4}$
	DES6	$0.82 \times 10^{-9} (\pm 0.08)$	$0.99 \times 10^{-9} (\pm 0.02)$	$4.99 \times 10^{-5}$
	DES7	$6.36 \times 10^{-9} (\pm 0.04)$	$6.83 \times 10^{-9} (\pm 0.05)$	$2.53 \times 10^{-4}$
	DES8	$2.13 \times 10^{-8} (\pm 0.10)$	$2.56 \times 10^{-8} (\pm 0.05)$	$4.11 \times 10^{-4}$
	DES9	$3.55 \times 10^{-9} (\pm 0.08)$	$3.60 \times 10^{-9} (\pm 0.06)$	$2.15 \times 10^{-4}$
	DES10	$2.98 \times 10^{-9} (\pm 0.08)$	$3.33 \times 10^{-9} (\pm 0.03)$	$1.63 \times 10^{-4}$
	DES11	$2.73 \times 10^{-8} (\pm 0.03)$	$2.89 \times 10^{-8} (\pm 0.04)$	$4.35 \times 10^{-4}$
	DES12	$2.44 \times 10^{-9} (\pm 0.06)$	$3.01 \times 10^{-9} (\pm 0.08)$	$1.02 \times 10^{-4}$
	DES13	$4.80 \times 10^{-9} (\pm 0.02)$	$5.01 \times 10^{-9} (\pm 0.05)$	$1.59 \times 10^{-4}$
	DES14	$2.82 \times 10^{-9} (\pm 0.06)$	$2.85 \times 10^{-9} (\pm 0.05)$	$1.14 \times 10^{-4}$
	DES15	$8.16 \times 10^{-10} (\pm 0.03)$	$8.28 \times 10^{-10} (\pm 0.09)$	$1.91 \times 10^{-5}$
	DES16	$3.68 \times 10^{-9} (\pm 0.08)$	$3.74 \times 10^{-9} (\pm 0.05)$	$1.02 \times 10^{-4}$

#### 4.2.5 Temperature dependence of the voltammetric data, $D$ and $k^0$ for Fc/Fc<sup>+</sup> and Cc<sup>+</sup>/Cc in DESs

Figures 4.14 indicate typical cyclic voltammograms for oxidation of Fc and reduction of Cc<sup>+</sup> in DES1, respectively, which are obtained from individually prepared 10 mM solutions in the temperature range 298–348 K. The voltammetric data of Fc and Cc<sup>+</sup> is summarized in Table 4.9. Fc and Cc<sup>+</sup> exhibit reversible reactions in all of the investigated DESs (according to the section 4.2.2). Figure 4.14 shows the anodic and cathodic peak current had increased substantially with increasing temperature for oxidation of Fc and reduction of Cc<sup>+</sup>, respectively. The peak potential separation ( $\Delta E_p$ ) was found to be in the range between 0.062 - 0.096 V for Fc and 0.063 - 0.1 V for Cc<sup>+</sup> (Table 4.9). It is observed in all cases that  $\Delta E_p$  decreases with increasing temperature and this at least partly reflects the faster electron kinetics. For DESs, the  $\Delta E_p$  was found to be higher than the theoretical value ( $\Delta E_p = 0.059$  V), attributing to the effect of either slow heterogeneous electron transfer kinetics or the enhanced impact of ohmic drop as was previously described by other researchers. Reversible kinetics was assumed for both Fc and Cc<sup>+</sup> following a similar presumption from work reported in the literature (Zhao et al., 2006, Sukardi et al., 2006).

Influential drifts in potential were perceived for the AgQRE wire dipped directly in DESs including electroactive compounds. Nevertheless, separation of Ag wire immersed in DESs from the bulk solution by means of a glass frit impeded this drift in potential. The  $E_{1/2}$  data inclined to decrease with the rise of temperature. Moreover, the  $E_{1/2}$  values changed significantly for different DESs at a given temperatures. It was demonstrated that  $E_{1/2}$  shifted toward more negative potentials for the oxidation of Fc and more positive potentials for the reduction of Cc<sup>+</sup> in DESs. The shift of  $E_{1/2}$  could be illustrated by donor-acceptor Lewis-type interactions (Keita et al., 1988).

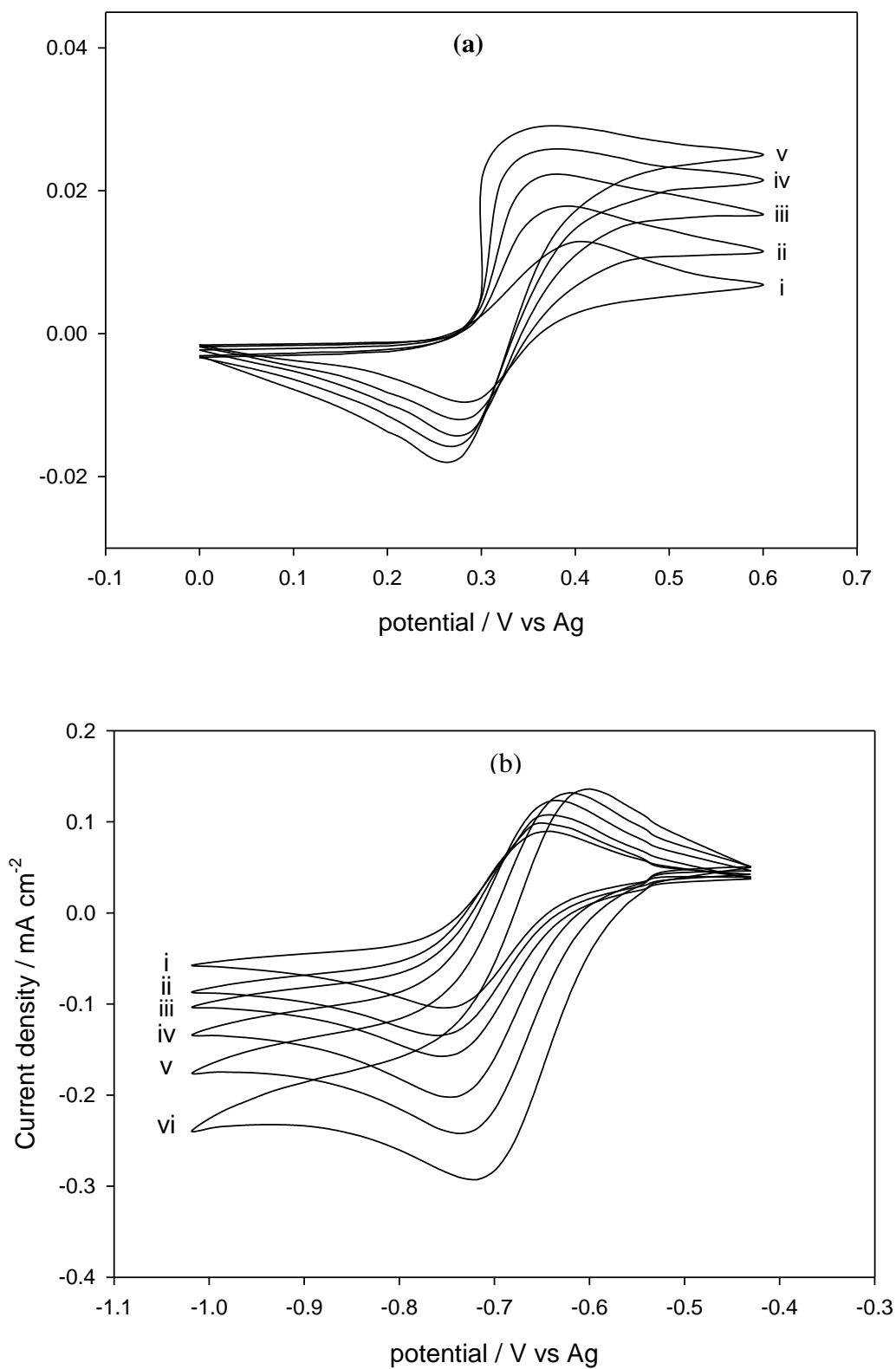


**Figure 4.14:** Cyclic voltammetry for; (a) oxidation of Fc and; (b) reduction of Cc<sup>+</sup> in the DES1 at varying temperatures of (i) 298 K, (ii) 308 K, (iii) 318 K, (iv) 328 K, (v) 338 K and (vi) 348 K, at 100 mV s<sup>-1</sup>.

**Table 4.9:** Experimental voltammetric data for Fc/Fc<sup>+</sup> and Cc<sup>+</sup>/Cc in DESs at different operating temperatures.

DESs	T/K	Fc/Fc <sup>+</sup>						Cc <sup>+</sup> /Cc					
		$j_{pa}/\text{mA cm}^{-2}$	$j_{pc}/\text{mA cm}^{-2}$	$E_{pa}/\text{V}$	$E_{pc}/\text{V}$	$\Delta E_p/\text{V}$	$E_{1/2}/\text{V}$	$j_{pa}/\text{mA cm}^{-2}$	$j_{pc}/\text{mA cm}^{-2}$	$E_{pa}/\text{V}$	$E_{pc}/\text{V}$	$\Delta E_p/\text{V}$	$E_{1/2}/\text{V}$
DES1	308	0.017	-0.012	0.375	0.282	0.093	0.328	0.097	-0.129	-0.659	-0.758	0.099	-0.708
	318	0.021	-0.015	0.360	0.275	0.085	0.317	0.107	-0.154	-0.649	-0.749	0.100	-0.699
	328	0.025	-0.016	0.350	0.269	0.081	0.309	0.136	-0.201	-0.639	-0.738	0.099	-0.688
	338	0.028	-0.018	0.341	0.265	0.076	0.303	0.145	-0.232	-0.619	-0.718	0.099	-0.668
DES2	308	0.035	-0.022	0.402	0.322	0.080	0.362	0.132	-0.162	-0.618	-0.710	0.092	-0.664
	318	0.040	-0.024	0.389	0.314	0.075	0.351	0.140	-0.187	-0.599	-0.685	0.086	-0.642
	328	0.043	-0.025	0.380	0.306	0.074	0.343	0.148	-0.231	-0.587	-0.666	0.079	-0.626
	338	0.047	-0.027	0.372	0.301	0.071	0.336	0.156	-0.259	-0.581	-0.654	0.073	-0.617
DES3	308	0.093	-0.076	0.417	0.321	0.096	0.369	0.087	-0.097	-0.665	-0.757	0.092	-0.711
	318	0.98	-0.079	0.411	0.319	0.092	0.365	0.096	-0.126	-0.654	-0.746	0.092	-0.700
	328	0.104	-0.083	0.400	0.314	0.086	0.357	0.111	-0.147	-0.643	-0.732	0.089	-0.687
	338	0.111	-0.086	0.388	0.306	0.082	0.347	0.124	-0.162	-0.631	-0.717	0.086	-0.674
DES9	308	0.026	-0.019	0.411	0.318	0.093	0.380	0.148	-0.183	-0.624	-0.722	0.098	-0.673
	318	0.031	-0.021	0.401	0.316	0.085	0.373	0.153	-0.192	-0.615	-0.711	0.096	-0.663
	328	0.035	-0.024	0.393	0.313	0.080	0.362	0.158	-0.221	-0.602	-0.694	0.092	-0.648
	338	0.038	-0.027	0.385	0.311	0.074	0.358	0.162	-0.245	-0.586	-0.673	0.087	-0.629
DES10	308	0.062	-0.048	0.416	0.330	0.086	0.373	0.116	-0.138	-0.653	-0.747	0.094	-0.700
	318	0.067	-0.052	0.406	0.323	0.083	0.364	0.124	-0.159	-0.642	-0.732	0.090	-0.687
	328	0.075	-0.055	0.395	0.313	0.082	0.354	0.132	-0.182	-0.633	-0.717	0.084	-0.675
	338	0.081	-0.059	0.388	0.309	0.079	0.348	0.141	-0.218	-0.618	-0.698	0.080	-0.658
DES11	308	0.071	0.061	0.421	0.339	0.082	0.380	0.096	-0.129	-0.648	-0.746	0.098	-0.697
	318	0.079	0.063	0.411	0.336	0.075	0.373	0.098	-0.138	-0.640	-0.733	0.093	-0.686
	328	0.088	0.066	0.398	0.327	0.071	0.362	0.103	-0.156	-0.635	-0.725	0.090	-0.680
	338	0.096	0.069	0.390	0.326	0.064	0.358	0.105	-0.188	-0.628	-0.716	0.088	-0.672
DES14	308	0.021	-0.013	0.421	0.325	0.096	0.373	0.146	-0.203	-0.655	-0.724	0.069	-0.689
	318	0.027	-0.017	0.411	0.319	0.092	0.365	0.192	-0.247	-0.648	-0.715	0.067	-0.681
	328	0.030	-0.020	0.401	0.312	0.089	0.356	0.223	-0.291	-0.641	-0.706	0.065	-0.673
	338	0.035	-0.024	0.392	0.306	0.086	0.349	0.258	-0.342	-0.637	-0.700	0.063	-0.668

'Table 4.9, continued'

DESs	T/K	Fc/Fc <sup>+</sup>						Cc <sup>+</sup> /Cc					
		$j_{pa}/\text{mA cm}^{-2}$	$j_{pc}/\text{mA cm}^{-2}$	$E_{pa}/\text{V}$	$E_{pc}/\text{V}$	$\Delta E_p/\text{V}$	$E_{1/2}/\text{V}$	$j_{pa}/\text{mA cm}^{-2}$	$j_{pc}/\text{mA cm}^{-2}$	$E_{pa}/\text{V}$	$E_{pc}/\text{V}$	$\Delta E_p/\text{V}$	$E_{1/2}/\text{V}$
DES15	308	0.028	-0.023	0.409	0.338	0.071	0.373	0.203	-0.246	-0.641	-0.736	0.095	-0.688
	318	0.035	-0.025	0.398	0.330	0.068	0.364	0.235	-0.302	-0.635	-0.727	0.092	-0.681
	328	0.046	-0.028	0.389	0.323	0.066	0.356	0.258	-0.333	-0.629	-0.718	0.089	-0.673
	338	0.052	-0.031	0.381	0.319	0.062	0.350	0.297	-0.389	-0.621	-0.709	0.088	-0.665
DES16	308	0.110	-0.092	0.425	0.334	0.091	0.379	0.339	-0.362	-0.652	-0.744	0.092	-0.698
	318	0.131	-0.125	0.419	0.331	0.088	0.375	0.351	-0.403	-0.649	-0.738	0.089	-0.693
	328	0.159	-0.142	0.411	0.325	0.086	0.368	0.379	-0.456	-0.638	-0.725	0.087	-0.681
	338	0.171	-0.161	0.405	0.320	0.085	0.362	0.402	-0.509	-0.634	-0.717	0.083	-0.675

The diffusion coefficient of both the Fc/Fc<sup>+</sup> and Cc<sup>+</sup>/Cc redox couples in DESs at different temperatures were determined through analysis of double chronoamperometric measurements conducted at Pt. microelectrodes. Figure 4.15 shows the best theoretical fit (o) to the experimental double potential step chronoamperograms (–) for the Fc/Fc<sup>+</sup> and Cc<sup>+</sup>/Cc redox couples at 293, 298, 303, 308, 313, and 318 K in DES1. The limiting currents of the first step incline regularly and the trend of the second step becomes slightly less steep as the temperature increases in both Fc and Cc<sup>+</sup>. It is reasonably established that  $D_{Fc}$  and  $D_{Cc^+}$  improves with increasing temperature in DESs (Table 4.10). The  $D$  of the electroactive species have been analyzed in terms of the Arrhenius exponential function of the temperature following the Eq:

$$D = D_0 \exp\left(\frac{-E_D}{RT}\right) \quad (4.10)$$

Where  $D_0$  is a constant corresponding to the hypothetical diffusion coefficient at infinite temperature, and  $E_D$  is the diffusional activation energy of the electroactive species.

Plot of  $\ln D$  against  $1/T$  resulted in a straight line and from the slope the activation energy for diffusion,  $E_D$ , was determined as shown in Figure 4.16 (least-squares correlation coefficient,  $R^2 > 0.98$  for Fc and Cc<sup>+</sup>). The calculated  $E_D$  for each sample is summarized in Table 4.11, which compares well with the value determined for the  $E_\eta$  in DESs and corresponds well to that observed in the literature for ILs (Rogers et al., 2008). The activation energies increased systematically with increasing viscosity in DESs. A slight deviation for activation energies of  $D_{Cc^+}$  is observed, which may be due to impeded diffusion of the reduced species as a result of stronger solvation by the DES.



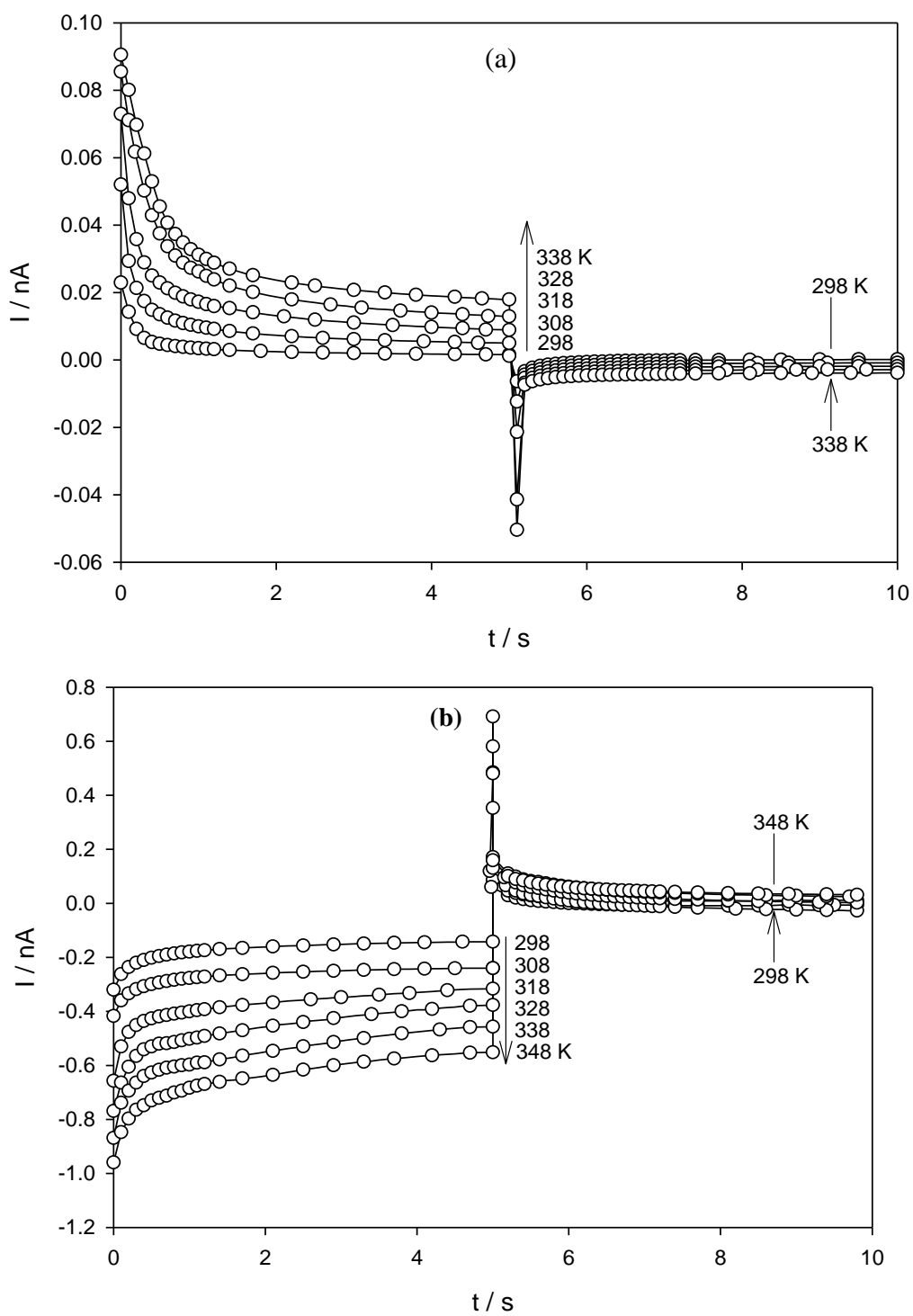


**Figure 4.15:** Double potential step chronoamperometry measured; (a) on the DES1 across the  $\text{Fc}/\text{Fc}^+$ ; (b) on the DES11 across the  $\text{Cc}^+/\text{Cc}$  at temperatures of 298, 308, 318 and 338 K.

**Table 4.10:** Temperature dependence of kinetic parameters and diffusion coefficients for Fc/Fc<sup>+</sup> and Cc<sup>+</sup>/Cc in DESs.

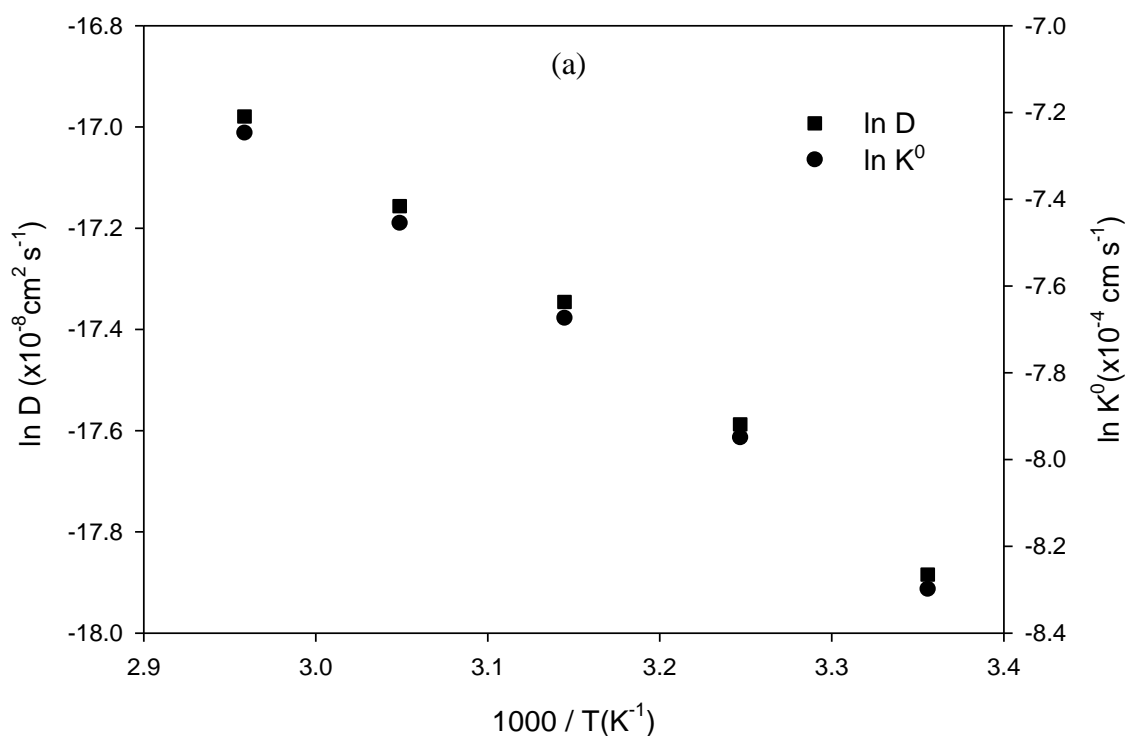
DESs	T/K	$D_{Fc}/\text{cm}^2\text{s}^{-1}$	$D_{Cc^+}/\text{cm}^2\text{s}^{-1}$	$k_{Fc}^0/\text{cm s}^{-1}$	$k_{Cc^+}^0/\text{cm s}^{-1}$
DES1	308	$2.30\times 10^{-8}(\pm 0.03)$	$1.06\times 10^{-8}(\pm 0.07)$	$3.53\times 10^{-4}(\pm 0.07)$	$3.61\times 10^{-4}(\pm 0.06)$
	318	$2.93\times 10^{-8}(\pm 0.05)$	$1.52\times 10^{-8}(\pm 0.04)$	$4.65\times 10^{-4}(\pm 0.08)$	$5.80\times 10^{-4}(\pm 0.06)$
	328	$3.54\times 10^{-8}(\pm 0.08)$	$2.04\times 10^{-8}(\pm 0.06)$	$5.79\times 10^{-4}(\pm 0.09)$	$8.83\times 10^{-4}(\pm 0.05)$
	338	$4.23\times 10^{-8}(\pm 0.04)$	$2.63\times 10^{-8}(\pm 0.03)$	$7.12\times 10^{-4}(\pm 0.05)$	$1.25\times 10^{-3}(\pm 0.04)$
DES2	308	$4.77\times 10^{-9}(\pm 0.05)$	$4.12\times 10^{-9}(\pm 0.07)$	$3.44\times 10^{-4}(\pm 0.07)$	$3.00\times 10^{-4}(\pm 0.08)$
	318	$5.46\times 10^{-9}(\pm 0.09)$	$4.98\times 10^{-9}(\pm 0.05)$	$4.73\times 10^{-4}(\pm 0.04)$	$4.16\times 10^{-4}(\pm 0.07)$
	328	$6.08\times 10^{-9}(\pm 0.06)$	$5.88\times 10^{-9}(\pm 0.08)$	$5.94\times 10^{-4}(\pm 0.04)$	$5.48\times 10^{-4}(\pm 0.08)$
	338	$6.86\times 10^{-9}(\pm 0.08)$	$6.88\times 10^{-9}(\pm 0.07)$	$7.89\times 10^{-4}(\pm 0.06)$	$7.23\times 10^{-4}(\pm 0.05)$
DES3	308	$3.48\times 10^{-8}(\pm 0.02)$	$2.60\times 10^{-8}(\pm 0.09)$	$5.99\times 10^{-4}(\pm 0.05)$	$5.37\times 10^{-4}(\pm 0.07)$
	318	$3.94\times 10^{-8}(\pm 0.04)$	$3.06\times 10^{-8}(\pm 0.02)$	$1.16\times 10^{-3}(\pm 0.08)$	$1.07\times 10^{-3}(\pm 0.03)$
	328	$4.38\times 10^{-8}(\pm 0.05)$	$3.56\times 10^{-8}(\pm 0.06)$	$2.21\times 10^{-3}(\pm 0.06)$	$2.11\times 10^{-3}(\pm 0.06)$
	338	$4.92\times 10^{-8}(\pm 0.04)$	$4.11\times 10^{-8}(\pm 0.06)$	$4.73\times 10^{-3}(\pm 0.07)$	$3.96\times 10^{-3}(\pm 0.07)$
DES9	308	$5.66\times 10^{-9}(\pm 0.09)$	$4.95\times 10^{-9}(\pm 0.07)$	$2.96\times 10^{-4}(\pm 0.07)$	$2.63\times 10^{-4}(\pm 0.06)$
	318	$6.85\times 10^{-9}(\pm 0.07)$	$6.37\times 10^{-9}(\pm 0.05)$	$3.59\times 10^{-4}(\pm 0.06)$	$3.13\times 10^{-4}(\pm 0.06)$
	328	$7.83\times 10^{-9}(\pm 0.04)$	$7.68\times 10^{-9}(\pm 0.08)$	$4.07\times 10^{-4}(\pm 0.05)$	$3.56\times 10^{-4}(\pm 0.08)$
	338	$9.00\times 10^{-9}(\pm 0.09)$	$9.22\times 10^{-9}(\pm 0.04)$	$4.61\times 10^{-4}(\pm 0.07)$	$4.01\times 10^{-4}(\pm 0.08)$
DES10	308	$4.14\times 10^{-9}(\pm 0.06)$	$4.43\times 10^{-9}(\pm 0.08)$	$2.51\times 10^{-4}(\pm 0.04)$	$2.42\times 10^{-4}(\pm 0.04)$
	318	$5.37\times 10^{-9}(\pm 0.07)$	$5.53\times 10^{-9}(\pm 0.06)$	$3.54\times 10^{-4}(\pm 0.05)$	$3.29\times 10^{-4}(\pm 0.03)$
	328	$6.65\times 10^{-9}(\pm 0.02)$	$6.71\times 10^{-9}(\pm 0.08)$	$4.70\times 10^{-4}(\pm 0.08)$	$4.35\times 10^{-4}(\pm 0.07)$
	338	$8.26\times 10^{-9}(\pm 0.04)$	$7.83\times 10^{-9}(\pm 0.05)$	$6.32\times 10^{-4}(\pm 0.06)$	$5.47\times 10^{-4}(\pm 0.06)$
DES11	308	$3.65\times 10^{-8}(\pm 0.04)$	$3.38\times 10^{-8}(\pm 0.04)$	$6.58\times 10^{-4}(\pm 0.07)$	$5.56\times 10^{-4}(\pm 0.08)$
	318	$3.99\times 10^{-8}(\pm 0.09)$	$3.84\times 10^{-8}(\pm 0.07)$	$7.69\times 10^{-4}(\pm 0.04)$	$6.85\times 10^{-4}(\pm 0.07)$
	328	$4.38\times 10^{-8}(\pm 0.06)$	$4.25\times 10^{-8}(\pm 0.05)$	$9.23\times 10^{-4}(\pm 0.05)$	$8.13\times 10^{-4}(\pm 0.06)$
	338	$4.82\times 10^{-8}(\pm 0.07)$	$4.84\times 10^{-8}(\pm 0.06)$	$1.14\times 10^{-3}(\pm 0.06)$	$1.02\times 10^{-3}(\pm 0.08)$
DES14	308	$4.23\times 10^{-9}(\pm 0.04)$	$3.69\times 10^{-9}(\pm 0.08)$	$2.58\times 10^{-4}(\pm 0.06)$	$3.21\times 10^{-4}(\pm 0.08)$
	318	$4.54\times 10^{-9}(\pm 0.08)$	$4.21\times 10^{-9}(\pm 0.07)$	$3.14\times 10^{-4}(\pm 0.05)$	$3.96\times 10^{-4}(\pm 0.07)$
	328	$5.20\times 10^{-9}(\pm 0.06)$	$4.76\times 10^{-9}(\pm 0.05)$	$5.27\times 10^{-4}(\pm 0.08)$	$4.08\times 10^{-4}(\pm 0.09)$
	338	$5.63\times 10^{-9}(\pm 0.09)$	$5.24\times 10^{-9}(\pm 0.04)$	$6.56\times 10^{-4}(\pm 0.09)$	$4.97\times 10^{-4}(\pm 0.06)$
DES15	308	$9.92\times 10^{-10}(\pm 0.06)$	$9.22\times 10^{-10}(\pm 0.08)$	$4.38\times 10^{-5}(\pm 0.05)$	$2.42\times 10^{-5}(\pm 0.08)$
	318	$1.38\times 10^{-9}(\pm 0.09)$	$1.98\times 10^{-9}(\pm 0.05)$	$5.16\times 10^{-5}(\pm 0.04)$	$4.53\times 10^{-5}(\pm 0.05)$
	328	$2.12\times 10^{-9}(\pm 0.07)$	$2.12\times 10^{-9}(\pm 0.06)$	$5.56\times 10^{-5}(\pm 0.09)$	$5.32\times 10^{-5}(\pm 0.08)$
	338	$2.86\times 10^{-9}(\pm 0.05)$	$2.66\times 10^{-9}(\pm 0.05)$	$5.96\times 10^{-5}(\pm 0.07)$	$6.12\times 10^{-5}(\pm 0.09)$
DES16	308	$4.92\times 10^{-9}(\pm 0.07)$	$4.56\times 10^{-9}(\pm 0.06)$	$3.88\times 10^{-4}(\pm 0.06)$	$2.56\times 10^{-4}(\pm 0.06)$
	318	$5.53\times 10^{-9}(\pm 0.05)$	$5.02\times 10^{-9}(\pm 0.09)$	$5.68\times 10^{-4}(\pm 0.08)$	$4.56\times 10^{-4}(\pm 0.08)$
	328	$6.12\times 10^{-9}(\pm 0.04)$	$5.51\times 10^{-9}(\pm 0.06)$	$7.43\times 10^{-4}(\pm 0.05)$	$6.31\times 10^{-4}(\pm 0.05)$
	338	$6.65\times 10^{-9}(\pm 0.08)$	$6.28\times 10^{-9}(\pm 0.07)$	$8.96\times 10^{-4}(\pm 0.05)$	$7.84\times 10^{-4}(\pm 0.05)$

Table 4.10 shows that the rate constants of Fc and Cc<sup>+</sup> increased with temperature, and Figure 4.16 displays an Arrhenius relationship for the obtained  $k^0$  values for Fc in DES1 and Cc<sup>+</sup> for DES11, respectively. Nearly identical slopes were established in the  $D$  and  $k^0$  Arrhenius plots for selected DESs. From these plots, the

activation energy of rate constants for Fc and Cc<sup>+</sup> were determined, which are listed in Table 4.11.

**Table 4.11:** Activation energies of the diffusion coefficients and rate constants for Fc/Fc<sup>+</sup> and Cc<sup>+</sup>/Cc in studied DESs.

DESs	$E_D(\text{Fc}) / \text{kJ mol}^{-1}$	$E_D(\text{Cc}^+) / \text{kJ mol}^{-1}$	$E_k^0(\text{Fc}) / \text{kJ mol}^{-1}$	$E_k^0(\text{Cc}^+) / \text{kJ mol}^{-1}$
DES1	22.82	21.97	21.81	26.62
DES2	27.01	28.52	25.20	30.33
DES3	21.65	21.04	19.63	20.57
DES9	24.73	25.50	22.18	28.02
DES10	29.68	30.88	27.51	36.29
DES11	20.08	17.57	15.15	17.44
DES14	28.36	29.45	26.30	31.48
DES15	49.35	52.32	38.23	58.41
DES16	24.05	22.93	22.07	27.63



‘Figure 4.16, continued’

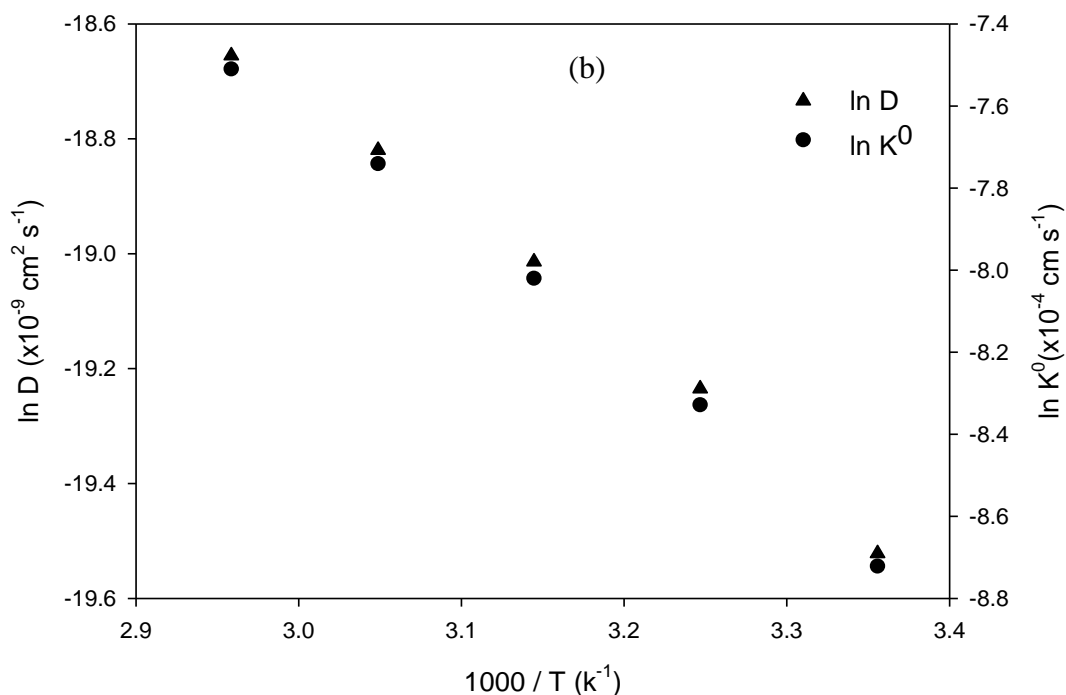


**Figure 4.16:** Dependence of diffusion and rate constant on temperature using Arrhenius rule for; (a) Fc/Fc<sup>+</sup> in DES1 and; (b) Cc<sup>+</sup>/Cc in DES11

#### 4.2.6 Concentration dependence of $D$ of Fc/Fc<sup>+</sup>

Data obtained for  $D_{Fc}$  from both cyclic voltammetry and chronoamperometry at various concentrations are presented in Table 4.12. Figure 4.17 shows potential step chronoamperometry for the oxidation of Fc at concentrations of 1.08, 5.21, 10.13, 20.18 and 30.06 mM in DESs on a 20  $\mu\text{m}$  diameter platinum electrode. The potential was stepped from 0.0 V (no Faradaic current) to 0.6 V vs. Ag wire QRE to oxidize the Fc to Fc<sup>+</sup>. The experimental data (–) fits the simulation data (o) well, referring to the fitting procedure indicated in the experimental section. Typical cyclic voltammetry was undertaken at a range of concentrations of Fc in DESs to determine  $D$  for Fc as a function of concentration. As expected, the peak current due to Fc oxidation increased with increasing concentration. However, the  $D$  of Fc did not change considerably. As can be seen, the ratio of  $D$  from both experimental techniques remained constant

throughout the whole concentration range showing that the diffusion coefficient was independent of the concentration in DESs.

**Table 4.12:** Concentration dependent of the diffusion coefficients of Fc in DESs solution

DESs	Concentration (mM)	$D_{CV}$ ( $\text{cm}^2 \text{s}^{-1}$ )	$D_{CA}$ ( $\text{cm}^2 \text{s}^{-1}$ )
DES1	1.08	$4.54 \times 10^{-9} (\pm 0.08)$	$4.30 \times 10^{-9} (\pm 0.05)$
	5.21	$4.32 \times 10^{-9} (\pm 0.10)$	$4.21 \times 10^{-9} (\pm 0.03)$
	10.13	$4.56 \times 10^{-9} (\pm 0.06)$	$3.86 \times 10^{-9} (\pm 0.08)$
	20.18	$4.23 \times 10^{-9} (\pm 0.04)$	$4.33 \times 10^{-9} (\pm 0.06)$
	30.06	$4.02 \times 10^{-9} (\pm 0.08)$	$4.36 \times 10^{-9} (\pm 0.08)$
DES2	1.08	$9.42 \times 10^{-10} (\pm 0.07)$	$8.65 \times 10^{-10} (\pm 0.04)$
	5.21	$8.96 \times 10^{-10} (\pm 0.05)$	$8.96 \times 10^{-10} (\pm 0.05)$
	10.13	$9.12 \times 10^{-10} (\pm 0.06)$	$8.88 \times 10^{-10} (\pm 0.05)$
	20.18	$9.03 \times 10^{-10} (\pm 0.08)$	$8.62 \times 10^{-10} (\pm 0.03)$
	30.06	$9.86 \times 10^{-10} (\pm 0.06)$	$8.49 \times 10^{-10} (\pm 0.10)$
DES3	1.08	$2.94 \times 10^{-8} (\pm 0.06)$	$3.46 \times 10^{-8} (\pm 0.06)$
	5.21	$3.11 \times 10^{-8} (\pm 0.10)$	$3.32 \times 10^{-8} (\pm 0.05)$
	10.13	$3.08 \times 10^{-8} (\pm 0.09)$	$3.12 \times 10^{-8} (\pm 0.04)$
	20.18	$3.22 \times 10^{-8} (\pm 0.08)$	$3.39 \times 10^{-8} (\pm 0.08)$
	30.06	$3.19 \times 10^{-8} (\pm 0.04)$	$2.98 \times 10^{-8} (\pm 0.08)$
DES9	1.08	$4.01 \times 10^{-9} (\pm 0.09)$	$3.82 \times 10^{-9} (\pm 0.10)$
	5.21	$3.90 \times 10^{-9} (\pm 0.10)$	$4.13 \times 10^{-9} (\pm 0.10)$
	10.13	$4.07 \times 10^{-9} (\pm 0.08)$	$3.96 \times 10^{-9} (\pm 0.09)$
	20.18	$3.96 \times 10^{-9} (\pm 0.04)$	$4.12 \times 10^{-9} (\pm 0.05)$
	30.06	$3.86 \times 10^{-9} (\pm 0.07)$	$4.08 \times 10^{-9} (\pm 0.05)$
DES10	1.08	$2.98 \times 10^{-8} (\pm 0.08)$	$4.01 \times 10^{-8} (\pm 0.03)$
	5.21	$3.20 \times 10^{-8} (\pm 0.05)$	$4.22 \times 10^{-8} (\pm 0.04)$
	10.13	$3.22 \times 10^{-8} (\pm 0.10)$	$3.95 \times 10^{-8} (\pm 0.02)$
	20.18	$3.26 \times 10^{-8} (\pm 0.06)$	$4.16 \times 10^{-8} (\pm 0.02)$
	30.06	$3.25 \times 10^{-8} (\pm 0.08)$	$3.89 \times 10^{-8} (\pm 0.08)$
DES11	1.08	$2.80 \times 10^{-9} (\pm 0.08)$	$3.65 \times 10^{-9} (\pm 0.06)$
	5.21	$3.08 \times 10^{-9} (\pm 0.09)$	$3.55 \times 10^{-9} (\pm 0.08)$
	10.13	$3.25 \times 10^{-9} (\pm 0.03)$	$3.40 \times 10^{-9} (\pm 0.04)$
	20.18	$2.97 \times 10^{-9} (\pm 0.08)$	$3.86 \times 10^{-9} (\pm 0.04)$
	30.06	$3.02 \times 10^{-9} (\pm 0.09)$	$3.93 \times 10^{-9} (\pm 0.03)$

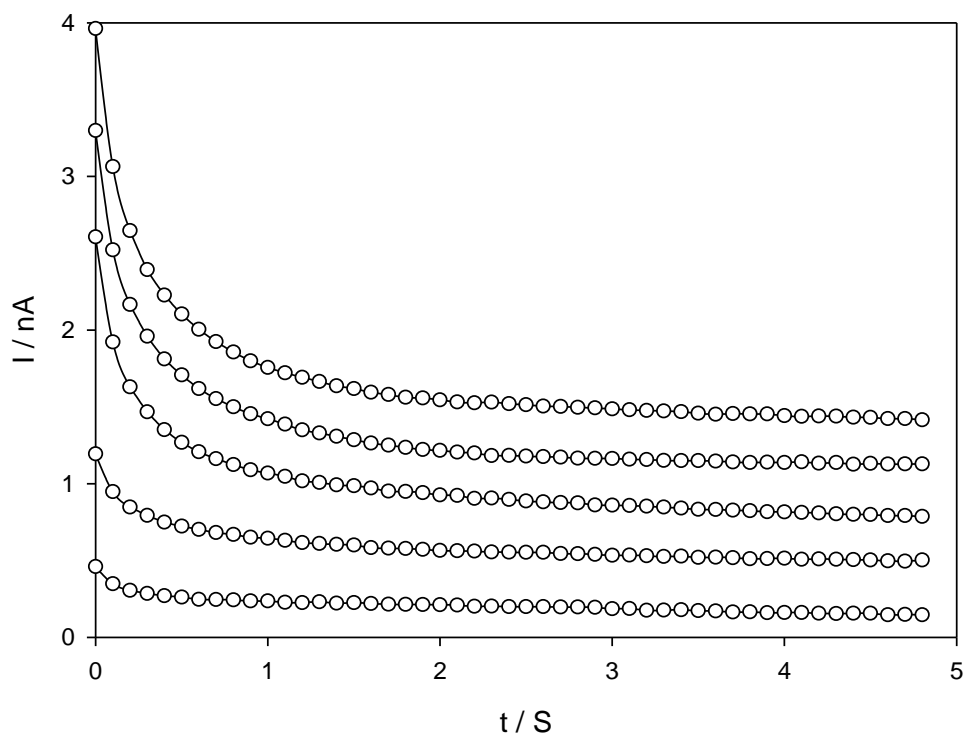


**Figure 4.17:** Experimental (–) and fitted theoretical (o) chronoamperometric transients for the oxidation of 1.08, 5.21, 10.13, 20.18 and 30.06 mM Fc in DES11 at a 20  $\mu\text{m}$  Pt microelectrode.

#### 4.2.7 Stokes–Einstein behaviour of metallocene derivatives

The mass transport properties of Fc and  $\text{Cc}^+$  in DESs can be predicted on the basis of the Stokes–Einstein expression (Eq. 4.11), which relates  $D$  and the dynamic viscosity of the medium,  $\eta$ . Here  $k_B$  is the Boltzmann constant,  $a$  is the hydrodynamic radius of the species, and  $T$  is the absolute temperature.

$$D = \frac{k_B T}{6\pi\eta a} \quad (4.11)$$

According to Eq. 4.11, a plot of  $D$  vs.  $\eta^{-1}$  should be linear with zero intercept. Figure 4.18 exhibited linear behaviour when  $D_{\text{Fc}}$  was plotted vs.  $\eta^{-1}$  for 10.13 mM Fc in DESs based on glycerol and ethylene glycol HBDs. Thus, it might be sensible to presume that the Stokes–Einstein relationship, as shown in Eq. 4.11, can be applied to the data reported herein. Furthermore, many reports in the literature indicated that the Stokes–Einstein equation applies for a range of redox species in various ILs (inclusive of Fc), as

indicated by linear plots of  $D$  vs.  $\eta^{-1}$  (Rogers et al., 2008). However, there is other report that Eq. 4.11 does not apply in ILs, particularly when the redox species is small in size (Huang et al., 2009).

Table 4.13 summarizes the calculated Stokes–Einstein products,  $D\eta/T$  of Fc and  $Cc^+$  in some DESs.  $D\eta/T$  of Fc in DESs is larger than that of  $Cc^+$  in the same solvent. Since  $D\eta/T$  of metallocene couples is dependent on the hydrodynamic radii of the diffusing species, their comparable values reveal that the radius of the diffusing entity is independent of the DESs. Consequently, one can estimate the viscosity of the new DES from the experimentally determined  $D$  as well as from  $D\eta/T$  values of Fc and  $Cc^+$ .

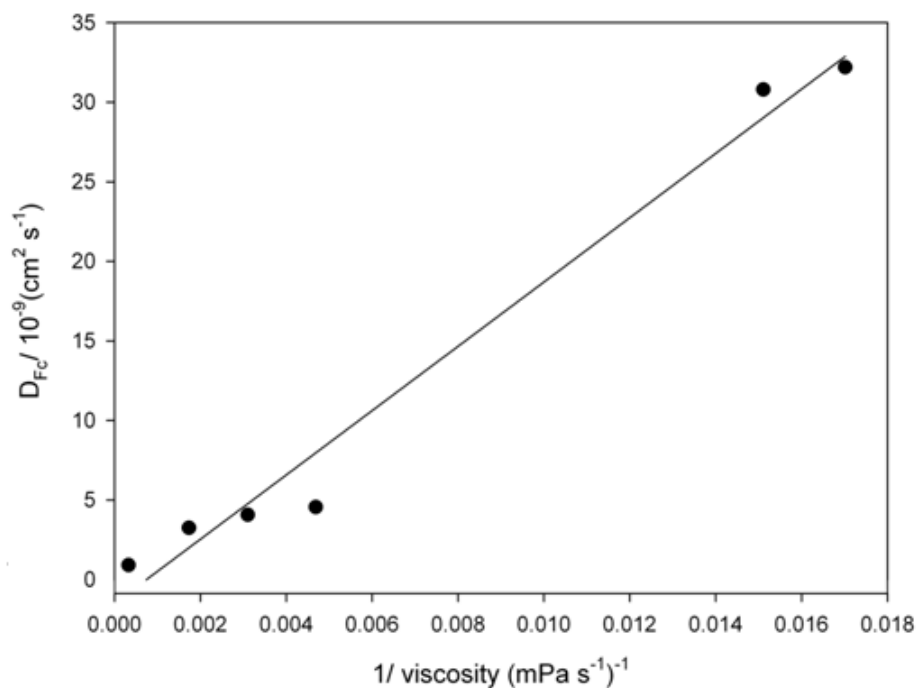


**Figure 4.18:** Plot of  $D$  against the inverse of viscosity ( $\eta^{-1}$ ) for the DESs based on glycerol and ethylene glycol HBDs

$D$  of Fc and  $Cc^+$  in the all studied DESs (Table 4.8) decrease as the viscosity of the solvent increases, as expected from the slower rate of mass transport to the electrode in the more viscous medium.

**Table 4.13:** Stokes–Einstein products of Fc and Cc<sup>+</sup> in some DESs

DESs	$\eta D T^{-1} / \text{g cm s}^{-2} \text{K}^{-1}$	
	Fc	Cc <sup>+</sup>
DES1	$3.79 \times 10^{-11}$	$3.29 \times 10^{-11}$
DES2	$6.23 \times 10^{-11}$	$4.09 \times 10^{-11}$
DES3	$3.26 \times 10^{-11}$	$2.79 \times 10^{-11}$
DES4	$3.09 \times 10^{-11}$	$2.45 \times 10^{-11}$
DES5	$8.62 \times 10^{-11}$	$6.64 \times 10^{-11}$
DES12	$6.16 \times 10^{-11}$	$5.47 \times 10^{-11}$
DES13	$3.66 \times 10^{-11}$	$2.75 \times 10^{-11}$

### 4.3 Electrochemical behaviour of V(acac)<sub>3</sub> in DESs

It was shown throughout this chapter that DES3, DES7, DES9, DES11, DES13 and DES16 are potential candidates as electrolytes to replace acetonitrile as a solvent for vanadium acetylacetonate (V(acac)<sub>3</sub>)-based redox batteries. This is mainly because of the higher solubility and ionic conductivity of these DESs compared to the other studied DESs. Additionally, PWs results of these DESs showed the stability of the V(acac)<sub>3</sub> active species in the selected DESs.

#### 4.3.1 Voltammetry of vanadium electrolytes in DESs

Preliminary experiments involved verifying the set-up proposed in this section using results reported in the literature (Liu et al., 2009, Zhang et al., 2012). For this purpose, 0.01 M V(acac)<sub>3</sub> was dissolved in an acetonitrile (CH<sub>3</sub>CN) solution consisting of 0.5 M TEABF<sub>4</sub> as the supporting electrolyte. Solutions were prepared and experiments carried out in an argon-filled glove box to ensure the chemicals and solutions were not exposed to environmental oxygen and water. Cyclic voltammograms at 0.1 V s<sup>-1</sup> scan rate is shown for both supporting and active electrolytes in Figure 4.19. Two redox couples were present within the solvent PW (-2.5 V to 1.5 V vs. Ag/Ag<sup>+</sup>).



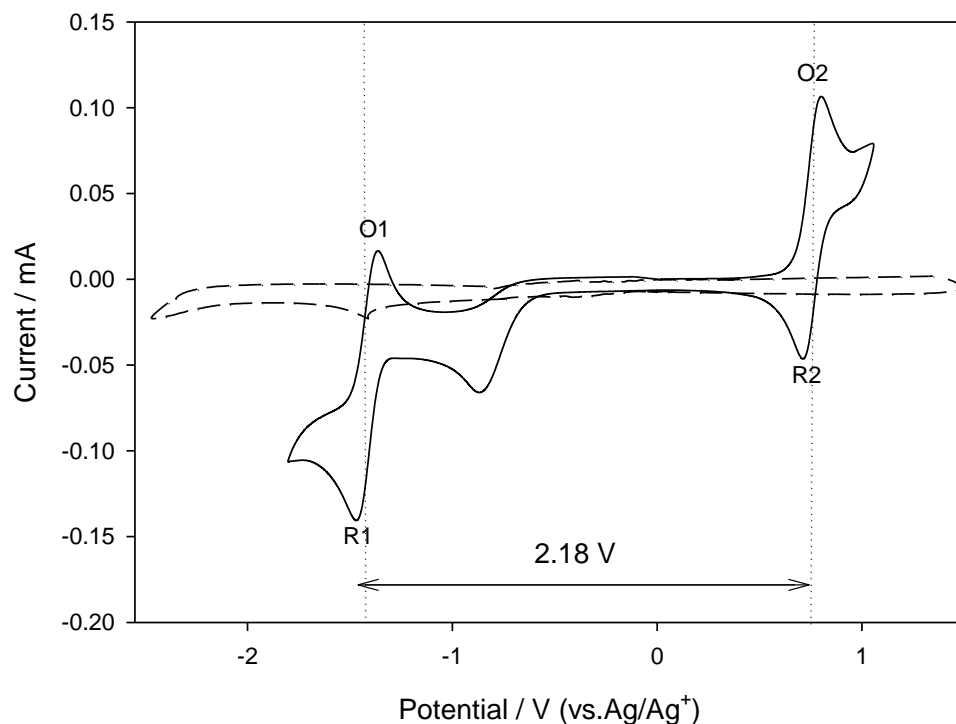
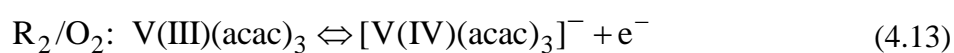
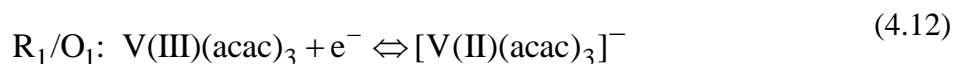


**Figure 4.19:** Cyclic voltammograms recorded at a glassy carbon electrode in 0.5 M TEABF<sub>4</sub> in CH<sub>3</sub>CN (---) and 0.01 M V(acac)<sub>3</sub> and 0.5 M TEABF<sub>4</sub> in CH<sub>3</sub>CN (—) at 0.1 V s<sup>-1</sup>.

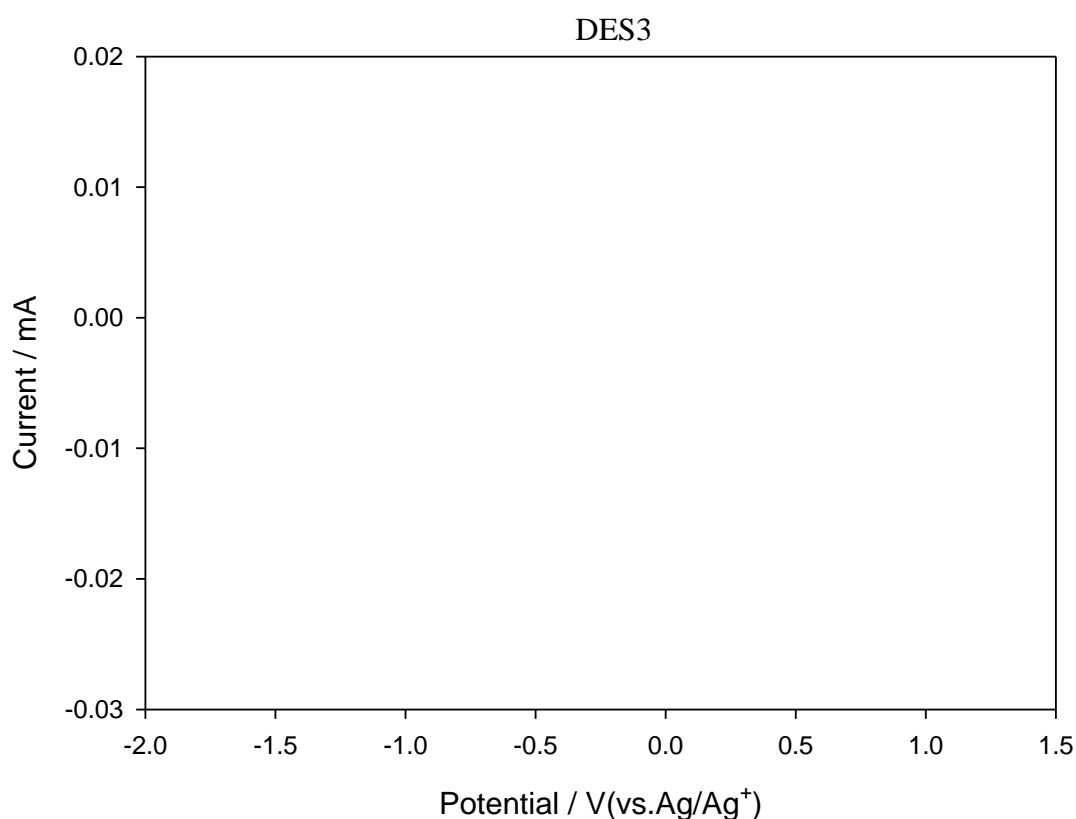
Although a direct similarity between the absolute values of reduction potentials reported earlier and those in this work is difficult (due to the different solvents used), the voltage difference between the first and second reductions show stark resemblance to those reported elsewhere (Shinkle et al., 2012) and therefore verifies the three-electrode set-up employed herein.

These current peaks attribute the redox couples observed in Figure 4.19 to the following reactions:

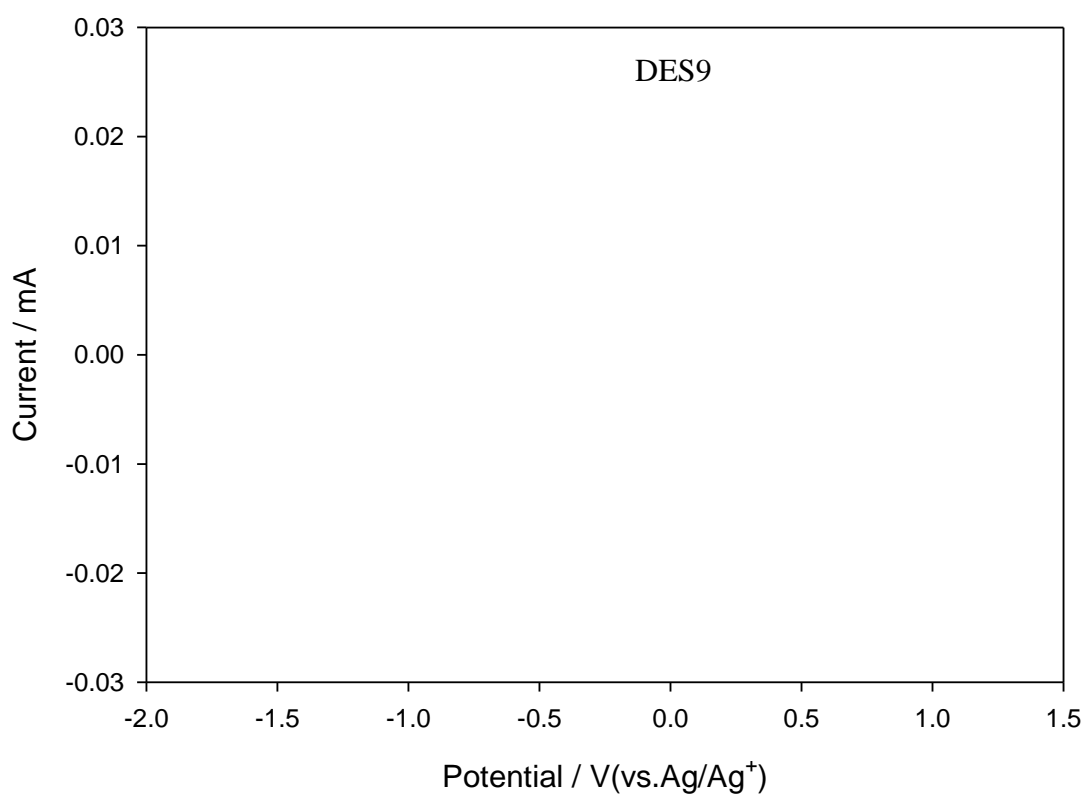
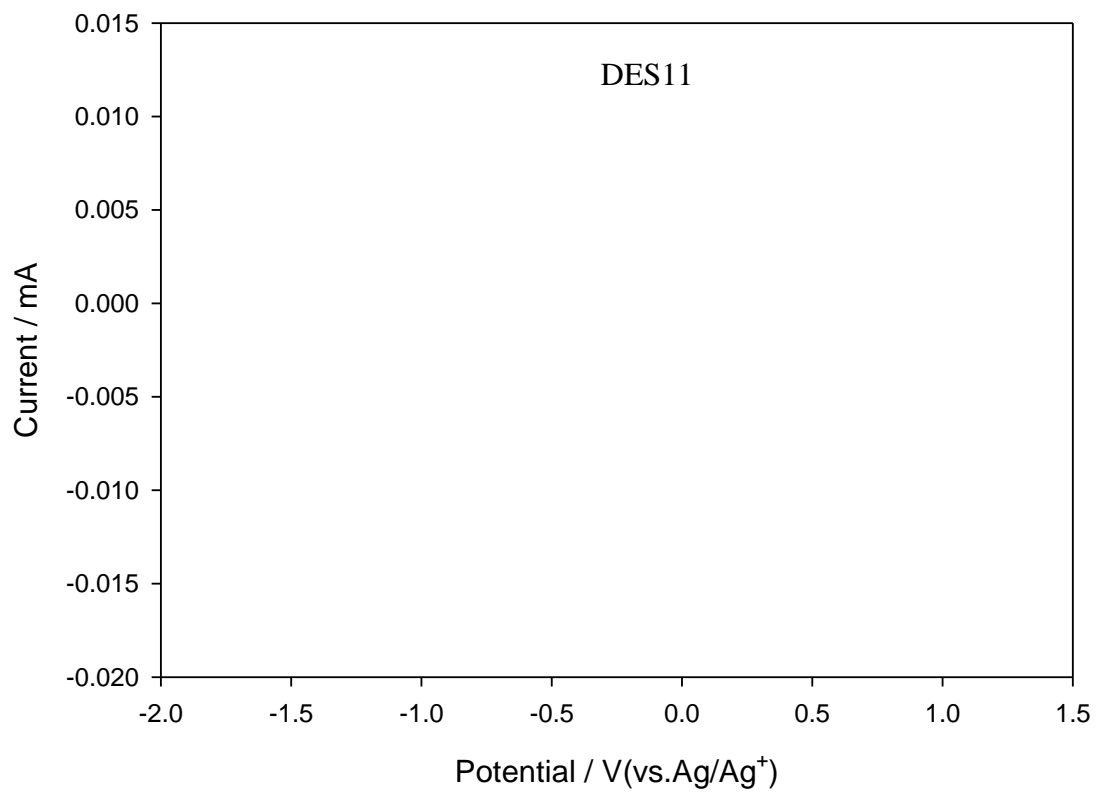


These standard open circuit cell potential indicated by the reactions in Figure 4.19 suggests that a system based on one-electron disproportionation of  $V(\text{acac})_3$  should yield a 2.18 V equilibrium cell potential. This is approximately 58 % higher than the potential reported for aqueous vanadium RFBs (1.26 V under standard conditions (Ponce de Leon et al., 2006)).

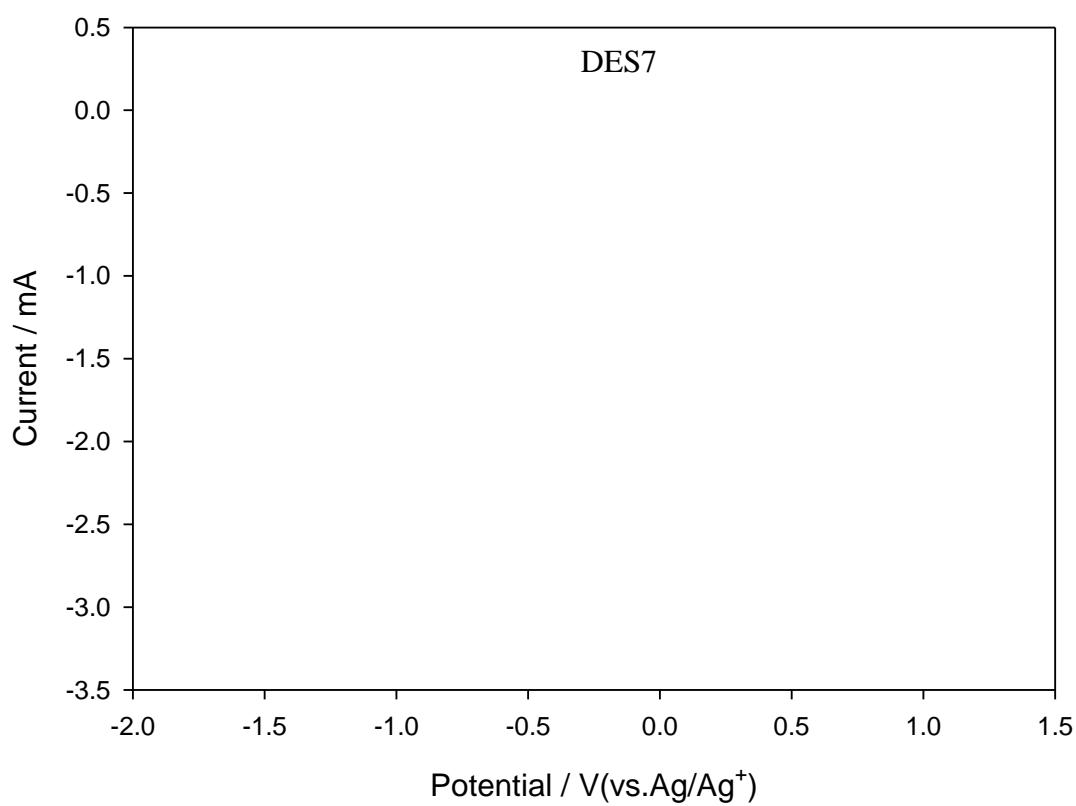
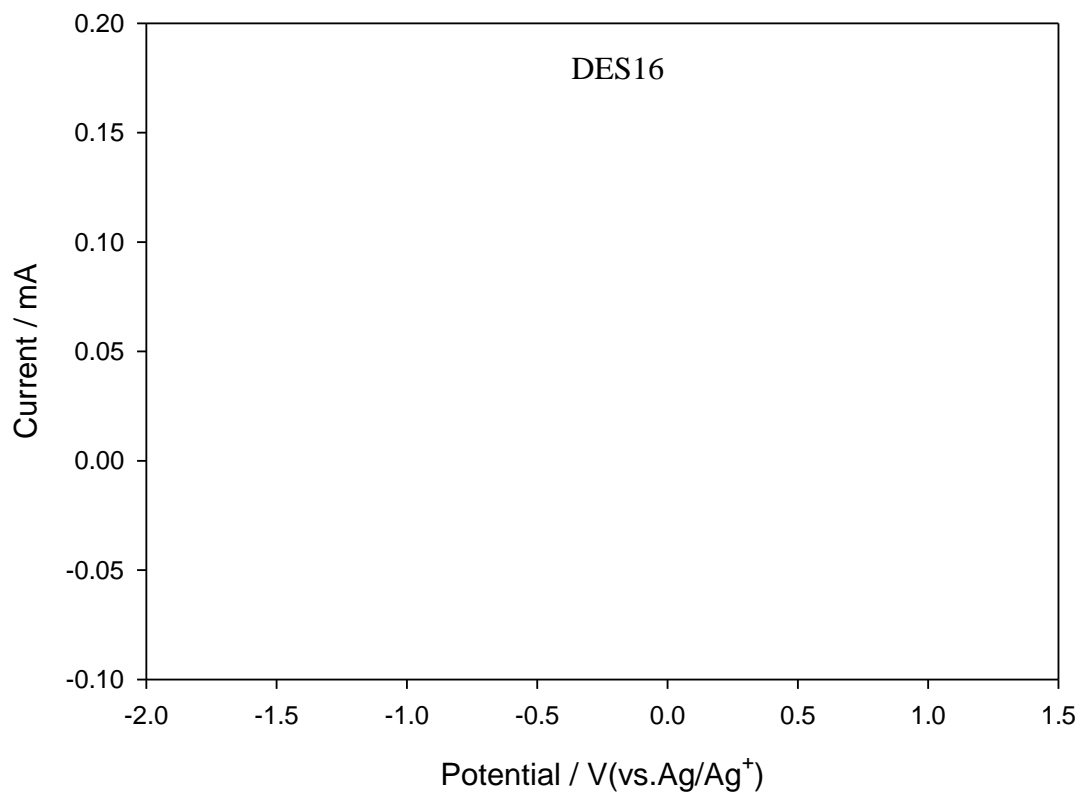
Figure 4.20 shows the voltammograms of 0.01 M  $V(\text{acac})_3$  in the six different DESs at a scan rate of  $0.1 \text{ V s}^{-1}$ . The results clearly show that DESs 3, 9 and 11 have potential for further evaluation and their standard open circuit cell potentials are listed in Table 4.14.



'Figure 4.20, continued'



'Figure 4.20, continued



‘Figure 4.20, continued’

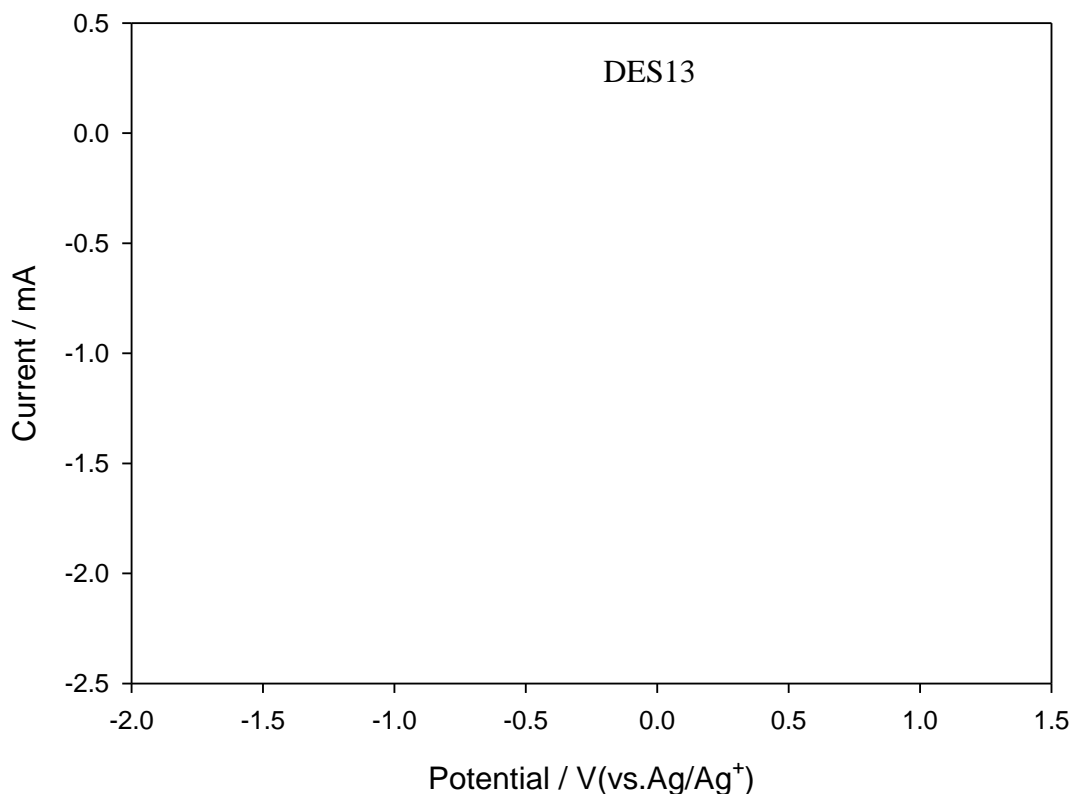


**Figure 4.20:** Cyclic voltammograms recorded at  $0.1 \text{ V s}^{-1}$  at a glassy carbon electrode in  $0.01 \text{ M V}(\text{acac})_3$  and  $0.5 \text{ M TEABF}_4$  in different DESs.

### 4.3.2 Kinetics of electrode reactions

A series of cyclic voltammograms at different scan rates from  $0.01$  to  $1 \text{ V s}^{-1}$  for electrolyte containing  $0.01 \text{ M V}(\text{acac})_3$  and  $0.5 \text{ M TEABF}_4$  in  $\text{CH}_3\text{CN}$  are shown in Figure 4.21. For the  $\text{V(II)/V(III)}$  couples, the  $\Delta E_p$  increased slightly with increasing scan rate from  $68$  to  $85 \text{ mV}$ . For the  $\text{V(III)/V(IV)}$  couples, the  $\Delta E_p$  remained constant at  $66 \text{ mV}$ . The ratios of anodic to cathodic peak currents were near unity for both reduction couples, suggesting reversible kinetics for reactions.

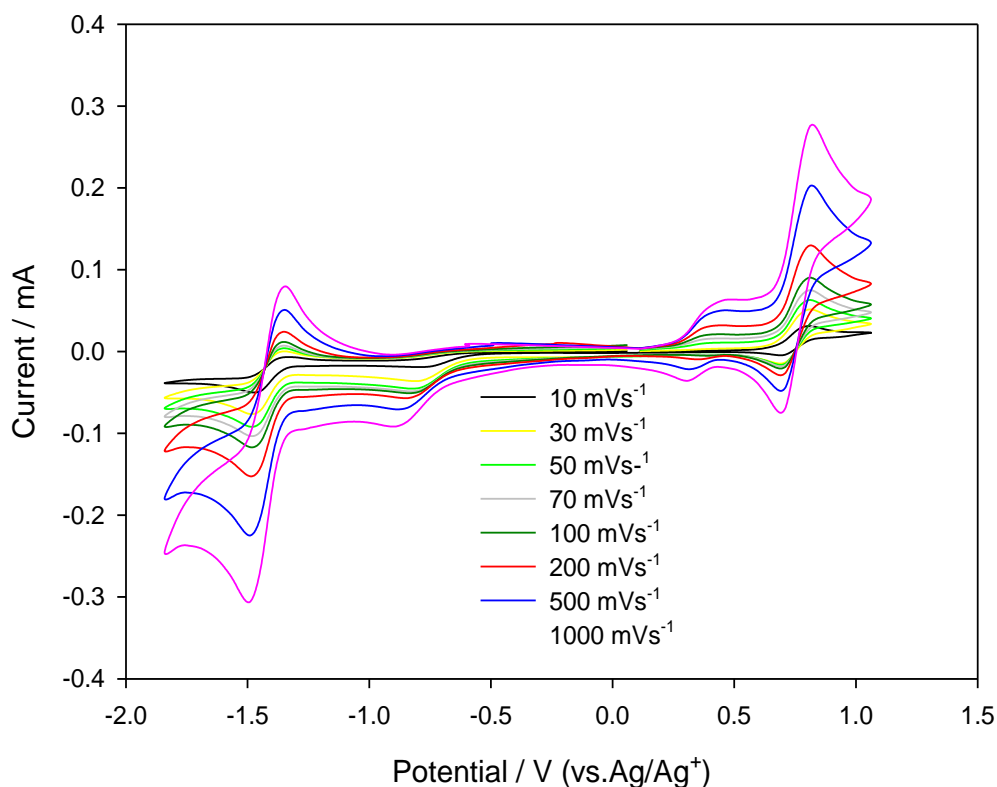


**Figure 4.21:** Cyclic voltammetry recorded at a glassy carbon electrode in 0.01 M  $V(acac)_3$  and 0.5 M TEABF<sub>4</sub> in CH<sub>3</sub>CN at different scan rate.

To determine the  $D$  of  $V(acac)_3$  in the electrolytic solutions, changes in peak height were measured as scan rates varied stepwise from 0.01-0.50  $V s^{-1}$ , as was done for the other active species discussed in sections 4.2.2. Based on equation 4.7, the  $D$  of the neutral complex is calculated to be  $3.5 \times 10^{-6} cm^2 s^{-1}$ .

Figure 4.22 shows the cyclic voltammograms for electrolyte containing 0.01 M  $V(acac)_3$  and 0.5 M TEABF<sub>4</sub> in DES3. For the V(II)/V(III) redox couple, the  $\Delta E_p$  increased from 60 to 90 mV and the ratio of anodic to cathodic peak currents increased from 0.97 to 1.20 as the scan rate is increased from 0.05 to 0.50  $V s^{-1}$ . For the V(III)/V(IV) redox couple,  $\Delta E_p$  increased from 65 to 80 mV but the ratio of anodic to cathodic peak currents decreased from 1.1 to 0.98 as the scan rate increased. The ratio of anodic to cathodic peak currents is approximately close to unity.

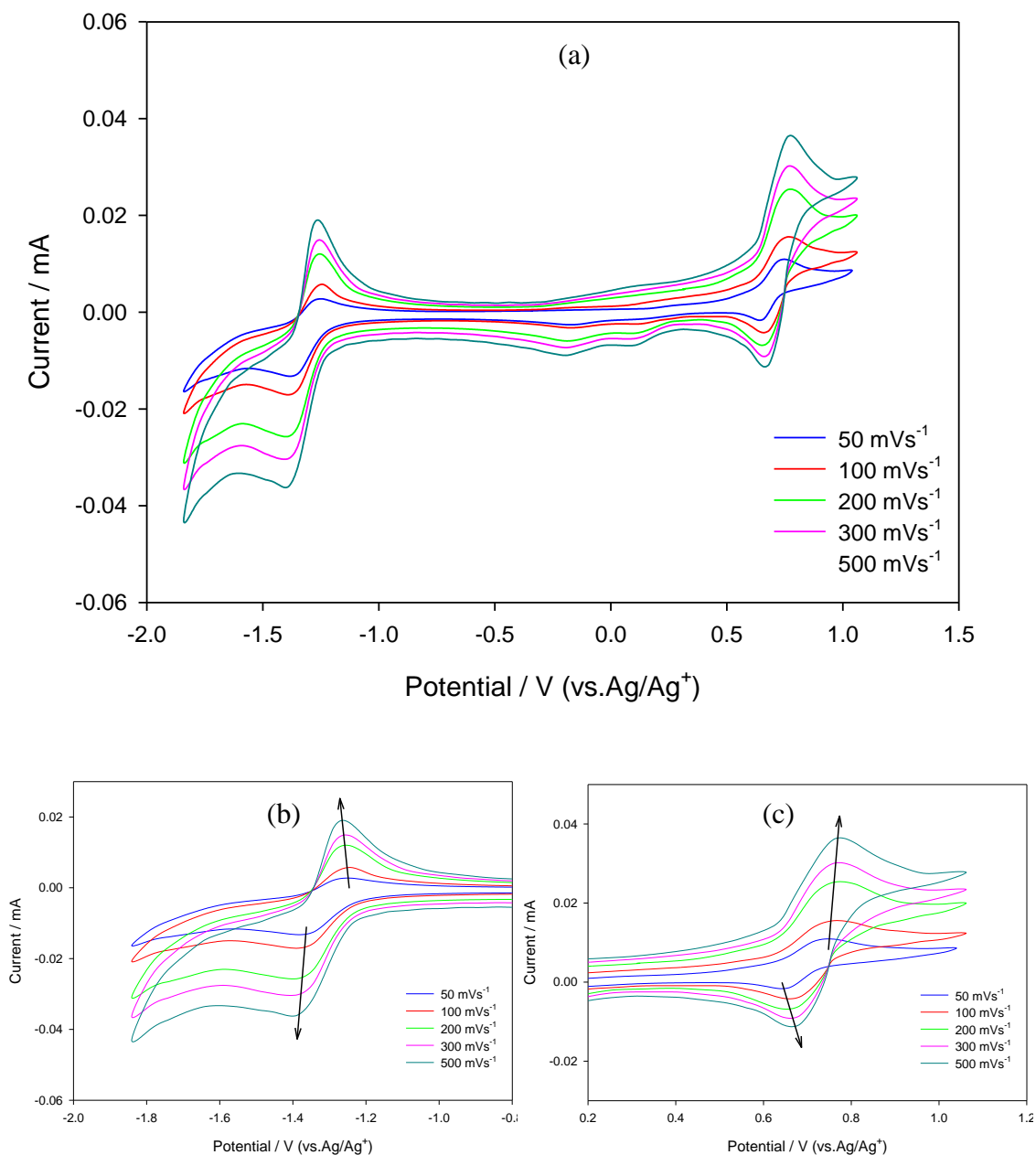


**Figure 4.22:** Cyclic voltammograms for (a)  $V(acac)_3$ , (b) the  $V(II)/V(III)$  redox couple and (c) the  $V(III)/V(IV)$  redox couple at a glassy carbon electrode in 0.01 M  $V(acac)_3/0.5$  M  $TEABF_4$  in DES3.

Figure 4.23 and 4.24 show the cyclic voltammograms for electrolyte containing 0.01 M  $V(acac)_3$  and 0.5 M  $TEABF_4$  in DES11 and DES9, respectively. For the  $V(II)/V(III)$  redox couple, the  $\Delta E_p$  increased from 80-116 mV and 92-135 mV for DES 11 and respectively. The ratio of anodic to cathodic peak currents increased from 0.33-0.54 (for DES11) and 0.25-0.51 (for DES9) as the scan rate is increased from 0.01 to

0.50 V s<sup>-1</sup>. For the V(III)/V(IV) redox couple,  $\Delta E_p$  increased from 85-122 mV ( for DES11) and 90-145 mV( for DES9) but the ratio of anodic to cathodic peak currents decreased from 0.92-0.55 ( for DES11) and 0.85-0.49 (for DES9) as the scan rate increased. From Figures 4.23 and 4.24, it can be deduced that both reactions 4.12 and 4.13 are quasi-reversible in DES11 and 9. For a reversible redox couple, the peak current  $i_p$  is given by Eq 4.7. For a totally irreversible redox couple, the peak current is given by:

$$i_p = 2.99 \times 10^5 n^{3/2} \alpha^{1/2} A C D_0^{1/2} v^{1/2} \quad (4.14)$$

Where  $n$  is the number of electrons transferred in the electrode reaction ( $n = 1$ ),  $A$  is the electrode area (cm<sup>2</sup>),  $C$  is the bulk concentration of primary reactant (mol l<sup>-1</sup>),  $D$  is the diffusion coefficient of primary reactant,  $v$  is the scan rate (V s<sup>-1</sup>) and  $\alpha$  is a constant. Since  $i_p$  is a function of  $v^{1/2}$ , a plot of  $i_p$  vs.  $v^{1/2}$  gives a straight line with a slope proportional to the  $D$  of the active species (Bard and Faulkner, 2001). Because the electrode reactions appear to be quasi-reversible in DES11 and 9, the value for the diffusion coefficient of V(acac)<sub>3</sub> would be located in between the results calculated from Eqs. 4.7 and 4.14. The  $D$  of V(acac)<sub>3</sub> based on the cathodic peak currents for the V(III)/V(IV) redox couple are listed in Table 4.14. The largest  $D$ ,  $0.69 \times 10^{-6}$  cm<sup>2</sup> s<sup>-1</sup>, is obtained at room temperature for DES3.



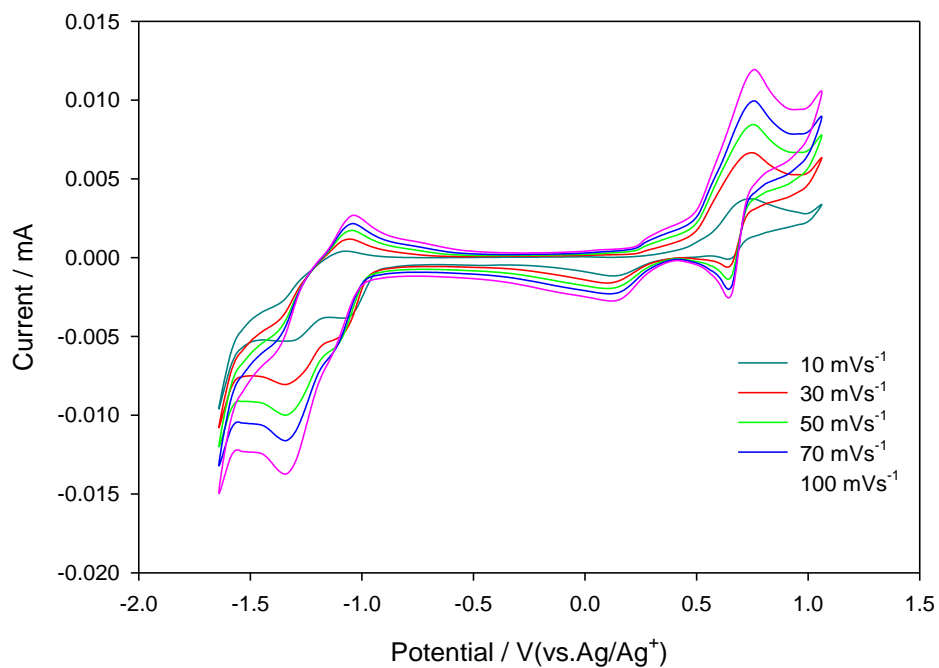


**Figure 4.23:** Cyclic voltammograms at a glassy carbon electrode in 0.01 M  $V(acac)_3/0.5$  M  $TEABF_4$  in DES11 at different scan rate.

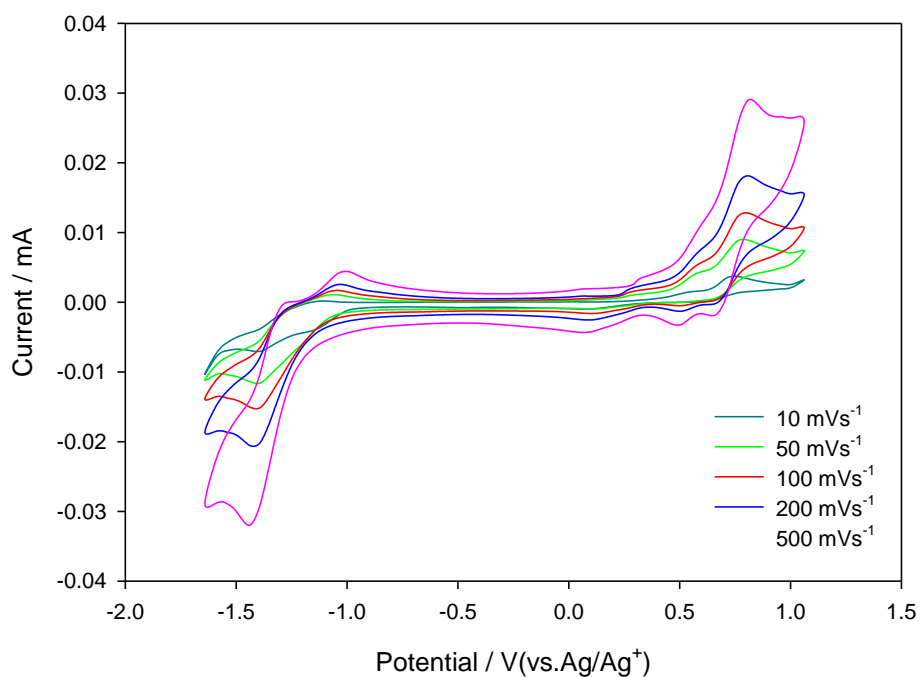


**Figure 4.24:** Cyclic voltammograms at a glassy carbon electrode in 0.01 M  $V(acac)_3/0.5$  M  $TEABF_4$  in DES9 at different scan rate.

The cell potential, number of electrons transferred, and concentration of active species determine the energy density of a VRFB. The active-species solubility limits can be used in place of its concentration to estimate the maximum energy densities for a particular chemistry. Solubility of CH<sub>3</sub>CN in energy densities and different DESs were calculated using a ICP-AES spectrometer, and are listed in Table 4.14. The method used to measure the solubility of a V(acac)<sub>3</sub> in DESs was given in Section 3.3. The solubility of V(acac)<sub>3</sub> in CH<sub>3</sub>CN were near 0.6 M, whereas the solubility of DESs were up to 0.25 M. Thus, the energy densities of V(acac)<sub>3</sub> in DES3 is 3 times smaller than CH<sub>3</sub>CN.

In order to select the more promising DESs, the reversibility of the reactions and its kinetics should be taken into account. The effective  $k^0$  was estimated using Eq. 4.9. The  $k^0$  of the reactions for DES3 and CH<sub>3</sub>CN were comparable, while those for DES9 were approximately 10 times smaller.

**Table 4.14:** Summary of V(acac)<sub>3</sub> performance characteristics in selected DESs and CH<sub>3</sub>CN.

Electrolyte	Cell Potential (V)	$D \times 10^{-6}$ (cm <sup>2</sup> s <sup>-1</sup> )	$k^0 \times 10^{-3}$ (cm s <sup>-1</sup> )		Solubility (M)	Energy Density (Wh L <sup>-1</sup> )
			V(II)/V(III)	V(III)/V(IV)		
CH <sub>3</sub> CN	2.18	3.50 (±0.06)	1.25(±0.08)	1.18(±0.07)	0.63(±0.05)	18.40
DES3	2.01	0.69 (±0.03)	0.74(±0.05)	1.02(±0.08)	0.25(±0.06)	6.73
DES9	1.98	0.02-0.13 (±0.05)	0.12(±0.07)	0.32(±0.02)	0.12(±0.04)	3.18
DES11	2.01	0.59-0.63 (±0.08)	0.53(±0.04)	0.85(±0.03)	0.19(±0.07)	5.11

The standard open circuit cell potential can be used to determine the potential of the system when no current is flowing through the system via the Nernst equation (supposing the reactants and products of redox reactions behave relatively ideally, so that activity coefficients are unity):

$$E = E^0 - \frac{RT}{nF} \ln \left( \frac{[\text{products}]}{[\text{reactants}]} \right) \quad (4.15)$$

where  $E$  is the measured potential,  $E^0$  is the cell potential measured from cyclic voltammetry,  $R$  is the universal gas constant,  $T$  is the absolute temperature,  $n$  is the

number of electrons, and  $F$  is Faraday's constant. For a single-electron disproportionation of a neutral intermediate active species, the product and reactant concentrations can be related to the total concentration of  $V$ ,  $[c]_{\text{total}}$ , and the fractional state of charge (SOC),  $x$ , through:

$$[\text{Products}] = [c]_{\text{total}} x \quad [\text{Reactants}] = [c]_{\text{total}}(1 - x) \quad (4.17)$$

Figure 4.25 indicates a plot of the cell potential as a function of the percent state of charge (%SOC=100x) in DES3, using the cell potential from Table 4.14 along with the condition that  $V(\text{acac})_3$  undergoes a single-electron disproportionation.

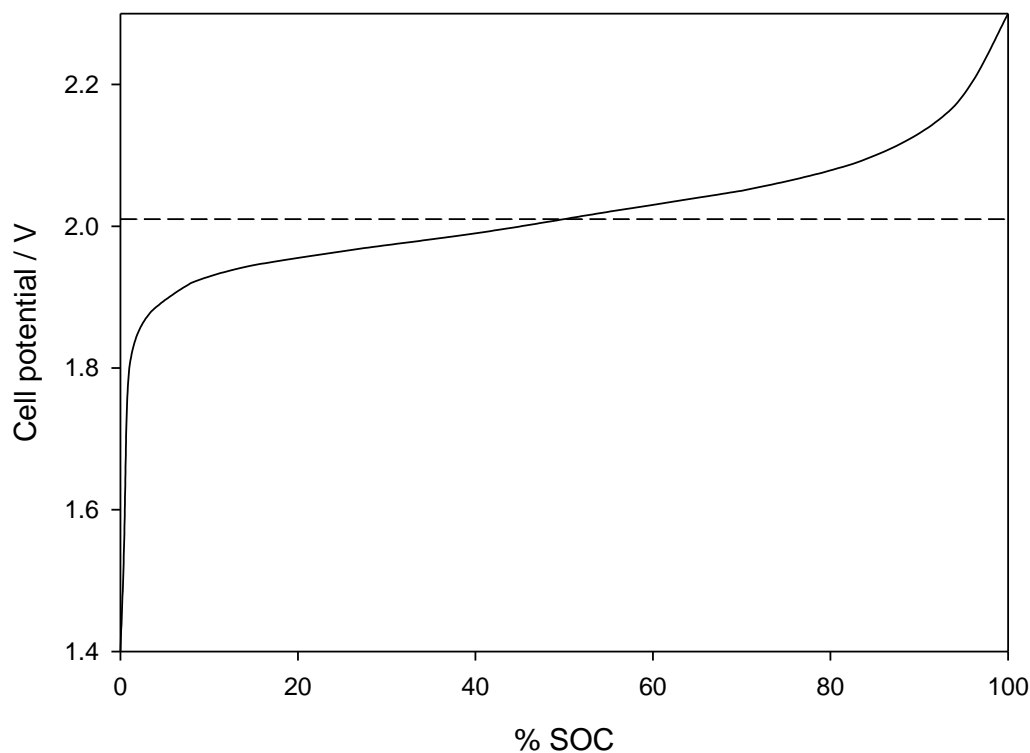


**Figure 4.25:** Plot of the Nernst equation for a single-electron disproportionation reaction with a 2.01 V cell potential (DES3).

The cell potential enhances dramatically while the first 8 % of the  $V(\text{III})$  is changed to  $V(\text{II})$  and  $V(\text{VI})$ . Then it increases slowly and passes through the equilibrium potential when half of the  $V(\text{III})$  is changed. When the solution is completely converted, the

potential again increases dramatically towards infinity at 100 % conversion. This dramatic increase is indicative of overcharging if it is observed in the charge/discharge curves.

#### 4.4 Charge/discharge performance

CH<sub>3</sub>CN has been used to validate the results obtained with DES3. Galvanostatic charge and discharge has been performed with 0.01 M V(acac)<sub>3</sub> in CH<sub>3</sub>CN consisting of 0.5 M TEABF<sub>4</sub> as reported above. The result is shown in Figure 4.26 for 2 cycles. The coulombic efficiency is also near 50% at 50% SOC herein (like similar experiments reported in the literature (Liu et al., 2009)), which confirms that the reactor employed is worthy for investigation using DES3.

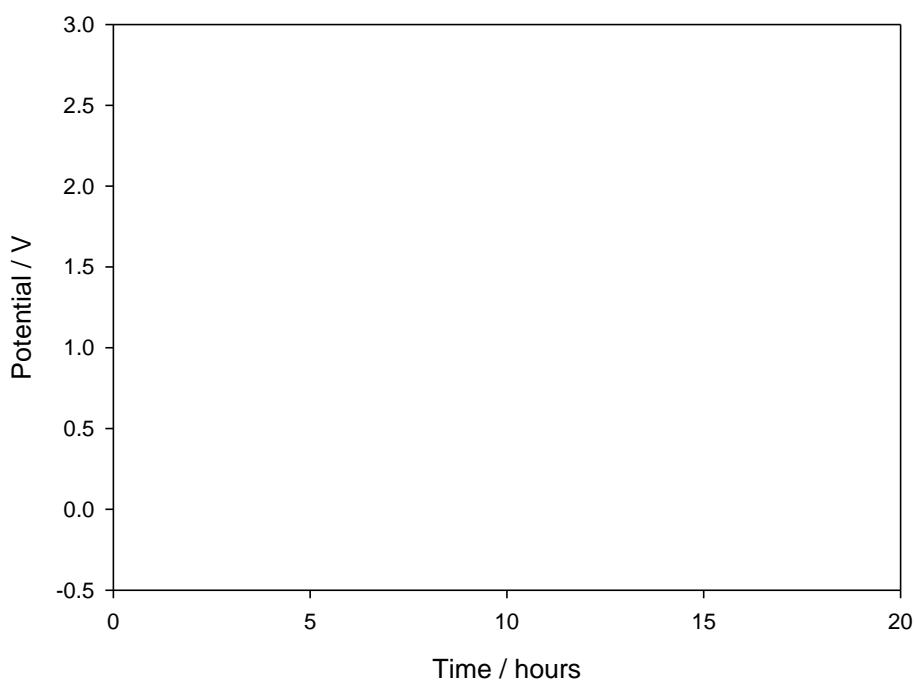


**Figure 4.26:** Charge/discharge curves for 0.01 M V(acac)<sub>3</sub>/0.5 M TEABF<sub>4</sub> in CH<sub>3</sub>CN. The charge current was 1 mA and the discharge current was 0.1 mA.

The charge/discharge cycle for the same electrolytes in DES3 was evaluated. Galvanostatic conditions were applied with potential cutoffs for both charge and discharge (Figure 4.27). The cut-off potential for charge was 2.40 V, higher than the 2.01 V cell potential detected in the voltammetry for the one-electron disproportionation

of  $V(\text{acac})_3$  in DES3. The cut-off potential for discharge was set at 0 V to enable the system to completely discharge without establishing side reactions. Further charge/discharge cycling was performed and the electrolyte was found to be stable after 10 cycles (Figure 4.28).

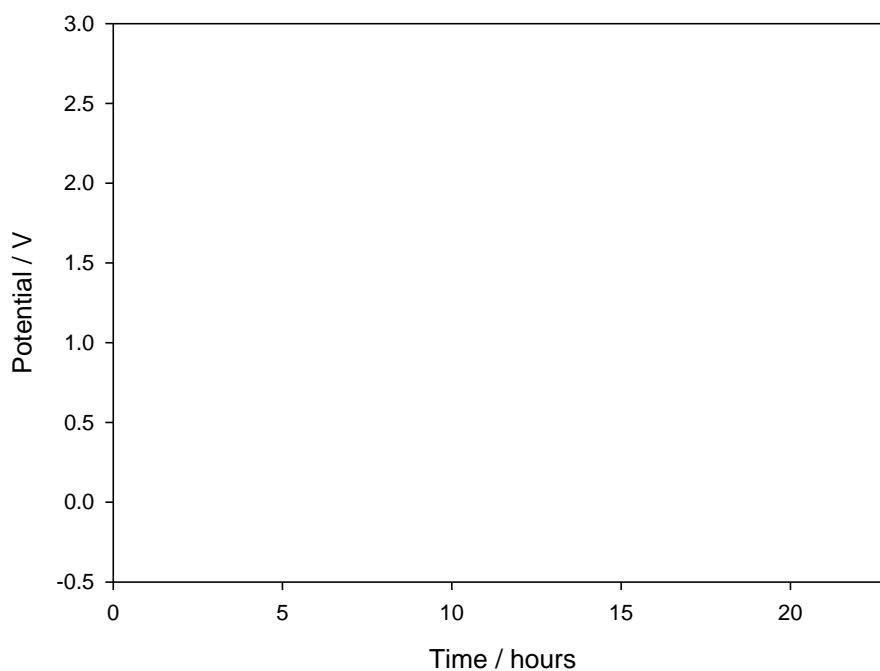


**Figure 4.27:** Charge/discharge curves for 0.01 M  $V(\text{acac})_3$ /0.5 M  $\text{TEABF}_4$  in DES3. The charge current was 0.1 mA and the discharge current was 0.01 mA.

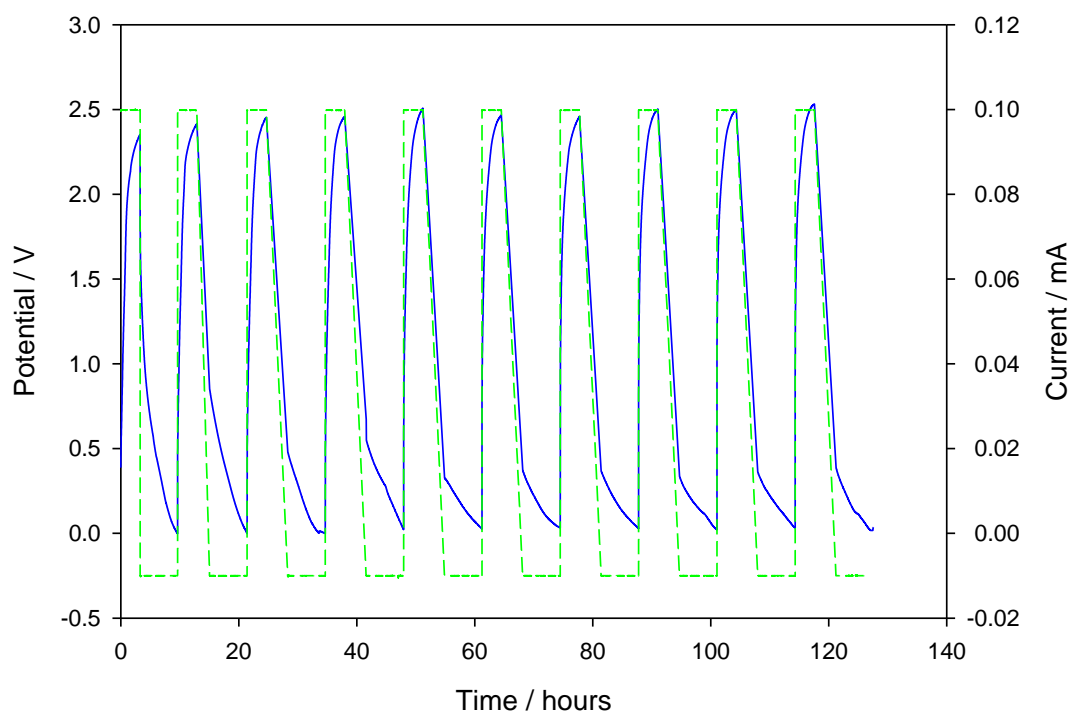
As shown in Figure 4.28, the charge voltage was as high as 2.40 V for the system, suggesting a total overpotential of 400 mV with respect to the 2.01 V formal potential associated with reaction. There is a small discharge voltage plateau in this system, around 0.5 V and 0.3 V for cycle 1-5 and cycle 6-12, respectively. The low discharge voltage may be because of the large ohmic drop and polarization in the H-type cell. Despite adding a supporting electrolyte, the ohmic drop was higher in the case of DES. Ohmic overpotential was probably important due to the low conductivity of the electrolyte, the relatively large distance between the two electrodes in the H-type cell, and the relatively low ionic conductivity of the membrane separator. The ohmic

overpotential decreased the energy efficiency. The coulombic and energy efficiencies obtained relatively constant values; with similar charge/discharge curves recorded.

Coulombic efficiency (CE) is the ratio of a cell's discharge capacity divided by its charge capacity, described as Eq. 4.18.

$$CE = \frac{I_D t_D}{I_C t_C} \times 100\% \quad (4.18)$$

Where  $I_D$  and  $I_C$  are discharge and charge cell currents,  $t_D$  and  $t_C$  are discharge and charge times.



The CE for TEABF<sub>4</sub>/ DES3 was 49.58 % in cycle 1. It can be seen that the CE was similar to that for CH<sub>3</sub>CN thereby giving significant relevance for considering DESs as suitable electrolytes for future evaluations. The low CE may be due to side reactions and/or the crossover of the active species through the anion-exchange membrane.

Energy efficiency (EE) is estimated from voltage efficiency (VE) and CE, as depicted in Eq. 4.19. VE is defined as the ratio of a cell's mean discharge voltage ( $V_D$ ) divided by its mean charge voltage ( $V_C$ ), displayed in Eq. 4.20.

$$EE = CE \times VE \quad (4.19)$$

$$VE = \frac{V_D}{V_C} \times 100\% \quad (4.20)$$

CE for cycles 1-12 ranged from 49-52 % at 50 % SOC. These low values may owe to crossover of the active species through the membrane. EE of approximately 25-31 % were achieved.

## CHAPTER 5: CONCLUSIONS

### 5.1. Summary and conclusions

Throughout the present work, sixteen DESs were synthesized. The DESs were characterized and selected DESs were used as electrolytes in charge/discharge tests using all-vanadium redox couples. The following conclusions were drawn from the results of the preliminary examinations that were carried out.

a) *DESs were produced at high purity using a simple and effective synthesis method*

DESs were easily prepared by mixing salts and HBDs with moderate heating. The synthesis procedure did not require sophisticated equipment. The purity of the resulting DES was completely dependent on the purity of the mixed components due to the absence of any chemical reaction.

Some DESs in this study were considered as novel DESs as they were not synthesized, characterized or employed previously.

b) *Different conditions are required for the synthesis of different combinations of DESs*

It was found that the types of salt and HBD were the principal factors that determine the optimum temperature needed for the preparation of DESs.

c) *Physicochemical properties of DESs are temperature dependent*

The prepared DESs were characterized by measuring selected important physicochemical properties, such as viscosity, density, conductivity, molar conductivity and pH over the temperature range from 298 to 368 K. As expected, the values of the measured properties changed with temperature. While the density and pH changed linearly with temperature, viscosity and ionic conductivity showed



exponential behavior. The activation energies for viscosity and conductivity for each DES were then calculated from the slopes of the Arrhenius plots. Walden plot was used to correlate viscosity and conductivity. The type of HBD was found to importantly affect the physical behaviour of the DES. For instance, the DESs synthesized from ethylene glycol and zinc nitrate hexahydrate HBDs had higher ionic conductivities than those made from other HBDs. Additionally, the DESs synthesized from ammonium salts showed higher conductivities than those made from phosphonium salts with same HBDs.

Some of the prepared DESs have favourable physical properties, e.g. low freezing point, moderate viscosity and high electrical conductivity. These make them potential solvents for many green applications.

d) *Electrochemical properties of Fc and Cc<sup>+</sup> are temperature dependent*

The electrochemical oxidation of Fc and Cc<sup>+</sup> has been studied by cyclic voltammetry and potential step chronoamperometry in different DESs. The potential windows of DESs have been determined electrochemically at Pt microelectrode and a GC electrode. The reductive and oxidative potential limits have been reported versus Ag/Ag QRE. In most cases, the DESs made up of ammonium salts had a larger potential window compared with the corresponding phosphonium based DESs.

Results show that  $D$  for Fc and Cc<sup>+</sup> does not change significantly with concentration. Fc/Fc<sup>+</sup> and Cc<sup>+</sup>/Cc complies with classical Stokes-Einstein behaviour in terms of the  $D$  vs  $\eta^{-1}$  dependence. The values of the calculated Stokes-Einstein product of Fc and Cc<sup>+</sup> in these DESs are less than those determined in other ILs. The kinetics of electron transfer across the DES/electrode interface have been studied using cyclic voltammetry and the highest  $k^0$  is determined to be  $5.44 \times 10^{-4}$  cm s<sup>-1</sup> and  $4.35 \times 10^{-4}$  cm s<sup>-1</sup> for Fc/Fc<sup>+</sup> and Cc<sup>+</sup>/Cc, respectively, in the ammonium based DES

prepared from N,N-diethylenethanol ammonium chloride and ethylene glycol.  $D$  and  $k^0$  of Fc and  $Cc^+$  in the DESs are found to be an order of magnitude lower than those reported in the literature in ILs under similar conditions.

The influence of temperature on the calculated electrochemical properties of studied DESs was discussed in detail. The  $D$  and  $k^0$  values tended to increase with the rise of temperature in DESs. The validity of the Arrhenius law was verified by examining the temperature dependencies of  $D$  and  $k^0$ . The trends of electrochemically derived activation energy from chronoamperometric characterization have relationships with  $E_\eta$  and  $E_\sigma$  evaluated from the experimental values. In addition,  $\Delta E_p$  was reduced with an increase in temperature and  $E_{1/2}$  values shifted towards more negative potentials for oxidation of Fc and more positive potentials for reduction of  $Cc^+$  in DESs with the enhancement in temperature.

Based on the performed electrochemical experiments, it was found that some of prepared DESs have the potential to be used in the evaluation of V(acac)<sub>3</sub> flow battery.

*e) Despite low solubility, good electrochemical performance is observed for DES3 by means of cyclic voltammetric studies*

V(acac)<sub>3</sub>/DESs system was evaluated for application in a non-aqueous VRFB. Results from voltammetry show that the V(acac)<sub>3</sub> complex can be simply reduced to  $[V(acac)_3]^-$  and oxidized to  $[V(acac)_3]^+$  at a GC electrode. In addition, the cyclic voltammograms indicate that TEABF<sub>4</sub> is stable in V(acac)<sub>3</sub> and DES3, 9 and 11 electrolytes in -2.5–1.5 V.

Kinetics of electrode reactions shows that both of V(II)/V(III) and V(III)/V(IV) reactions are reversible in DES3 and quasi-reversible in DES 9 and DES11 electrolytes. The  $D$  for DESs is in the range of  $0.02\text{--}0.69 \times 10^{-6} \text{ cm}^2 \text{ s}^{-1}$  at room temperature.

$V(\text{acac})_3$  has reversible electrochemistry in DES3, but a much higher solubility is required to compete with aqueous systems.

The energy density of a VRFB electrolyte is dictated by the solubility of active species, the voltage at which the active species react and the number of electrons transferred in the cell reaction. In this study, the energy density of a VRFB is lower due to the low solubility and limitations in the cell.

*f) Charge and discharge using DES3 shows similar coulombic efficiency as for  $CH_3CN$*

The charge/discharge characteristics for the all-vanadium system were evaluated using an H-cell with an anion-exchange membrane separator for the first time. Coulombic and energy efficiencies of the electrolyte containing  $V(\text{acac})_3/0.5$  M TEABF<sub>4</sub> in DES3 were obtained as 49-52 % and 25-31 %, respectively, when charging from 0% to 50% of theoretical maximum SOC for the cycles 1-12. The low CE may be indebted to crossover of the active species through the separator, or to the loss of active vanadium to a parasitic reaction. However, the CE was similar to that for  $CH_3CN$  thereby giving significant relevance for considering DESs as suitable electrolytes for future evaluations. Charge and discharge voltages are respectively higher and lower than the formal cell potential obtained by voltammetry. Ohmic drop in the DES results from the low conductivity of the electrolyte and the relatively large distance between the two electrodes in the H-cell.

## **5.2. Recommendations for future work**

Other types of DESs could be synthesized using various salts and HBDs and a similar investigation could be conducted to optimize the performance and tune up the process.

This study showed that DESs could be used effectively as electrolytes for RFBs. However, the solubility was found to be low and tests with other DESs is recommended to determine optimum performance in terms of high solubility and good efficiencies. One means of improving solubility could be to operate the cell at 50 °C, akin to results reported by Lloyd and co-workers for an all-copper redox flow cell (Lloyd et al., 2013).

## REFERENCES

- Abbott, A. P. (2004). Application of Hole Theory to the Viscosity of Ionic and Molecular Liquids. *ChemPhysChem*, 5(8), 1242-1246.
- Abbott, A. P., Barron, J. C., Ryder, K. S., Wilson, D. (2007b). Eutectic-based ionic liquids with metal-containing anions and cations. *Chemistry – A European Journal*, 13(22), 6495-6501.
- Abbott, A. P., Bell, T. J., Handa, S., Stoddart, B. (2005). O-Acetylation of cellulose and monosaccharides using a zinc based ionic liquid. *Green Chemistry*, 7(10), 705-707.
- Abbott, A. P., Boothby, D., Capper, G., Davies, D. L., Rasheed, R. K. (2004). Deep Eutectic Solvents Formed between Choline Chloride and Carboxylic Acids: Versatile Alternatives to Ionic Liquids. *Journal of the American Chemical Society*, 126(29), 9142-9147.
- Abbott, A. P., Capper, G., Davies, D. L., McKenzie, K. J., Obi, S. U. (2006). Solubility of metal oxides in deep eutectic solvents based on choline chloride. *Journal of Chemical & Engineering Data*, 51(4), 1280-1282.
- Abbott, A. P., Capper, G., Davies, D. L., Rasheed, R. K. (2004). Ionic Liquid Analogues Formed from Hydrated Metal Salts. *Chemistry – A European Journal*, 10(15), 3769-3774.
- Abbott, A. P., Capper, G., Davies, D. L., Rasheed, R. K., Tambyrajah, V. (2003). Novel solvent properties of choline chloride/urea mixtures. *Chemical Communications*(1), 70-71.
- Abbott, A. P., Capper, G., McKenzie, K. J., Ryder, K. S. (2007). Electrodeposition of zinc-tin alloys from deep eutectic solvents based on choline chloride. *Journal of Electroanalytical Chemistry*, 599(2), 288-294.
- Abbott, A. P., El Ttaib, K., Frisch, G., McKenzie, K. J., Ryder, K. S. (2009). Electrodeposition of copper composites from deep eutectic solvents based on choline chloride. *Physical Chemistry Chemical Physics*, 11(21), 4269-4277.
- Abbott, A. P., Frisch, G., Gurman, S. J., Hillman, A. R., Hartley, J., Holyoak, F., et al. (2011b). Ionometallurgy: designer redox properties for metal processing. *Chemical Communications*, 47(36), 10031-10033.
- Abbott, A. P., Frisch, G., Hartley, J., Ryder, K. S. (2011a). Processing of metals and metal oxides using ionic liquids. *Green Chemistry*, 13(3), 471-481.
- Abbott, A. P., Griffith, J., Nandhra, S., O'Connor, C., Postlethwaite, S., Ryder, K. S., et al. (2008). Sustained electroless deposition of metallic silver from a choline chloride-based ionic liquid. *Surface and Coatings Technology*, 202(10), 2033-2039.
- Abbott, A. P., Harris, R. C., Ryder, K. S. (2007c). Application of Hole Theory to Define Ionic Liquids by their Transport Properties. *The Journal of Physical Chemistry B*, 111(18), 4910-4913.
- Adamova, G., Gardas, R. L., Nieuwenhuyzen, M., Puga, A. V., Rebelo, L. P. N., Robertson, A. J., et al. (2012). Alkyltributylphosphonium chloride ionic liquids: synthesis, physicochemical properties and crystal structure. *Dalton Transactions*, 41(27), 8316-8332.

- Adams, R.N., *Electrochemistry at solid electrodes* M. Dekker, New York, 1969, xiii+402.
- Aki, S. N. V. K., Brennecke, J. F., Samanta, A. (2001). How polar are room temperature ionic liquids? *Chemical Communications*. 413–414.
- AlNashef, I. M., Leonard, M. L., Kittle, M. C., Matthews, M. A., Weidner, J. W. (2001). Electrochemical generation of superoxide in room-temperature ionic liquids. *Electrochemical and Solid-State Letters*, 4(11), D16-D18.
- AlNashef, I. M., Leonard, M. L., Matthews, M. A., Weidner, J. W. (2002). Superoxide electrochemistry in an ionic liquid. *Industrial & Engineering Chemistry Research*, 41(18), 4475-4478.
- Anderson, C. J., Deakin, M. R., Choppin, G. R., D'Olieslager, W., Heerman, L., Pruett, D. J. (1991). Spectroscopy and electrochemistry of uranium(IV)/uranium(III) in basic aluminum chloride-1-ethyl-3-methylimidazolium chloride. *Inorganic Chemistry*, 30(21), 4013-4016.
- Anderson, T. M., Ingersoll, D., Rose, A. J., Staiger, C. L., Leonard, J. C. (2010). Synthesis of an ionic liquid with an iron coordination cation. *Dalton Transactions*, 39(37), 8609-8612.
- Angell, C. A., Byrne, N., Belieres, J.-P. (2007). Parallel Developments in Aprotic and Protic Ionic Liquids: Physical Chemistry and Applications. *Accounts of Chemical Research*, 40(11), 1228-1236.
- Appetecchi, G. B., Montanino, M., Zane, D., Carewska, M., Alessandrini, F., Passerini, S. (2009). Effect of the alkyl group on the synthesis and the electrochemical properties of N-alkyl-N-methyl-pyrrolidinium bis(trifluoromethanesulfonyl)imide ionic liquids. *Electrochimica Acta*, 54(4), 1325-1332.
- Appetecchi, G. B., Scaccia, S., Tizzani, C., Alessandrini, F., Passerini, S. (2006). Synthesis of hydrophobic ionic liquids for electrochemical applications. *Journal of The Electrochemical Society*. 153(9), A1685–A1691.
- Armand, M., Endres, F., MacFarlane, D. R., Ohno, H., Scrosati, B. (2009). Ionic-liquid materials for the electrochemical challenges of the future. *Nat Mater*, 8(8), 621-629.
- Arora, P., Zhang, Z. (2004). Battery Separators. *Chemical Reviews*, 104(10), 4419-4462.
- Asensio, J. A., Sanchez, E. M., Gomez-Romero, P. (2010). Proton-conducting membranes based on benzimidazole polymers for high-temperature PEM fuel cells. A chemical quest. *Chemical Society Reviews*, 39(8), 3210-3239.
- Assink, R. A. (1984). Fouling mechanism of separator membranes for the iron/chromium redox battery. *Journal of Membrane Science*, 17(2), 205-217.
- Audrieth, L. F., Long, A., Edwards, R. E. (1936). Fused "Onium" Salts as Acids. Reactions in Fused Pyridinium Hydrochloride. *Journal of the American Chemical Society*, 58(3), 428-429.
- Bae, C., Roberts, E. P. L., Chakrabarti, M. H., Saleem, M. (2011). All-Chromium Redox Flow Battery for Renewable Energy Storage. *International Journal of Green Energy*, 8(2), 248-264.

- Bandres, I., Alcalde, R., Lafuente, C., Atilhan, M., Aparicio, S. (2011). On the Viscosity of Pyridinium Based Ionic Liquids: An Experimental and Computational Study. *The Journal of Physical Chemistry B*, 115(43), 12499-12513.
- Banos, R., Manzano-Agugliaro, F., Montoya, F. G., Gil, C., Alcayde, A., Gomez, J. (2011). Optimization methods applied to renewable and sustainable energy: A review. *Renewable and Sustainable Energy Reviews*, 15(4), 1753-1766.
- Bao, W. L., Wang, Z. M., Li, Y. X. (2003). Synthesis of chiral ionic liquids from natural amino acids. *Journal of Organic Chemistry*. 68, 591–593
- Bard, A. J., Faulkner, L. R., *Electrochemical Methods: Fundamentals and Applications*, 2nd ed., Wiley, New York, USA, 2001.
- Barnartt, S., Forejt, D. A. (1964). Bromine-Zinc Secondary Cells. *Journal of The Electrochemical Society*, 111(11), 1201-1204.
- Barrosse-Antle, L. E., Bond, A. M., Compton, R. G., O'Mahony, A. M., Rogers, E. I., Silvester, D. S. (2010). Voltammetry in Room Temperature Ionic Liquids: Comparisons and Contrasts with Conventional Electrochemical Solvents. *Chemistry – An Asian Journal*, 5(2), 202-230.
- Bartolozzi, M. (1989). Development of redox flow batteries. A historical bibliography. *Journal of Power Sources*, 27(3), 219-234.
- Batra, D., Seifert, S., Varela, L. M., Liu, A. C. Y., Firestone, M. A. (2007). Solvent-Mediated Plasmon Tuning in a Gold-Nanoparticle–Poly(Ionic Liquid) Composite. *Advanced Functional Materials*, 17(8), 1279-1287.
- Besenhard, J. O., Schollhorn, R. (1976). The discharge reaction mechanism of the MoO<sub>3</sub> electrode in organic electrolytes. *Journal of Power Sources*, 1(3), 267-276.
- Bhatt, A. I., Bond, A. M. (2008). Electrodeposition of silver from the 'distillable' ionic liquid, DIMCARB in the absence and presence of chemically induced nanoparticle formation. *Journal of Electroanalytical Chemistry*, 619-620, 1-10.
- Bhatt, A., Bond, A., Zhang, J. (2007). Electrodeposition of lead on glassy carbon and mercury film electrodes from a distillable room temperature ionic liquid, DIMCARB. *Journal of Solid State Electrochemistry*, 11(12), 1593-1603.
- Boisset, A., Menne, S., Jacquemin, J., Balducci, A., Anouti, M. (2013). Deep eutectic solvents based on N-methylacetamide and a lithium salt as suitable electrolytes for lithium-ion batteries. *Physical Chemistry Chemical Physics*, 15(46), 20054-20063.
- Bond, A. M., Oldham, K. B., Snook, G. A. (2000). Use of the Ferrocene Oxidation Process to Provide Both Reference Electrode Potential Calibration and a Simple Measurement (via Semiintegration) of the Uncompensated Resistance in Cyclic Voltammetric Studies in High-Resistance Organic Solvents. *Analytical Chemistry*, 72(15), 3492-3496.
- Bonhote, P., Dias, A.-P., Papageorgiou, N., Kalyanasundaram, K., Gratzel, M. (1996). Hydrophobic, Highly Conductive Ambient-Temperature Molten Salts. *Inorganic Chemistry*, 35(5), 1168-1178.
- Boxall, D. L., O'Dea, J. J., Osteryoung, R. A. (2002). Apparent Anomaly during Rotating Disk Voltammetry in Ionic Liquids. *Journal of The Electrochemical Society*, 149(11), E468-E471.

- Brooks, C. A., Doherty, A. P. (2004). Concentration-dependent diffusion in room temperature ionic liquids: a microelectrode study. *Electrochemistry Communications*, 6(8), 867-871.
- Burt, R., Birkett, G., Zhao, X. S. (2014). A review of molecular modelling of electric double layer capacitors. *Physical Chemistry Chemical Physics*, 16(14), 6519-6538.
- Buzzeo, M. C., Evans, R. G., Compton, R. G. (2004). Non-Haloaluminate Room-Temperature Ionic Liquids in Electrochemistry—A Review. *ChemPhysChem*, 5(8), 1106-1120.
- Buzzeo, M. C., Klymenko, O. V., Wadhawan, J. D., Hardacre, C., Seddon, K. R., Compton, R. G. (2003). Voltammetry of Oxygen in the Room-Temperature Ionic Liquids 1-Ethyl-3-methylimidazolium Bis((trifluoromethyl)sulfonyl)imide and Hexyltriethylammonium Bis((trifluoromethyl)sulfonyl)imide: One-Electron Reduction To Form Superoxide. Steady-State and Transient Behavior in the Same Cyclic Voltammogram Resulting from Widely Different Diffusion Coefficients of Oxygen and Superoxide. *The Journal of Physical Chemistry A*, 107(42), 8872-8878.
- Caban, K., Donten, M., Stojek, Z. (2003). Electroformation of Microlayers of Ionic Liquids in Undiluted Nitromethane and Its Homologues. Unusual Oscillations behind the Range of Limiting Steady-State Current. *The Journal of Physical Chemistry B*, 108(3), 1153-1159.
- Carmichael, A. J., Seddon, K. R. (2000). Polarity study of some 1-alkyl-3-methylimidazolium ambient-temperature ionic liquids with the solvatochromic dye, Nile red. *Journal of Physical and Organic Chemistry*, 13, 591-595.
- Carriazo, D., Serrano, M. C., Gutierrez, M. C., Ferrer, M. L., del Monte, F. (2012). Deep-eutectic solvents playing multiple roles in the synthesis of polymers and related materials. *Chemical Society Reviews*, 41(14), 4996-5014.
- Carter, M. T., Hussey, C. L., Strubinger, S. K. D., Osteryoung, R. A. (1991). Electrochemical reduction of dioxygen in room-temperature imidazolium chloride-aluminum chloride molten salts. *Inorganic Chemistry*, 30(5), 1149-1151.
- Chakrabarti M. H, Dryfe, R. A. W, Roberts, E. P. L. ( 2007) Organic electrolytes for redox flow batteries. *Journal of the Chemical Society of Pakistan*, 29, 294-300.
- Chakrabarti, M. H., Dryfe, R. A. W., Roberts, E. P. L. (2007). Evaluation of electrolytes for redox flow battery applications. *Electrochimica Acta*, 52(5), 2189-2195.
- Chakrabarti, M. H., Dryfe, R. A.W., Roberts E. P. L. (2007). Organic electrolytes for redoxflow batteries, *Journal of the Chemical Society of Pakistan*, 29(4), 294-300.
- Chakrabarti, M. H., Mjalli, F. S., AlNashef, I. M., Hashim, M. A., Hussain, M. A., Bahadori, L., et al. (2014). Prospects of applying ionic liquids and deep eutectic solvents for renewable energy storage by means of redox flow batteries. *Renewable and Sustainable Energy Reviews*, 30, 254-270.
- Chakrabarti, M. H., Roberts, E. P. L., Bae, C., Saleem, M. (2011). Ruthenium based redox flow battery for solar energy storage. *Energy Conversion and Management*, 52(7), 2501-2508.



- Chakrabarti, M., Brandon, N., Mjalli, F., Bahadori, L., Al Nashef, I., Hashim, M. A., Hussain, M. A., Low, J., Yufit, V. (2013). Cyclic Voltammetry of Metallic Acetylacetonate Salts in Quaternary Ammonium and Phosphonium Based Deep Eutectic Solvents. *Journal of Solution Chemistry*, 42(12), 2329-2341.
- Chen C. (2001). Synthesis and characterization of new cathode materials for lithium ion batteries. Thesis, Binghamton University, New York.
- Choi, Y. H., van Spronsen, J., Dai, Y., Verberne, M., Hollmann, F., Arends, I. W. C. E., et al. (2011). Are Natural Deep Eutectic Solvents the Missing Link in Understanding Cellular Metabolism and Physiology? *Plant Physiology*, 156(4), 1701-1705.
- Chum, H. L., Koch, V. R., Miller, L. L., Osteryoung, R. A. (1975). Electrochemical scrutiny of organometallic iron complexes and hexamethylbenzene in a room temperature molten salt. *Journal of American Chemical Society*. 97, 3264–3267.
- Dai, Y., van Spronsen, J., Witkamp, G.-J., Verpoorte, R., Choi, Y. H. (2013). Natural deep eutectic solvents as new potential media for green technology. *Analytica Chimica Acta*, 766, 61-68.
- De Souza, R. F., Padilha, J. C., Goncalves, R. S., Dupont, J. (2003). Room temperature dialkylimidazolium ionic liquid-based fuel cells. *Electrochemistry Communications*, 5(8), 728-731.
- Devanathan, R. (2008). Recent developments in proton exchange membranes for fuel cells. *Energy & Environmental Science*, 1(1), 101-119.
- Diaz-Gonzalez, F., Sumper, A., Gomis-Bellmunt, O. Villafafila-Robles, R. (2012). A review of energy storage technologies for wind power applications. *Renewable and Sustainable Energy Reviews*, 16(4), 2154-2171.
- Doyle, M., Choi, S. K., Proulx, G. (2000). High-Temperature Proton Conducting Membranes Based on Perfluorinated Ionomer Membrane-Ionic Liquid Composites. *Journal of The Electrochemical Society*, 147(1), 34-37.
- Du, Z., Li, Z., Guo, S., Zhang, J., Zhu, L., Deng, Y. (2005). Investigation of Physicochemical Properties of Lactam-Based Brønsted Acidic Ionic Liquids. *The Journal of Physical Chemistry B*, 109(41), 19542-19546.
- Dullius, J. E. L., Suarez, P. A. Z., Einloft, S., de Souza, R. F., Dupont, J., Fischer, J., et al. (1998). Selective Catalytic Hydrodimerization of 1,3-Butadiene by Palladium Compounds Dissolved in Ionic Liquids. *Organometallics*, 17(5), 815-819.
- Dupont, J., Fonseca, G. S., Umpierre, A. P., Fichtner, P. F. P., Teixeira, S. R. (2002). Transition-Metal Nanoparticles in Imidazolium Ionic Liquids: Recyclable Catalysts for Biphasic Hydrogenation Reactions. *Journal of the American Chemical Society*, 124(16), 4228-4229.
- Dzyuba, S. V., Bartsch, R. A. (2002). Influence of Structural Variations in 1-Alkyl(aralkyl)-3-Methylimidazolium Hexafluorophosphates and Bis(trifluoromethylsulfonyl)imides on Physical Properties of the Ionic Liquids. *ChemPhysChem*, 3(2), 161-166.
- Earle, M. J., Esperanca, J. M. S. S., Gilea, M. A., Canongia Lopes, J. N., Rebelo, L. P. N., Magee, J. W., et al. (2006). The distillation and volatility of ionic liquids. *Nature*, 439(7078), 831-834.

- Earle, M. J., Seddon, K. R. (2000). Ionic liquids. Green solvents for the future. *Pure and Applied Chemistry*, 72 (7), 1391–1398.
- Eisele, S., Schwarz, M., Speiser, B., Tittel, C. (2006). Diffusion coefficient of ferrocene in 1-butyl-3-methylimidazolium tetrafluoroborate - concentration dependence and solvent purity. *Electrochimica Acta*, 51(25), 5304-5306.
- Endres, F. (2004). Ionic Liquids: Promising Solvents for Electrochemistry, *Zeitschrift für Physikalische Chemie* (Vol. 218, pp. 255).
- Endres, F., MacFarlane, D. R., Abbott, A. P. (2008). Electrodeposition from Ionic Liquids;
- Endres, F., Zein El Abedin, S. (2006). Air and water stable ionic liquids in physical chemistry. *Physical Chemistry Chemical Physics*, 8(18), 2101-2116.
- Erdinc, O., Uzunoglu, M. (2012). Optimum design of hybrid renewable energy systems: Overview of different approaches. *Renewable and Sustainable Energy Reviews*, 16(3), 1412-1425.
- Evans, A., Strezov, V., Evans, T. J. (2012). Assessment of utility energy storage options for increased renewable energy penetration. *Renewable and Sustainable Energy Reviews*, 16(6), 4141-4147.
- Evans, R. G., Klymenko, O. V., Hardacre, C., Seddon, K. R., Compton, R. G. (2003). Oxidation of N,N,N,N-tetraalkyl-para-phenylenediamines in a series of room temperature ionic liquids incorporating the bis(trifluoromethylsulfonyl)imide anion. *Journal of Electroanalytical Chemistry*, 556(0), 179-188.
- Fabjan, C., Garche, J., Harrer, B., Jorissen, L., Kolbeck, C., Philippi, F. (2001). The vanadium redox-battery: an efficient storage unit for photovoltaic systems. *Electrochimica Acta*, 47(5), 825-831.
- Fang, B., Iwasa, S., Wei, Y., Arai, T., Kumagai, M. (2002). A study of the Ce(III)/Ce(IV) redox couple for redox flow battery application. *Electrochimica Acta*, 47(24), 3971-3976.
- Fernicola, A., Navarra, M., Panero, S. (2008). Aprotic ionic liquids as electrolyte components in protonic membranes. *Journal of Applied Electrochemistry*, 38(7), 993-996.
- Fernicola, A., Scrosati, B., Ohno, H. (2006). Potentialities of ionic liquids as new electrolyte media in advanced electrochemical devices. *Ionics*, 12(2), 95-102.
- Figure 2.6 from : < <http://www.leicester-ils.co.uk/deepeutectics.html> >
- Fonseca, G. S., Umpierre, A. P., Fichtner, P. F. P., Teixeira, S. R., Dupont, J. (2003). The Use of Imidazolium Ionic Liquids for the Formation and Stabilization of Ir<sup>0</sup> and Rh<sup>0</sup> Nanoparticles: Efficient Catalysts for the Hydrogenation of Arenes. *Chemistry – A European Journal*, 9(14), 3263-3269.
- Fontaine, O., Lagrost, C., Ghilane, J., Martin, P., Trippe, G., Fave, C., et al. (2009). Mass transport and heterogeneous electron transfer of a ferrocene derivative in a room-temperature ionic liquid. *Journal of Electroanalytical Chemistry*, 632, 88-96.
- Fraser, K. J., MacFarlane, D. R. (2009). Phosphonium-Based Ionic Liquids: An Overview. *Australian Journal of Chemistry*, 62(4), 309-321.

- Fredlake, C. P., Crosthwaite, J. M., Hert, D. G., Aki, S. N. V. K., Brennecke, J. F. (2004). Thermophysical Properties of Imidazolium-Based Ionic Liquids. *Journal of Chemical & Engineering Data*, 49(4), 954-964.
- Fu, C., Aldous, L., Dickinson, E. J. F., Manan, N. S. A., Compton, R. G. (2011). The Kinetics of Ferrocene Volatilisation from an Ionic Liquid. *ChemPhysChem*, 12(9), 1708-1713.
- Fukumoto, K., Yoshizawa, M., Ohno, H. (2005). Room Temperature Ionic Liquids from 20 Natural Amino Acids. *Journal of the American Chemical Society*, 127(8), 2398-2399.
- Fuller, J., Carlin, R. T., Osteryoung, R. A. (1997). The room temperature ionic liquid 1-ethyl-3-methylimidazolium tetrafluoroborate: Electrochemical couples and physical properties. *Journal of The Electrochemical Society*, 144 (11), 3881-3886.
- Gagne, R. R., Koval, C. A., Lisensky, G. C. (1980). Ferrocene as an internal standard for electrochemical measurements. *Inorganic Chemistry*, 19(9), 2854-2855.
- Galinski, M., Lewandowski, A., Stepniak, I. (2006). Ionic liquids as electrolytes. *Electrochimica Acta*, 51(26), 5567-5580.
- Garcia, B. a., Lavallee, S., Perron, G. r., Michot, C., Armand, M. (2004). Room temperature molten salts as lithium battery electrolyte. *Electrochimica Acta*, 49(26), 4583-4588.
- Gathergood, N., Scammells, P. J., Garcia, M. T. (2006). Biodegradable ionic liquids Part III. The first readily biodegradable ionic liquids. *Green Chemistry*, 8(2), 156-160.
- Gattrell, M., Park, J., MacDougall, B., Apte, J., McCarthy, S., Wu, C. W. (2004). Study of the Mechanism of the Vanadium 4+/5+ Redox Reaction in Acidic Solutions. *Journal of The Electrochemical Society*, 151(1), A123-A130.
- Gau, W.-j., Sun, I.-W. (1996). Electrochemical and Spectroscopic Studies of Ytterbium in the Aluminum Chloride-1-methyl-3-ethylimidazolium Chloride Room Temperature Molten Salt. *Journal of The Electrochemical Society*, 143(1), 170-174.
- Ge, S. H., Yi, B. L., Zhang, H. M. (2004). Study of a high power density sodium polysulfide/bromine energy storage cell. *Journal of Applied Electrochemistry*, 34(2), 181-185.
- Ghatee, M. H., Zare, M., Moosavi, F., Zolghadr, A. R. (2010). Temperature-Dependent Density and Viscosity of the Ionic Liquids 1-Alkyl-3-methylimidazolium Iodides: Experiment and Molecular Dynamics Simulation. *Journal of Chemical & Engineering Data*, 55(9), 3084-3088.
- Gratzel, M. (2001). Photoelectrochemical cells. *Nature*, 414(6861), 338-344.
- Gritzner, G., Kuta, J. (1984). recommendations on reporting electrode potentials in nonaqueous solvents. *Pure and Applied Chemistry*, 56(4), 461-466.
- Gu, Z., Brennecke, J. F. (2002). Volume Expansivities and Isothermal Compressibilities of Imidazolium and Pyridinium-Based Ionic Liquids. *Journal of Chemical & Engineering Data*, 47(2), 339-345.

- Hagiwara, R., Hirashige, T., Tsuda, T., Ito, Y. (2002). A Highly Conductive Room Temperature Molten Fluoride: EMIF 2.3HF. *Journal of The Electrochemical Society*, 149(1), D1-D6.
- Hajimolana, S. A., Hussain, M. A., Daud, W. M. A. W., Soroush, M., Shamiri, A. (2011). Mathematical modeling of solid oxide fuel cells: A review. *Renewable and Sustainable Energy Reviews*, 15(4), 1893-1917.
- Hall, P. J., Bain, E. J. (2008). Energy-storage technologies and electricity generation. *Energy Policy*, 36(12), 4352-4355.
- Handa, N., Sugimoto, T., Yamagata, M., Kikuta, M., Kono, M., Ishikawa, M. (2008). A neat ionic liquid electrolyte based on FSI anion for electric double layer capacitor. *Journal of Power Sources*, 185(2), 1585-1588.
- Hart, E. K., Stoutenburg, E. D., Jacobson, M. Z. (2012). The Potential of Intermittent Renewables to Meet Electric Power Demand: Current Methods and Emerging Analytical Techniques. *Proceedings of the IEEE*, 100(2), 322-334.
- Hayashi, K., Nemoto, Y., Akuto, K., Sakurai, Y. (2005). Alkylated imidazolium salt electrolyte for lithium cells. *Journal of Power Sources*, 146, 689-692.
- Hayyan, A., Mjalli, F. S., AlNashef, I. M., Al-Wahaibi, Y. M., Al-Wahaibi, T., Hashim, M. A. (2013). Glucose-based deep eutectic solvents: physical properties. *Journal of Molecular Liquids*. 178, 137 – 141.
- Hayyan, M., Mjalli, F. S., Hashim, M. A., AlNashef, I. M., Al-Zahrani, S. M., Chooi, K. L. (2012). Long term stability of superoxide ion in piperidinium, pyrrolidinium and phosphonium cations-based ionic liquids and its utilization in the destruction of chlorobenzenes. *Journal of Electroanalytical Chemistry*, 664(0), 26-32.
- Herr, T., Fischer, P., Tubke, J., Pinkwart, K., Elsner, P. (2014). Increasing the energy density of the non-aqueous vanadium redox flow battery with the acetonitrile-1,3-dioxolane-dimethyl sulfoxide solvent mixture. *Journal of Power Sources*, 265, 317-324.
- Hirao, M., Sugimoto, H., Ohno, H. (2000). Preparation of Novel Room Temperature Molten Salts by Neutralization of Amines. *Journal of The Electrochemical Society*, 147(11), 4168-4172.
- Holbrey, J. D., Reichert, W. M., Reddy, R. G., Rogers, R. D. (2003). Heat capacities of ionic liquids and their applications as thermal fluids. *ACS Symposium Series: Ionic Liquids as Green Solvents*. 856, 121–133.
- Hoogerstraete, T. V, Brooks, N. R., Norberg, B., Wouters, J., Van Hecke, K., Van Meervelt, L., et al. (2012). Crystal structures of low-melting ionic transition-metal complexes with N-alkylimidazole ligands. *CrystEngComm*, 14(15), 4902-4911.
- Hou, Y., Gu, Y., Zhang, S., Yang, F., Ding, H., Shan, Y. (2008). Novel binary eutectic mixtures based on imidazole. *Journal of Molecular Liquids*. 143, 154–159.
- Huang, K.-L., Li, X.-g., Liu, S.-q., Tan, N., Chen, L.-q. (2008). Research progress of vanadium redox flow battery for energy storage in China. *Renewable Energy*, 33(2), 186-192.
- Huang, X.-J., Rogers, E. I., Hardacre, C., Compton, R. G. (2009). The Reduction of Oxygen in Various Room Temperature Ionic Liquids in the Temperature Range 293-318 K: Exploring the Applicability of the Stokes-Einstein

Relationship in Room Temperature Ionic Liquids. *The Journal of Physical Chemistry B*, 113(26), 8953-8959.

- Hultgren, V. M., Mariotti, A. W. A., Bond, A. M., Wedd, A. G. (2002). Reference Potential Calibration and Voltammetry at Macrodisk Electrodes of Metallocene Derivatives in the Ionic Liquid [bmim][PF<sub>6</sub>]. *Analytical Chemistry*, 74(13), 3151-3156.
- Hurley, F. H., Wier, T. P. (1951). Electrodeposition of Metals from Fused Quaternary Ammonium Salts. *Journal of The Electrochemical Society*, 98(5), 203-206.
- Inzelt, G. r., Lewenstam, A., Scholz, F., Gritzner, G. (2013). Reference Redox Systems in Nonaqueous Systems and the Relation of Electrode Potentials in Nonaqueous and Mixed Solvents to Standard Potentials in Water. In *Handbook of Reference Electrodes* (pp. 25-31): Springer Berlin Heidelberg.
- Ishikawa, M., Sugimoto, T., Kikuta, M., Ishiko, E., Kono, M. (2006). Pure ionic liquid electrolytes compatible with a graphitized carbon negative electrode in rechargeable lithium-ion batteries. *Journal of Power Sources*, 162(1), 658-662.
- Itoh, H., Naka, K., Chujo, Y. (2004). Synthesis of Gold Nanoparticles Modified with Ionic Liquid Based on the Imidazolium Cation. *Journal of the American Chemical Society*, 126(10), 3026-3027.
- Jacquemin, J., Ge, R., Nancarrow, D. W., Costa Gomes, M. F., Padua, A. A. H., Hardacer, C. (2008). Prediction of ionic liquid properties. I. Volumetric properties as a function of temperature at 0.1 MPa. *Journal of Chemical Engineering Data*. 53 (3), 716–726.
- Jacquemin, J., Husson, P., Padua, A. A. H., Majer, V. (2006). Density and viscosity of several pure and water-saturated ionic liquids. *Green Chemistry*, 8(2), 172-180.
- Jhong, H.-R., Wong, D. S.-H., Wan, C.-C., Wang, Y.-Y., Wei, T.-C. (2009). A novel deep eutectic solvent-based ionic liquid used as electrolyte for dye-sensitized solar cells. *Electrochemistry Communications*, 11(1), 209-211.
- Joerissen, L., Garche, J., Fabjan, C., Tomazic, G. (2004). Possible use of vanadium redox-flow batteries for energy storage in small grids and stand-alone photovoltaic systems. *Journal of Power Sources*, 127(1-2), 98-104.
- Ju, Y.-J., Lien, C.-H., Chang, K.-H., Hu, C.-C., Wong, D. S.-H. (2012). Deep Eutectic Solvent-based Ionic Liquid Electrolytes for Electrical Double-layer Capacitors. *Journal of the Chinese Chemical Society*, 59(10), 1280-1287.
- Kareem, M. A., Mjalli, F. S., Hashim, M. A., AlNashef, I. M. (2010). Phosphonium-based ionic liquids analogues and their physical properties. *Journal of Chemical and Engineering Data*. 55, 4632–4637.
- Katayama, Y., Konishiike, I., Miura, T., Kishi, T. (2002). Redox reaction in 1-ethyl-3-methylimidazolium-iron chlorides molten salt system for battery application. *Journal of Power Sources*, 109(2), 327-332.
- Katayama, Y., Konishiike, I., Miura, T., Kishi, T. (2002). Redox reaction in 1-ethyl-3-methylimidazolium-iron chlorides molten salt system for battery application. *Journal of Power Sources*, 109(2), 327-332.
- Kazacos, M., Skyllas-Kazacos, M. (1989). Performance Characteristics of Carbon Plastic Electrodes in the All-Vanadium Redox Cell. *Journal of The Electrochemical Society*, 136(9), 2759-2760.

- Kear, G., Shah, A. A., Walsh, F. C. (2012). Development of the all-vanadium redox flow battery for energy storage: a review of technological, financial and policy aspects. *International Journal of Energy Research*, 36(11), 1105-1120.
- Keita, B., Bouaziz, D., Nadj, L. (1988). Solvent Effects on the Redox Potentials of Potassium 12-Tungstosilicate and 18-Tungstodiphosphate. *Journal of The Electrochemical Society*, 135(1), 87-91
- Keskin, S., Kayrak-Talay, D., Akman, U., Hortaçsu, Ö. (2007). A review of ionic liquids towards supercritical fluid applications. *Journal of Supercritical Fluids*, 43, 150–180.
- Kirchner, B., Clare, B., Sirwardana, A., MacFarlane, D. (2010). Synthesis, Purification and Characterization of Ionic Liquids. In *Ionic Liquids* (Vol. 290, pp. 1-40): Springer Berlin Heidelberg.
- Kölle, P., Dronskowski, R. (2004). Synthesis, crystal structures and electrical conductivities of the ionic liquid compounds butyl dimethylimidazolium tetrafluoroborate, hexafluoroborate and hexafluoroantimonate. *European Journal of Inorganic Chemistry*, 2313–2320.
- Kuang, D., Wang, P., Ito, S., Zakeeruddin, S. M., Gratzel, M. (2006). Stable Mesoscopic Dye-Sensitized Solar Cells Based on Tetracyanoborate Ionic Liquid Electrolyte. *Journal of the American Chemical Society*, 128(24), 7732-7733.
- Kuhnel, R. S., Bockenfeld, N., Passerini, S., Winter, M., Balducci, A. (2011). Mixtures of ionic liquid and organic carbonate as electrolyte with improved safety and performance for rechargeable lithium batteries. *Electrochimica Acta*, 56(11), 4092-4099.
- Laher, T. M., Hussey, C. L. (1982). Electrochemical studies of chloro complex formation in low-temperature chloroaluminate melts. 1. Iron(II), iron(III), and nickel(II). *Inorganic Chemistry*, 21(11), 4079-4083.
- Largeot, C., Taberna, P. L., Gogotsi, Y., Simon, P. (2011). Microporous Carbon-Based Electrical Double Layer Capacitor Operating at High Temperature in Ionic Liquid Electrolyte. *Electrochemical and Solid-State Letters*, 14(12), A174-A176.
- Leron, R. B., Li, M.-H. (2012). High-pressure density measurements for choline chloride: Urea deep eutectic solvent and its aqueous mixtures at T= (298.15 to 323.15) K and up to 50 MPa. *The Journal of Chemical Thermodynamics*, 54(0), 293-301.
- Lessner, P. M., McLarnon, F. R., Winnick, J., Cairns, E. J. (1992). Aqueous polysulphide flow-through electrodes: Effects of electrocatalyst and electrolyte composition on performance. *Journal of Applied Electrochemistry*, 22(10), 927-934.
- Leung, P., Li, X., Ponce De Leon, C., Berlouis, L., Low, C. T. J., Walsh, F. C. (2012). Progress in redox flow batteries, remaining challenges and their applications in energy storage. *RSC Advances*, 2(27), 10125-10156.
- Lewandowski, A., Swiderska-Mocek, A. (2009). Ionic liquids as electrolytes for Li-ion batteries-An overview of electrochemical studies. *Journal of Power Sources*, 194(2), 601-609.

- Lewandowski, A., Swiderska-Mocek, A. (2010). Lithium-metal potential in Li<sup>+</sup> containing ionic liquids. *Journal of Applied Electrochemistry*, 40(3), 515-524.
- Lewandowski, A., Waligora, L., Galinski, M. (2013). Electrochemical Behavior of Cobaltocene in Ionic Liquids. *Journal of Solution Chemistry*, 42(2), 251-262.
- Li, H., Wang, Y., Na, H., Liu, H., Zhou, H. (2009). Rechargeable Ni-Li Battery Integrated Aqueous/Nonaqueous System. *Journal of the American Chemical Society*, 131(42), 15098-15099.
- Li, L., Kim, S., Wang, W., Vijayakumar, M., Nie, Z., Chen, B., et al. (2011). A Stable Vanadium Redox-Flow Battery with High Energy Density for Large-Scale Energy Storage. *Advanced Energy Materials*, 1(3), 394-400.
- Li, X., Zhang, H., Mai, Z., Zhang, H., Vankelecom, I. (2011). Ion exchange membranes for vanadium redox flow battery (VRB) applications. *Energy & Environmental Science*, 4(4), 1147-1160.
- Liang, H., Li, H., Wang, Z., Wu, F., Chen, L., Huang, X. (2001). New Binary Room-Temperature Molten Salt Electrolyte Based on Urea and LiTFSI. *The Journal of Physical Chemistry B*, 105(41), 9966-9969.
- Lim, H. S., Lackner, A. M., Knechtli, R. C. (1977). Zinc-Bromine Secondary Battery. *Journal of The Electrochemical Society*, 124(8), 1154-1157.
- Liming, H. (2009). Financing rural renewable energy: A comparison between China and India. *Renewable and Sustainable Energy Reviews*, 13(5), 1096-1103.
- Lindberg, D., de la Fuente Revenga, M., Widersten, M. (2010). Deep eutectic solvents (DESs) are viable cosolvents for enzyme-catalyzed epoxide hydrolysis. *Journal of Biotechnology*, 147, 169-171.
- Lipsztajn, M., Osteryoung, R. A. (1985). Electrochemistry in neutral ambient-temperature ionic liquids. 1. Studies of iron(III), neodymium(III), and lithium(I). *Inorganic Chemistry*, 24(5), 716-719.
- Liu, Q., Shinkle, A. A., Li, Y., Monroe, C. W., Thompson, L. T., Sleightholme, A. E. S. (2010). Non-aqueous chromium acetylacetonate electrolyte for redox flow batteries. *Electrochemistry Communications*, 12(11), 1634-1637.
- Liu, Q., Sleightholme, A. E. S., Shinkle, A. A., Li, Y., Thompson, L. T. (2009). Non-aqueous vanadium acetylacetonate electrolyte for redox flow batteries. *Electrochemistry Communications*, 11(12), 2312-2315.
- Lloyd, D., Vainikka, T., Kontturi, K. s. (2013a). The development of an all copper hybrid redox flow battery using deep eutectic solvents. *Electrochimica Acta*, 100(0), 18-23.
- Lloyd, D., Vainikka, T., Murtomaki, L., Kontturi, K., Ahlberg, E. (2011). The kinetics of the Cu<sup>2+</sup>/Cu<sup>+</sup> redox couple in deep eutectic solvents. *Electrochimica Acta*, 56(14), 4942-4948.
- Lloyd, D., Vainikka, T., Ronkainen, M., Kontturi, K. s. (2013b). Characterisation and application of the Fe(II)/Fe(III) redox reaction in an ionic liquid analogue. *Electrochimica Acta*, 109(0), 843-851.
- Lockett, V., Sedev, R., Ralston, J., Horne, M., Rodopoulos, T. (2008). Differential Capacitance of the Electrical Double Layer in Imidazolium-Based Ionic Liquids: Influence of Potential, Cation Size, and Temperature. *The Journal of Physical Chemistry C*, 112(19), 7486-7495.

- Low, C. T. J., Walsh, F. C., Chakrabarti, M. H., Hashim, M. A., Hussain, M. A. (2013). Electrochemical approaches to the production of graphene flakes and their potential applications. *Carbon*, 54(0), 1-21.
- Lu, W., Qu, L., Henry, K., Dai, L. (2009). High performance electrochemical capacitors from aligned carbon nanotube electrodes and ionic liquid electrolytes. *Journal of Power Sources*, 189(2), 1270-1277.
- Lu, X., Burrell, G., Separovic, F., Zhao, C. (2012). Electrochemistry of Room Temperature Protic Ionic Liquids: A Critical Assessment for Use as Electrolytes in Electrochemical Applications. *The Journal of Physical Chemistry B*, 116(30), 9160-9170.
- Lund, H., Mathiesen, B. V. (2009). Energy system analysis of 100% renewable energy systems-The case of Denmark in years 2030 and 2050. *Energy*, 34(5), 524-531.
- MacFarlane, D. R., Forsyth, M., Howlett, P. C., Pringle, J. M., Sun, J., Annat, G., et al. (2007). Ionic Liquids in Electrochemical Devices and Processes: Managing Interfacial Electrochemistry. *Accounts of Chemical Research*, 40(11), 1165-1173.
- MacFarlane, D. R., Forsyth, M., Izgorodina, E. I., Abbott, A. P., Annat, G., Fraser, K. (2009). On the concept of ionicity in ionic liquids. *Physical Chemistry Chemical Physics*, 11(25), 4962-4967.
- MacFarlane, D. R., Meakin, P., Sun, J., Amini, N., Forsyth, M. (1999). Pyrrolidinium Imides: A New Family of Molten Salts and Conductive Plastic Crystal Phases. *The Journal of Physical Chemistry B*, 103(20), 4164-4170.
- Mai, Z., Zhang, H., Li, X., Bi, C., Dai, H. (2011). Sulfonated poly(tetramethyldiphenyl ether ether ketone) membranes for vanadium redox flow battery application. *Journal of Power Sources*, 196(1), 482-487.
- Marques, A. n. C., Fuinhas, J. A. (2011). Drivers promoting renewable energy: A dynamic panel approach. *Renewable and Sustainable Energy Reviews*, 15(3), 1601-1608.
- Martino, W., de la Mora, J. F., Yoshida, Y., Saito, G., Wilkes, J. (2006). Surface tension measurements of highly conducting ionic liquids. *Green Chemistry*, 8(4), 390-397.
- Matsuda, Y., Tanaka, K., Okada, M., Takasu, Y., Morita, M., Matsumura-Inoue, T. (1988). A rechargeable redox battery utilizing ruthenium complexes with non-aqueous organic electrolyte. *Journal of Applied Electrochemistry*, 18(6), 909-914.
- McCluskey, A., Geoffrey, A. L., Sarah, K. L., Michael, P. O., Ian, C. H. (2002). Ionic Liquids and Metal Ions: From Green Chemistry to Ore Refining. In *Ionic Liquids* (Vol. 818, pp. 199-212): American Chemical Society.
- McEwen, A. B., McDevitt, S. F., Koch, V. R. (1997). Nonaqueous Electrolytes for Electrochemical Capacitors: Imidazolium Cations and Inorganic Fluorides with Organic Carbonates. *Journal of The Electrochemical Society*, 144(4), L84-L86.
- McHale, G., Hardacre, C., Ge, R., Doy, N., Allen, R. W. K., MacInnes, J. M., et al. (2008). Density-Viscosity Product of Small-Volume Ionic Liquid Samples Using Quartz Crystal Impedance Analysis. *Analytical Chemistry*, 80(15), 5806-5811.



- Menne, S., Pires, J., Anouti, M., Balducci, A. (2013). Protic ionic liquids as electrolytes for lithium-ion batteries. *Electrochemistry Communications*, 31(0), 39-41.
- Mohammadi, T., Skyllas-Kazacos, M. (1995). Preparation of sulfonated composite membrane for vanadium redox flow battery applications. *Journal of Membrane Science*, 107(1-2), 35-45.
- Montanino, M., Moreno, M., Alessandrini, F., Appetecchi, G. B., Passerini, S., Zhou, Q., et al. (2012). Physical and electrochemical properties of binary ionic liquid mixtures: (1-x) PYR14TFSI-(x) PYR14IM14. *Electrochimica Acta*, 60(0), 163-169.
- Morrison, H. G., Sun, C. C., Neervannan, S. (2009). Characterization of thermal behavior of deep eutectic solvents and their potential as drug solubilization vehicles. *International Journal of Pharmaceutics*, 378, 136-139.
- Nagy, L., Gyetvai, G., Kollar, L., Nagy, G. (2006). Electrochemical behavior of ferrocene in ionic liquid media. *Journal of Biochemical and Biophysical Methods*, 69(1-2), 121-132.
- Nakamoto, H., Watanabe, M. (2007). Bronsted acid-base ionic liquids for fuel cell electrolytes. *Chemical Communications*(24), 2539-2541.
- Nanjundiah, C., Osteryoung, R. A. (1983). Electrochemical Studies of Cu(I) and Cu(II) in an Aluminum Chloride-N-(n-Butyl)Pyridinium Chloride Ionic Liquid. *Journal of The Electrochemical Society*, 130(6), 1312-1318.
- Nanjundiah, C., Shimizu, K., Osteryoung, R. A. (1982). Electrochemical Studies of Fe(II) and Fe(III) in an Aluminum Chloride-Butylpyridinium Chloride Ionic Liquid. *Journal of The Electrochemical Society*, 129(11), 2474-2480.
- Negro, S. O., Alkemade, F., Hekkert, M. P. (2012). Why does renewable energy diffuse so slowly? A review of innovation system problems. *Renewable and Sustainable Energy Reviews*, 16(6), 3836-3846.
- Nicholson, R. S. (1965). Theory and Application of Cyclic Voltammetry for Measurement of Electrode Reaction Kinetics. *Analytical Chemistry*, 37(11), 1351-1355.
- Nkuku, C. A., Lesuer, R. J. (2007). Electrochemistry in Deep Eutectic Solvents. *The Journal of Physical Chemistry B*, 111(46), 13271-13277.
- Nuli, Y., Yang, J., Wang, J., Xu, J., Wang, P. (2005). Electrochemical Magnesium Deposition and Dissolution with High Efficiency in Ionic Liquid. *Electrochemical and Solid-State Letters*, 8(11), C166-C169.
- O'Donnell, P.M., R.F. Gahn, and J.L. Pfeiffer, The Redox Flow System for Solar Photovoltaic Energy Storage, N.T. 73562, Editor. 1976: Lewis Research Center.
- O'Mahony, A. M., Silvester, D. S., Aldous, L., Hardacre, C., Compton, R. G. (2008). Effect of Water on the Electrochemical Window and Potential Limits of Room-Temperature Ionic Liquids. *Journal of Chemical & Engineering Data*, 53(12), 2884-2891.
- Ong, S. P., Andreussi, O., Wu, Y., Marzari, N., Ceder, G. (2011). Electrochemical Windows of Room-Temperature Ionic Liquids from Molecular Dynamics and Density Functional Theory Calculations. *Chemistry of Materials*, 23(11), 2979-2986.

- Oriji, G., Katayama, Y., Miura, T. (2004). Investigation on V(IV)/V(V) species in a vanadium redox flow battery. *Electrochimica Acta*, 49(19), 3091-3095.
- Oriji, G., Katayama, Y., Miura, T. (2005). Investigations on V(IV)/V(V) and V(II)/V(III) redox reactions by various electrochemical methods. *Journal of Power Sources*, 139(1-2), 321-324.
- Padilha, J. C., Basso, J., da Trindade, L. G., Martini, E. M. A., de Souza, M. O., de Souza, R. F. (2010). Ionic liquids in proton exchange membrane fuel cells: Efficient systems for energy generation. *Journal of Power Sources*, 195(19), 6483-6485.
- Palacin, M. R. (2009). Recent advances in rechargeable battery materials: a chemist's perspective. *Chemical Society Reviews*, 38(9), 2565-2575.
- Pang, K., Hou, Y., Wu, W., Guo, W., Peng, W., Marsh, K. N. (2012). Efficient separation of phenols from oils via forming deep eutectic solvents. *Green Chemistry*, 14(9), 2398-2401.
- Panwar, N. L., Kaushik, S. C., Kothari, S. (2011). Role of renewable energy sources in environmental protection: A review. *Renewable and Sustainable Energy Reviews*, 15(3), 1513-1524.
- Paulenova, A., Creager, S. E., Navratil, J. D., Wei, Y. (2002). Redox potentials and kinetics of the Ce<sup>3+</sup>/Ce<sup>4+</sup> redox reaction and solubility of cerium sulfates in sulfuric acid solutions. *Journal of Power Sources*, 109(2), 431-438.
- Plechkova, N. V., Seddon, K. R. (2008). Applications of ionic liquids in the chemical industry. *Chemical Society Reviews*, 37(1), 123-150.
- Ponce de Leon, C., Frías-Ferrer, A., González-García, J., Szánto, D. A., Walsh, F. C. (2006). Redox flow cells for energy conversion. *Journal of Power Sources*, 160(1), 716-732.
- Posner, A. M. (1955) Redox fuel cell. *Fuel*, 34, 330–338.
- Pratt, H. D., Leonard, J. C., Steele, L. A. M., Staiger, C. L., Anderson, T. M. (2013). Copper ionic liquids: Examining the role of the anion in determining physical and electrochemical properties. *Inorganica Chimica Acta*, 396(0), 78-83.
- Pratt H. D., Rose, A. J., Staiger, C. L., Ingersoll, D., Anderson, T. M. (2011). Synthesis and characterization of ionic liquids containing copper, manganese, or zinc coordination cations. *Dalton Transactions*, 40(43), 11396-11401.
- Price, A., Bartley, S., Male, S., Cooley, G. (1999). A novel approach to utility scale energy storage [regenerative fuel cells]. *Power Engineering Journal*, 13(3), 122-129.
- Quinn, B. M., Ding, Z., Moulton, R., Bard, A. J. (2002). Novel Electrochemical Studies of Ionic Liquids. *Langmuir*, 18(5), 1734-1742.
- Rahman, F., Skyllas-Kazacos, M. (2009). Vanadium redox battery: Positive half-cell electrolyte studies. *Journal of Power Sources*, 189(2), 1212-1219.
- Rahman, F., Skyllas-Kazacos, M. (1998). Solubility of vanadyl sulfate in concentrated sulfuric acid solutions. *Journal of Power Sources*, 72(2), 105-110.
- Randles, J. E. B. (1948). A cathode ray polarograph. Part II.-The current-voltage curves. *Transactions of the Faraday Society*, 44, 327-338.

- Rauter, A. I. P., Vogel, P., Queneau, Y., Chiappe, C., Marra, A., Mele, A. (2010). Synthesis and Applications of Ionic Liquids Derived from Natural Sugars. In *Carbohydrates in Sustainable Development II* (Vol. 295, pp. 177-195): Springer Berlin Heidelberg.
- Rezaei, B., Mallakpour, S., Taki, M. (2009). Application of ionic liquids as an electrolyte additive on the electrochemical behavior of lead acid battery. *Journal of Power Sources*, 187(2), 605-612.
- Rogers, E. I., Silvester, D. S., Poole, D. L., Aldous, L., Hardacre, C., Compton, R. G. (2008). Voltammetric Characterization of the Ferrocene|Ferrocenium and Cobaltocenium|Cobaltocene Redox Couples in RTILs. *The Journal of Physical Chemistry C*, 112(7), 2729-2735.
- Rub, C., Konig, B. (2012). Low melting mixtures in organic synthesis - an alternative to ionic liquids? *Green Chemistry*, 14(11), 2969-2982.
- Rychcik, M., Skyllas-Kazacos, M. (1988). Characteristics of a new all-vanadium redox flow battery. *Journal of Power Sources*, 22(1), 59-67.
- S. Eckroad, Technical Report, EPRI-1014836, Electric Power Research Institute, Palo Alto, CA, USA, 2007.
- Sahir, M. H., Qureshi, A. H. (2008). Assessment of new and renewable energy resources potential and identification of barriers to their significant utilization in Pakistan. *Renewable and Sustainable Energy Reviews*, 12(1), 290-298.
- Sanchez, L. G., Espel, J. R., Onink, F., Meindersma, G. W., Haan, A. B. d. (2009). Density, Viscosity, and Surface Tension of Synthesis Grade Imidazolium, Pyridinium, and Pyrrolidinium Based Room Temperature Ionic Liquids. *Journal of Chemical & Engineering Data*, 54(10), 2803-2812.
- Sato, T., Maruo, T., Marukane, S., Takagi, K. (2004). Ionic liquids containing carbonate solvent as electrolytes for lithium ion cells. *Journal of Power Sources*, 138(1-2), 253-261.
- Sato, T., Masuda, G., Takagi, K. (2004). Electrochemical properties of novel ionic liquids for electric double layer capacitor applications. *Electrochimica Acta*, 49(21), 3603-3611.
- Savinell, R. F., Liu, C. C., Galasco, R. T., Chiang, S. H., Coetzee, J. F. (1979). Discharge Characteristics of a Soluble Iron-Titanium Battery System. *Journal of The Electrochemical Society*, 126(3), 357-360.
- Scordilis-Kelley, C., Fuller, J., Carlin, R. T., Wilkes, J. S. (1992). Alkali Metal Reduction Potentials Measured in Chloroaluminate Ambient-Temperature Molten Salts. *Journal of The Electrochemical Society*, 139(3), 694-699.
- Sekhon, S. S., Krishnan, P., Singh, B., Yamada, K., Kim, C. S. (2006). Proton conducting membrane containing room temperature ionic liquid. *Electrochimica Acta*, 52(4), 1639-1644.
- Shahbaz, K., Baroutian, S., Mjalli, F. S., Hashim, M. A., AlNashef, I. M. (2012a). Densities of ammonium and phosphonium based deep eutectic solvents: Prediction using artificial intelligence and group contribution techniques. *Thermochimica Acta*. 527, 59-66.
- Shahbaz, K., Mjalli, F. S., Hashim, M. A., AlNashef, I. M. (2010). Using deep eutectic solvents for the removal of glycerol from palm-oil based biodiesel. *Journal of applied sciences*. 10 (24), 3349-3354.

- Shahbaz, K., Mjalli, F. S., Hashim, M. A., AlNashef, I. M. (2011). Using Deep Eutectic Solvents Based on Methyl Triphenyl Phosphonium Bromide for the Removal of Glycerol from Palm-Oil-Based Biodiesel. *Energy & Fuels*, 25(6), 2671-2678.
- Shahbaz, K., Mjalli, F. S., Hashim, M. A., AlNashef, I. M. (2011c). Prediction of deep eutectic solvents densities at different temperatures. *Thermochimica Acta*. 515, 67–72.
- Shan, C., Li, F., Yuan, F., G. Yang, L. Niu, Zhang, Q. (2008). Size-controlled synthesis of monodispersed gold nanoparticles stabilized by polyelectrolyte-functionalized ionic liquid. *Nanotechnology*, 19(28), 285601.
- Sheikh, M. A. (2010). Energy and renewable energy scenario of Pakistan. *Renewable and Sustainable Energy Reviews*, 14(1), 354-363.
- Sheldon, R. A., Lau, R. M., Sorgedrager, F., Rantwijk, K. V., Seddon, K. R. (2002). Biocatalysis in ionic liquids. *Green Chemistry*. 4, 147–151.
- Shiddiky, M. J. A., Torriero, A. A. J. (2011). Application of ionic liquids in electrochemical sensing systems. *Biosensors and Bioelectronics*, 26(5), 1775-1787.
- Shinkle, A. A., Pomaville, T. J., Sleightholme, A. E. S., Thompson, L. T., Monroe, C. W. (2014). Solvents and supporting electrolytes for vanadium acetylacetonate flow batteries. *Journal of Power Sources*, 248, 1299-1305.
- Shinkle, A. A., Sleightholme, A. E. S., Griffith, L. D., Thompson, L. T., Monroe, C. W. (2012). Degradation mechanisms in the non-aqueous vanadium acetylacetonate redox flow battery. *Journal of Power Sources*, 206(0), 490-496.
- Shoup, D., Szabo, A. (1982). Chronoamperometric current at finite disk electrodes. *Journal of Electroanalytical Chemistry and Interfacial Electrochemistry*, 140(2), 237-245.
- Skyllas-Kazacos M. Vanadium/polyhalideredox flow battery. US Patent 7320844; 2008.
- Skyllas-Kazacos, M. (2003). Novel vanadium chloride/polyhalide redox flow battery. *Journal of Power Sources*, 124(1), 299-302.
- Skyllas-Kazacos, M., Chakrabarti, M. H., Hajimolana, S. A., Mjalli, F. S., Saleem, M. (2011). Progress in Flow Battery Research and Development. *Journal of The Electrochemical Society*, 158(8), R55-R79.
- Skyllas-Kazacos, M., Kasherman, D., Hong, D. R., Kazacos, M. (1991). Characteristics and performance of 1 kW UNSW vanadium redox battery. *Journal of Power Sources*, 35(4), 399-404.
- Skyllas-Kazacos, M., Kazacos, G., Poon, G., Verseema, H. (2010). Recent advances with UNSW vanadium-based redox flow batteries. *International Journal of Energy Research*, 34(2), 182-189.
- Skyllas-Kazacos, M., Menictas, C., Kazacos, M. (1996). Thermal Stability of Concentrated V(V) Electrolytes in the Vanadium Redox Cell. *Journal of The Electrochemical Society*, 143(4), L86-L88.
- Skyllas-Kazacos, M., Rychcik, M., Robins, R., Fane, A., Green, M. (1986). New all-vanadium redox flow cell. *Journal of The Electrochemical Society*, 133(5), 1057-1058.

- Sleightholme, A. E. S., Shinkle, A. A., Liu, Q., Li, Y., Monroe, C. W., Thompson, L. T. (2011). Non-aqueous manganese acetylacetonate electrolyte for redox flow batteries. *Journal of Power Sources*, 196(13), 5742-5745.
- Snook, G. A., Best, A. S., Pandolfo, A. G., Hollenkamp, A. F. (2006). Evaluation of a Ag/Ag<sup>+</sup> reference electrode for use in room temperature ionic liquids. *Electrochemistry Communications*, 8(9), 1405-1411.
- Soloveichik, G. L. (2011). Battery Technologies for Large-Scale Stationary Energy Storage. *Annual Review of Chemical and Biomolecular Engineering*, 2(1), 503-527.
- Steichen, M., Thomassey, M., Siebentritt, S., Dale, P. J. (2011). Controlled electrodeposition of Cu-Ga from a deep eutectic solvent for low cost fabrication of CuGaSe<sub>2</sub> thin film solar cells. *Physical Chemistry Chemical Physics*, 13(10), 4292-4302.
- Strubinger, S. K. D., Sun, I. W., Cleland, W. E., Hussey, C. L. (1990). Electrochemical and spectroscopic studies of rhenium(IV) monomeric and dimeric chloride complexes in the basic aluminum chloride-1-methyl-3-ethylimidazolium chloride room-temperature molten salt. *Inorganic Chemistry*, 29(21), 4246-4252.
- Suarez, P. A. Z., Einloft, S., Dullius, J. E. L., de Souza, R. F., Dupont, J. (1998). Synthesis and physical-chemical properties of ionic liquids based on 1-butyl-3-methylimidazolium cation. *J. Chim. Phys.*, 95(7), 1626-1639.
- Suarez, P. A. Z., Selbach, V. n. M., Dullius, J. E. L., Einloft, S., Piatnicki, C. M. S., Azambuja, D. S., et al. (1997). Enlarged electrochemical window in dialkyl-imidazolium cation based room-temperature air and water-stable molten salts. *Electrochimica Acta*, 42(16), 2533-2535.
- Sukkar, T., Skyllas-Kazacos, M. (2003). Water transfer behaviour across cation exchange membranes in the vanadium redox battery. *Journal of Membrane Science*, 222(1-2), 235-247.
- Sum, E., Rychcik, M., Skyllas-kazacos, M. (1985). Investigation of the V(V)/V(IV) system for use in the positive half-cell of a redox battery. *Journal of Power Sources*, 16(2), 85-95.
- Sum, E., Skyllas-Kazacos, M. (1985). A study of the V(II)/V(III) redox couple for redox flow cell applications. *Journal of Power Sources*, 15(2-3), 179-190.
- Sun, B., Skyllas-Kazacos, M. (1991). Chemical modification and electrochemical behaviour of graphite fibre in acidic vanadium solution. *Electrochimica Acta*, 36(3-4), 513-517.
- Sun, I. W., Hussey, C. L. (1989). Electrochemistry of niobium chloride and oxide chloride complexes in the basic aluminum chloride-1-methyl-3-ethylimidazolium chloride room-temperature ionic liquid. *Inorganic Chemistry*, 28(14), 2731-2737.
- Susan, M. A. B. H., Noda, A., Mitsushima, S., Watanabe, M. (2003). Bronsted acid-base ionic liquids and their use as new materials for anhydrous proton conductors. *Chemical Communications*(8), 938-939.
- Tang, B., Row, K. (2013). Recent developments in deep eutectic solvents in chemical sciences. *Monatshefte fur Chemie - Chemical Monthly*, 144(10), 1427-1454.

- Tang, S., Baker, G. A., Zhao, H. (2012). Ether- and alcohol-functionalized task-specific ionic liquids: attractive properties and applications. *Chemical Society Reviews*, 41(10), 4030-4066.
- Tatumi, R., Fujihara, H. (2005). Remarkably stable gold nanoparticles functionalized with a zwitterionic liquid based on imidazolium sulfonate in a high concentration of aqueous electrolyte and ionic liquid. *Chemical Communications*(1), 83-85.
- Thaller L. H. ( 1974). Electrically rechargeable redox flow cells. Proc. Ninth Intersoc. Energy Conv. Eng. Conf., San Francisco, CA, August 26 - 30 , pp. 924 – 928. NASATMX-71540.
- Torriero, A. A. J., Sunarso, J., Howlett, P. C. (2012). Critical evaluation of reference systems for voltammetric measurements in ionic liquids. *Electrochimica Acta*, 82, 60-68.
- Tsierkezos, N. (2007). Cyclic Voltammetric Studies of Ferrocene in Nonaqueous Solvents in the Temperature Range from 248.15 to 298.15 K. *Journal of Solution Chemistry*, 36(3), 289-302.
- Tsuda, I., Nozaki, K., Sakuta, K., Kurokawa, K. (1997). Improvement of performance in redox flow batteries for PV systems. *Solar Energy Materials and Solar Cells*, 47(1-4), 101-107.
- Tsunashima, K., Sugiya, M. (2007). Physical and electrochemical properties of low-viscosity phosphonium ionic liquids as potential electrolytes. *Electrochemistry* 75, 734–736.
- Ue, M., Takeda, M., Toriumi, A., Kominato, A., Hagiwara, R., Ito, Y. (2003). Application of Low-Viscosity Ionic Liquid to the Electrolyte of Double-Layer Capacitors. *Journal of The Electrochemical Society*, 150(4), A499-A502.
- Vafiadis, H., Skyllas-Kazacos, M. (2006). Evaluation of membranes for the novel vanadium bromine redox flow cell. *Journal of Membrane Science*, 279(1-2), 394-402.
- Wadia, C., Albertus, P., Srinivasan, V. (2011). Resource constraints on the battery energy storage potential for grid and transportation applications. *Journal of Power Sources*, 196(3), 1593-1598.
- Waligora, L., Lewandowski, A., Gritzner, G. (2009). Electrochemical studies of four organometallic redox couples as possible reference redox systems in 1-ethyl-3-methylimidazolium tetrafluoroborate. *Electrochimica Acta*, 54(5), 1414-1419.
- Wandschneider, F. T., Rohm, S., Fischer, P., Pinkwart, K., Tubke, J., & Nirschl, H. (2014). A multi-stack simulation of shunt currents in vanadium redox flow batteries. *Journal of Power Sources*, 261, 64-74.
- Wang, P., Wenger, B., Humphry-Baker, R., Moser, J.-E., Teuscher, J. I., Kantlehner, W., et al. (2005). Charge Separation and Efficient Light Energy Conversion in Sensitized Mesoscopic Solar Cells Based on Binary Ionic Liquids. *Journal of the American Chemical Society*, 127(18), 6850-6856.
- Wang, P., Zakeeruddin, S. M., Humphry-Baker, R., Gratzel, M. (2004). A Binary Ionic Liquid Electrolyte to Achieve  $\geq 7\%$  Power Conversion Efficiencies in Dye-Sensitized Solar Cells. *Chemistry of Materials*, 16(14), 2694-2696.

- Wang, P., Zakeeruddin, S. M., Moser, J.-E., Gratzel, M. (2003). A New Ionic Liquid Electrolyte Enhances the Conversion Efficiency of Dye-Sensitized Solar Cells. *The Journal of Physical Chemistry B*, 107(48), 13280-13285.
- Wasserscheid, P., Hal, R. V., Bösmann, A. (2002). 1-n-butyl-3-methylimidazolium ([bmim]) octylsulfate an even 'greener' ionic liquid. *Green Chemistry*, 4, 400-404.
- Wasserscheid, P., Keim, W. (2000). Ionic Liquids—New “solutions” for transition metal catalysis. *Angewandte Chemie International Edition*, 39, 3773-3789.
- Watt-Smith, M. J., Ridley, P., Wills, R. G. A., Shah, A. A., Walsh, F. C. (2013). The importance of key operational variables and electrolyte monitoring to the performance of an all vanadium redox flow battery. *Journal of Chemical Technology & Biotechnology*, 88(1), 126-138.
- Weber, A., Mench, M., Meyers, J., Ross, P., Gostick, J., Liu, Q. (2011). Redox flow batteries: a review. *Journal of Applied Electrochemistry*, 41(10), 1137-1164.
- Wei, D., Ivaska, A. (2008). Applications of ionic liquids in electrochemical sensors. *Analytica Chimica Acta*, 607(2), 126-135.
- Wen, Y. H., Zhang, H. M., Qian, P., Zhou, H. T., Zhao, P., Yi, B. L., et al. (2006). A study of the Fe(III)/Fe(II)-triethanolamine complex redox couple for redox flow battery application. *Electrochimica Acta*, 51(18), 3769-3775.
- Whitehead, J. A., Lawrance, G. A., McCluskey, A. (2004). Green leaching: recyclable and selective leaching of gold-bearing ore in an ionic liquid. *Green Chemistry*, 6(7), 313-315.
- Wiedemann, E., Heintz, A., Lichtenthaler, R. N. (1998). Transport properties of vanadium ions in cation exchange membranes: Determination of diffusion coefficients using a dialysis cell. *Journal of Membrane Science*, 141(2), 215-221.
- Wiley: Weinheim, Germany; p 387.
- Wilkes, J. S. (2004). Properties of ionic liquid solvents for catalysis. *Journal of Molecular Catalysis A: Chemical*, 214(1), 11-17.
- Wilkes, J. S., Levisky, J. A., Wilson, R. A., Hussey, C. L. (1982). Dialkylimidazolium chloroaluminate melts: a new class of room-temperature ionic liquids for electrochemistry, spectroscopy and synthesis. *Inorganic Chemistry*, 21, 1263-1264.
- Wilkes, J. S., Zaworotko, M. J. (1992). Air and water stable 1-ethyl-3-methylimidazolium based ionic liquids. *Journal of the Chemical Society, Chemical Communications*, 965-967.
- Wu, T. Y., Su, S. G., Gung, S. T., Lin, M. W., Lin, Y. C., Ou-Yang, W. C., et al. (2011). Synthesis and characterization of protic ionic liquids containing cyclic amine cations and tetrafluoroborate anion. *Journal of the Iranian Chemical Society*, 8(1), 149-165.
- Wu, T.-Y., Su, S.-G., Wang, H. P., Sun, I. W. (2011). Glycine-based ionic liquids as potential electrolyte for electrochemical studies of organometallic and organic redox couples. *Electrochemistry Communications*, 13(3), 237-241.
- Wu, X., Angell, C. A. (2003). Solvent-Free Electrolytes with Aqueous Solution-Like Conductivities. *Science*, 302, 422-425.

- Wu, X., Xu, H., Xu, P., Shen, Y., Lu, L., Shi, J. (2014). Microwave-treated graphite felt as the positive electrode for all-vanadium redox flow battery. *Journal of Power Sources*, 263, 104-109.
- Xia, X., Liu, H.-T., & Liu, Y. (2002). Studies of the Feasibility of a  $\text{Ce}^{4+}/\text{Ce}^{3+}$   $\text{V}^{2+}/\text{V}^{3+}$  Redox Cell. *Journal of The Electrochemical Society*, 149(4), A426-A430.
- Xue, F.-Q., Wang, Y.-L., Wang, W.-H., Wang, X.-D. (2008). Investigation on the electrode process of the Mn(II)/Mn(III) couple in redox flow battery. *Electrochimica Acta*, 53(22), 6636-6642.
- Yamagata, M., Katayama, Y., Miura, T. (2006). Electrochemical Behavior of Samarium, Europium, and Ytterbium in Hydrophobic Room-Temperature Molten Salt Systems. *Journal of The Electrochemical Society*, 153(1), E5-E9.
- Yamagata, M., Tachikawa, N., Katayama, Y., Miura, T. (2007). Electrochemical behavior of several iron complexes in hydrophobic room-temperature ionic liquids. *Electrochimica Acta*, 52(9), 3317-3322.
- Yamamura, T., Shiokawa, Y., Yamana, H., Moriyama, H. (2002). Electrochemical investigation of uranium  $\beta$ -diketonates for all-uranium redox flow battery. *Electrochimica Acta*, 48(1), 43-50.
- Yang, Z., Zhang, J., Kintner-Meyer, M. C. W., Lu, X., Choi, D., Lemmon, J. P., et al. (2011). Electrochemical Energy Storage for Green Grid. *Chemical Reviews*, 111(5), 3577-3613.
- Ye, H., Huang, J., Xu, J. J., Kodiweera, N. K. A. C., Jayakody, J. R. P., Greenbaum, S. G. (2008). New membranes based on ionic liquids for PEM fuel cells at elevated temperatures. *Journal of Power Sources*, 178(2), 651-660.
- Yoshida, Y., Baba, O., Saito, G. (2007). Ionic Liquids Based on Dicyanamide Anion: Influence of Structural Variations in Cationic Structures on Ionic Conductivity. *The Journal of Physical Chemistry B*, 111(18), 4742-4749.
- Yufit, V., Hale, B., Matian, M., Mazur, P., Brandon, N. P. (2013). Development of a Regenerative Hydrogen-Vanadium Fuel Cell for Energy Storage Applications. *Journal of The Electrochemical Society*, 160(6), A856-A861.
- Yuyama, K., Masuda, G., Yoshida, H., Sato, T. (2006). Ionic liquids containing the tetrafluoroborate anion have the best performance and stability for electric double layer capacitor applications. *Journal of Power Sources*, 162(2), 1401-1408.
- Zhang, D., Liu, Q., Shi, X., Li, Y. (2012). Tetrabutylammonium hexafluorophosphate and 1-ethyl-3-methyl imidazolium hexafluorophosphate ionic liquids as supporting electrolytes for non-aqueous vanadium redox flow batteries. *Journal of Power Sources*, 203(0), 201-205.
- Zhang, H., Shen, P. K. (2012). Recent Development of Polymer Electrolyte Membranes for Fuel Cells. *Chemical Reviews*, 112(5), 2780-2832.
- Zhang, H., Zhang, H., Li, X., Mai, Z., Zhang, J. (2011). Nanofiltration (NF) membranes: the next generation separators for all vanadium redox flow batteries (VRBs)? *Energy & Environmental Science*, 4(5), 1676-1679.
- Zhang, J., Bond, A. M., Belcher, W. J., Wallace, K. J., Steed, J. W. (2003). Electrochemical Studies on the Modular Podand 1,3,5-Tris(3-(ferrocenylmethyl)amino)pyridiniumyl)-2,4,6-triethylbenzene



Hexafluorophosphate in Conventional Solvents and Ionic Liquids. *The Journal of Physical Chemistry B*, 107(24), 5777-5786.

- Zhang, Q., De Oliveira Vigier, K., Royer, S., Jerome, F. (2012). Deep eutectic solvents: syntheses, properties and applications. *Chemical Society Reviews*, 41(21), 7108-7146.
- Zhang, S., Sun, N., He, X., Lu, X., Zhang, X. (2006). Physical Properties of Ionic Liquids: Database and Evaluation. *Journal of Physical and Chemical Reference Data*, 35(4), 1475-1517.
- Zhao, C., Burrell, G., Torriero, A. A. J., Separovic, F., Dunlop, N. F., MacFarlane, D. R., Bond, A. (2008). Electrochemistry of room temperature protic ionic liquids. *The Journal of Physical Chemistry B*, 112(23), 6923-6936.
- Zhao, C., Burrell, G., Torriero, A. A. J., Separovic, F., Dunlop, N. F., MacFarlane, D. R. (2008). Electrochemistry of Room Temperature Protic Ionic Liquids. *The Journal of Physical Chemistry B*, 112(23), 6923-6936.
- Zhao, H., Baker, G. A. (2012). Ionic liquids and deep eutectic solvents for biodiesel synthesis: a review. *Journal of Chemical Technology & Biotechnology*, 88(1), 3-12.
- Zhao, H., Baker, G. A. (2013). Ionic liquids and deep eutectic solvents for biodiesel synthesis: a review. *Journal of Chemical Technology & Biotechnology*, 88(1), 3-12.
- Zhao, H., Baker, G. A., Holmes, S. (2011). New eutectic ionic liquids for lipase activation and enzymatic preparation of biodiesel. *Organic & Biomolecular Chemistry*, 9(6), 1908-1916.
- Zhao, P., Zhang, H., Zhou, H., Chen, J., Gao, S., Yi, B. (2006). Characteristics and performance of 10 kW class all-vanadium redox-flow battery stack. *Journal of Power Sources*, 162(2), 1416-1420.
- Zhao, P., Zhang, H., Zhou, H., Yi, B. (2005). Nickel foam and carbon felt applications for sodium polysulfide/bromine redox flow battery electrodes. *Electrochimica Acta*, 51(6), 1091-1098.
- Zhou, Z.-B., Takeda, M., Ue, M. (2004). New hydrophobic ionic liquids based on perfluoroalkyltrifluoroborate anions. *Journal of Fluorine Chemistry*, 125(3), 471-476.

## List of Publications and Papers Presented

### Journal papers

- 1- The electrochemical behaviour of ferrocene in deep eutectic solvents based on quaternary ammonium and phosphonium salts. **Laleh Bahadori**, Ninie Suhana Abdul Manan, Mohammed Harun Chakrabarti, Mohd. Ali Hashim, Farouq Sabri Mjalli, Inas Muen AlNashef, Mohd. Azlan Hussain, Chee Tong John Low. *J. Physical Chemistry Chemical Physics*. 2013, 15, 1707-1714.
- 2- Physicochemical properties of ammonium-based deep eutectic solvents and their electrochemical evaluation using organometallic reference redox systems. **Laleh Bahadori**, Mohammed Harun Chakrabarti, Farouq Sabri Mjalli, Inas Muen AlNashef, Ninie Suhana Abdul Manan, Mohd Ali Hashim. *Electrochimica Acta*, 2013, 113, 205-211.
- 3- Temperature effects on the kinetics of ferrocene and cobaltocenium in methyltriphenylphosphonium bromide based deep eutectic solvents. **Laleh Bahadori**, Mohammed Harun Chakrabarti, Mohd Ali Hashim, Ninie Suhana Abdul Manan, Inas Muen AlNashef, Farouq Sabri Mjalli. *Journal of The Electrochemical Society*, 2015, 162 (9) H617-H624.
- 4- Prospects of applying ionic liquids and deep eutectic solvents for renewable energy storage by means of redox flow batteries. Mohammed Harun Chakrabarti, Farouq Sabri Mjalli, Inas Muen AlNashef, Mohd. Ali Hashim, Mohd. Azlan Hussain, **Laleh Bahadori**, Chee Tong John Low. *Renewable and Sustainable Energy Reviews*, 2014, 30, 254-270.
- 5- Cyclic voltammetry of iron (III) acetylacetonate in quaternary ammonium and phosphonium based deep eutectic solvents. Mohammed Harun Chakrabarti, Nigel P. Brandon, Mohd. Ali Hashim, Farouq Sabri Mjalli, Inas Muen

- AlNashef, **Laleh Bahadori**, Ninie Suhana Abdul Manan, Mohd. Azlan Hussain, Vladimir Yufit. International Journal of Electrochemical Science, 2013, 8, 9652-9676.
- 6- Cyclic voltammetry of metallic acetylacetonate salts in quaternary ammonium and phosphonium based deep eutectic solvents. Mohammed Harun Chakrabarti, Nigel P. Brandon, Farouq Sabri Mjalli, **Laleh Bahadori**, Inas Muen AlNashef, Mohd. Ali Hashim, Mohd. Azlan Hussain, Chee Tong John Low, Vladimir Yufi. Journal of Solution Chemistry, 2013, 13, 2329-2341.
- 7- Evaluation of deep eutectic solvents as electrolytes for a non-aqueous vanadium redox battery. **Laleh Bahadori**, Mohammed Harun Chakrabarti, Ninie Suhana Abdul Manan, Farouq Sabri Mjalli, Inas Muen AlNashef, Mohd. Ali Hashim, Nigel P. Brandon. Journal of power sources, 2015, Under Review.
- 8- The effect of temperature on kinetics and diffusion coefficients of metallocene derivatives in polyol-based deep eutectic solvents. **Laleh Bahadori**, Mohammed Harun Chakrabarti, Mohd Ali Hashim, Ninie Suhana Abdul Manan, Inas Muen AlNashef, Farouq Sabri Mjalli. PLOS ONE, 2015, Under Review.

## Conferences

- 1- Electrochemical studies of ferrocene and ferrocenium ion in ammonium and phosphonium based deep eutectic solvents. **Laleh Bahadori**, Ninie Suhana Abdul Manan, Mohammed Harun Chakrabarti, Mohd. Ali Hashim, Farouq Sabri Mjalli, Inas Muen AlNashef, Mohd. Azlan Hussain, Chee Tong John Low. The Asia-Oceania Top University League on Engineering (AOTULE 2012), Kuala Lumpur, Malaysia.
- 2- Investigation of physicochemical and electrochemical properties of organometallic derivatives in ammonium based deep eutectic solvents. **Laleh Bahadori**, Mohammed Harun Chakrabarti, Mohd Ali Hashim, Ninie Suhana Abdul Manan, Inas Muen AlNashef, Farouq Sabri Mjalli. International Conference on Ionic Liquids (ICIL 2013), Langkawi, Malaysia.
- 3- Electrochemical behaviour of metallocene in deep eutectic solvents for possible applications as solvents for redox flow batteries. **Laleh Bahadori**, Seyedahmad Hajimolana, Mohammed Harun Chakrabarti, Mohd Ali Hashim, Ninie Suhana Abdul Manan, Inas Muen AlNashef, Farouq Sabri Mjalli. International Conference on Ionic Liquids (ICIL 2013), Langkawi, Malaysia.
- 4- Electrochemical and physicochemical properties of alcohol based deep eutectic solvents. **Laleh Bahadori**, Mohammed Harun Chakrabarti, Mohd Ali Hashim, Ninie Suhana Abdul Manan, Inas Muen AlNashef, Farouq Sabri Mjalli. 4<sup>th</sup> International congress on Green Process Engineering (GPE 2014), Seville, Spain.
- 5- Electrochemical studies of non-aqueous vanadium acetylacetonate redox flow battery in deep eutectic solvents. **Laleh Bahadori**, Mohammed Harun Chakrabarti, Mohd Ali Hashim, Inas Muen AlNashef, Farouq Sabri Mjalli,

Ninie Suhana Abdul Manan. 19th Annual Green Chemistry & Engineering Conference (2015 GC&E), North Bethesda, USA.

- 6- Evaluation of deep eutectic solvents as electrolytes for a non-aqueous vanadium redox battery. **Laleh Bahadori**, Mohammed Harun Chakrabarti, Mohd Ali Hashim, Inas Muen AlNashef, Farouq Sabri Mjalli, Ninie Suhana Abdul Manan. 2<sup>nd</sup> International Conference on Past and Present Research systems of Green Chemistry (Green Chemistry-2015), Orlando, USA.